

NEW ADVANCES IN SYNCHRONIZATION OF DIGITAL
COMMUNICATION RECEIVERS

A Dissertation

by

YAN WANG

Submitted to the Office of Graduate Studies of
Texas A&M University
in partial fulfillment of the requirements for the degree of

DOCTOR OF PHILOSOPHY

December 2003

Major Subject: Electrical Engineering

NEW ADVANCES IN SYNCHRONIZATION OF DIGITAL
COMMUNICATION RECEIVERS

A Dissertation

by

YAN WANG

Submitted to Texas A&M University
in partial fulfillment of the requirements
for the degree of

DOCTOR OF PHILOSOPHY

Approved as to style and content by:

Erchin Serpedin
(Chair of Committee)

Costas N. Georghiadis
(Member)

Andrew K. Chan
(Member)

Du Li
(Member)

Chanan Singh
(Head of Department)

December 2003

Major Subject: Electrical Engineering

ABSTRACT

New Advances in Synchronization of Digital

Communication Receivers. (December 2003)

Yan Wang, B.S., Peking University, P.R. China;

M.S., Beijing University of Posts & Telecommunications, P.R. China

Chair of Advisory Committee: Dr. Erchin Serpedin

Synchronization is a challenging but very important task in communications. In digital communication systems, a hierarchy of synchronization problems has to be considered: carrier synchronization, symbol timing synchronization and frame synchronization. For bandwidth efficiency and burst transmission reasons, the former two synchronization steps tend to favor non-data aided (NDA or blind) techniques, while in general, the last one is usually solved by inserting repetitively known bits or words into the data sequence and is referred to as a data-aided (DA) approach.

Over the last two decades, extensive research work has been carried out to design nondata-aided timing recovery and carrier synchronization algorithms. Despite their importance and spread use, most of the existing blind synchronization algorithms are derived in an *ad-hoc* manner without exploiting optimally the entire available statistical information. In most cases their performance is evaluated by computer simulations; rigorous and complete performance analysis has not been performed yet. It turns out that a theoretical oriented approach is indispensable for studying the limit or bound of algorithms and for comparing different methods.

The main goal of this dissertation is to develop several novel signal processing frameworks that enable one to analyze and improve the performance of the existing timing recovery and carrier synchronization algorithms. As byproducts of this analy-

sis, unified methods for designing new computationally and statistically efficient (i.e., minimum variance estimators) blind feedforward synchronizers are developed.

This work consists of three tightly coupled research directions. First, a general and unified framework is proposed to develop optimal nonlinear least-squares (NLS) carrier recovery scheme for burst transmissions. A family of blind constellation-dependent optimal “matched” NLS carrier estimators is proposed for synchronization of burst transmissions fully modulated by PSK and QAM-constellations in additive white Gaussian noise channels. Second, a cyclostationary statistics based framework is proposed for designing computationally and statistically efficient robust blind symbol timing recovery for time-selective flat-fading channels. Lastly, dealing with the problem of frame synchronization, a simple and efficient data-aided approach is proposed for jointly estimating the frame boundary, the frequency-selective channel and the carrier frequency offset.

To my family and life

ACKNOWLEDGMENTS

I am greatly indebted to my advisor, Professor Erchin Serpedin, who provided the continual and thoughtful inspiration and guidance, enthusiastic encouragement, as well as tremendous technical support throughout my years at Texas A&M University. He has made invaluable effort and impact on the accomplishment of this work. My gratitude for this dissertation also goes to Dr. Philippe Ciblat of ENST, France, for our pleasurable and successful cooperation.

I would like to express my deep appreciation to Professor Costas N. Georghiadis, Professor Andrew K. Chan and Professor Du Li for serving as members of my dissertation committee and for their valuable comments and time.

I am also thankful to Professors Krishna R. Narayanan, Professor Don R. Halverson, and Professor X. Wang of Columbia University for their instruction and teaching, inside and outside of the classroom.

Finally, it is my pleasure to acknowledge my colleagues in the Wireless Communications Lab of Texas A&M University, in particular, Dr. Zigang Yang, Dr. Zhongmin Liu, Dr. Yu Zhang, Dr. Ben Lu, Dr. Jing Li, Yongzhe Xie, Wenyan He, Kai Shi, Hui Liu, and Jun Zheng. I have benefited from numerous technical discussions with them.

TABLE OF CONTENTS

CHAPTER		Page
I	INTRODUCTION	1
	A. Background of Digital Synchronization	1
	B. Classifications of Digital Synchronization	2
	C. An Overview of the Dissertation	5
	D. Abbreviations and Notations	7
II	OPTIMAL BLIND CARRIER SYNCHRONIZATION FOR PSK/QAM TRANSMISSIONS	10
	A. Optimal Blind Carrier Recovery for M-PSK Burst Trans- missions	10
	1. Introduction	10
	2. Problem Formulation	11
	3. Nonlinear Carrier Synchronizer	12
	4. Monomial Nonlinearity Estimators	17
	5. Extension to Flat Ricean-fading Channels	20
	6. HAF-based Estimator	23
	7. Simulation Experiments	24
	8. Conclusions	30
	B. Optimal Blind Carrier Recovery for General QAM Mod- ulations	30
	1. Introduction	30
	2. Estimators for Square QAM Constellations	33
	3. Extension to Cross QAM Constellations	38
	4. Implementation of the Optimal Estimator	39
	5. Simulation Experiments	41
	6. Conclusions and Discussions	44
III	BLIND NLS FREQUENCY OFFSET ESTIMATORS FOR FADING CHANNELS	47
	A. Blind Feedforward NLS Carrier Frequency Offset Esti- mators for QAM Constellations in ISI Channels	48
	1. Introduction	48
	2. Modeling Assumptions	49

CHAPTER	Page
3. Carrier Frequency Offset Estimators	51
4. Asymptotic Performance Analysis	54
5. Simulations	57
6. Conclusions	62
B. On a Blind Fractionally-sampling Based Carrier Frequency Offset Estimator for Non-circular Transmissions . .	62
1. Introduction	62
2. Proposed Estimator	63
3. Influence of the Oversampling Factor	66
4. Simulations	67
5. Conclusions	70
 IV	
BLIND FEEDFORWARD CYCLOSTATIONARITY-BASED TIMING ESTIMATION FOR LINEAR MODULATIONS	71
A. Performance Analysis of Blind Frequency Offset and Symbol Timing Estimators GG and GSD	73
1. Introduction	73
2. Modeling Assumptions	73
3. Frequency Offset and Symbol Timing Estimators for Time-invariant Channels	74
4. Performance Analysis for Time-invariant Channels . .	79
5. Extension to Time-selective Channels	83
6. Simulation Experiments	85
7. Conclusions	90
B. Blind Feedforward Symbol Timing Estimators: Further Results	91
1. System Model and Assumptions	91
2. Second-Order CS Statistics-based Timing Estimators .	92
3. Joint Second and Fourth-Order CS-based Timing Estimator	102
4. Simulation Experiments	108
5. Conclusions	109
C. An Alternative Blind Feedforward Symbol Timing Estimator Using Two Samples per Symbol	111
1. Introduction	111
2. A New Blind Feedforward CS-based Symbol Timing Estimator	112
3. Performance Analysis for Estimators	114

CHAPTER	Page
4. Simulation Experiments	115
5. Conclusions	117
V CONTINUOUS-MODE FRAME SYNCHRONIZATION FOR FREQUENCY-SELECTIVE CHANNELS	118
A. Introduction	118
B. System Model	120
C. Joint Frame Synchronization and Channel Acquisition . . .	123
D. Synchronization in the Presence of Frequency offset	126
E. Simulation Results	129
F. Conclusion	132
VI SUMMARY	133
REFERENCES	134
APPENDIX A	149
APPENDIX B	150
APPENDIX C	154
APPENDIX D	160
APPENDIX E	164
APPENDIX F	168
VITA	173

LIST OF TABLES

TABLE	Page
I (a) OPT-estimate of $\hat{\alpha}_1$ versus SNR and (b) OPT-estimate of $\hat{\alpha}_1$ versus ϵ	106

LIST OF FIGURES

FIGURE		Page
1	Block diagram of a coherent communication system	3
2	Frame structure	5
3	Feedback and feedforward topologies	5
4	Theoretical degradation of $\hat{\omega}_l^{(k)}$ w.r.t. the optimal estimator	25
5	Performance loss w.r.t. the UCRB versus SNR	25
6	a) MSEs of $\hat{\theta}$, b) MSEs of $\widehat{F_e T}$, c) MSEs of $\widehat{\eta T^2}$	26
7	a) MSEs of $\hat{\theta}$, b) MSEs of $\widehat{F_e T}$, c) MSEs of $\widehat{\eta T^2}$	27
8	MSEs of \hat{f}_e in the presence of a flat Ricean-fading channel	28
9	MSEs of \hat{f}_e in the presence of timing error	28
10	MSEs of \hat{f}_e	29
11	16-QAM constellation	32
12	Theoretical bounds of $\hat{\theta}$ versus SNR	39
13	a) F_{\min} versus ρ (16-QAM constellation at SNR= 20dB) b) F_{\min} versus ρ (16-QAM constellation at varying SNRs)	41
14	Comparison of MSEs of $\hat{\theta}$ (16-QAM constellation)	42
15	Comparison of MSEs of \hat{f}_e (16-QAM constellation)	42
16	Comparison of MSEs of $\hat{\theta}$ (32-QAM constellation)	43
17	SER curves versus SNR (16-QAM and 32-QAM)	44
18	SER curves versus SNR (64-QAM and 256-QAM)	45

FIGURE	Page
19	MSE and SER versus SNR (128-QAM constellation) 45
20	Star 16QAM constellation 46
21	MSEs of $\widehat{F_e T}$ versus SNR 59
22	Amplitudes of harmonics 59
23	MSEs of $\widehat{F_e T}$ versus ϵ 60
24	MSEs of $\widehat{F_e T}$ versus L 60
25	MSEs of $\widehat{F_e T}$ versus oversampling factor P 61
26	MSEs of $\widehat{F_e T}$ versus SNR in frequency-selective channels 61
27	Lower bound for N_s 68
28	MSE versus N_s 68
29	MSE versus SNR 69
30	MSE versus ρ 69
31	MSE of $\widehat{F_e T}$ and $\widehat{\epsilon}$ vs. P for BPSK and time-invariant channel 86
32	MSE of $\widehat{F_e T}$ and $\widehat{\epsilon}$ vs. ρ for BPSK and time-invariant channel 87
33	MSE of $\widehat{F_e T}$ and $\widehat{\epsilon}$ vs. L for BPSK and time-invariant channel 88
34	MSE of $\widehat{F_e T}$ and $\widehat{\epsilon}$ vs. SNR for BPSK and time-invariant channel . . . 88
35	MSE of $\widehat{F_e T}$ and $\widehat{\epsilon}$ vs. P for QPSK and time-selective channel 89
36	MSE of $\widehat{F_e T}$ and $\widehat{\epsilon}$ vs. ρ for QPSK and time-selective channel 90
37	Common structure of blind feedforward timing estimators 92
38	Theoretical performance of SLN-estimate $\widehat{\epsilon}$ for different values of τ_m with (a) $\rho = 0.2$ and (b) $\rho = 0.9$ 98
39	Cost function of SLN estimator ($\rho = 0.9$, SNR=20dB) 100

FIGURE	Page
40	Comparison of asymptotic variances versus SNR with (a) $\rho = 0.1$ and (b) $\rho = 0.9$ 109
41	Improvement of OPT over SLN versus ρ (SNR= 20dB) 110
42	Comparison of MSEs with (a) $\rho = 0.1$ and (b) $\rho = 0.9$ 111
43	Asymptotic bias of $\hat{\epsilon}_{Lee}$ 115
44	MSEs versus SNR ($\rho = 0.1$) 115
45	MSEs versus SNR ($\rho = 0.35$) 116
46	MSEs versus SNR ($\rho = 0.5$) 116
47	Frame synchronization model 122
48	FAP vs. SNR with fixed N 129
49	MSCEE vs. SNR with fixed N 129
50	FAP vs. SNR with varying N 130
51	MSCEE vs. SNR with varying N 130
52	Improvement of FAP with multiple-frame synchronization 131
53	Improvement of MSCEE with multiple-frame synchronization 131
54	FAP in the presence of f_e 132
55	MSCEE in the presence of f_e 132
56	$MSE(\hat{f}_e)$ in the presence of f_e 132

CHAPTER I

INTRODUCTION

When Charles V retired in weariness from the greatest throne in the world to the solitude of this monastery at Yuste, he occupied his leisure for some weeks in trying to regulate two clocks. It proved very difficult. One day, it is recorded, he turned to his assistant and said: "To think that I attempted to force the reason and conscience of thousands of men into one mold, and I cannot make two clocks agree!"

(Ellis: *The Tasks of Social Hygiene*)

A. Background of Digital Synchronization

Clock regulation turned out an extremely difficult task for Charles V, even though he was such a mighty emperor that governed the people throughout half of Europe and most of America in sixteenth century. Five hundred years passed, and now the art of "making two clocks agree" has become the foundation of synchronous digital communications [94], and also, the coverage of synchronization has been extended tremendously.

Synchronization is a critical task in communications and its failure may have catastrophic effects on the system performance [63]. In any physical communication systems, the information data sequences are first modulated to time-continuous uniformly spaced waveforms at the transmitter and then transmitted through certain channels. As a consequence, in addition to the data, the received signal at the receiver depends on a group of unknown variables referred to as reference parameters, among which some are related to the implementation of the transmitter and the receiver,

The journal model is *IEEE Transactions on Automatic Control*.

and other are generated during propagation over the channel. The ultimate task of the receiver is to retrieve the data by means of decision devices and can be properly performed only after these reference parameters are estimated accurately. Therefore, synchronization is such a vital function for this measure of reference parameters [63], [64].

During the last several decades, digital realizations of receivers are of growing interest due to the increasing need of data transmission and the enormous progress in semiconductor and integrated circuits technology, which allows to implement complex algorithms into small size and low cost components in a more reliable and economical way to achieve bit rates close to the information theoretical limits [63], [64], [83]. As a result, the digital implementation of synchronization implies that the reference parameters mentioned above should be recovered entirely by means of digital signal processing based only on signal samples generated at a suitable rate. Generally, synchronization circuits possess such a large portion of the receiver hardware that their implementation has a substantial impact on the overall costs [63]. Therefore, there is always a great demand for developing innovative and efficient synchronization structures for digital communications.

B. Classifications of Digital Synchronization

In digital communication systems, a hierarchy of synchronization problems has to be considered. When passband communications and coherent demodulation are involved, there is the problem of carrier synchronization which concerns the generation of a local reference carrier with the phase and frequency closely matched to that of the incoming carrier [35]. In some specific applications, other phase parameters, such as Doppler rate, have also to be considered. Another problem is the synchronization of symbol

timing, which is the process of synchronizing the receiver clock with the baseband data sequence to obtain the optimum sampling times located at the “peaks” of the signal pulse corresponding to the maximum eye opening. Clearly, the locations of the pulse peaks must be accurately determined for reliable detection [63].

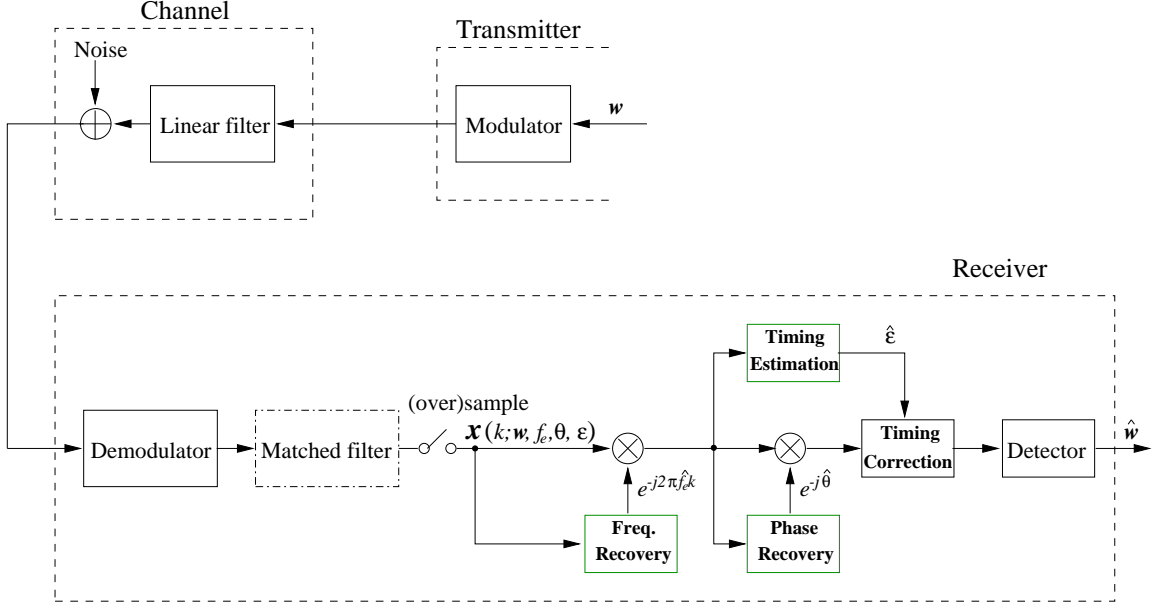


Fig. 1. Block diagram of a coherent communication system

The phase, frequency offset and symbol timing are the main parameters to be concerned in this research work. The block diagram of Fig. 1 illustrates sketchily the structure of digital communication systems and the synchronization process discussed above. In Fig. 1, the digital information data sequence $\{w\}$ is modulated and transmitted through physical channels, which in reality have different characteristics corresponding to different applications, and generally can be mathematically modeled as a linear filter with additive noise. At the end of the receiver, it is common to first translate the received signal in frequency down to baseband (demodulation), matched filter and sample (or oversample) the corresponding low-frequency waveform,

and then operate on the resulting discrete-time samples [63].

Once symbol timing recovery is achieved, frame synchronization may be encountered further down the hierarchy [35], which is indispensable in systems for which the unit of information is not a symbol, but rather a frame of symbols, hence, the boundaries of frames have to be identified [37]. It is obvious that the prerequisite for frame synchronization is that the symbol timing synchronization must be achieved. However, it does not need carrier recovery to be done. Actually, in many cases, carrier estimation is performed after frame synchronization. A feature that distinguishes the frame synchronization from those of carrier and symbol timing recoveries is that it is usually solved by repetitive insertion of bits or words (training symbols) with known special patterns into the data sequence solely for synchronization purpose [35]. Fig. 2 depicts such structure, where the bit stream is composed of sync words (shown shaded) and useful information data. Using these known symbols, the frame synchronization is performed, and in many cases, the unknown channel parameters are also estimated in the shaded bit stream segments [64]. This data-aided (DA) approach has the advantage of separating the task of the estimation of reference parameters from the data detection, and makes the complexity of receiver design reduced drastically. On the other hand, the overall efficiency of the channel is sacrificed. In addition, burst mode transmission of digital data is currently used in many applications such as satellite time-division multiple access (TDMA) systems and terrestrial mobile cellular radio, which tends to favor non-data aided (NDA or blind) synchronization techniques since the preambles represent wasted capacity that should be kept low or eliminated altogether [44], [71]. Therefore, it is desirable that the carrier and symbol timing synchronizations are established without using any training sequence, but only based on the same signal for symbol detection.

From the operating principle point of view, two categories of synchronizers are

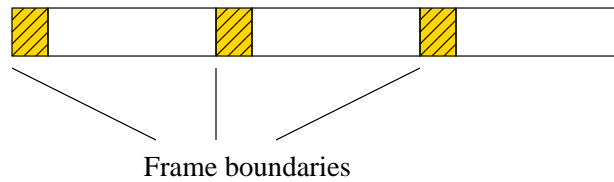


Fig. 2. Frame structure

distinguished, i.e., feedback (or closed-loop) synchronizers and feedforward (or open-loop) synchronizers [64], whose features are shown in Fig. 3(a) and (b), respectively. Although the feedback schemes have good tracking performance, they have rather high implementation complexity and may exhibit comparatively long acquisitions due to hangup phenomena, which is not desirable in short burst [63], [71]. Therefore, in this dissertation, we only concentrate on blind feedforward synchronization structures of carrier and symbol timing recovery. On the other hand, when dealing with the problem of frame synchronization, the DA method will be exploited.



Fig. 3. Feedback and feedforward topologies

C. An Overview of the Dissertation

Over the last two decades, extensive research work has been carried out to design nondata-aided timing recovery and carrier synchronization algorithms. These blind methods have found applications in many areas such as digital HDTV systems and digital cable modems, equalization of wireless GSM systems, design of bandwidth

efficient wireless ATM networks, feedforward synchronization schemes for magnetic-recording channels, and so on. Despite their importance and spread use, most of the existing blind synchronization algorithms are derived in an *ad-hoc* manner without exploiting optimally the entire available statistical information. In essence, these algorithms are derived based on a truncated Taylor series approximation of the stochastic (unconditional) maximum likelihood (ML) function that is further simplified to a form that enables estimation of the unknown synchronization parameters directly from certain second or fourth-order moments of the received data [2], [44], [61], [64]. Moreover, in most cases their performance is only evaluated by computer simulations, and rigorous and complete performance analysis has not been reported yet. It turns out that a theoretical oriented approach is indispensable for studying the performance of algorithms and ascertain their relative merits.

The main goal of this dissertation is to develop several novel signal processing frameworks that enable one to analyze and improve the performance of the existing timing recovery and carrier synchronization algorithms. As byproducts of this analysis, unified methods for designing new computationally and statistically efficient (i.e., minimum variance estimators) blind feedforward synchronizers are proposed. Specifically, we seek to derive non-data aided synchronization algorithms that exploit optimally the entire statistical information and take advantage of the structured information available: knowledge of the pulse-shape filter, input modulation, and the cyclostationary statistics induced by oversampling of the received waveform.

This work consists of three tightly coupled research directions. First, in Chapters II and III, a general and unified framework is proposed to develop optimal carrier recovery schemes for burst transmissions. The proposed blind feedforward NLS joint estimation set-up can be interpreted as a generalized form of the Maximum Likelihood algorithm and represent an extension of the classic blind carrier phase estimator

proposed by Andrew Viterbi and Audrey Viterbi [102] for synchronization of fully modulated M-PSK modulations. This carrier phase estimator is referred in the literature as the Viterbi and Viterbi (V&V) algorithm [63, p. 280], [64, p. 316]. A family of blind constellation-dependent optimal “matched” NLS carrier estimators is proposed for synchronization of burst transmissions fully modulated by PSK and QAM constellations in additive white Gaussian noise channels. Second, a cyclostationary statistics based framework is proposed in Chapter IV for designing computationally and statistically efficient robust blind symbol timing recovery for time-selective flat-fading channels. Lastly, dealing with the problem of frame synchronization, Chapter V proposes a simple and efficient data-aided approach for jointly estimating the frame boundary, the frequency-selective channel and the carrier frequency offset.

The design of new and more efficient signal processing algorithms with improved performance for synchronization is a lasting and challenging task. We believe that this dissertation brings significant new advances and considerable in-depth insights, and fill in a large number of gaps in the analysis of digital synchronizers.

D. Abbreviations and Notations

The following abbreviations are used in this dissertation:

AWGN	Additive White Gaussian Noise
BPSK	Binary Phase Shift Keying
CRB	Cramèr-Rao Bound
CS	Cyclostationary
DA	Data Aided
FAP	False Acquisition Probabilities
FFT	Fast Fourier Transform

FT	Fourier Transform
GG	Gini-Giannakis estimator [44]
GSD	Ghogho-Swami-Durrani estimator [41]
i.i.d.	independently and identically distributed
ISI	Inter-Symbol-Interference
LHS	Left Hand Side
ML	Maximum Likelihood
MSCEE	Mean Square Channel Estimation Error
MSE	Mean Square Error
NLS	Nonlinear Least Squares
NDA	Non-Data Aided
O&M	Oerder and Meyr estimator [75]
OPT	optimal estimator
pdf	probability density function
PSK	Phase Shift Keying
QAM	Quadrature Amplitude Modulation
QPSK	Quadrature Phase Shift Keying
RHS	Right Hand Side
RV	Random Variable
SER	Symbol Error Rate
SNR	Signal-to-Noise Ratio
V&V	Viterbi and Viterbi estimator [102]
w.r.t.	with respect to
WSS	Wide Sense Stationary

Notations used throughout this dissertation are standard. Vectors and matrices

are denoted in boldface by lowercase and capitals or calligraphic capitals, respectively.

Other symbols used are

$*$	vector or matrix complex conjugate (superscript)
T	vector or matrix transpose (superscript)
H	vector or matrix complex conjugate transpose (superscript)
c	a continuous-time signal (subscript)
$:=$	is defined as
$\operatorname{re}\{\cdot\}$	real part of a complex scalar, vector, or matrix
$\operatorname{im}\{\cdot\}$	imaginary part of a complex scalar, vector, or matrix
$\mathsf{E}\{\cdot\}$	statistical expectation
$ \cdot $	modulus of a scalar, or determinant of a matrix
$\ \cdot\ $	2-norm of a vector
\mathbf{I}_m	the $m \times m$ identity matrix
$\mathbf{\Gamma}_{k,l}$	(k, l) th-entry of matrix $\mathbf{\Gamma}$
$\delta_d(\cdot)$	Dirac delta function
$\delta(\cdot)$	Kronecker delta function
$*$	linear convolution
\otimes	circular convolution
$\hat{\cdot}$	the estimate of the unknown parameter

CHAPTER II

OPTIMAL BLIND CARRIER SYNCHRONIZATION FOR PSK/QAM TRANSMISSIONS

A. Optimal Blind Carrier Recovery for M-PSK Burst Transmissions

1. Introduction

Burst transmission of digital data and voice is employed in time division-multiple access (TDMA) and packet demand-assignment multiple-access (DAMA) satellite communication and terrestrial mobile cellular radio systems. Conventionally, carrier synchronization of burst transmissions requires a large number of overhead symbols, which results in reduced spectral efficiency and increased transmission delays [17].

Non-data aided or blind feedforward carrier synchronization of burst M-PSK transmissions has received much attention in the literature. A generalized form of the Maximum Likelihood feedforward algorithm was originally proposed by A. J. Viterbi and A. M. Viterbi as a blind carrier phase estimator with improved performance at low and intermediate SNRs [77], [102]. This carrier phase estimator is referred to as the Viterbi and Viterbi (V&V) algorithm [23], [51], [63, p. 280], and has been used to design blind frequency offset estimators for burst M-PSK modulations transmitted through AWGN channels [3], [4], [6], [7], [24]. Extensions of the V&V carrier estimator for flat Rayleigh and Ricean fading channels were reported in [93] and [33]. The V&V estimator exhibits several desirable features: its good performance at low SNRs translates into improved bit error probability (BEP) performance in fading channels that tend to be dominated by times when the signal experiences a deep fade (low SNR), and its open loop operation enables fast reliable acquisitions after deep fades [93]. Reference [23] introduces a different class of blind carrier frequency estimators

that assume fractionally sampling of the received signal. However, the statistical properties of the resulting estimators are partially analyzed based on certain approximations [23]. A quite general blind NLS estimator for the carrier phase, frequency offset and Doppler rate was proposed in [59]. However, the performance of the NLS-type estimator was not analyzed and exploited to develop carrier recovery algorithms with improved performance [59].

In this section, a family of blind feedforward joint carrier phase, frequency offset and Doppler rate NLS estimators for carriers that are fully modulated by M-PSK modulations is proposed based on the V&V algorithm. The corresponding thorough and rigorous analysis of their statistical properties is presented for the cases of AWGN and flat Ricean-fading channels to develop the optimal or “matched” nonlinear estimator that achieves the smallest asymptotic (large sample) variance within the family of blind NLS estimators. Monomial nonlinear estimators that do not require knowledge of the SNR are also developed and shown to perform similarly as the matched nonlinear estimator [110].

As we shall see, in the case of AWGN channels, the proposed family of blind NLS estimators presents high convergence rates, provides accurate estimates for phase, frequency offset and Doppler rate, and admits low complexity digital implementations, without being necessary to oversample (or fractionally-sample) the received signal faster than the Nyquist rate [23]. The performance of these algorithms coincides with the CRB of an unmodulated carrier at medium and high SNRs, and is robust to Ricean fading effects and timing errors.

2. Problem Formulation

Consider the baseband representation of an M-PSK modulated signal transmitted through an AWGN channel. Assume that filtering is evenly split between transmitter

and receiver so that the overall channel satisfies the first Nyquist condition. Filtering the received waveform through a matched filter and sampling at the right time instants yields:

$$\begin{aligned} x(n) &= w(n)e^{j\phi(n)} + v(n), \quad n = 0, \dots, N-1, \\ \phi(n) &= \theta + 2\pi F_e T n + \eta T^2 n^2, \end{aligned} \quad (2.1)$$

where $\{w(n)\}$ is the sequence of zero-mean unit variance ($\sigma_w^2 := E\{|w(n)|^2\} = 1$) i.i.d. M-PSK symbols, θ , F_e and η stand for carrier phase, frequency offset and Doppler rate, respectively, T denotes the symbol period, and $\{v(n)\}$ is a zero-mean circular white Gaussian noise process independent of $w(n)$ and with variance $\sigma_v^2 := E\{|v(n)|^2\}$. The Signal-to-Noise Ratio is defined as $\text{SNR} := 10 \log_{10}(\sigma_w^2/\sigma_v^2)$.

As depicted by (2.1), the problem that we pose is to estimate the unknown phase parameters (θ , F_e and η) of a random amplitude chirp signal $\exp(j\phi(n))$ embedded in unknown additive noise, assuming knowledge of the received samples $\{x(n)\}_{n=0}^{N-1}$. The solution that we pursue consists of evaluating first certain moments of the output that will remove the unwanted multiplicative effects introduced by the M-PSK modulated sequence $w(n)$. It turns out that the resulting problem reduces to the standard problem of estimating the phase parameters of a constant amplitude chirp signal embedded in additive noise, for which standard NLS-type estimators can be developed and their statistical properties analyzed in a rigorous manner.

3. Nonlinear Carrier Synchronizer

Consider the polar representation of $x(n)$:

$$x(n) = \rho(n)e^{j\varphi(n)}, \quad (2.2)$$

and define the process $y(n)$ via the nonlinear transformation:

$$y(n) := F(\rho(n))e^{jM\varphi(n)}, \quad (2.3)$$

where $F(\cdot)$ is a real-valued nonlinear function.

Conditioned on the M-PSK symbol $w(n)$, $x(n)$ is normally distributed with the pdf $f(x(n)|w(n) = \exp(j2\pi m/M), 0 \leq m \leq M-1) \sim \mathcal{N}(w(n)\exp(j\phi(n)), \sigma_v^2)$.

Due to (2.2), it follows that:

$$f(\rho(n), \varphi(n)|w(n) = e^{j\frac{2\pi m}{M}}) = \frac{\rho(n)}{\pi\sigma_v^2} e^{-(\rho^2(n)+1)/\sigma_v^2} e^{2\rho(n)\cos[\varphi(n)-2\pi m/M-\phi(n)]/\sigma_v^2}. \quad (2.4)$$

Based on (2.4), the joint pdf of $\rho(n)$ and $\varphi(n)$, and the marginal pdf of $\rho(n)$ take the expressions:

$$\begin{aligned} f(\rho(n), \varphi(n)) &= \frac{1}{M} \sum_{m=0}^{M-1} f(\rho(n), \varphi(n)|w(n) = \exp(j\frac{2\pi m}{M})) \\ &= \frac{1}{M} \sum_{m=0}^{M-1} \frac{\rho(n)}{\pi\sigma_v^2} e^{-\frac{\rho^2(n)+1}{\sigma_v^2}} e^{\frac{2\rho(n)}{\sigma_v^2} \cos[\varphi(n)-\frac{2\pi m}{M}-\phi(n)]}, \end{aligned} \quad (2.5)$$

$$f(\rho(n)) = \int_{-\pi}^{\pi} f(\rho(n), \varphi(n)) d\varphi(n) = \frac{2\rho(n)}{\sigma_v^2} e^{-(\rho^2(n)+1)/\sigma_v^2} I_0\left(\frac{2\rho(n)}{\sigma_v^2}\right), \quad (2.6)$$

where $I_0(\cdot)$ stands for the zero-order modified Bessel function of the first kind [1, eq. (9.6.16)]. Moreover, it is not difficult to find that the joint pdf of the RVs $\rho(n_1), \varphi(n_1), \rho(n_2), \varphi(n_2)$ satisfies the following relation for $n_1 \neq n_2$:

$$f(\rho(n_1), \varphi(n_1), \rho(n_2), \varphi(n_2)) = f(\rho(n_1), \varphi(n_1)) \cdot f(\rho(n_2), \varphi(n_2)). \quad (2.7)$$

Exploiting (2.5) and (2.6), some calculations, whose details are provided in the Appendix A, lead to the following relations:

$$\mathbb{E}\{y(n)\} = \mathbb{E}\{F(\rho(n))e^{jM\varphi(n)}\} = \mathcal{C}e^{jM\phi(n)}, \quad (2.8)$$

$$\mathcal{C} := |\mathbb{E}\{y(n)\}| = \mathbb{E}\left\{F(\rho(n))\frac{I_M\left(\frac{2\rho(n)}{\sigma_v^2}\right)}{I_0\left(\frac{2\rho(n)}{\sigma_v^2}\right)}\right\}, \quad (2.9)$$

where $I_M(\cdot)$ denotes the M th-order modified Bessel function of the first kind [1, eq. (9.6.19)], the expectation in (2.9) is w.r.t. the marginal distribution of $\rho(n)$ (2.6) and the resulting amplitude \mathcal{C} is a real-valued constant which does not depend on n . Since $w(n)$ and $v(n)$ are i.i.d. and mutually independent, from (2.7), it follows that $u(n) := y(n) - \mathbb{E}\{y(n)\}$ is wide sense stationary (WSS) i.i.d., too. Consequently,

$$y(n) = \mathcal{C}e^{jM\phi(n)} + u(n), \quad n = 0, 1, \dots, N-1, \quad (2.10)$$

and $y(n)$ can be viewed as a constant amplitude chirp signal $\exp(jM\phi(n))$ embedded in additive WSS white noise. Note that, in general, the WSS white noise process $u(n)$ is neither Gaussian distributed nor circular [81].

Let $\boldsymbol{\omega} := [\mathcal{C} \ \omega_0 \ \omega_1 \ \omega_2]^T = [\mathcal{C} \ M\theta \ 2\pi MF_e T \ M\eta T^2]^T$, and introduce the following NLS estimator (c.f. [40], [59]):

$$\hat{\boldsymbol{\omega}} = \arg \min_{\bar{\boldsymbol{\omega}}} J(\bar{\boldsymbol{\omega}}), \quad (2.11)$$

$$J(\bar{\boldsymbol{\omega}}) = \frac{1}{2} \sum_{n=0}^{N-1} \left| y(n) - \bar{\mathcal{C}} e^{j \sum_{l=0}^2 \bar{\omega}_l n^l} \right|^2. \quad (2.12)$$

By equating to zero the gradient of $J(\bar{\boldsymbol{\omega}})$, some simple algebra calculations lead to the following expressions for the NLS estimates of ω_l , $l = 0, 1, 2$, [40] [110]:

$$\begin{aligned} (\hat{\omega}_1, \hat{\omega}_2) &= \arg \max_{\bar{\omega}_1, \bar{\omega}_2} \frac{1}{N} \left| \sum_{n=0}^{N-1} y(n) e^{-j \sum_{l=1}^2 \bar{\omega}_l n^l} \right|^2, \\ \hat{\omega}_0 &= \text{angle} \left\{ \sum_{n=0}^{N-1} y(n) e^{-j \sum_{l=1}^2 \hat{\omega}_l n^l} \right\}. \end{aligned} \quad (2.13)$$

It is well-known that estimator (2.11) is asymptotically unbiased and consistent, and also almost asymptotically efficient at high SNR [8], [39] and [40].

Following a procedure similar to the one presented in [40], one can derive the asymptotic variances of estimates $\hat{\omega}_l$, $l = 0, 1, 2$. These calculations are established in the Appendix B and are summarized in the following theorem [110]:

Theorem 1 *The asymptotic variances of the NLS estimates $\hat{\omega}_l$, $l = 0, 1, 2$, in (2.11)-(2.13) are given by [110]:*

$$\text{avar}(\hat{\omega}_l) = \frac{\mathcal{B} - \mathcal{D}}{\mathcal{C}^2} \cdot \frac{1}{2N^{2l+1}} \cdot \frac{1}{2l+1} \cdot \left[\frac{(l+3)!}{(l!)^2(2-l)!} \right]^2, \quad (2.14)$$

$$\mathcal{B} := \mathbb{E}\{|y(n)|^2\} = \mathbb{E}\{F^2(\rho(n))\}, \quad (2.15)$$

$$\mathcal{D} := |\mathbb{E}\{y^2(n)\}| = |\mathbb{E}\{F^2(\rho(n))e^{j2M\varphi(n)}\}| = \mathbb{E}\left\{ F^2(\rho(n)) \frac{I_{2M}\left(\frac{2\rho(n)}{\sigma_v^2}\right)}{I_0\left(\frac{2\rho(n)}{\sigma_v^2}\right)} \right\}, \quad (2.16)$$

and \mathcal{C} is defined in (2.9).

Some remarks are now in order:

Remark 1 From (2.14)–(2.16), one can observe that the asymptotic variances of $\hat{\omega}_l$, $l = 0, 1, 2$, are independent of the unknown phase parameters θ , F_e and η .

Remark 2 It is of interest to compare the asymptotic variances (2.14) with the CRB. In [34] and [39], the CRB is derived for the case when the random amplitude $w(n)$ of model (2.1) is a stationary Gaussian process. In [40], the CRB is obtained by assuming that the additive noise $u(n)$ of model (2.10) is colored Gaussian and circularly symmetric. Note that in our case, both models (2.1) and (2.10) do not satisfy these assumptions. Therefore, here we adopt the CRB for an unmodulated carrier wave (UCRB), i.e., $M = 1$ (c.f. [102]), which is a special case of the CRB presented in [34], [39] and [40]:

$$\text{UCRB}(\hat{\omega}_l) = \frac{\sigma_v^2}{2N^{2l+1}} \cdot \frac{1}{2l+1} \cdot \left[\frac{(l+3)!}{(l!)^2(2-l)!} \right]^2. \quad (2.17)$$

Based on (2.14), one can observe that the asymptotic variances $\text{avar}(\hat{\omega}_l)$ of the NLS estimates $\hat{\omega}_l$, $l = 0, 1, 2$, decay at the same rate as the UCRB, i.e., $\mathcal{O}(1/N^{2l+1})$.

Remark 3 Estimator (2.13) involves a two dimensional (2-D) maximization problem which could be too intensive if a good initial estimate can not be provided. In our

work, the initial values of F_e and η are obtained by the so-called high-order ambiguity function (HAF) approach, which has become a “standard” tool for analyzing constant amplitude chirp signals since it provides a computationally efficient yet statistically accurate estimator [8]. We will briefly introduce the HAF-based estimator in Subsection 6.

Remark 4 The estimates of phase parameters θ , F_e and η present M -fold ambiguity, which can be counteracted by applying differential encoding [59] or unique word decoding method [93]. The estimation range due to the ambiguity, e.g., for F_e , is $|F_e| < 1/(2MT)$.

Next, we determine the optimal or “matched” nonlinearity $F(\cdot)$ which minimizes the asymptotic variance $\text{avar}(\hat{\omega}_l)$. Since in (2.14), only the terms \mathcal{B} , \mathcal{C} , \mathcal{D} depend on $F(\cdot)$, finding an optimal $F(\cdot)$ resorts to solving the optimization problem:

$$F_{\min}(\rho(n)) = \arg \min_{F(\cdot)} \frac{\mathcal{B} - \mathcal{D}}{\mathcal{C}^2}.$$

Using (2.9), (2.15) and (2.16), we obtain:

$$\frac{\mathcal{B} - \mathcal{D}}{\mathcal{C}^2} = \frac{\mathbb{E}\left\{F^2(\rho(n))\left(1 - \frac{I_{2M}\left(\frac{2\rho(n)}{\sigma_v^2}\right)}{I_0\left(\frac{2\rho(n)}{\sigma_v^2}\right)}\right)\right\}}{\mathbb{E}\left\{F(\rho(n))\frac{I_M\left(\frac{2\rho(n)}{\sigma_v^2}\right)}{I_0\left(\frac{2\rho(n)}{\sigma_v^2}\right)}\right\}}.$$

Using Cauchy-Schwarz’ inequality, the optimum nonlinearity F_{\min} is given by the following theorem:

Theorem 2 *The optimal or “matched” nonlinearity $F_{\min}(\cdot)$ that minimizes the asymptotic variances of the proposed family of NLS estimators (2.11) is given by [110]:*

$$F_{\min}(\rho(n)) = \lambda \frac{I_M\left(\frac{2\rho(n)}{\sigma_v^2}\right)}{I_0\left(\frac{2\rho(n)}{\sigma_v^2}\right) - I_{2M}\left(\frac{2\rho(n)}{\sigma_v^2}\right)}, \quad (2.18)$$

where λ is an arbitrary nonzero constant.

Plugging (2.18) back into (2.9), (2.15), and (2.16), and substituting these values into (2.14), the minimal asymptotic variances of $\hat{\omega}_l$, $l = 0, 1, 2$, can be expressed as:

$$\text{avar}_{\min}(\hat{\omega}_l) = \frac{1}{2N^{2l+1}} \cdot \frac{1}{2l+1} \cdot \left[\frac{(l+3)!}{(l!)^2(2-l)!} \right]^2 \cdot \frac{1}{\mathbb{E} \left\{ \frac{I_M^2\left(\frac{2\rho(n)}{\sigma_v^2}\right)}{I_0^2\left(\frac{2\rho(n)}{\sigma_v^2}\right) - I_0\left(\frac{2\rho(n)}{\sigma_v^2}\right)I_{2M}\left(\frac{2\rho(n)}{\sigma_v^2}\right)} \right\}}. \quad (2.19)$$

4. Monomial Nonlinearity Estimators

As can be observed from (2.18), $F_{\min}(\rho(n))$ is a function that depends on the SNR. This is not a restrictive requirement since blind SNR estimators that exhibit good performance can be used [80]. However, if the SNR-estimation step is not desirable, we show next that there exist optimal monomial approximations $\rho^k(n)$, $k = 0, \dots, M$, of the matched nonlinearity $F_{\min}(\rho(n))$ that exhibit almost the same asymptotic variance as (2.19) and their implementation does not require knowledge of the SNR.

Exploiting the asymptotic formula [1, eq. (9.7.1)] in (2.18), it turns out that at high SNRs ($\text{SNR} \rightarrow \infty$) the optimal monomial is $G_h(\rho(n)) = \rho(n)$. Similarly, based on [1, eq. (9.6.7)], it turns out that at low SNRs ($\text{SNR} \rightarrow -\infty$), the optimal monomial is $G_l(\rho(n)) = \rho^M(n)$. These results parallel the derivations reported in [77] and do not depend on the value of the frequency shift or Doppler rate. In order to obtain a better understanding, next we establish the asymptotic performance of the monomial NLS estimators.

Define the class of processes $y_k(n)$ by means of the monomial transformations:

$$y_k(n) = \rho^k(n)e^{jM\varphi(n)}, \quad k = 0, 1, \dots, M, \quad (2.20)$$

and the zero-mean processes: $u_k(n) := y_k(n) - \mathbb{E}\{y_k(n)\}$, $k = 0, \dots, M$. As before, it turns out that $\mathbb{E}\{y_k(n)\}$ is a constant amplitude chirp signal, and hence $y_k(n) =$

$E\{y_k(n)\} + u_k(n)$ can be interpreted as a constant amplitude chirp signal embedded in white noise. As a special case of (2.11), we introduce the following class of monomial NLS estimators:

$$\hat{\omega}^{(k)} = \arg \min_{\bar{\omega}^{(k)}} \frac{1}{2} \sum_{n=0}^{N-1} \left| y_k(n) - \bar{C}^{(k)} e^{j \sum_{l=0}^2 \bar{\omega}_l^{(k)} n^l} \right|^2, \quad (2.21)$$

whose asymptotic variances for $\hat{\omega}_l^{(k)}$, $l = 0, 1, 2$, are provided by the following theorem:

Theorem 3 *The asymptotic variances of the NLS estimates $\hat{\omega}_l^{(k)}$, $l = 0, 1, 2$, in (2.21), are given by [110]:*

$$\begin{aligned} \text{avar}(\hat{\omega}_l^{(k)}) &= \frac{\mathcal{B}_k - \mathcal{D}_k}{\mathcal{C}_k^2} \cdot \frac{1}{2N^{2l+1}} \cdot \frac{1}{2l+1} \cdot \left[\frac{(l+3)!}{(l!)^2(2-l)!} \right]^2, \\ \mathcal{B}_k &:= E\{|y_k(n)|^2\} = E\{\rho^{2k}(n)\}, \\ \mathcal{C}_k &:= |E\{y_k(n)\}| = |E\{\rho^k(n)e^{jM\varphi(n)}\}|, \\ \mathcal{D}_k &:= |E\{y_k^2(n)\}| = |E\{\rho^{2k}(n)e^{j2M\varphi(n)}\}|. \end{aligned} \quad (2.22)$$

Exploiting (2.6) and [46, eq. (6.643.4)], the following relation was derived in [102, (A17)]:

$$\mathcal{B}_k = \sum_{q=0}^k \binom{k}{q}^2 \sigma_v^{2q} \cdot q!. \quad (2.23)$$

Using (2.5), we can obtain that:

$$\begin{aligned} E\{y_k(n)\} &= \int_0^\infty \int_{-\pi}^\pi \rho^k(n) e^{jM\varphi(n)} f(\rho(n), \varphi(n)) d\varphi(n) d\rho(n) \\ &= \frac{1}{M} \sum_{m=0}^{M-1} \int_0^\infty \frac{\rho^{k+1}(n)}{\pi \sigma_v^2} e^{-\frac{\rho^2(n)+1}{\sigma_v^2}} \int_{-\pi}^\pi e^{jM\varphi(n)} e^{\frac{2\rho(n)}{\sigma_v^2} \cos[\varphi(n) - \frac{2\pi m}{M} - \phi(n)]} d\varphi(n) d\rho(n) \\ &= \frac{1}{\alpha^k} e^{jM\phi(n)} e^{-\frac{\gamma}{2}} \int_0^\infty \zeta^{k+1} e^{-\frac{\zeta^2}{2}} I_M(\alpha\zeta) d\zeta, \end{aligned} \quad (2.24)$$

where: $\alpha := \sqrt{2}/\sigma_v$, $\gamma := \alpha^2$ and $\zeta := \alpha\rho(n)$. Based on [46, eq. (6.643,2)] and [1, eq. (13.1.32)], \mathcal{C}_k can be expressed in terms of the confluent hypergeometric function

$\Phi(\cdot, \cdot, \cdot)$ for $k = 0, 1, \dots, M$:

$$\mathcal{C}_k = \frac{\Gamma(\frac{k+M}{2} + 1)e^{-\frac{\gamma}{2}}}{\Gamma(M+1)\sigma_v^{M-k}} \Phi\left(\frac{k+M}{2} + 1, M+1, \frac{\gamma}{2}\right). \quad (2.25)$$

Similarly,

$$\mathcal{D}_k = \frac{\Gamma(k+M+1)e^{-\frac{\gamma}{2}}}{\Gamma(2M+1)\sigma_v^{2M-2k}} \Phi\left(k+M+1, 2M+1, \frac{\gamma}{2}\right). \quad (2.26)$$

It should be pointed out that when k is even (M is usually a power of two), following a similar approach to that presented in [102] or the formula [1, eq. (13.5.1)], one can obtain a slightly more compact expression for the confluent hypergeometric function in (2.25):

$$\begin{aligned} \mathcal{C}_k &= \frac{1}{\gamma^t} \left[\gamma^t \sum_{p=0}^{s+t} p! \binom{s+t}{p} \binom{s-t+p-1}{p} \left(\frac{-2}{\gamma}\right)^p + (-1)^{s+t+1} 2^t e^{-\frac{\gamma}{2}} \left(\frac{2}{\gamma}\right)^{t+1} \right. \\ &\quad \cdot \left. \sum_{p=0}^{s-t-1} \binom{s+t+p}{p} \frac{(s+t)!}{(s-t-p-1)!} \left(\frac{2}{\gamma}\right)^p \right], \text{ if } k = 0, 2, \dots, M-2, \\ \mathcal{C}_k &= 1, \text{ if } k = M, \end{aligned}$$

where $s := M/2$ and $t := k/2$. Similarly,

$$\begin{aligned} \mathcal{D}_k &= \frac{1}{\gamma^k} \left[\gamma^k \sum_{p=0}^{M+k} p! \binom{M+k}{p} \binom{M-k+p-1}{p} \left(\frac{-2}{\gamma}\right)^p + (-1)^{M+k+1} 2^k e^{-\frac{\gamma}{2}} \left(\frac{2}{\gamma}\right)^{k+1} \right. \\ &\quad \cdot \left. \sum_{p=0}^{M-k-1} \binom{M+k+p}{p} \frac{(M+k)!}{(M-k-p-1)!} \left(\frac{2}{\gamma}\right)^p \right], \text{ if } k = 0, 1, \dots, M-1, \quad (2.27) \\ \mathcal{D}_k &= 1, \text{ if } k = M. \end{aligned}$$

Plugging (2.23), (2.25) and (2.26) back into (2.22), closed-form expressions for the asymptotic variances $\text{avar}(\hat{\omega}_l^{(k)})$ for $k = 0, 1, \dots, M$, and $l = 0, 1, 2$, are obtained.

Note that at very high SNR ($1/\sigma_v^2 \rightarrow \infty$), using [1, eq. (13.1.4)], some calculations show that:

$$\lim_{\text{SNR} \rightarrow \infty} \mathcal{C}_k = 1, \quad (2.28)$$

for any $k = 0, 1, \dots, M$. Hence, based on (2.22), (2.23), (2.27) and (2.28), we obtain:

$$\text{avar}(\hat{\omega}_l^{(k)}) \propto \frac{M^2}{\text{SNR}} \cdot \frac{1}{N^{2l+1}},$$

which does not depend on the estimator order k , i.e., it turns out that at very high SNRs, the performance of estimators (2.21) for different nonlinearity orders k is asymptotically the same.

We close this subsection with the following remark.

Remark 5 Assume that $\eta = 0$, i.e., the received signal is affected only by phase offset and frequency offset. Then, the estimator (2.21) reduces to:

$$\begin{aligned} \hat{f}_e^{(k)} &= \frac{1}{M} \arg \max_{|\bar{f}_0| < 1/2} \frac{1}{N} \left| \sum_{n=0}^{N-1} y_k(n) e^{-j2\pi \bar{f}_0 n} \right|, \\ \hat{\theta}^{(k)} &= \frac{1}{M} \text{angle} \left\{ \sum_{n=0}^{N-1} y_k(n) e^{-j2\pi M \hat{f}_e^{(k)} n} \right\}, \end{aligned} \quad (2.29)$$

with $f_e := F_e T$. Based on the eq. (2.29), the frequency offset estimator can be implemented efficiently by means of the FFT algorithm applied on the sequence $y_k(n)$, which is generally zero-padded with a sufficiently large number of zeros to achieve the precision provided by the asymptotic (Cramer-Rao) bound ($O(1/N^3)$). The following corollary is obtained directly from Theorem 3:

Corollary 1 The asymptotic variance of the class of NLS estimators (2.29) for f_e is given by:

$$\text{avar}(\hat{f}_e^{(k)}) = \frac{6(\mathcal{B}_k - \mathcal{D}_k)}{4\pi^2 M^2 \mathcal{C}_k^2 N^3}, \quad (2.30)$$

where \mathcal{B}_k , \mathcal{C}_k and \mathcal{D}_k are defined in Theorem 3.

5. Extension to Flat Ricean-fading Channels

In the foregoing discussion, we assumed AWGN channels. In this subsection, we will see that the NLS estimators (2.11) remain asymptotically unbiased and consistent in

the presence of flat Ricean-fading channels. To simplify our derivation, we will only concentrate on the extension of the frequency offset estimators (2.29).

Assuming a flat Ricean-fading channel model, the input-output relationship of the channel can be expressed as:

$$x(n) = \mu(n)w(n)e^{j2\pi F_e T n} + v(n), \quad n = 0, \dots, N - 1, \quad (2.31)$$

where $\mu(n) = \rho_\mu(n) \exp(j\varphi_\mu(n))$ is the fading process with non-zero mean $E\{\mu(n)\} := \rho_1 \exp(j\varphi_1)$ and variance $\sigma_\mu^2 := E\{|\mu(n) - E\{\mu(n)\}|^2\}$. Using the Jakes model, the second-order correlations of the fading are given by $E\{[\mu(n) - E\{\mu(n)\}]^* \cdot [\mu(n + \tau) - E\{\mu(n + \tau)\}]\} = \sigma_\mu^2 J_0(2\pi f_d \tau)$, where $J_0(\cdot)$ denotes the zero-order Bessel function of the first kind, and f_d stands for the normalized Doppler spread. The joint pdf of $\rho_\mu(n)$ and $\varphi_\mu(n)$, and the marginal pdf of $\rho_\mu(n)$ are given by:

$$f(\rho_\mu(n), \varphi_\mu(n)) = \frac{\rho_\mu(n)}{\pi \sigma_\mu^2} e^{-\frac{\rho_\mu^2(n) + \rho_1^2 - 2\rho_\mu(n)\rho_1 \cos(\varphi_\mu(n) - \varphi_1)}{\sigma_\mu^2}}, \quad (2.32)$$

$$f(\rho_\mu(n)) = \frac{2\rho_\mu(n)}{\sigma_\mu^2} e^{-\frac{\rho_\mu^2(n) + \rho_1^2}{\sigma_\mu^2}} I_0\left(\frac{2\rho_\mu(n)\rho_1}{\sigma_\mu^2}\right). \quad (2.33)$$

Conditioned on the fading process $\mu(n)$ and the input symbol $w(n)$, the joint pdf of $\rho(n)$ and $\varphi(n)$ takes the form:

$$f(\rho(n), \varphi(n) | w(n)) = \exp\left(\frac{j2\pi l}{M}\right), \rho_\mu(n), \varphi_\mu(n) = \frac{\rho(n)}{\pi \sigma_v^2} e^{-(\rho^2(n) + \rho_\mu^2(n))/\sigma_v^2} \cdot e^{2\rho(n)\rho_\mu(n) \cos[\varphi(n) - \varphi_\mu(n) - 2\pi(l + M f_e n)/M]/\sigma_v^2}. \quad (2.34)$$

Using (2.31) through (2.34), in a similar way to that presented in the former subsections, some straightforward but lengthy calculations lead to:

$$E\{y_k(n)\} = C_k e^{jM\varphi_1} e^{j2\pi M f_e n}, \quad k = 0, 1, \dots, M,$$

$$\mathcal{C}_k := \frac{\Gamma(\frac{k+M}{2} + 1)e^{-\frac{\gamma_1}{2}}\rho_1^M}{\Gamma(M+1)\sigma_1^{M-k}}\Phi\left(\frac{k+M}{2} + 1, M+1, \frac{\gamma_1}{2}\right),$$

with $\sigma_1^2 := \sigma_\mu^2 + \sigma_v^2$ and $\gamma_1 := 2\rho_1^2/\sigma_1^2$. Hence, $y_k(n)$ can still be viewed as a constant amplitude harmonic embedded in additive noise $u_k(n) := y_k(n) - \mathbb{E}\{y_k(n)\}$, and the unbiasedness and consistency of estimators (2.29) hold true in the presence of flat Ricean-fading channels. However, we should note that due to the fading effect, $u_k(n)$ is not white any more, but a zero-mean colored process. Establishing the asymptotic variance of estimators (2.29) in flat Ricean-fading effects for any k is generally, if not impossible, at least very complicated for $k = 0, \dots, M-1$. In the special case $k = M$, $u_M(n)$ is a circular noise process, whose autocorrelation and spectral density are given by $r_{u_M}(\tau) := \mathbb{E}\{u_M^*(n)u_M(n+\tau)\}$ and $S_{u_M}(f) := \sum_\tau r_{u_M}(\tau)\exp(-j2\pi f\tau)$, respectively. Therefore, the asymptotic variance of (2.29) is now given by [98]:

$$\text{avar}(\hat{f}_e^{(M)}) = \frac{6S_{u_M}(Mf_e)}{4\pi^2 M^2 \mathcal{C}_M^2 N^3}. \quad (2.35)$$

The calculation of the power spectral density $S_{u_M}(\cdot)$ is tractable and is briefly detailed next. Define the following variables:

$$\begin{aligned} c_v^{(k)} &:= \mathbb{E}\{|v(n)|^{2k}\} = k! \cdot \sigma_v^{2k}, \\ c_\mu^{(k)} &:= \mathbb{E}\{|\mu(n) - \mathbb{E}\{\mu(n)\}|^{2k}\} = k! \cdot \sigma_\mu^{2k}, \\ r_\mu^{(k)} &:= \mathbb{E}\{|\mu(n)|^{2k}\} = \rho_1^{2k} + \sum_{l=1}^k \binom{k}{l}^2 \rho_1^{2k-2l} c_\mu^{(l)}. \end{aligned}$$

Some direct but lengthy calculations lead to the following expression:

$$S_{u_M}(Mf_e) = \sum_\tau \sum_{k=1}^M \binom{M}{k}^2 \rho_1^{2M-2k} c_\mu^{(k)} J_0^k(2\pi f_d \tau) + \sum_{k=1}^M \binom{M}{k}^2 c_v^{(k)} r_\mu^{(M-k)}. \quad (2.36)$$

Plugging (2.36) back into (2.35), a closed-form expression of the asymptotic variance $\text{avar}(\hat{f}_e^{(M)})$ in the presence of flat Ricean-fading effects is obtained.

6. HAF-based Estimator

As mentioned in Subsection 3, a HAF-based estimator is a simple and computational efficient approach to provide the initial estimates of NLS estimator (2.13), and combines the use of the HAF in order to reduce the order of the polynomial phase $\phi(n)$ and that of the NLS approach in order to estimate the parameters of an exponential signal embedded in noise [8].

First, let us rewrite (2.10) as:

$$y(n) = \mathcal{C}e^{j(M\theta + 2\pi MF_e T n + M\eta T^2 n^2)} + u(n) ,$$

and define the following process:

$$y_2(n; \tau) := y^*(n)y(n + \tau) = \mathcal{C}^2 e^{j(2\pi MF_e T \tau + M\eta T^2 \tau^2)} e^{j2M\eta T^2 n \tau} + u'(n) , \quad (2.37)$$

where $\tau > 0$ and $u'(n)$ is a zero-mean noise composed of noise \times signal and noise \times noise terms. For a fixed τ , $y_2(n; \tau)$ is an exponential signal with constant amplitude $\mathcal{C}^2 \exp(j(2\pi MF_e T \tau + M\eta T^2 \tau^2))$ embedded in additive noise $u'(n)$. Hence, it is natural to use an NLS estimator to obtain an estimate of η as follows:

$$\hat{\eta} = \frac{1}{2MT^2\tau} \arg \max_{|\bar{\omega}| < \pi} \frac{1}{N} \left| \sum_{n=0}^{N-1} y_2(n; \tau) e^{-j\bar{\omega}n} \right| . \quad (2.38)$$

Once $\hat{\eta}$ is available, demodulate $y(n)$ to obtain:

$$z(n) := y(n) \cdot e^{-jM\hat{\eta}T^2 n^2} \simeq \mathcal{C}e^{j(M\theta + 2\pi MF_e T n)} + u''(n) ,$$

where $u''(n)$ combines the estimation errors in $\hat{\eta}$ and the effect of additive noise [8].

Similarly, F_e can be obtained as:

$$\hat{F}_e = \frac{1}{MT} \arg \max_{|\bar{f}_0| < 1/2} \frac{1}{N} \left| \sum_{n=0}^{N-1} z(n) e^{-j2\pi \bar{f}_0 n} \right| . \quad (2.39)$$

The HAF-based estimators (2.38) and (2.39) can decrease computational complexity and provide good initial values for NLS estimator (2.13). Examining its performance is beyond the scope of this work. We refer the reader to [8] for the detailed performance analysis of HAF-based estimator.

7. Simulation Experiments

In this subsection, we study thoroughly the performance of estimators (2.11), (2.21) and (2.29) using computer simulations. The experimental MSE results of these estimators will be compared with the theoretical asymptotic bounds and the CRB-like bounds. The experimental results are obtained by performing a number of 200 Monte Carlo trials, the additive noise is generated as zero-mean Gaussian white noise with variance σ_v^2 and unless otherwise noted, all the simulations are performed assuming the carrier phase $\theta = 0.1$, frequency offset $F_e T = 0.011$ and Doppler rate $\eta T^2 = 0.03$. *Experiment 1-Performance loss of estimators (2.20)-(2.21) w.r.t. the matched estimator (2.18)-(2.11):* Fig. 4 plots the loss in performance of estimators (2.20)-(2.21) w.r.t. the optimal estimator (2.18)-(2.11) ($-10 \log_{10}[\text{avar}(\hat{\omega}_l^{(k)})/\text{avar}_{\min}(\hat{\omega}_l)]$) in the case of a BPSK modulation ($M = 2$) and QPSK modulation ($M = 4$), respectively. It turns out that in almost the entire SNR region of interest, the optimal nonlinearity $F_{\min}(\rho(n))$ can be approximated without much loss in performance by $\rho(n)$ (BPSK) and $\rho(n)$ or $\rho^2(n)$ (QPSK, depending on SNR), respectively.

Experiment 2-Asymptotic variances of estimators (2.18)-(2.11) and (2.20)-(2.21) w.r.t. the UCRB: Fig. 5 depicts the performance loss of the asymptotic variances (2.19) and (2.22) w.r.t. the UCRB (i.e., $-10 \log_{10}[\text{avar}(\hat{\omega}_l)/\text{UCRB}(\hat{\omega}_l)]$), assuming BPSK and QPSK modulations, respectively. It can be seen that the proposed estimators exhibit good accuracy. In high SNR range they coincide with the UCRB, therefore, are asymptotically efficient. In low SNR range (near 0 dB), monomial nonlinear estima-

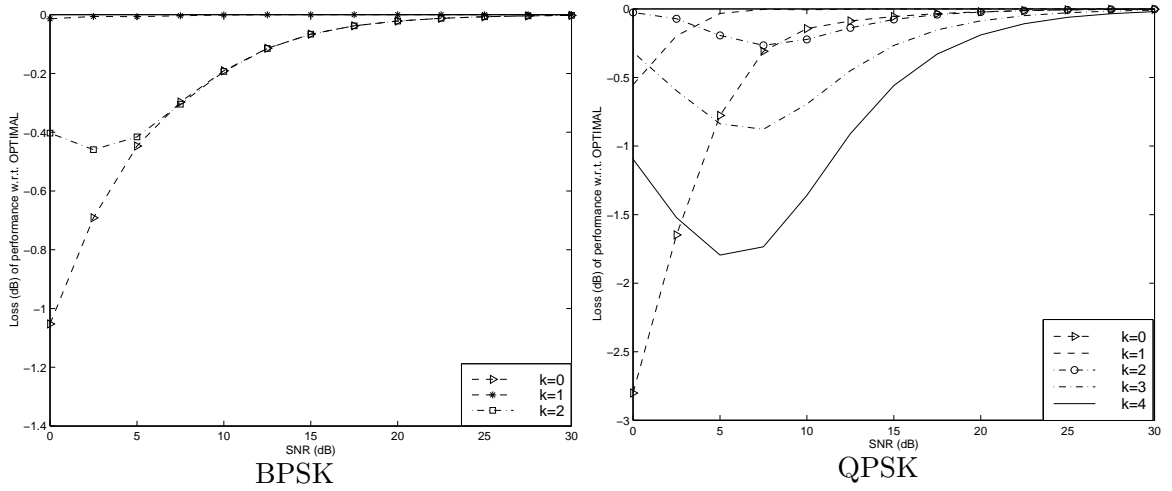


Fig. 4. Theoretical degradation of $\hat{\omega}_l^{(k)}$ w.r.t. the optimal estimator

tors with improved performance can be obtained by adopting low order nonlinearities ($k = 1$ and 2 for BPSK and QPSK modulations, respectively). Although the matched nonlinear estimator is optimal in the entire SNR range, its performance improvement relative to the monomial estimators is observable only at low SNRs. From Figs. 4–5, we can also observe that at very high SNRs, the monomial estimators (2.20)–(2.21) for different orders k exhibit the same asymptotic variance.

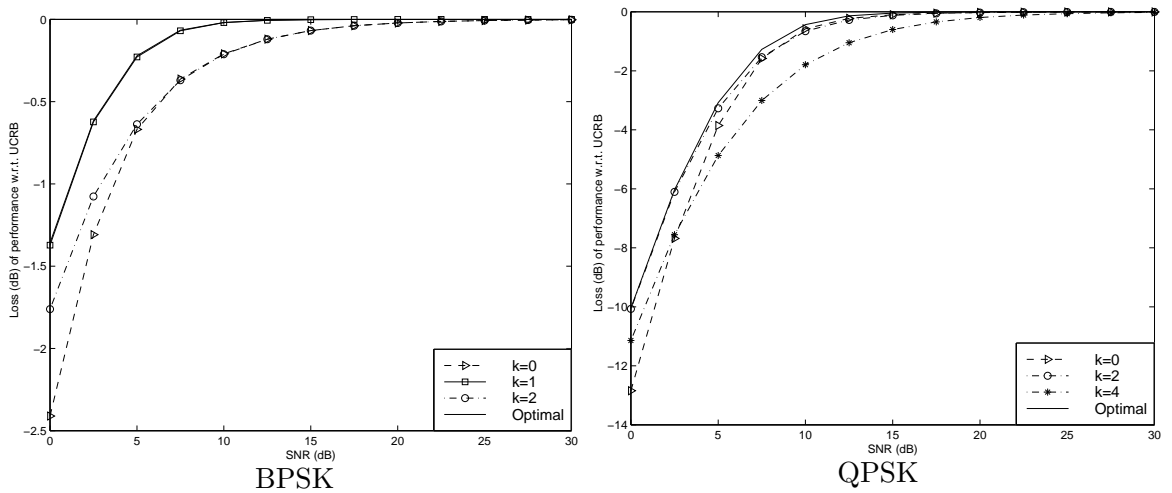


Fig. 5. Performance loss w.r.t. the UCRB versus SNR

Experiment 3-Comparison of the MSE of estimators (2.21) with the theoretical bounds versus SNR: In Fig. 6, the theoretical bounds (2.22) are compared with the experimental MSEs of estimators (2.21) versus SNR, assuming $k = 1$, $N = 50$ symbols and BPSK modulation. This figure shows that for medium and high SNR, the experimental results are well predicted by the asymptotic bounds derived in Subsection 4, and the proposed estimators provide very good estimates of carrier phase, frequency offset and Doppler rate, even when a reduced number of samples is used ($N = 50$). This shows the potential of these estimators for fast synchronization of burst transmissions.

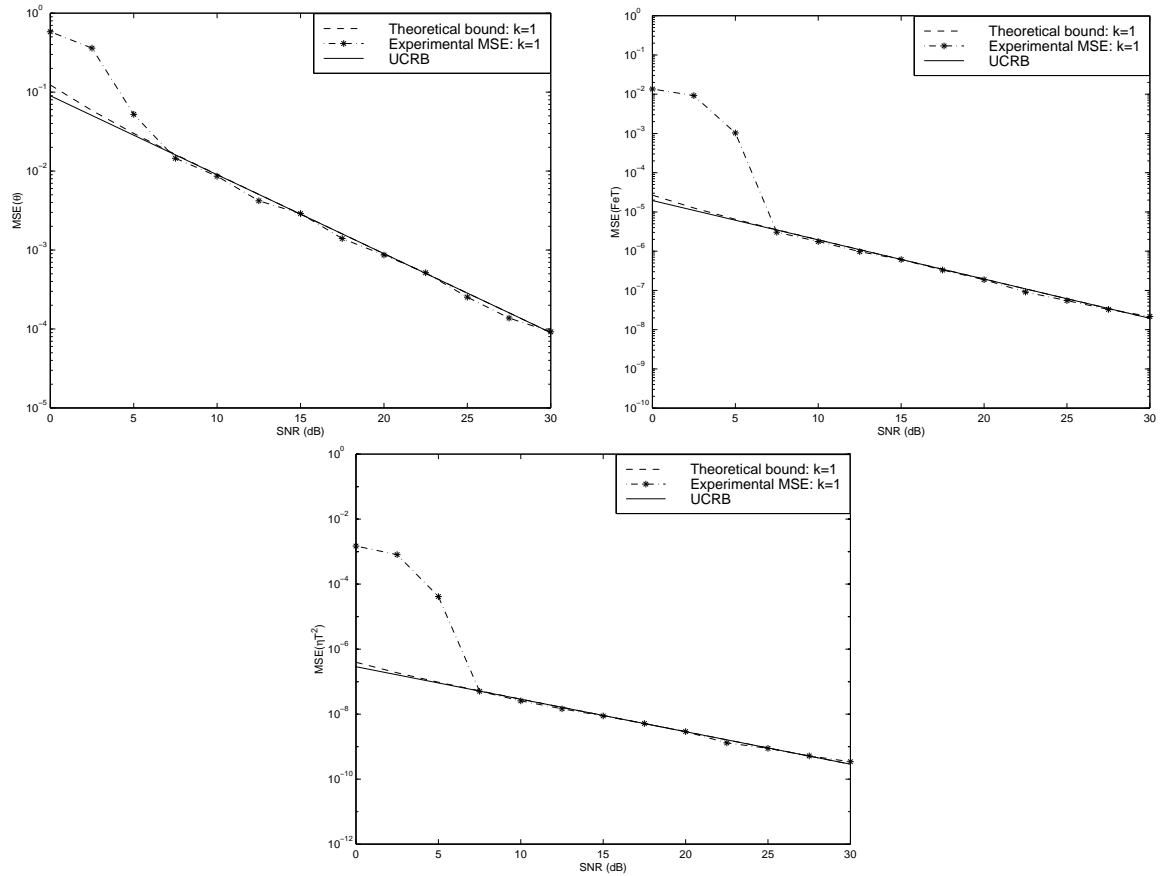


Fig. 6. a) MSEs of $\hat{\theta}$, b) MSEs of $\hat{F}_e T$, c) MSEs of $\hat{\eta} T^2$

Experiment 4-Comparison of MSE of estimators (2.21) with the theoretical bounds versus number of samples N : Fig. 7 displays the influence of the number of samples N on the performance of the estimators (2.21), assuming $k = 1$, SNR=5 dB and a BPSK input modulation. One can observe from this figure that even at low SNR, the proposed NLS estimators (2.21) can approach very closely the UCRB using a small number of samples ($N = 70$ or 80 samples), i.e., a lower threshold of SNR, at which large estimation errors of frequency offset and Doppler rate begin to occur, can be achieved with a reduced number of samples.

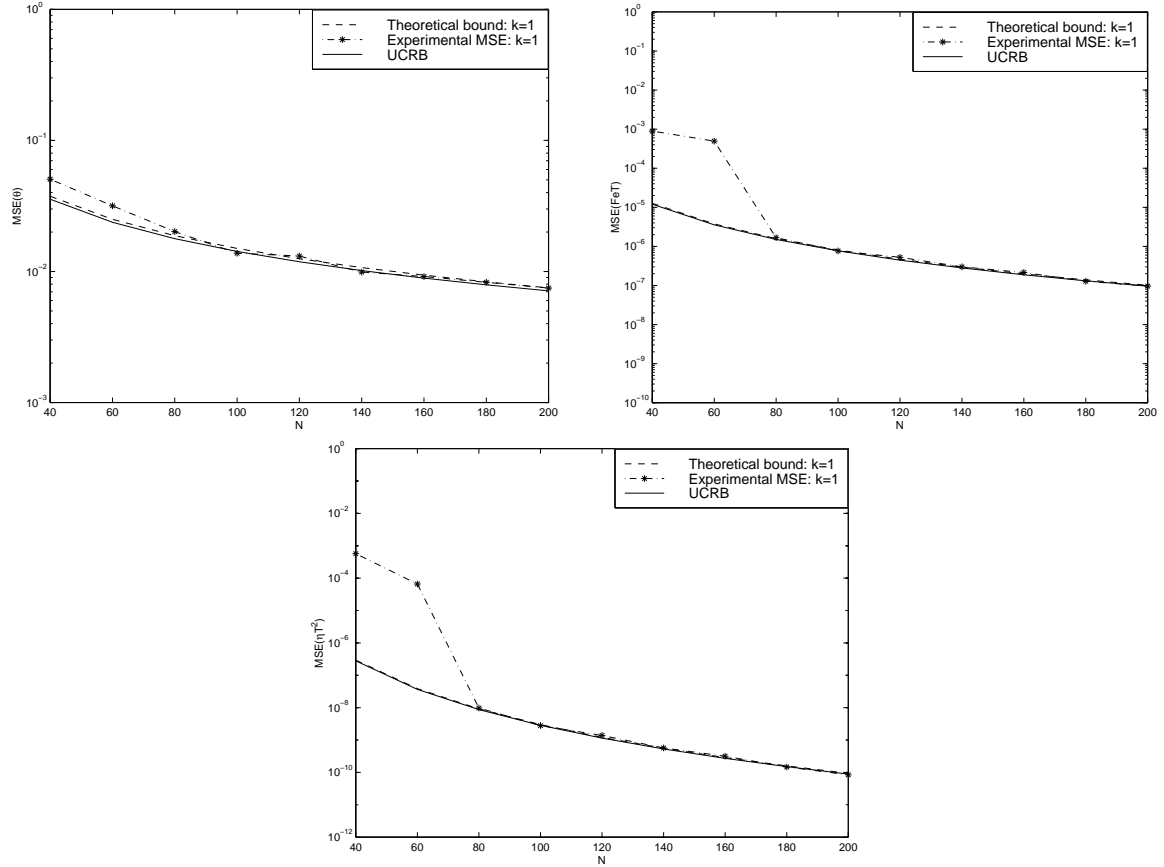


Fig. 7. a) MSEs of $\hat{\theta}$, b) MSEs of $\hat{F}_e T$, c) MSEs of $\hat{\eta T}^2$

Experiment 5-Performance of frequency estimators (2.29) in flat Ricean-fading channels: This experiment illustrates that the proposed frequency offset estimators (2.29) still perform well in the presence of Ricean-fading effects. In Fig. 8, the asymptotic variance (2.35) and the modified Cramér-Rao bound (MCRB) for NDA frequency offset estimation in flat Ricean-fading channel are plotted versus SNR. The latter was derived in [45], and with the notations adopted so far admits the following expression for large N : $\text{MCRB}(\hat{f}_e) = 6\sigma_v^2/[4\pi^2N^3(\rho_1^2 + \sigma_\mu^2)]$. We assume that the Ricean-fading process has a normalized energy (i.e., $E\{|\mu(n)|^2\} = 1$) and the Ricean factor $\kappa := \rho_1^2/\sigma_\mu^2 = 1$. The Doppler spread f_d is chosen as 0.005, 0.05 and 0.5, respectively. The transmitted symbol is BPSK and the number of samples is chosen as $N = 200$. In Fig. 8, the MSE of estimator (2.29) with $k = 2$ and $f_d = 0.005$ is also plotted. From Fig. 8, it turns out that although there exists an error floor due to the random fading effects, the accuracy of the proposed frequency offset estimators is still satisfying at medium and high SNRs, and improves for large Doppler spreads.

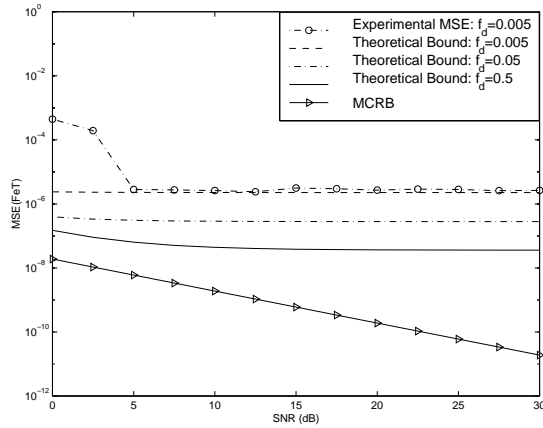


Fig. 8. MSEs of \hat{f}_e in the presence of a flat Ricean-fading channel

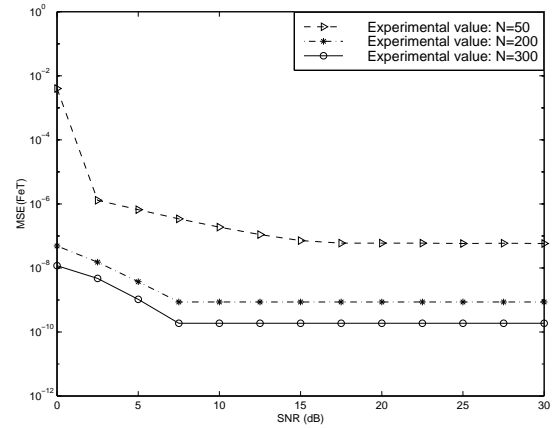


Fig. 9. MSEs of \hat{f}_e in the presence of timing error

Experiment 6-Performance of frequency offset estimators (2.29) in the presence of

timing error: Until now, we assumed a perfect timing reference at receiver. The simulation results presented in Fig. 9 illustrate that estimators (2.29) are robust to timing errors. In this simulation, we assume that there is a normalized timing-error $\epsilon T = 0.1$, the transmit and receive filters are square-root raised cosine filters with roll-off factor $\beta = 0.5$. The symbol modulation is BPSK, $k = 2$ and the number of samples is chosen as $N = 50, 200$ and 300 , respectively.

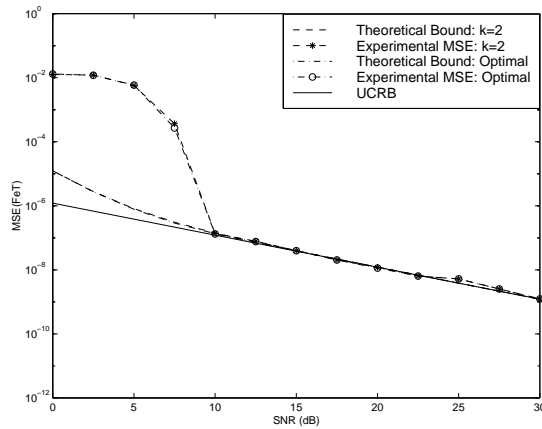


Fig. 10. MSEs of \hat{f}_e

Experiment 7-Performance of frequency offset estimator with optimal nonlinearity : For the sake of completeness, we illustrate in Fig. 10 the performance of frequency offset estimator (2.29) with optimal nonlinearity (2.18), compared with that of $k = 2$. Both theoretical bounds are shown, too. The constellation is QPSK and the number of samples is $N = 50$. In stead of using fixed value, this experiment assumes that the true frequency offset is taken randomly from the interval $[-0.1, 0.1]$ in each simulation run. It can be seen that Fig. 10 shows again the merit of the performance analysis presented in this work.

8. Conclusions

In this section, we have introduced and analyzed a family of blind feedforward joint estimators for the carrier phase, frequency offset and Doppler rate of burst-mode M-PSK modulations. A matched nonlinear estimator together with a class of monomial nonlinear estimators were introduced and their performance established in closed-form. It has been shown that the proposed estimators exhibit high convergence rates and good accuracy, and are robust to Ricean fading effects and timing errors.

B. Optimal Blind Carrier Recovery for General QAM Modulations

1. Introduction

Quadrature amplitude modulation (QAM) is a highly bandwidth efficient transmission technique for digital communications. Currently, large quadrature amplitude modulations are widely used in throughput efficient high speed communication applications such as digital TV and TDMA systems, and demodulation of a large QAM constellation signal requires accurate carrier recovery at the receiver, which generally involves the acquisition of carrier frequency and phase. Unfortunately, the conventional carrier tracking schemes frequently fail to converge for large QAM.

Recently, assuming that the frequency recovery has already been achieved, a number of blind feedforward phase estimators for square and cross QAM modulations were reported in [12]–[14], [28], [29], [38], [63, pp. 281–282] and [67], and analyzed in [86] and [92]. These estimators exploit the angle information contained in the fourth or higher-order statistics of the received signal. Reference [92] has shown that the seemingly different estimators [12], [63, pp. 281–282] and [67] are equivalent to the standard fourth-power estimator, while the estimator [14] exhibits a larger asymptotic (large sample) variance than the former class [12], [67]. A so-called reduced-

constellation (RC) fourth-power algorithm, which slightly improves the performance of the classic fourth-power estimator, is proposed in [38]. However, it is well-known that both the RC and the standard fourth-power estimators exhibit relatively poor performance in the case of cross QAM transmissions [38]. Also, reference [38] introduces two SNR dependent methods that outperform the performance of standard and RC fourth-power estimators in the case of cross and square QAM constellations, at moderate to high SNR levels, respectively. However, in the case of square QAM constellations and low SNRs, the performance of these two methods is inferior to the fourth-power algorithm [38]. Based on the V&V algorithm, Efstathiou and Aghvami have introduced blind carrier phase and frequency offset estimators for 16-QAM modulated transmissions [28], [29], which are similar to the RC fourth-power algorithm in the sense that they tend to emphasize the weight of the four corner points in the signal constellation. Morelli *et al.* pointed out that this solution was unsatisfactory with short bursts and proposed a new blind scheme with superior performance to previous methods [70]. However, it appears that it is not straightforward to extend this algorithm to general QAM modulations that are different from 16-QAM.

In this section, based on the fact that a QAM can be represented in terms of a set of PSK constellations, each of them defined by a specific amplitude and phase shift, we extend the result presented in Section A for M-PSK modulations, and introduce the optimal NLS estimators as well as computationally efficient approximate matched carrier estimators for general QAM modulations. Fig. 11 illustrates the example of a 16-QAM constellation consisting of four 4-QAM (QPSK) constellations.

The proposed matched estimators are constellation-dependent and are optimally designed such that their asymptotic variance is minimized. The performance of these matched algorithms is compared with the CRB, calculated according to [86], and shown that the optimal matched estimator exhibits superior performance (smaller

symbol error rate (SER)) w.r.t. the classic fourth-power estimator at any SNR level, but significant improvements are observable especially at medium and high SNRs. The proposed estimation techniques represent a quite general and unifying framework to design blind carrier synchronizers with improved performance. It appears that some of the existing synchronizers [70], [89] may be obtained as special cases of the proposed estimation framework.

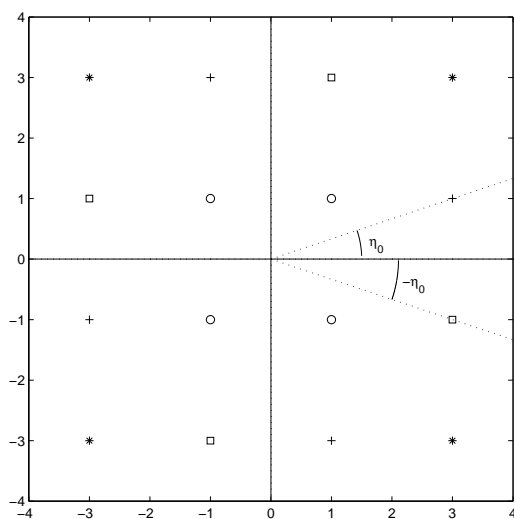


Fig. 11. 16-QAM constellation

We consider the following model similar to (2.1):

$$x(n) = w(n)e^{j\eta(n)} + v(n), \quad n = 0, \dots, N - 1, \quad (2.40)$$

$$\eta(n) := \theta + 2\pi F_e T n ,$$

where $\{w(n)\}$ now is the i.i.d. input M-QAM symbol stream with zero-mean and unit variance ($\sigma_w^2 := E\{|w(n)|^2\} = 1$).

As stated in Remark 4, the estimates of θ and F_e present 4-fold ambiguities for QAM constellation, which can be counteracted by applying differential encoding.

Without any loss of generality, we assume that the unknown phase θ lies in the interval $(-\pi/4, \pi/4)$ and $|f_e| := |F_e T| < 1/8$.

2. Estimators for Square QAM Constellations

First, let us consider square QAM constellations (i.e., with sizes $M = 2^{2m}$, $m = 1, 2, \dots$). With normalized energy, $w(n)$ takes a value from the set $(1/r_w)\{\pm(1+2l) \pm j(1+2k), (l, k) \in \mathcal{A}_M\}$ with $\mathcal{A}_M := \{(0, 1, 2, \dots, 2^{m-1} - 1)^2\}$ and:

$$r_w^2 := \frac{4}{M} \sum_{(l,k) \in \mathcal{A}_M} [(1+2l)^2 + (1+2k)^2].$$

a. Matched Nonlinear Carrier Synchronizer

Following the similar procedure presented in Section A, we represent $x(n)$ in its polar form:

$$x(n) = \rho(n)e^{j\phi(n)}, \quad (2.41)$$

and define the process $y(n)$ via the nonlinear transformation:

$$y(n) := F(\rho(n))e^{j4\phi(n)}, \quad (2.42)$$

where $F(\cdot)$ is a real-valued non-negative arbitrary nonlinear function. It is interesting to remark that the transformation (2.42) differs from the class of nonlinear transformations introduced in Section A. This difference is due to the fact that all QAM constellations exhibit quadrant symmetries which translate into non-zero fourth-order moments ($E\{w^4(n)\} \neq 0$), and consequently justify the special form of the exponential factor in (2.42).

Due to (2.41), it follows that:

$$f(\rho(n), \phi(n)|w(n) = \rho_w(n)e^{j\phi_w(n)}) = \frac{\rho(n)}{\pi\sigma_v^2} e^{-\frac{\rho^2(n)+\rho_w^2(n)}{\sigma_v^2}} e^{\frac{2\rho(n)\rho_w(n)\cos[\phi(n)-\phi_w(n)-\eta(n)]}{\sigma_v^2}},$$

where $\rho_w(n)$ and $\phi_w(n)$ denote the amplitude and phase angle of $w(n)$, respectively, and:

$$f(\rho(n), \phi(n)) = \frac{\rho(n)}{M\pi\sigma_v^2} \sum_{(l,k) \in \mathcal{A}_M} \sum_{m=0}^3 e^{-\frac{1}{\sigma_v^2}[\rho^2(n)+\varrho_{l,k}^2]} e^{\frac{2\rho(n)\varrho_{l,k}}{\sigma_v^2} \cos[\phi(n)-\psi_{l,k}-\frac{m\pi}{2}-\eta(n)]}, \quad (2.43)$$

$$f(\rho(n)) = \frac{8\rho(n)}{M\sigma_v^2} \sum_{(l,k) \in \mathcal{A}_M} e^{-(\rho^2(n)+\varrho_{l,k}^2)/\sigma_v^2} I_0\left(\frac{2\rho(n)\varrho_{l,k}}{\sigma_v^2}\right), \quad (2.44)$$

where $\varrho_{l,k} := \sqrt{[(1+2l)^2 + (1+2k)^2]}/r_w$, $\psi_{l,k} := \arctan((1+2k)/(1+2l))$. Then, the following NLS estimator can be introduced:

$$\hat{\omega}_1 := 8\pi\hat{f}_e = \arg \max_{\hat{\omega}_1} \frac{1}{N} \left| \sum_{n=0}^{N-1} y(n)e^{-j\hat{\omega}_1 n} \right|^2, \quad (2.45)$$

$$\hat{\omega}_0 := 4\hat{\theta} = \text{angle} \left\{ - \sum_{n=0}^{N-1} y(n)e^{-j\hat{\omega}_1 n} \right\}. \quad (2.46)$$

From (2.45) and (2.46), it can be seen that the overall estimation procedure includes two steps. First, a coarse estimate of the frequency offset f_e is determined efficiently by means of the FFT algorithm applied on the sequence $y(n)$, which is generally zero-padded with a sufficiently large number of zeros to achieve the precision provided by the asymptotic (Cramér-Rao) bound ($O(1/N^3)$). Then, a fine frequency offset estimate is obtained by means of interpolation or using a gradient algorithm. Finally, a closed-form estimate of the carrier phase is obtained based on (2.46), which assumes knowledge of the frequency estimate \hat{f}_e . As the estimator (2.11), estimators (2.45) and (2.46) are asymptotically unbiased and consistent [98], and also asymptotically efficient in the sense that it achieves the performance of the maximum likelihood estimator [8], [40] and [98], if the distribution of additive noise $u(n)$ is approximated to be circular normal. As the simulation experiments illustrate, this approximation holds true for small order QAM constellations (e.g., QPSK), and the departure from circularity becomes more dominant for larger-order QAM constellations.

The following theorems for the case of square QAM modulations can be obtained similarly [111] and [104]:

Theorem 4 *The asymptotic variances of the NLS estimates $\hat{\omega}_l$, $l = 0, 1$ in (2.45)-(2.46) are given by:*

$$\text{avar}(\hat{\omega}_l) = \frac{\mathcal{B} - \mathcal{D}}{\mathcal{C}^2} \cdot \frac{4l + 2}{N^{2l+1}}, \quad (2.47)$$

$$\mathcal{B} := \mathbb{E}\{|y(n)|^2\} = \mathbb{E}\{F^2(\rho(n))\} = \int_0^\infty F^2(\rho(n))\xi_1(\rho(n))d\rho(n), \quad (2.48)$$

$$\mathcal{C} := |\mathbb{E}\{y(n)\}| = |\mathbb{E}\{F(\rho(n))e^{j4\phi(n)}\}| = \int_0^\infty F(\rho(n))\xi_2(\rho(n))d\rho(n), \quad (2.49)$$

$$\mathcal{D} := |\mathbb{E}\{y^2(n)\}| = |\mathbb{E}\{F^2(\rho(n))e^{j8\phi(n)}\}| = \int_0^\infty F^2(\rho(n))\xi_3(\rho(n))d\rho(n), \quad (2.50)$$

where for $i = 1, 2, 3$ the following relations hold:

$$\xi_i(\rho(n)) := (-1)^{i-1} \frac{8\rho(n)}{M\sigma_v^2} e^{-\frac{\rho^2(n)}{\sigma_v^2}} \sum_{l,k \in \mathcal{A}_M} \cos(4(i-1)\varphi_{l,k}) e^{-\frac{q_{l,k}^2}{\sigma_v^2}} I_{4(i-1)}\left(\frac{2\rho(n)q_{l,k}}{\sigma_v^2}\right), \quad (2.51)$$

and $\varphi_{l,k} := \psi_{\max\{l,k\}, \min\{l,k\}}$.

Theorem 5 *The optimal “matched” nonlinearity $F_{\min}(\cdot)$ that minimizes the asymptotic variances of the proposed family of NLS estimators is given by:*

$$F_{\min}(\rho(n)) = \lambda \frac{\xi_2(\rho(n))}{\xi_1(\rho(n)) - \xi_3(\rho(n))}, \quad (2.52)$$

where λ is an arbitrary nonzero constant selected such that $F_{\min}(\cdot)$ is non-negative.

Plugging (2.52) back into (2.48)–(2.50), and substituting these values into (2.47), the asymptotic variances corresponding to the optimal matched estimates $\hat{\omega}_l$, $l = 0, 1$, can be expressed as:

$$\text{avar}_{\min}(\hat{\omega}_l) = \frac{4l + 2}{N^{2l+1}} \cdot \frac{1}{\int_0^\infty \frac{\xi_2^2(\rho(n))}{\xi_1(\rho(n)) - \xi_3(\rho(n))} d\rho(n)}. \quad (2.53)$$

In [86], the CRBs for carrier phase and frequency offset estimates are derived for fully QAM-modulated carriers, and with the notations adopted so far admit the

following expression for large N :

$$\text{CRB}(\hat{\omega}_l) = \text{CRB}_{\text{CW}}(\hat{\omega}_l) \cdot R(\sigma_v^2) = \frac{(4l+2)\sigma_v^2}{N^{2l+1}} \cdot R(\sigma_v^2), \quad (2.54)$$

where CRB_{CW} corresponds to the CRB for an unmodulated carrier wave, and $R(\sigma_v^2)$ denotes the constellation-dependent ratio of the true CRB to CRB_{CW} , which can be evaluated by means of numerical integration or Monte Carlo evaluations (MCE) [86].

In the absence of frequency offset (f_e), the proposed NLS estimator reduces to the phase estimator:

$$\hat{\theta} = \frac{1}{4} \text{angle} \left\{ - \sum_{n=0}^{N-1} y(n) \right\}, \quad (2.55)$$

whose asymptotic variance is one quarter of that corresponding to the case of joint phase and frequency offset estimation [86], and is given by:

$$\text{avar}(\hat{\theta}) = \frac{\mathcal{B} - \mathcal{D}}{32N\mathcal{C}^2}. \quad (2.56)$$

b. Monomial Nonlinear Estimators

As illustrated in Section A, the conventional Viterbi-like nonlinearities rely on the monomial transformations $F_k(\rho(n)) = \rho^k(n)$, $k = 0, \dots, 4$, and exhibit computational efficiency and simplicity when compared with the optimal matched estimator. Following a similar approach to that presented in Section A, one can obtain the class of monomial NLS estimators as:

$$\hat{\omega}^{(k)} = \arg \min_{\bar{\omega}^{(k)}} \frac{1}{2} \sum_{n=0}^{N-1} \left| y_k(n) - \bar{\mu}^{(k)} e^{j \sum_{l=0}^1 \bar{\omega}_l^{(k)} n^l} \right|^2, \quad (2.57)$$

whose asymptotic variances for $\hat{\omega}_l^{(k)}$, $l = 0, 1$, are provided by the following theorem [111] and [104]:

Theorem 6 *The asymptotic variances of the NLS estimates $\hat{\omega}_l^{(k)}$, $l = 0, 1$, in (2.57),*

are given by:

$$\text{avar}(\hat{\omega}_l^{(k)}) = \frac{\mathcal{B}_k - \mathcal{D}_k}{\mathcal{C}_k^2} \cdot \frac{4l + 2}{N^{2l+1}}, \quad (2.58)$$

$$\mathcal{B}_k = \frac{4\sigma_v^{2k}}{M} \sum_{q=0}^k \binom{k}{q}^2 q! \sum_{l,p \in \mathcal{A}_M} \left(\frac{\varrho_{l,p}^2}{\sigma_v^2} \right)^{k-q}, \quad (2.59)$$

$$\mathcal{C}_k = -\frac{4\sigma_v^{k-4}\Gamma(\frac{k}{2} + 3)}{M\Gamma(5)} \sum_{(l,p) \in \mathcal{A}_M} \cos(4\varphi_{l,p}) e^{-\frac{\varrho_{l,p}^2}{\sigma_v^2}} \varrho_{l,p}^4 \Phi\left(\frac{k}{2} + 3, 5, \frac{\varrho_{l,p}^2}{\sigma_v^2}\right), \quad (2.60)$$

$$\mathcal{D}_k = \frac{4\sigma_v^{2k-8}\Gamma(k + 5)}{M\Gamma(9)} \sum_{(l,p) \in \mathcal{A}_M} \cos(8\varphi_{l,p}) e^{-\frac{\varrho_{l,p}^2}{\sigma_v^2}} \varrho_{l,p}^8 \Phi\left(k + 5, 9, \frac{\varrho_{l,p}^2}{\sigma_v^2}\right). \quad (2.61)$$

When k is even (M is usually a power of two), the following expressions hold:

$$\mathcal{C}_k = -\frac{4}{M} \sum_{(l,p) \in \mathcal{A}_M} \cos(4\varphi_{l,p}) \mathcal{H}\left(\frac{k}{2}, 2, \frac{\varrho_{l,p}^2}{\sigma_v^2}\right), \quad \text{if } k = 0, 2,$$

$$\mathcal{C}_k = -\frac{4}{M} \sum_{(l,p) \in \mathcal{A}_M} \cos(4\varphi_{l,p}) \varrho_{l,p}^4, \quad \text{if } k = 4,$$

$$\begin{aligned} \mathcal{H}(s, t, \gamma) := & \left(\frac{\sigma_v^2}{2}\right)^t \left[\gamma^t \sum_{p=0}^{s+t} p! \binom{s+t}{p} \binom{s-t+p-1}{p} \left(\frac{-2}{\gamma}\right)^p \right. \\ & \left. + (-1)^{s+t+1} 2^t e^{-\frac{\gamma}{2}} \left(\frac{2}{\gamma}\right)^{t+1} \sum_{p=0}^{s-t-1} \binom{s+t+p}{p} \frac{(s+t)!}{(s-t-p-1)!} \left(\frac{2}{\gamma}\right)^p \right]. \end{aligned}$$

Similarly,

$$\mathcal{D}_k = \frac{4}{M} \sum_{(l,p) \in \mathcal{A}_M} \cos(8\varphi_{l,p}) \mathcal{H}\left(k, 4, \frac{\varrho_{l,p}^2}{\sigma_v^2}\right), \quad \text{if } k = 0, 1, 2, 3,$$

$$\mathcal{D}_k = \frac{4}{M} \sum_{(l,p) \in \mathcal{A}_M} \cos(8\varphi_{l,p}) \varrho_{l,p}^8, \quad \text{if } k = 4.$$

Note that when $k = 4$, the phase estimator (2.55) is just the standard fourth-power estimator [12], [63, pp. 281–282] and [67], and (2.56) coincides with the expression established earlier in [92, eq. (13)].

3. Extension to Cross QAM Constellations

Following a similar approach to the one presented above, one can develop an optimal matched joint carrier phase and frequency offset estimator for general cross QAM modulations (i.e., with sizes $M = 2^{2m+1}$, $m = 2, 3, \dots$). Observe that for general cross QAM constellations, $w(n)$ takes a value from the set $(1/r_w)\{\pm(1+2l) \pm j(1+2k)\}$, $(l, k) \in \mathcal{A}_M\}$, with $\mathcal{A}_M := \{(0, 1, \dots, 3 \cdot 2^{m-2} - 1)^2 - (2^{m-1}, \dots, 3 \cdot 2^{m-2} - 1)^2\}$ and r_w an energy normalization constant. Therefore, we can still express the joint and marginal pdf of $\rho(n)$ and $\phi(n)$ as in (2.43) and (2.44). Similarly to the derivations presented in Subsection 2, it is not difficult to find that all the estimators proposed for square QAM modulations can be applied to cross QAM constellations, and all the expressions for the asymptotic variances still hold true without any change. The constants $\mathcal{B}_k, \mathcal{C}_k, \mathcal{D}_k$ are constellation-dependent and their values should be computed accordingly, whose detailed derivations will not be presented.

Assuming the number of samples $N = 500$, Fig. 12 illustrates the theoretical asymptotic variances for 16-QAM (square) and 32-QAM (cross), respectively. Since the difference between the asymptotic variances of $\hat{\theta}$ and \hat{f}_e is just a constant for a given SNR, only the variance of $\hat{\theta}$ (2.56) is plotted. From Fig. 12, one can observe that at low SNRs, both the optimal estimator and the fourth-power estimator achieve CRB, which means that at very low SNRs, the classic fourth-power estimator is always the best choice. This is not a surprising result since the fourth-power estimator is simply a low-SNR approximation of the ML estimator [67]. However, in the more practical regime of medium and high SNRs, the optimum nonlinear estimator provides a significant improvement over the class of monomial estimators while the latter exhibits the error floor due to its self-induced noise [67], [86]. This conclusion is different from the result presented in Fig. 4 where the optimal nonlinearity $F_{\min}(\rho(n))$

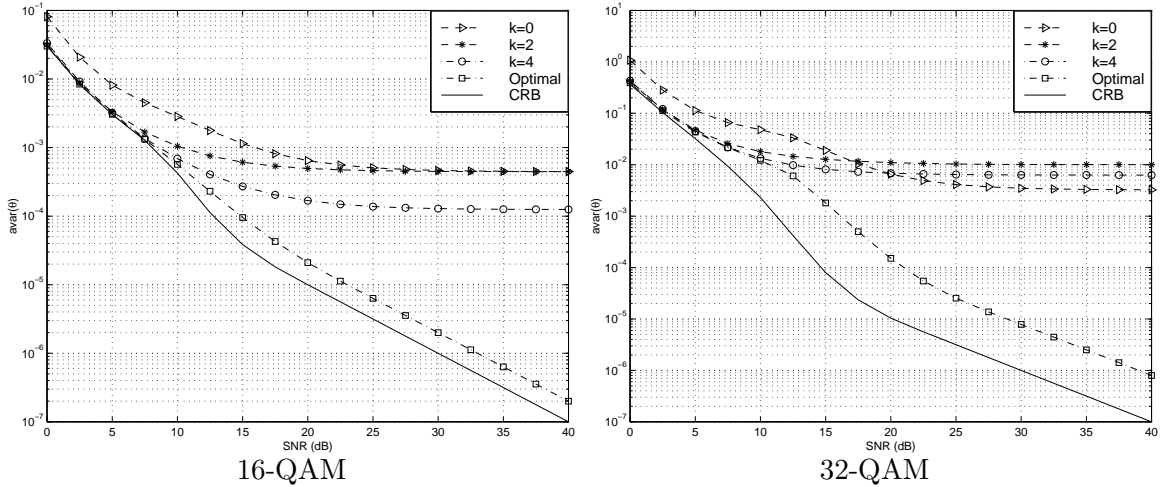


Fig. 12. Theoretical bounds of $\hat{\theta}$ versus SNR

can be approximated without much loss in performance by certain monomial function in almost the entire SNR region of interest.

4. Implementation of the Optimal Estimator

The results shown in Fig. 12 illustrate the good property of the optimal nonlinearity (2.52) for higher-order (higher than 4) QAM modulations at medium and high SNR ranges. As can be observed from (2.51) and (2.52), $F_{\min}(\rho(n))$ is a function that depends on the SNR, and presents high implementation complexity, which makes the optimal estimator impractical. Fortunately, computer simulations indicate that the sensitivity of the optimal estimator to SNR is limited in medium and high SNR ranges. By considering approximations of (2.52), we propose next computationally efficient SNR-independent estimators, which will be referred to as APP-estimators.

We select 16-QAM as an example to illustrate the derivation of the constellation-dependent APP estimator. Fig. 13 (a) plots the optimal nonlinearity (2.52) versus the magnitude ρ of the received data at SNR= 20dB for 16-QAM modulation, while Fig. 13 (b) depicts the optimal nonlinearity (2.52) for a set of varying SNRs. The

curve presented in Fig. 13-a suggests that for 16-QAM a good design for the APP estimator is a piecewise linear approximation of the following form:

$$F_{\text{APP}_{16}}(\rho(n)) = \begin{cases} 122.2733\rho(n) & \text{if } \rho(n) \leq 0.7 , \\ 331.885\rho(n) - 30.4524 & \text{if } \rho(n) \geq 1.2 , \\ 0 & \text{elsewhere .} \end{cases} \quad (2.62)$$

Similarly for 32-QAM and 64-QAM, since the optimal nonlinearity (2.52) appears to be well modeled by piecewise linear approximations, we can obtain the APP estimators:

$$F_{\text{APP}_{32}}(\rho(n)) = \begin{cases} 206.9958\rho(n) & \text{if } \rho(n) \leq 0.5 , \\ 608.4586\rho(n) + 2.2689 & \text{if } 0.84 \leq \rho(n) \leq 1.02 , \\ 0 & \text{elsewhere ,} \end{cases}$$

$$F_{\text{APP}_{64}}(\rho(n)) = \begin{cases} 106.4159\rho(n) & \text{if } \rho(n) \leq 0.34 , \\ 321.2425\rho(n) & \text{if } 0.59 \leq \rho(n) \leq 0.69 , \\ 717\rho(n) & \text{if } \rho(n) \geq 1.44 , \\ 0 & \text{elsewhere ,} \end{cases}$$

respectively. Since $F_{\text{APP}}(\cdot)$ is constellation-dependent, we will not present the detailed expressions of F_{APP} for other QAM modulations in this paper. The APP nonlinearities for general QAM constellations can be obtained in a similar way. It is interesting to observe that $F_{\text{APP}_{16}}$ (2.62) is quite similar to the nonlinearity introduced in the Morelli *et al.* estimator (V&V-SEL) [70], which takes the following expression:

$$F_{\text{V\&V-SEL}}(\rho(n)) = \begin{cases} 0.4472\rho(n) & \text{if } \rho(n) \leq 0.7236 , \\ 1.3416\rho(n) & \text{if } \rho(n) \geq 1.1708 , \\ 0 & \text{elsewhere .} \end{cases}$$

Careful examination of the expressions of APP nonlinearities illustrates that the in-

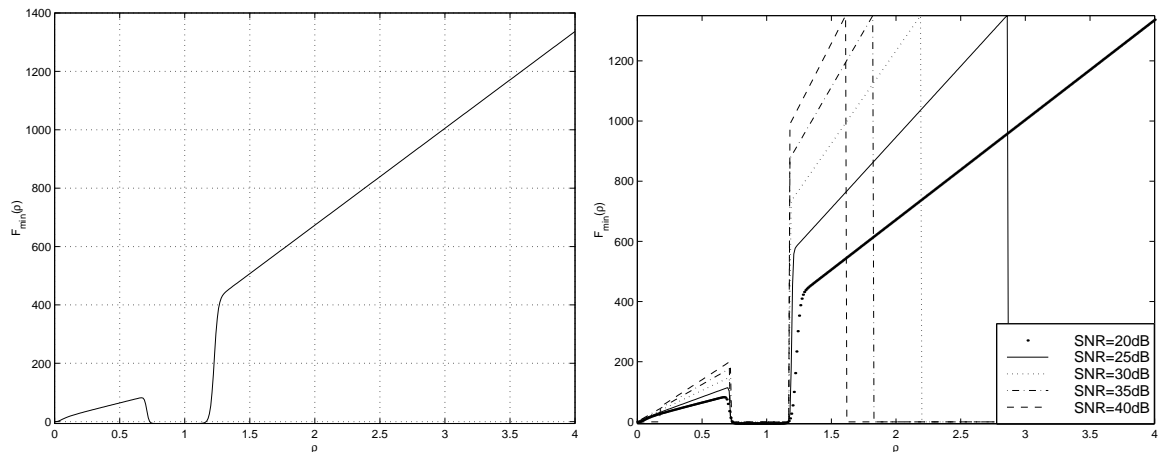


Fig. 13. a) F_{\min} versus ρ (16-QAM constellation at SNR= 20dB) b) F_{\min} versus ρ (16-QAM constellation at varying SNRs)

intrinsic principle of APP estimators is to emphasize the weight of the points located on the diagonals of the signal constellation, and discard all the off-diagonal points. It appears also that only a subset of the points located on the diagonals is selected. This principle was implicitly exploited by V&V-SEL estimator [70] for 16-QAM, and by Sari and Moridi for 16-QAM and 64-QAM under quite different circumstances [89]. In the next subsection, we will present simulation experiments to corroborate the theoretical performance analysis and to illustrate the performance of the proposed optimal estimators for both square and cross QAM constellations.

5. Simulation Experiments

In this subsection, we study thoroughly the performance of estimators (2.45), (2.46), (2.55) and (2.57) using computer simulations. The experimental MSE results of the proposed estimators will be compared with the theoretical asymptotic bounds and the CRB. The impact of the nonlinearity $F(\cdot)$ on SER is also assessed. The additive noise is generated as zero-mean Gaussian white noise, the number of samples is assumed $N = 500$, and the experimental results are obtained by performing a number of

$MC = 1,000$ Monte Carlo trials (Figs. 14–16) except in Figs. 17–19, where we use a larger number $MC = 100,000$ to ensure accuracy. Unless otherwise noted, the carrier phase $\theta = 0.2$ and frequency offset $F_e T = 0.05$.

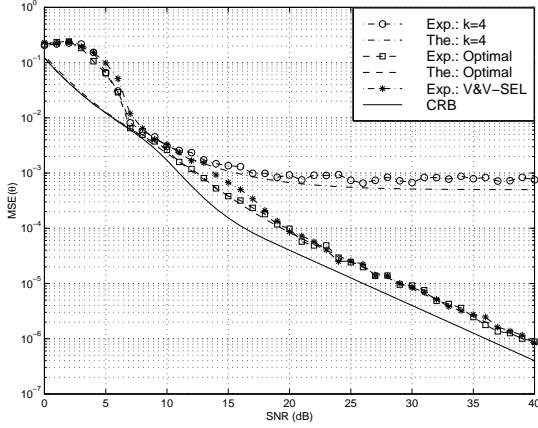


Fig. 14. Comparison of MSEs of $\hat{\theta}$ (16-QAM constellation)

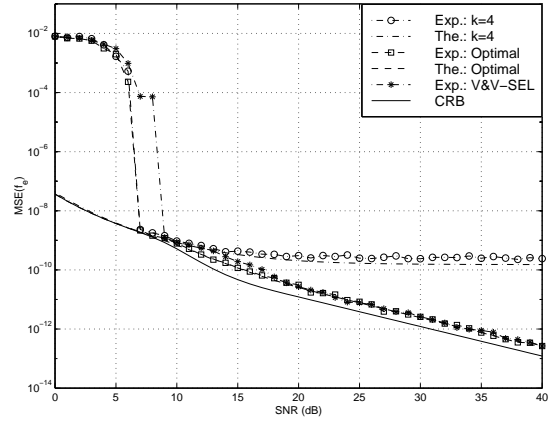


Fig. 15. Comparison of MSEs of \hat{f}_e (16-QAM constellation)

Experiment 1-Comparison of the MSE of the proposed estimators with the theoretical bounds versus SNR: This experiment compares the theoretical (The.) bounds with the experimental (Exp.) MSEs of the proposed estimators for 16-QAM (Figs. 14–15) and 32-QAM (Fig. 16) assuming no frequency offset. In Figs. 14 and 15, the performance of V&V-SEL estimator [70] is illustrated, too, while in Fig. 16, we also plot the MSE-result of the eighth-order statistics based phase estimator (EOE) proposed for cross QAM in [13]. These figures show that for medium and high SNRs, the experimental results of the optimal estimator and the fourth-power estimator are well predicted by the asymptotic bounds derived in this paper. Note that at low SNR (0dB), the MSE of the phase estimator (2.55) asymptotically converges toward the constant value $\pi^2/48$, which represents the variance of a uniformly distributed phase estimate over the range $[-\pi/4, \pi/4]$ [86], [102]. From Figs. 14 and 15, we can observe that for

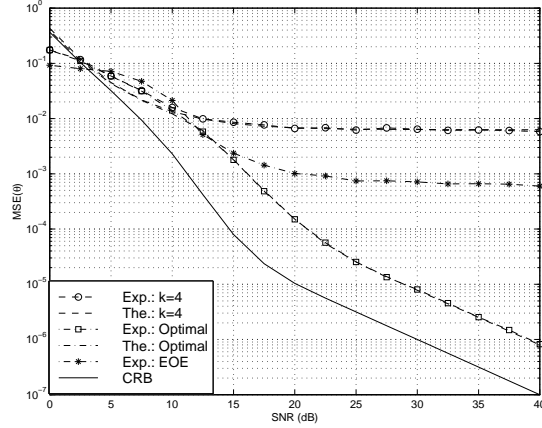


Fig. 16. Comparison of MSEs of $\hat{\theta}$ (32-QAM constellation)

16-QAM, the performance of the optimal estimator and the V&V-SEL estimator is essentially identical, and both of them outperform significantly the standard fourth-power estimator in the medium and high SNR ranges, and are very close to CRB. In the case of cross QAM constellations, the proposed optimal phase estimator provides considerable improvement over the fourth-power estimator and EOE.

Experiment 2-The impact of the nonlinearity on SER: In Fig. 17, we show the SER performance of the carrier synchronizers exploiting different nonlinearities and QAM modulations. Because the choice of nonlinearity $F(\cdot)$ is the same for both carrier phase and frequency offset estimators, for simplicity we only concentrate on the carrier phase estimator assuming the absence of frequency offset. Fig. 17 compares the performance of the proposed optimal and APP estimators with that of the classic fourth-power estimator, V&V-SEL estimator and EOE for 16-QAM with $\theta = 0.75$ and 32-QAM with $\theta = 0.2$, respectively. To show the superior performance of the optimal estimator, we also plot as a lower bound the SER curves in the case of perfect carrier recovery, i.e., in the case when the transmitted symbols are only corrupted by

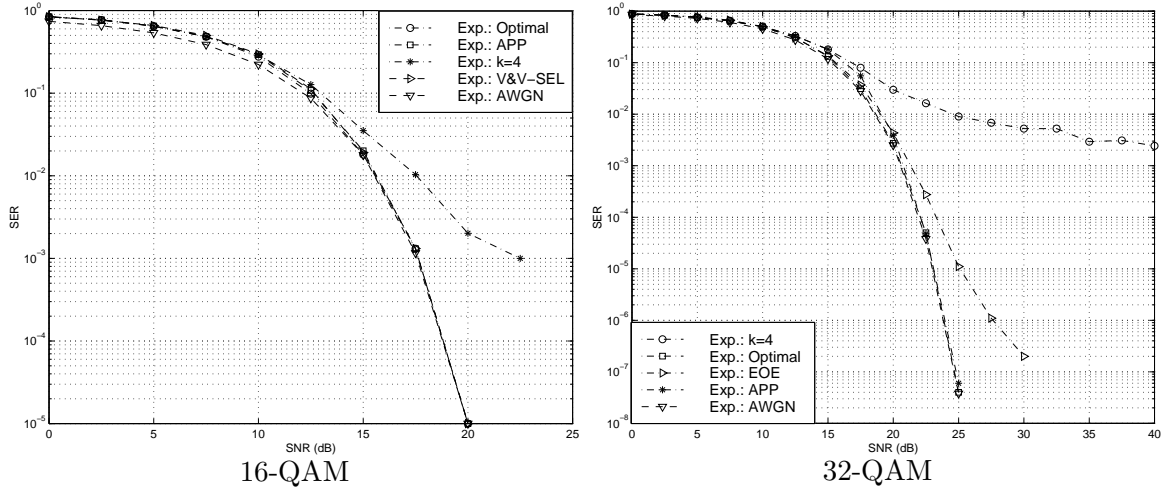


Fig. 17. SER curves versus SNR (16-QAM and 32-QAM)

additive white Gaussian noise. Fig. 17 indicates that the proposed optimal estimator approaches closely this lower bound, and improves significantly the performance of the conventional fourth-power estimator and EOE for medium and high SNRs. We can also observe that APP is a satisfying realizable alternative to the optimal estimator.

Experiment 3-The performance of the proposed estimators in the case of higher-order QAM modulations: Figs. 18–19 illustrate the performance of the optimal estimator and APP for larger-order QAM modulations (64-QAM with $\theta = 0.75$, 256-QAM and 128-QAM, respectively), compared with the existing methods. Since higher-order QAM modulations often operate at larger SNRs, we pay special attention to the medium and high SNRs, where the SER is in the range $SER \leq 10^{-3}$. These figures show again the merit of the proposed optimal estimator and APP, and justify again our derivation of the asymptotic variance.

6. Conclusions and Discussions

In this section, we have introduced and analyzed a family of blind feedforward joint carrier phase and frequency offset estimators for general QAM modulations. Based

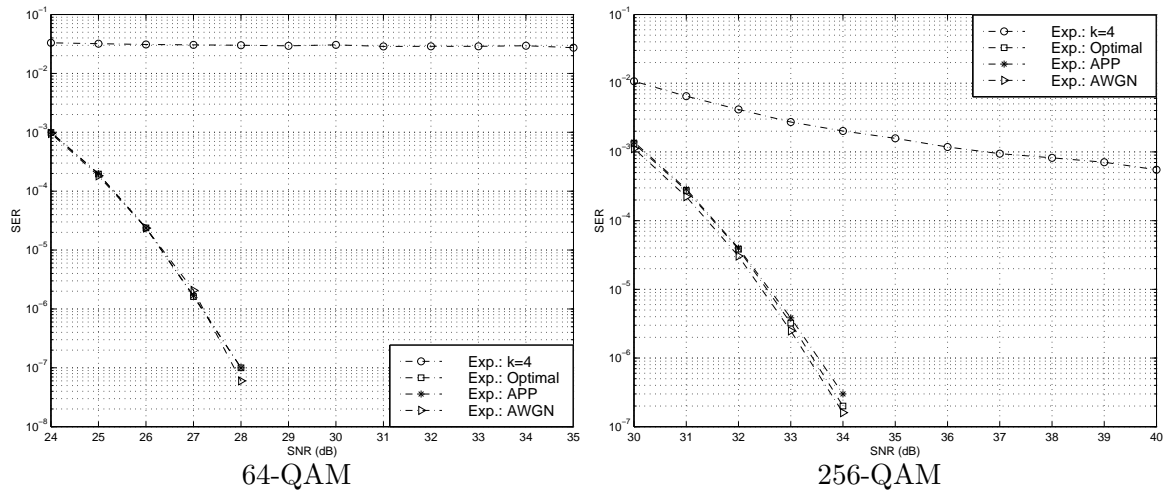


Fig. 18. SER curves versus SNR (64-QAM and 256-QAM)

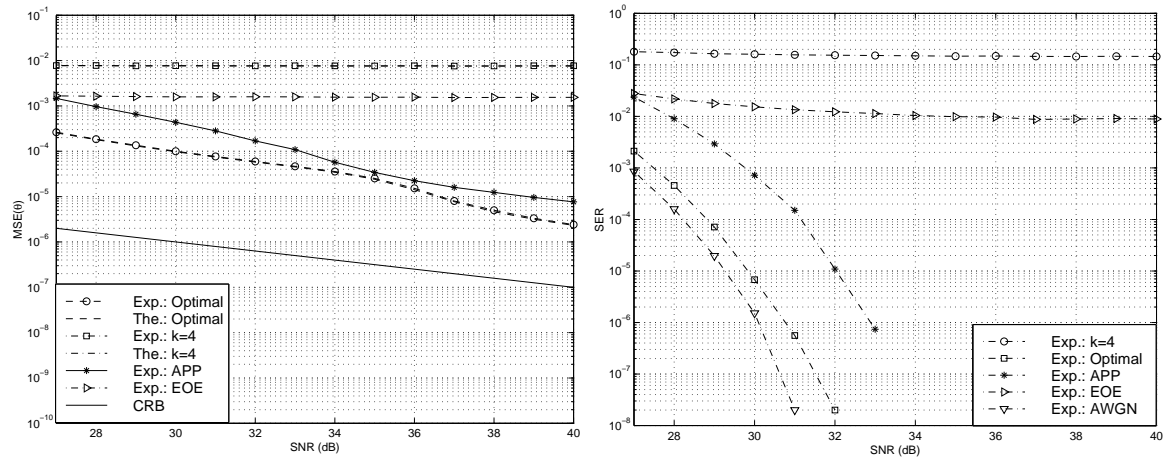


Fig. 19. MSE and SER versus SNR (128-QAM constellation)

on a generalization of the V&V algorithm, a matched nonlinear estimator together with a class of monomial nonlinear estimators were introduced and their performance established in closed-form expressions. A framework for designing computationally efficient approximations of the proposed optimal estimator without incurring much performance loss, is also proposed. The proposed (approximate) optimal estimator exhibits better performance when compared with the existing methods. Simulation results indicate the merit of the performance analysis presented in this section.

A future work may include analyzing the performance of a generalized NLS estimator that exploits the information provided by the two spectral lines present in the process: $y(n) := F_1(\rho(n))e^{j4\phi(n)} + F_2(\rho(n))e^{j8\phi(n)}$, where $F_1(\cdot)$ and $F_2(\cdot)$ are two arbitrary nonlinearities. It appears that for square QAM or small-order cross QAM there is not too much room for improvement, a fact that is corroborated by the SER curves depicted in Figs. 17 and 18. However, for larger-order cross QAM, the exploitation of additional harmonics (lines) may provide some performance gains. Another type of QAM constellations is star QAM modulation, which exhibit lower

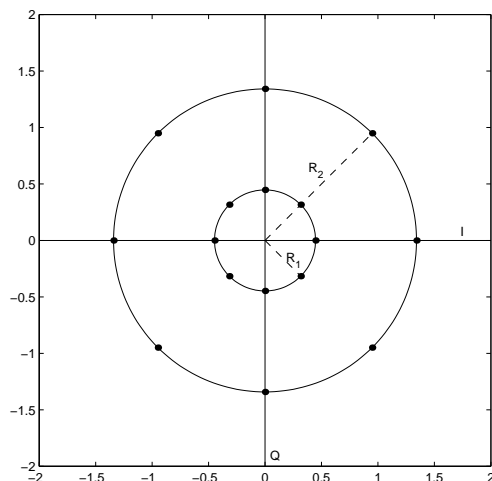


Fig. 20. Star 16QAM constellation

peak-to-average power ratio than square QAM modulations [87], [113]. Specifically, the star 16QAM constellation consists of 16 points arranged into two rings, each of which has 8 points uniformly spaced at $\pi/4$ intervals, and can be regarded as an 8-PSK modulation, as shown in Fig. 20. Our research work concerning the optimal carrier recovery scheme for Star 16QAM based on V&V algorithm can be found in [107].

CHAPTER III

BLIND NLS FREQUENCY OFFSET ESTIMATORS FOR FADING CHANNELS

In the previous chapter, we assume AWGN channels, which are relatively stationary and predictable, e.g., the wired channels. However, in the radio/wireless communication systems, the transmission path between the transmitter and the receiver can vary from simple line-of-sight to one that is severely obstructed by buildings, mountains, and foliage [84]. Therefore, in this case we have to model the channels in a more complex way, i.e., to characterize them as flat-fading or frequency-selective fading channels with ISI. For the characterization of fading channels, please refer to [83] and [84].

In this chapter, we consider the carrier recovery problem for linear modulations in the presence of flat-fading or frequency-selective fading ISI channels. To simplify the discussion, we will concentrate only on the acquisition of carrier frequency offset. According to the nature of the transmitted signal constellation, this chapter is composed of the following two sections, each to deal with one of the following categories of input signals: circular or non-circular constellations, where the essential difference between them, in terms of the statistical property, is that for a non-circular signal sequence w_k , $E\{w_k^2\} \neq 0$, while this relation does not hold for a circular signal. In this dissertation, we will consider the QAM modulations as the representative class of circular signals.

A. Blind Feedforward NLS Carrier Frequency Offset Estimators for QAM Constellations in ISI Channels

1. Introduction

The growth of mobile wireless communications systems has prompted an increased interest in designing digital receivers operating on samples of the fractionally-sampled (oversampled) received signal. The main reason is that oversampling gives rise to cyclostationarity (CS), which implies that more statistical information can be used for designing digital receivers with improved performance, and has been extensively exploited in communication systems to perform tasks of synchronization, blind channel identification and equalization (see e.g., [9], [17], [18], [27], [32], [42], [41], [44], [48], [49], [60], [90], [91] and [114]). It should be pointed out that CS statistics can also be induced by filtering the received discrete-time sequence through a nonlinear filter without oversampling, e.g., [9], [18], [91], [114], and the fourth-order NLS estimator proposed in Chapter II, will be rederived later on from a CS point of view.

Several carrier frequency-offset estimators for flat-fading channels that exploit the unconjugate second-order cyclostationary statistics of the oversampled received signal were proposed in [41, 44, 90]. A high performance blind Maximum Likelihood (ML) framework to estimate the Doppler shift in the presence of an unknown frequency selective channel was proposed in [22]. However, the proposed ML-solution relies on an iterative Baum-Welch type algorithm, whose large numerical complexity and possible lack of convergence prohibit its use for many practical applications [22]. Reference [99] proposed a different solution for blind joint detection and carrier recovery in the presence of an unknown multipath channel using a Viterbi-like algorithm. Since this solution relies on a critical channel identifiability condition, which may not be always satisfied, the applicability of this algorithm is also limited [99].

Based on oversampled signals, this section proposes a family of blind NLS frequency offset estimators for QAM modulations, that does not require knowledge of the multipath channel, and incorporates as a particular case the frequency offset estimator (2.45) with the oversampling factor (or rate) $P = 1$. The proposed family of synchronizers admits a feedforward structure that may be easily implemented in digital form, does not present high computational complexity, exhibits much faster convergence rates ($O(1/N^3)$, N denotes the number of available data samples) than the algorithms [41, 44, 90], whose convergence rates are $O(1/N)$, and their convergence and consistency are guaranteed even in the presence of unknown multipath effects [106].

2. Modeling Assumptions

Suppose that a QAM signal is transmitted through a flat-fading channel. The complex envelope of the received signal is affected by the carrier frequency offset and/or Doppler shift F_e and is expressed as [44], [83, Ch. 14]:

$$r_c(t) = e^{j2\pi F_e t} \sum_l w(l) h_c^{(tr)}(t - lT - \epsilon T) + v_c(t), \quad (3.1)$$

where $w(l)$'s are the transmitted complex information symbols, $h_c^{(tr)}(t)$ denotes the transmitter's signaling pulse, $v_c(t)$ is the complex-valued additive noise assumed independently distributed w.r.t. the input symbol sequence $w(n)$, T is the symbol period, and ϵ is an unknown normalized timing error introduced by the channel. After matched filtering with $h_c^{(rec)}(t)$, the resulting signal is (over)sampled at a period $T_s := T/P$, where the oversampling factor $P \geq 1$ is an integer. Under the common assumption that the frequency offset achieves small values ($F_e T < 0.1$), the following

equivalent discrete-time model can be deduced:

$$x(n) = e^{j2\pi f_e n} \sum_l w(l)h(n - lP) + v(n) , \quad (3.2)$$

where $f_e := F_e T_s$, $x(n) := (r_c(t) * h_c^{(rec)}(t))|_{t=nT_s}$, $v(n) := (v_c(t) * h_c^{(rec)}(t))|_{t=nT_s}$ and $h(n) := (h_c^{(tr)}(t) * h_c^{(rec)}(t))|_{t=nT_s - \epsilon T}$. For large frequency offset ($F_e T \geq 0.1$), a very similar model to eq. (3.2) results. Indeed, from (3.1), the receiver output after sampling can be expressed as:

$$\begin{aligned} x(n) &:= (r_c(t) * h_c^{(rec)}(t))|_{t=nT_s} \\ &= \sum_l w(l) \int h_c^{(rec)}(\tau) h_c^{(tr)}(nT_s - \tau - lT - \epsilon T) e^{j2\pi F_e (nT_s - \tau)} d\tau + v(nT_s) \\ &= e^{j2\pi F_e nT_s} \sum_l w(l) \int h_c^{(rec)}(\tau) h_c^{(tr)}(nT_s - \tau - lT - \epsilon T) e^{-j2\pi F_e \tau} d\tau + v(nT_s) \\ &= e^{j2\pi f_e n} \sum_l w(l) h'(n - lP) + v(n) , \end{aligned} \quad (3.3)$$

where $h'(n) := h'_c(t)|_{t=nT_s - \epsilon T}$ and $h'_c(t) = h_c^{(tr)}(t) * h_c^{(rec)}(t) \exp(-j2\pi F_e t)$. Substituting $h(n)$ with $h'(n)$, we observe the equivalence between the two models (3.2) and (3.3): small and large carrier frequency offsets, respectively. Because estimation of large and small frequency offsets can be achieved using the same estimation framework, in what follows we restrict our analysis to the problem of estimating small carrier frequency offsets assuming the channel model (3.2). Moreover, since no knowledge of the timing delay is assumed, the proposed FO-estimators will apply also for general frequency-selective channels.

In order to derive the asymptotic performance of the FO-estimators, without any loss of generality the following assumptions are imposed:

(AS1) $w(n)$ is a zero-mean i.i.d. sequence with values drawn from a QAM constellation with unit variance, i.e., $\sigma_{2w}^2 := E\{|w(n)|^2\} = 1$.

(AS2) $v_c(t)$ is white circularly distributed Gaussian noise with zero mean and power

spectral density N_0 .

(AS3) the transmitter and receiver filters are square-root raised cosine pulses of bandwidth $[-(1 + \rho)/(2T), (1 + \rho)/(2T)]$, where the parameter ρ represents the roll-off factor ($0 \leq \rho < 1$) [83, Ch. 9].

(AS4) $v(n)$ satisfies the so-called mixing condition [10, pp. 8, 25-27], [91], [114], which states that the k th-order cumulant of $v(n)$ at lag $\boldsymbol{\tau} := (\tau_1, \tau_2, \dots, \tau_{k-1})$, denoted by $c_{kv}(\boldsymbol{\tau}) := \text{cum}\{v(n), v(n + \tau_1), \dots, v(n + \tau_{k-1})\}$, is absolutely summable: $\sum_{\boldsymbol{\tau}} |c_{kv}(\boldsymbol{\tau})| < \infty, \forall k$. The mixing condition is a reasonable assumption in practice since it is satisfied by all signals with finite memory. Assumption **(AS4)** will prove useful in facilitating calculation of the asymptotic performance of the proposed estimators.

3. Carrier Frequency Offset Estimators

Estimating f_e from $x(n)$ in (3.2) amounts to retrieving a complex exponential embedded in multiplicative noise $\sum_l w(l)h(n - lP)$ and additive noise $v(n)$. The underlying idea for estimating the frequency offset is to interpret the higher-order statistics of the received signal as a sum of several constant amplitude harmonics embedded in (CS) noise, and to extract the frequency offset from the frequencies of these spectral lines. Unlike in Chapter II, we will solve this spectral estimation problem by interpreting it from a CS-statistics viewpoint. Due to their $\pi/2$ -rotationally invariant symmetry properties, all QAM constellations satisfy the moment conditions $E\{w^2(n)\} = E\{w^3(n)\} = 0, E\{w^4(n)\} \neq 0$. This property will be exploited next to design FO-estimators based on the fourth-order CS-statistics of the received sequence.

Define the fourth-order conjugate time-varying correlations (for QAM constellations, the fourth-order cumulants and moments coincide) of the received sequence

$x(n)$ via: $\tilde{c}_{4x}(n; \mathbf{0}) := \text{E}\{x^4(n)\}$, with $\mathbf{0} := [0 \ 0 \ 0]$. For $P = 1$, it turns out that:

$$\tilde{c}_{4x}(n; \mathbf{0}) = \tilde{\kappa}_4 e^{j2\pi^4 f_e n} \sum_l h^4(l), \quad (3.4)$$

with $\tilde{\kappa}_4 := \text{cum}\{w(n), w(n), w(n), w(n)\} = \text{E}\{w^4(n)\}$. Similarly, for $P > 1$, we obtain:

$$\tilde{c}_{4x}(n; \mathbf{0}) = \tilde{\kappa}_4 e^{j2\pi^4 f_e n} \sum_l h^4(n - lP). \quad (3.5)$$

Being almost periodic with respect to n , the generalized Fourier Series (FS) coefficient of $\tilde{c}_{4x}(n; \mathbf{0})$, termed conjugate cyclic correlation, can be expressed for $P = 1$ as (c.f. [50], [73]):

$$\tilde{C}_{4x}(\alpha; \mathbf{0}) := \lim_{N \rightarrow \infty} \frac{1}{N} \sum_{n=0}^{N-1} \tilde{c}_{4x}(n; \mathbf{0}) e^{-j2\pi\alpha n} = \tilde{C}_{4x}(\alpha_0; \mathbf{0}) \delta(\alpha - \alpha_0), \quad (3.6)$$

where $\tilde{C}_{4x}(\alpha_0; \mathbf{0}) = \tilde{\kappa}_4 \sum_l h^4(l)$ and $\alpha_0 := 4f_e$. When $P > 1$, it follows that:

$$\tilde{C}_{4x}(\alpha; \mathbf{0}) = \sum_{k=0}^{P-1} \tilde{C}_{4x}\left(\alpha_0 + \frac{k}{P}; \mathbf{0}\right) \delta\left(\alpha - \left(\alpha_0 + \frac{k}{P}\right)\right), \quad (3.7)$$

where $\tilde{C}_{4x}(\alpha_0 + k/P; \mathbf{0}) = (\tilde{\kappa}_4/P) \sum_n h^4(n) \exp(-j2\pi kn/P)$.

Thus, $\tilde{C}_{4x}(\alpha; \mathbf{0})$ consists of a single spectral line located at $4f_e$ when $P = 1$, and P spectral lines located at the cyclic frequencies $4f_e + k/P$, $k = 0, 1, \dots, P-1$ when $P > 1$. An estimator of f_e can be obtained by determining the location of the spectral line present in $\tilde{C}_{4x}(\alpha; \mathbf{0})$ (see (3.6)):

$$f_e = \frac{1}{4} \left(\arg \max_{\dot{\alpha} \in (-0.5, 0.5)} \left| \tilde{C}_{4x}(\dot{\alpha}; \mathbf{0}) \right|^2 \right), \quad (3.8)$$

where the variable with a dot denotes a trial value. In practice, a computationally efficient FFT-based implementation of (3.8) can be obtained by adopting an asymptotically consistent sample estimate for conjugate cyclic correlation $\tilde{C}_{4x}(\alpha; \mathbf{0})$, which

takes the following form:

$$\hat{C}_{4x}(\alpha; \mathbf{0}) := \frac{1}{N} \sum_{n=0}^{N-1} x^4(n) e^{-j2\pi\alpha n} . \quad (3.9)$$

Plugging (3.9) back into (3.8), we obtain the estimator [91], [114]:

$$\hat{f}_e = \frac{1}{4} \left(\arg \max_{\hat{\alpha} \in (-0.5, 0.5)} \left| \hat{C}_{4x}(\hat{\alpha}; \mathbf{0}) \right|^2 \right) = \frac{1}{4} \left(\arg \max_{\hat{\alpha} \in (-0.5, 0.5)} \left| \frac{1}{N} \sum_{n=0}^{N-1} x^4(n) e^{-j2\pi\hat{\alpha}n} \right|^2 \right), \quad (3.10)$$

which is equivalent to (2.45) obtained in Chapter II with monomial order equal to 4.

In the case when $P > 1$, it is possible to design a FO-estimator that extracts f_e solely from knowledge of the location information of the spectral line of largest magnitude ($k = 0$). However, this approach leads again to the estimator (3.10). A different alternative is to extract the frequency offset by exploiting jointly the location information of all the P spectral lines. In this case, the FFT-based FO-estimator is obtained:

$$\begin{aligned} \hat{\alpha}_N &:= 4\hat{f}_e = \arg \max_{|\hat{\alpha}| < 1/(2P)} J_N(\hat{\alpha}), \quad (3.11) \\ J_N(\hat{\alpha}) &:= \sum_{k=0}^{P-1} \left| \hat{C}_{4x}\left(\hat{\alpha} + \frac{k}{P}; \mathbf{0}\right) \right|^2 = \sum_{k=0}^{P-1} \left| \frac{1}{N} \sum_{n=0}^{N-1} x^4(n) e^{-j2\pi(\hat{\alpha} + \frac{k}{P})n} \right|^2. \end{aligned}$$

Note that the condition $|F_e T| \leq 1/8$ is required in (3.10) and (3.11) in order to ensure identifiability of $F_e T$.

In the next subsection, we will establish in an unified manner the asymptotic performance of the proposed frequency estimators (3.10) and (3.11), and show the interrelation between the present class of cyclic estimators and the family of NLS estimators.

4. Asymptotic Performance Analysis

In order to show the equivalence between the present carrier frequency offset estimation problem and the problem of estimating the frequencies of a number of harmonics embedded in noise, it is helpful to observe that the conjugate time-varying correlation $\tilde{c}_{4x}(n; \mathbf{0})$ can be expressed as:

$$\tilde{c}_{4x}(n; \mathbf{0}) = \sum_{k=0}^{P-1} \tilde{C}_{4x}\left(\alpha_0 + \frac{k}{P}; \mathbf{0}\right) e^{j2\pi(\alpha_0 + \frac{k}{P})n} = \sum_{k=0}^{P-1} \lambda_k e^{j(\omega_k n + \phi_k)}, \quad (3.12)$$

where: $\lambda_k \exp(j\phi_k) := \tilde{C}_{4x}(\alpha_0 + k/P; \mathbf{0})$ and $\omega_k := (2\pi k/P) + 2\pi\alpha_0$.

Defining the zero-mean stochastic process $e(n)$ as:

$$e(n) := x^4(n) - \mathbb{E}\{x^4(n)\} = x^4(n) - \sum_{k=0}^{P-1} \tilde{C}_{4x}\left(\alpha_0 + \frac{k}{P}; \mathbf{0}\right) e^{j2\pi(\frac{k}{P} + \alpha_0)n}, \quad (3.13)$$

it follows that:

$$x^4(n) = \sum_{k=0}^{P-1} \tilde{C}_{4x}\left(\alpha_0 + \frac{k}{P}; \mathbf{0}\right) e^{j2\pi(\frac{k}{P} + \alpha_0)n} + e(n) = \sum_{k=0}^{P-1} \lambda_k e^{j(\omega_k n + \phi_k)} + e(n). \quad (3.14)$$

Thus, $x^4(n)$ can be interpreted as the sum of P constant amplitude harmonics corrupted by the cyclostationary noise $e(n)$ [18], [91].

Consider the NLS estimator:

$$\hat{\boldsymbol{\theta}} := \arg \min_{\boldsymbol{\theta}} J(\dot{\boldsymbol{\theta}}), \quad (3.15)$$

$$J(\dot{\boldsymbol{\theta}}) := \frac{1}{2N} \sum_{n=0}^{N-1} \left| x^4(n) - \sum_{k=0}^{P-1} \dot{\lambda}_k e^{j\dot{\phi}_k} e^{j2\pi(\dot{\alpha} + \frac{k}{P})n} \right|^2, \quad (3.16)$$

with the vector $\dot{\boldsymbol{\theta}} := [\dot{\lambda}_0 \cdots \dot{\lambda}_{P-1} \dot{\phi}_0 \cdots \dot{\phi}_{P-1} \dot{\alpha}]^T$. It has been shown that the FFT-based estimator (3.11) is asymptotically equivalent to the NLS-estimator (3.15) (see e.g., [91]). Hence, the proposed cyclic frequency offset estimator can be viewed as the NLS-estimator and the estimate $\hat{\alpha}_N$ is asymptotically unbiased and consistent [11], [47] and [91]. In order to compute the asymptotic performance of estimator

(3.11), it suffices to establish the asymptotic performance of NLS-estimator (3.15).

The following result, whose proof is deferred to Appendix C, holds [106]:

Theorem 7 *The asymptotic variance of the estimate $\hat{\alpha}_N$ is given by:*

$$\gamma := \lim_{N \rightarrow \infty} N^3 \mathbf{E}\{(\hat{\alpha}_N - \alpha_0)^2\} = \frac{3 \sum_{l_1, l_2=0}^{P-1} \mathbf{R}_{l_1}^H \mathbf{G}_{l_1, l_2} \mathbf{R}_{l_2}}{\pi^2 (\sum_{l=0}^{P-1} \mathbf{R}_l^H \mathbf{R}_l)^2}, \quad (3.17)$$

with

$$\mathbf{R}_l := \begin{bmatrix} \tilde{C}_{4x}(\alpha_0 + \frac{l}{P}; \mathbf{0}) \\ \tilde{C}_{4x}^*(\alpha_0 + \frac{l}{P}; \mathbf{0}) \end{bmatrix},$$

$$\mathbf{G}_{l_1, l_2} := \begin{bmatrix} S_{2e}(\frac{l_1 - l_2}{P}; \alpha_0 + \frac{l_1}{P}) & -\tilde{S}_{2e}(2\alpha_0 + \frac{l_1 + l_2}{P}; \alpha_0 + \frac{l_1}{P}) \\ -\tilde{S}_{2e}^*(2\alpha_0 + \frac{l_1 + l_2}{P}; \alpha_0 + \frac{l_1}{P}) & S_{2e}^*(\frac{l_1 - l_2}{P}; \alpha_0 + \frac{l_1}{P}) \end{bmatrix},$$

and $S_{2e}(\alpha; f)$ and $\tilde{S}_{2e}(\alpha; f)$ stand for the unconjugate and conjugate cyclic spectrum of $e(n)$ at cycle α and frequency f , respectively.

As an immediate corollary of Theorem 7, in the case when only the spectral line with the largest magnitude is considered, we obtain that the asymptotic variance of estimator (3.10) is given by:

$$\lim_{N \rightarrow \infty} N^3 \mathbf{E}\{(\hat{\alpha}_N - \alpha_0)^2\} = \frac{3 \mathbf{R}_0^H \mathbf{G}_{0,0} \mathbf{R}_0}{\pi^2 \|\mathbf{R}_0\|^4}. \quad (3.18)$$

Note that when $P = 1$, the autocorrelation $c_{2e}(n; \tau) := \mathbf{E}\{e^*(n)e(n+\tau)\}$ depends only on the lag τ , hence $e(n)$ is stationary w.r.t. its second-order autocorrelation function and the cyclic spectrum $S_{2e}(0; \alpha_0)$ coincides with the second-order stationary spectrum $S_{2e}(\alpha_0)$. The result (3.18) shows that the asymptotic variance of $\widehat{F_e T}$ converges as $O(N^{-3})$ and depends inversely proportionally to the SNR corresponding to the $k = 0$ spectral line $\text{SNR}_0 := |\tilde{C}_{4x}(\alpha_0; \mathbf{0})|^2 / \text{re}\{S_{2e}(0; \alpha_0) - \tilde{S}_{2e}(2\alpha_0; \alpha_0)\}$.

Evaluation of asymptotic variance (3.17) requires calculation of the unconju-

gate/conjugate cyclic spectra: $S_{2e}(\alpha; f)$ and $\tilde{S}_{2e}(\alpha; f)$, whose closed-form expressions will be presented in what follows.

Define the variables:

$$\kappa_8 := \text{cum}\left\{\underbrace{w^*(n), \dots, w^*(n)}_4, \underbrace{w(n), \dots, w(n)}_4\right\}, \quad \tilde{\kappa}_8 := \text{cum}\left\{\underbrace{w(n), \dots, w(n)}_8\right\},$$

and the fourth and sixth-order ($l = 4, 6$) moments/cyclic moments of $x(n)$ as follows:

$$m_{lx}(n; \underbrace{0, \dots, 0}_{l/2-1}, \underbrace{\tau, \dots, \tau}_{l/2}) := \mathbb{E}\{x^{*l/2}(n)x^{l/2}(n + \tau)\},$$

$$M_{lx}(k; \underbrace{0, \dots, 0}_{l/2-1}, \underbrace{\tau, \dots, \tau}_{l/2}) := \frac{1}{P} \sum_{n=0}^{P-1} m_{lx}(n; \underbrace{0, \dots, 0}_{l/2-1}, \underbrace{\tau, \dots, \tau}_{l/2}) e^{-j2\pi kn/P}.$$

Some lengthy calculations, whose details are illustrated in Appendix D, show that the following results hold [106]:

Proposition 1 *For $P = 1$, the unconjugate/conjugate cyclic spectra of $e(n)$ are given by:*

$$S_{2e}(\alpha_0) = \sum_{\tau} \left[16m_{2x}(\tau)m_{6x}(0, 0, \tau, \tau, \tau) + 18m_{4x}^2(0, \tau, \tau) \right. \\ \left. - 144m_{2x}^2(\tau)m_{4x}(0, \tau, \tau) + 144m_{2x}^4(\tau) \right] e^{-j2\pi\alpha_0\tau} + \frac{\kappa_8}{\tilde{\kappa}_4^2} |\tilde{C}_{4x}(\alpha_0; \mathbf{0})|^2,$$

$$\tilde{S}_{2e}(2\alpha_0; \alpha_0) = \sum_{\tau} \left[\tilde{\kappa}_8 \sum_l h^4(l)h^4(l + \tau) + 16\tilde{\kappa}_4^2 \sum_l h(l)h^3(l + \tau) \right. \\ \left. \cdot \sum_l h^3(l)h(l + \tau) + 18\tilde{\kappa}_4^2 \left(\sum_l h^2(l)h^2(l + \tau) \right)^2 \right],$$

respectively.

Proposition 2 *For $P > 1$, the unconjugate/conjugate cyclic spectra of $e(n)$ are given by:*

$$S_{2e}\left(\frac{k}{P}; \alpha_0 + \frac{l}{P}\right) = \sum_{\tau} [16\mathcal{V}_1 + 18\mathcal{V}_2 - 144\mathcal{V}_3 + 144\mathcal{V}_4] e^{-j2\pi(\alpha_0 + \frac{l}{P})\tau} \\ + \frac{\kappa_8 P}{\tilde{\kappa}_4^2} \tilde{C}_{4x}\left(\alpha_0 + \frac{l}{P}; \mathbf{0}\right) \tilde{C}_{4x}^*\left(\alpha_0 + \frac{l-k}{P}; \mathbf{0}\right),$$

$$\tilde{S}_{2e}\left(2\alpha_0 + \frac{k}{P}; \alpha_0 + \frac{l}{P}\right) = \sum_{\tau} [16\tilde{\mathcal{V}}_1 + 18\tilde{\mathcal{V}}_2 + \tilde{C}_{8x}(k; \tau)] e^{-j2\pi\frac{l}{P}\tau},$$

where:

$$\begin{aligned} \mathcal{V}_1 &:= \sum_{\substack{k_1, k_2=0 \\ k_1+k_2-k \equiv 0 \pmod{P}}}^{P-1} M_{2x}(k_1; \tau) M_{6x}(k_2; 0, 0, \tau, \tau, \tau), \\ \mathcal{V}_2 &:= \sum_{\substack{k_1, k_2=0 \\ k_1+k_2-k \equiv 0 \pmod{P}}}^{P-1} M_{4x}(k_1; 0, \tau, \tau) M_{4x}(k_2; 0, \tau, \tau), \\ \mathcal{V}_3 &:= \sum_{\substack{k_1, k_2, k_3=0 \\ k_1+k_2+k_3-k \equiv 0 \pmod{P}}}^{P-1} M_{2x}(k_1; \tau) M_{2x}(k_2; \tau) M_{4x}(k_3; 0, \tau, \tau), \\ \mathcal{V}_4 &:= \sum_{\substack{k_i=0 \\ \sum_i k_i - k \equiv 0 \pmod{P}}}^{P-1} \prod_{i=0}^3 M_{2x}(k_i; \tau), \\ \tilde{\mathcal{V}}_1 &:= \sum_{\substack{k_1, k_2=0 \\ k_1+k_2-k \equiv 0 \pmod{P}}}^{P-1} \tilde{C}_{4x_1}(k_1; \tau) \tilde{C}_{4x_3}(k_2; \tau), \\ \tilde{\mathcal{V}}_2 &:= \sum_{\substack{k_1, k_2=0 \\ k_1+k_2-k \equiv 0 \pmod{P}}}^{P-1} \tilde{C}_{4x_2}(k_1; \tau) \tilde{C}_{4x_2}(k_2; \tau), \\ \tilde{C}_{4x_i}(k; \tau) &:= \frac{\tilde{\kappa}_4}{P} \sum_n h^i(n) h^{4-i}(n + \tau) e^{-j2\pi\frac{kn}{P}}, \quad i = 1, 2, 3, \\ \tilde{C}_{8x}(k; \tau) &:= \frac{\tilde{\kappa}_8}{P} \sum_n h^4(n) h^4(n + \tau) e^{-j2\pi\frac{kn}{P}}. \end{aligned}$$

When $P = 1$, the discrete-time additive noise $v(n)$ is white. Then, it is not difficult to show that neither $S_{2e}(\alpha_0)$ nor $\tilde{S}_{2e}(2\alpha_0; \alpha_0)$ depends on f_e . Therefore, the asymptotic variance (3.18) is independent of the unknown frequency offset. The same conclusion holds in the case of $P > 1$ if the SNR is large enough ($N_0 \ll 1$).

5. Simulations

In this subsection, the experimental MSE results and theoretical asymptotic bounds will be compared. The experimental results are obtained by performing a number of

200 Monte Carlo trials assuming that the transmitted symbols are selected from a 4-QAM constellation with $\sigma_{2w}^2 = 1$. The transmitter and receiver filters are square-root raised cosine filters with roll-off factor $\rho = 0.5$, and the additive noise is generated by passing Gaussian white noise with variance N_0 through the square-root raised cosine filter. The signal-to-noise ratio is defined as: $\text{SNR} := 10 \log_{10}(\sigma_{2w}^2/N_0)$. All the simulations are performed assuming the frequency offset $F_e T = 0.011$ and unless otherwise noted, the number of transmitted symbols is $L = 128$.

In all figures except Figs. 22 and 25, the theoretical bounds of estimators (3.11) and (3.10) for $P = 1$ and $P = 4$ are represented by the solid line, dash-dot line and dash line, respectively. Their corresponding experimental results are plotted using solid line with squares, dash-dot line with circles, and dash line with stars, respectively.

Experiment 1-Performance w.r.t. SNR: Assuming the timing error $\epsilon = 0.3$, in Fig. 21 we compare the MSEs of the FO-estimators (3.10) and (3.11) with their theoretical asymptotic variances and the stochastic Cramér-Rao Bound (SCRb), which is represented by the solid line with triangles and evaluated as the inverse of the stochastic Fisher information matrix:

$$\begin{aligned} \mathbb{E}\{(\hat{f}_e - f_e)^2\} &\geq \mathbf{J}^{-1}(f_e) = \frac{N_0}{8\pi^2 T^2 \sum_{n=0}^{N-1} n^2 \sum_{l=0}^{N-1} |h(n-l)|^2} \\ &\doteq \frac{3N_0}{8\pi^2 T^2 N^3 \sum_{m=0}^M |h(m)|^2}, \\ \mathbf{J}(f_e) &= -\mathbb{E}_{\mathbf{w}} \mathbb{E} \left\{ \frac{\partial^2 \ln[f_{\mathbf{x}}(\mathbf{x}|\mathbf{w}, f_e)]}{\partial f_e^2} \right\} = \frac{8\pi^2 T^2}{N_0} \sum_{n=0}^{N-1} n^2 \sum_{l=0}^{N-1} |h(n-l)|^2, \end{aligned}$$

where M is the order of channel $\{h(m)\}$. It turns out that in the presence of ISI, the performance of FO-estimator (3.10) can be significantly improved by oversampling the output signal. This result is further illustrated by Fig. 23, where the MSE of the FO-estimator (3.10) is plotted vs. timing error ϵ , assuming again two different values

for the oversampling factor $P = 1$ and $P = 4$.

In the case of $P = 4$, from the comparison of the performances of estimators (3.10) and (3.11), which estimate f_e by taking into account the information provided by only one spectral line and all the P spectral lines of $\tilde{C}_{4x}(\alpha; 0)$, respectively, one can observe that both the theoretical and experimental results depicted in Fig. 21 show that estimator (3.11) does not improve significantly the performance of (3.10), especially in the more practical low and medium SNR ranges. In fact, the experimental MSE-results of (3.11) are even worse than those of (3.10) in the low SNR regime. This is due to the fact that the additional harmonics that are exploited in (3.11) have small magnitudes and their location information can be easily corrupted by the additive noise. Fig. 22 shows the magnitudes of these harmonics versus the cyclic frequency. Thus, taking into account all the harmonics appears not to be justifiable from a computational and performance viewpoint.

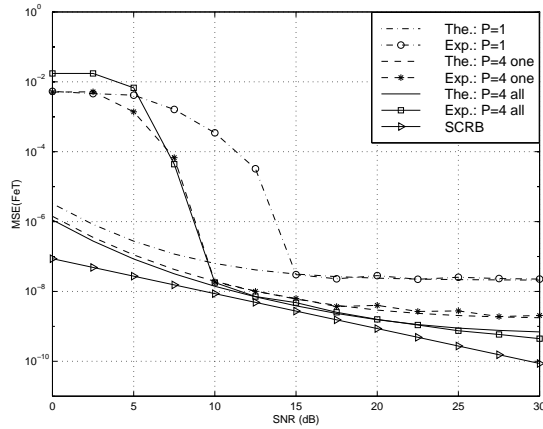


Fig. 21. MSEs of $\widehat{F_e T}$ versus SNR

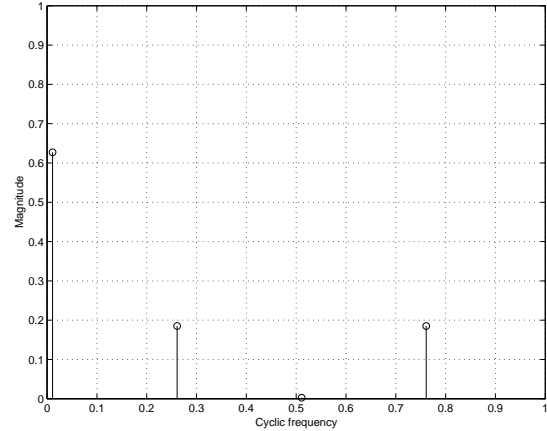


Fig. 22. Amplitudes of harmonics

Experiment 2-Performance w.r.t. timing error ϵ : In Fig. 23, the theoretical and experimental MSEs of the FO-estimator (3.10) are plotted versus the timing error ϵ ,

assuming the following parameters: SNR= 15 dB, and two oversampling factors $P = 1$ and $P = 4$. It turns out once again that oversampling of the received signal helps to improve the performance of symbol-spaced estimators and a significant improvement is achieved (several orders of magnitude) in the presence of large timing offsets ($\epsilon \approx 0.5$). Moreover, the oversampling-based FO-estimator is quite robust against the timing errors.

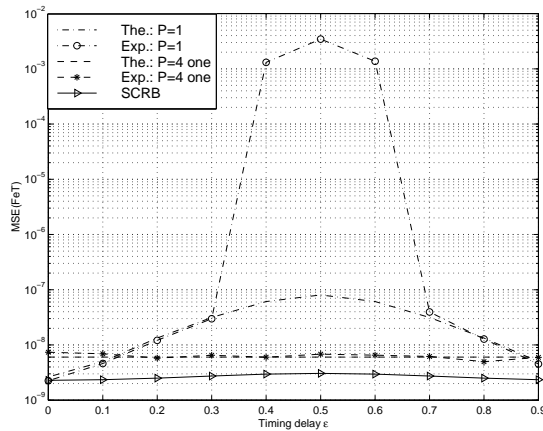


Fig. 23. MSEs of $\widehat{F_e T}$ versus ϵ

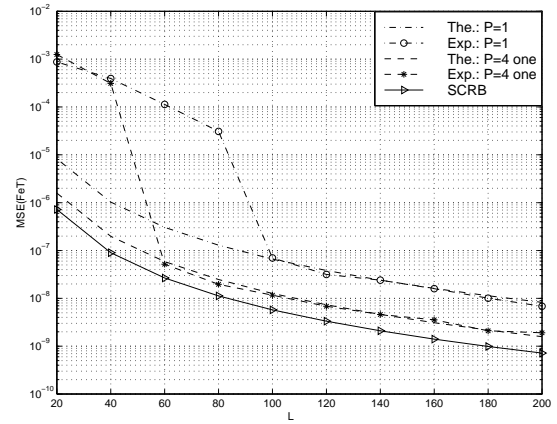


Fig. 24. MSEs of $\widehat{F_e T}$ versus L

Experiment 3-Performance w.r.t. the number of input symbols L : In Fig. 24, the theoretical and experimental MSEs of the FO-estimator (3.10) are plotted versus the number of input symbols L , assuming SNR= 15 dB, and timing delay $\epsilon = 0.3$. It can be seen that when the number of input symbols L increases, the experimental MSE-results are well predicted by the theoretical bounds derived above. This plot also shows the potential of these estimators for fast synchronization of burst transmissions since the proposed frequency estimator with $P > 1$ provides very good frequency estimates even when a reduced number of symbols are used ($L = 60 \div 80$ symbols).

Experiment 4-Performance w.r.t. the oversampling factor P : In this experiment, we

study more thoroughly the effect of the oversampling rate P on FO-estimators. By fixing $\text{SNR}=15\text{dB}$, $\epsilon = 0.3$ and varying the oversampling rate P , we compare the experimental MSEs of estimator (3.10) with its theoretical variance. The result is depicted in Fig. 25. It turns out that increasing P does not improve the performance of the FO-estimator as long as $P \geq 2$. This is a pleasing property since large sampling rates result in higher implementation complexity and hardware cost, which are not desirable for high-rate transmissions.

Experiment 5-Performance w.r.t. SNR in frequency-selective channels: Fig. 26 shows the results when the FO-estimator (3.10) is applied assuming a two-ray frequency-selective channel. Assuming the baseband channel impulse response $h_c^{(ch)}(t) = 1.4\delta(t-0.2T)+0.6\delta(t-0.5T)$, we compare the experimental MSEs with the theoretical asymptotic variances for estimator (3.10) in two scenarios: $P = 1$ and $P = 4$, respectively. Fig. 26 shows again the merit of the FO-estimator with $P > 1$.

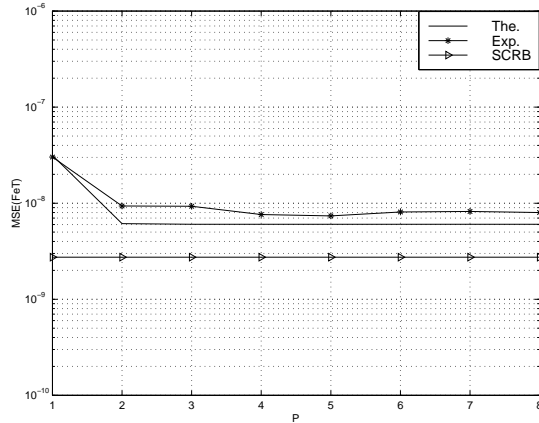


Fig. 25. MSEs of $\widehat{F_e T}$ versus oversampling factor P

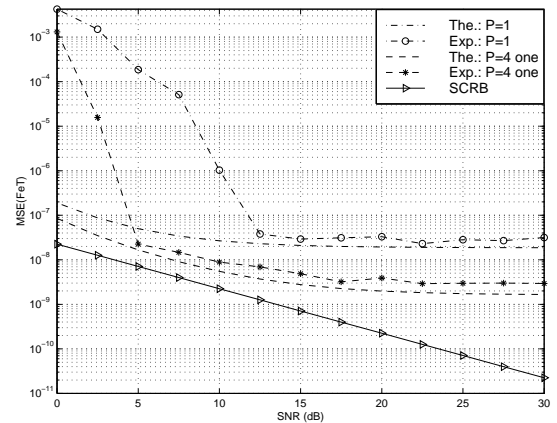


Fig. 26. MSEs of $\widehat{F_e T}$ versus SNR in frequency-selective channels

6. Conclusions

This section analyzed the performance of a class of non-data aided feedforward carrier frequency offset estimators for linearly modulated QAM-signals. It is shown that this class of cyclic frequency offset estimators is asymptotically a family of NLS-estimators that can be used for signals transmitted through unknown flat-fading or frequency-selective channels. The asymptotic performance of these estimators is established in closed-form expression and compared with the stochastic CRB. It is shown that this class of FO-estimators exhibits a high convergence rate, and in the presence of ISI-effects, its performance can be improved significantly by oversampling the received signal with a small oversampling factor ($P = 2$). This proposed work can be extended straightforwardly to other types of modulations (M-PSK, MSK).

B. On a Blind Fractionally-sampling Based Carrier Frequency Offset Estimator for Non-circular Transmissions

1. Introduction

This section shows that the estimation of the carrier frequency offset estimation can be significantly simplified when the constellation is non-circular (e.g., real-valued constellation such as BPSK), and accordingly, the performance analysis admits tractable forms due to the relatively simpler constellation structure compared with circular modulations [20].

In this section, the frequency offset estimator is designed in an optimized manner by exploiting efficiently all the conjugate second-order statistics that are present in the received waveform. We will prove rigorously the minimum MSE of the resulting carrier estimator invariant w.r.t. the oversampling factor P as soon as $P \geq 2$. Thus, selecting a low oversampling factor (e.g., $P = 2$) leads to an optimal carrier recovery

scheme that requires a low complexity receiver. From this perspective, the present carrier synchronizer represents a generalization of the estimators reported earlier by the authors in [18] and [112], which exploit only a subset of the received signal's conjugate second-order CS statistics.

We remark also that [21] represents a different extension of the results reported in [18], which proposes a unifying carrier frequency estimation framework that can be used for systems employing linear block precoders at the transmitter. However, only CDMA and OFDM modulation schemes are analyzed within this unifying transmitter precoding set-up [21].

Since the operation of oversampling the received waveform may be interpreted as a transmitter precoding scheme, the theoretical asymptotic performance analysis framework in [18] and [21] is exploited herein to design optimized frequency recovery schemes that operate on asynchronous signal samples taken at a rate faster than the symbol rate.

2. Proposed Estimator

We focus on single-carrier and single-user wireless communications channels. The continuous-time base-band received signal $y_c(t)$ can be expressed as follows :

$$y_c(t) = \left(\sum_{k \in \mathbf{Z}} s_k h_c(t - kT) \right) e^{2i\pi F_c t} + w_c(t),$$

where the symbol sequence $\{s_k\}$ transmitted at the baud rate $1/T$ is assumed to be non-circular (i.e., $E[s_k^2] \neq 0$), i.i.d. with zero-mean and unit-variance. The filter $h_c(t)$, with the FT $H_c(F)$, which is assumed to be time-limited and causal, and results from the convolution of the multipath propagation channel and the shaping filter, supposed of bandwidth $[-(1+\rho)/2T, (1+\rho)/2T]$, with the roll-off factor $\rho \in [0, 1]$. The additive noise $w_c(t)$ is assumed to be white circularly and normally distributed with power

spectral density $2N_0$. Finally, F_e stands for the analog carrier frequency offset, which may be induced by the local oscillator drifts and Doppler effects.

In general, the parameters F_e and $h_c(t)$ are unknown and have to be estimated in order to detect the transmitted data s_k . This section proposes an optimized frequency-offset compensator that does not require knowledge of the channel impulse response or training sequence. The proposed frequency estimator is implemented digitally and assumes at the front end of the receiver an anti-aliasing filter (AAF) $g_c(t)$, whose output is sampled at the rate $1/T_s = P/T$, where the oversampling factor P is an integer (see e.g., [63, p. 139]). The AAF is assumed to be an ideal low-pass filter (although less stringent conditions on the frequency response of the AAF may be adopted) with bandwidth B sufficiently large in order to preserve all the signal components at the filter output. The output of the AAF, denoted by $z_c(t)$, is sampled so that Nyquist's condition is satisfied $1/T_s = 2B$ (i.e., $B = P/2T$). Since $z_c(t) := g_c(t) * y_c(t)$, the following discrete-time channel model is obtained:

$$z(k) := z_c(kT_s) = \left(\sum_{m=0}^L l_m v_{k-m} \right) e^{2i\pi f_e k} + n(k), \quad (3.19)$$

where $\{v_k\}$ stands for the sequence obtained by padding $P - 1$ zeros between any two consecutive symbols $\{s_k\}$. Define also: $l(z) := \sum_{m=0}^L l_m z^{-m}$, with $l_m := (g_c(t) * h_c(t))|_{t=mT_s}$, the digital frequency offset $f_e := F_e T_s$, and the discrete-time white noise sequence $n(k) := (g_c(t) * w_c(t))|_{t=kT_s}$ of variance $\sigma^2 := \text{E}[|n(k)|^2] = 2N_0/T_s$.

Since the channel model (3.19) works as if one has transmitted the block sequence $[v_{kP}, \dots, v_{kP+P-1}] = \mathbf{k}^T s_n$, with $\mathbf{k} = [1, \mathbf{0}_{1,P-1}]^T$, (3.19) can be interpreted as a linearly precoded system. Consequently, we can use the frequency offset estimator [21] that holds for general linear precoders, described by a tall matrix \mathbf{K} . Let $\tilde{r}(n, \tau) := \text{E}[z(n + \tau)z(n)]$ denote the conjugate correlation at lag τ of $z(n)$, and define $\alpha_0 :=$

($2f_e$ modulo 1). Considering a Fourier series expansion of $\tilde{r}(n, \tau)$, we obtain:

$$\tilde{r}(n, \tau) = \sum_{p=0}^{P-1} \tilde{r}^{(\alpha_0+p/P)}(\tau) e^{2i\pi(\alpha_0+p/P)n}, \quad (3.20)$$

where $\tilde{r}^{(\alpha)}(\tau)$ stands for the conjugate cyclic correlation at lag τ and cyclic frequency α . Let \mathcal{A}_0 be a compact set included in $(0, \min(1/2, 1/P))$. According to (3.20), we get

$$\forall \alpha \in \mathcal{A}_0, \alpha \neq \alpha_0, \forall \tau, \forall p, \quad \tilde{r}^{(\alpha+p/P)}(\tau) = 0.$$

Then, an asymptotically unbiased and consistent estimate $\hat{\alpha}_N$ of α_0 is obtained as follows:

$$\hat{\alpha}_N := \arg \max_{\alpha \in \mathcal{A}_0} J_N(\alpha), \quad J_N(\alpha) := \sum_{p=0}^{P-1} \left\| \hat{\mathbf{r}}_{c,N}^{(\alpha+p/P)} \right\|_{\mathbf{W}_p}^2$$

where $\hat{\mathbf{r}}_{c,N}^{(\alpha)} := [\hat{r}_{c,N}^{(\alpha)}(-M), \dots, \hat{r}_{c,N}^{(\alpha)}(M)]^T$, M denotes a positive integer ($M \geq L$), and $\{\mathbf{W}_p\}_{p=0}^{P-1}$ is a sequence of positive-definite Hermitian matrices¹. The term $\hat{r}_{c,N}^{(\alpha)}(\tau) := (1/N) \sum_{n=0}^{N-1} z(n)z(n+\tau)e^{-2i\pi\alpha n}$ denotes a sample estimate of $\tilde{r}^{(\alpha)}(\tau)$, assuming N observations available.

A few observations are now in order. The introduced estimate is an extension of the estimator [112], which exploits only one cyclic correlation lag ($M = 0$). Second, the introduced estimator may be interpreted as a special case of the estimators proposed in [21], which are associated with different precoding schemes. Nevertheless, the design and analysis of the new estimator reported herein remain of interest and have not been reported in the literature.

By exploiting the results of [21], the consistency and asymptotic normality of $\hat{\alpha}_N$ can be established. In addition, a closed-form expression for the asymptotic

¹If \mathbf{x} and \mathbf{W} denote a vector and a positive Hermitian matrix, respectively, then by definition $\|\mathbf{x}\|_{\mathbf{W}}^2 := \mathbf{x}^H \mathbf{W} \mathbf{x}$.

covariance defined as:

$$\gamma := \lim_{N \rightarrow \infty} N^3 \mathbb{E}[(\hat{\alpha}_N - \alpha_0)^2], \quad (3.21)$$

may be obtained. Furthermore, in order to minimize the asymptotic variance γ , it can be shown that it is optimal to consider $M = L$ and $\mathbf{W}_p = \delta(p)\mathbf{I}_{2L+1}$ [21]. Simply stated, the extraction of the frequency offset should be performed based solely on the harmonic $\alpha_0 + p/P$ with $p = 0$, and all the cyclic correlation lags have to be taken into account. These results may be derived using similar techniques as the ones presented in [18] and [21], and will not be detailed herein. In the sequel, we focus on the estimate associated with such an optimal design setting and analyze its asymptotic performance.

3. Influence of the Oversampling Factor

As $M = L$ and $\mathbf{W}_p = \delta(p)\mathbf{I}_{2L+1}$, the closed-form expression of γ given in [21] can be reduced to

$$\gamma = \frac{3P\sigma^2}{\pi^2 a^2} (P\sigma^2 a + 2b),$$

with: $a := \int_{-1/2}^{1/2} |l(e^{2i\pi f})|^2 |l(e^{-2i\pi f})|^2 df$, and $b := \int_{-1/2}^{1/2} |l(e^{2i\pi f})|^4 |l(e^{-2i\pi f})|^2 df$.

To properly study the influence of the oversampling factor P on the performance of frequency estimator $\hat{\alpha}_N$, we evaluate the following term:

$$E_P = \mathbb{E}[(F_e T - \widehat{F_e T}|_{P, N_s})^2], \quad (3.22)$$

with $\widehat{F_e T}|_{P, N_s} := \hat{\alpha}_N P/2$ and $N_s := N/P$. In fact, E_P represents the theoretical mean-square error of the analog frequency offset estimate normalized with the symbol duration, assuming that the duration of the observation window is $N_s T$. From (3.21) and (3.22), it turns out that:

$$E_P = \frac{\gamma}{4PN_s^3}. \quad (3.23)$$

After some quite straightforward but very long calculations based on Poisson's formulae, (3.23) can be expressed as [20]:

$$E_P = \frac{3N_0}{\pi^2 N_s^3 \zeta_P^{(1)^2}} (N_0 T \zeta_P^{(1)} + \zeta_P^{(2)}),$$

with:

$$\begin{cases} \zeta_1^{(1)} := \int_{-1/2T}^{1/2T} |H_c(F)|^2 |H_c(-F)|^2 dF \\ \zeta_1^{(2)} := \int_{-1/2T}^{1/2T} |H_c(F)|^4 |H_c(-F)|^2 dF \end{cases} \quad \text{for } P = 1,$$

and

$$\begin{cases} \zeta_P^{(1)} := \int_{-1/T}^{1/T} |H_c(F)|^2 |H_c(-F)|^2 dF \\ \zeta_P^{(2)} := \int_{-1/T}^{1/T} |H_c(F)|^4 |H_c(-F)|^2 dF \end{cases} \quad \text{for } P \geq 2.$$

As soon as $P \geq 2$, $\zeta_P^{(1)}$ and $\zeta_P^{(2)}$ do not depend on P . Thus, the theoretical mean-square error is independent of P , a result which has been shown for QAM modulations by computer simulations in Fig. 25 and intuitively might be predicted based on Shannon's interpolation theorem, and is equal to zero in the noiseless case ($N_0 = 0$) (i.e., an asymptotically jitter-free timing recovery scheme).

4. Simulations

The Signal-to-Noise Ratio is expressed regardless of the oversampling factor as $\text{SNR} := \int_{\mathbb{R}} |H_c(F)|^2 dF / 2N_0$. We fix also $\rho = 0.2$, $f_e = 0.05$, $T = 3\mu s$, and the circularly distributed noise $n(k)$ is assumed white and Gaussian. The theoretical and experimental MSE of the frequency estimator are obtained by averaging E_P and $\|F_e T - \widehat{F_e T}\|_{P, N_s}^2$ over $MC = 100$ Monte-Carlo trials, respectively. At each trial, a (slow Rayleigh) fading multipath propagation channel with three paths is adopted. The complex amplitudes of the paths are normally distributed and the timing delays assume uniform distributions in $[0, 3T]$. As it is usually performed, we proceed in two steps to obtain the frequency offset estimate: first, a *coarse* search step is performed to maximize

the criterion $J_N(\alpha)$ via a FFT. Then, a *fine* search step is performed based on a gradient algorithm, initialized with the estimate provided by the coarse search step. Since the asymptotic analysis studies the behavior of the criterion around the true point α_0 , this analysis does not provide any relevant information on the performance of the first step, which optimizes the criterion over an FFT grid of frequencies spread on the entire interval $[0, 1/P]$. The performance of the first step can be relevantly evaluated by means of the occurrence probability of a wrong detection of the peak, which normally should occur around α_0 . Figure 27 depicts the number of samples N_s with respect to SNR for which the probability of failure is less than 1%. In fact, the amplitude of the spectral line localized at frequency α_0 depends on the terms $\zeta_P^{(k)}$, $k = 1, 2$. We have observed that the false detection occurs whenever the terms $\zeta_P^{(k)}$, $k = 1, 2$, are numerically weak, in general smaller than the noise variance.

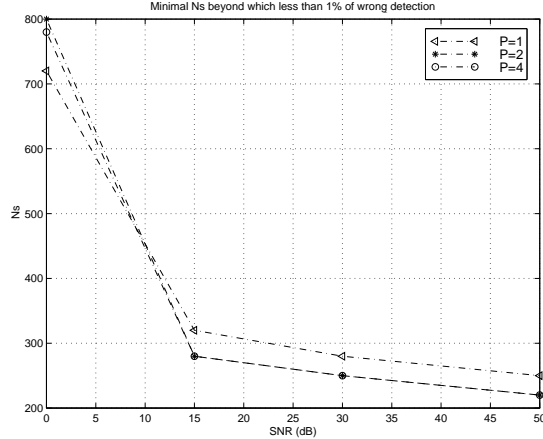


Fig. 27. Lower bound for N_s

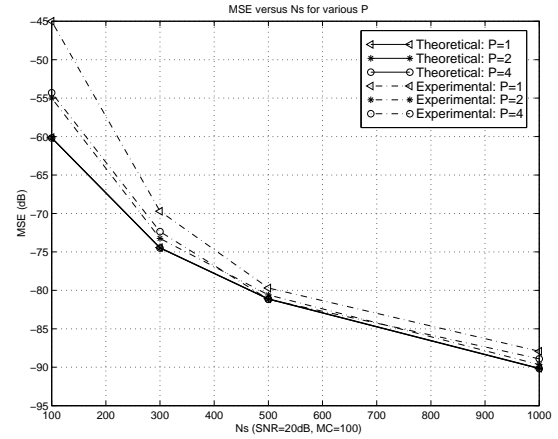


Fig. 28. MSE versus N_s

In the sequel, we only consider the trials which succeeded to detect the right peak. Figure 28 plots the MSE versus N_s . We observe that the MSE is proportional to $O(1/N_s^3)$. For the remaining simulations, we fix $N_s = 500$. Figure 29 plots the

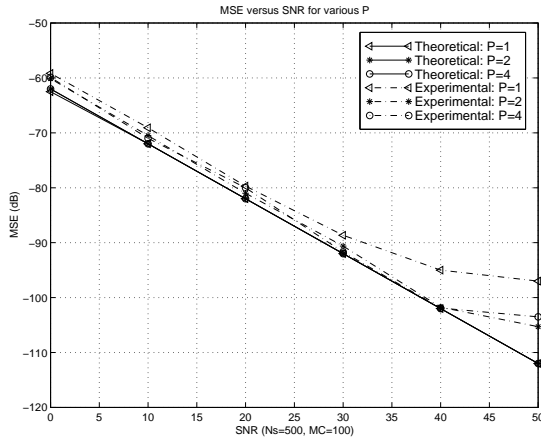
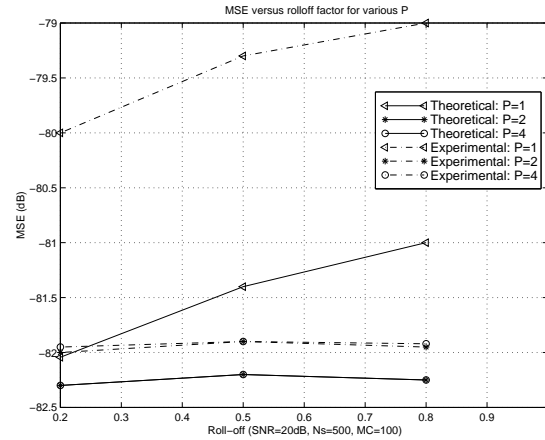


Fig. 29. MSE versus SNR

Fig. 30. MSE versus ρ

MSE versus SNR, and shows that the performance of the baud-rate estimator is worse than the performance of the oversampled estimator. In Figure 30, we depict the MSE versus ρ . For $P \geq 2$, the performance is quite the same with respect to ρ . On the contrary, for $P = 1$, the theoretical and experimental performances slightly degrade as ρ increases. Indeed, as the roll-off factor increases, the loss of information becomes more important. Judicious exploitation of the entire statistical information requires to select $P > 1$. In all the figures, one can observe that the performance is independent of the oversampling factor P as soon as $P \geq 2$. In addition, the estimation performance corresponding to the oversampled case ($P \geq 2$) is always better than the baud-rate case ($P = 1$).

5. Conclusions

We have investigated the theoretical and experimental MSE-performances of a blind frequency offset estimator based on the conjugate cyclostationary statistics of the oversampled received signal. In perfect agreement with Shannon's interpolation theorem, we deduced that for optimum performance the oversampling factor does not need to be larger than two. Consequently, receivers with reduced sampling rates (complexity) may be designed without any loss in performance.

CHAPTER IV

BLIND FEEDFORWARD CYCLOSTATIONARITY-BASED TIMING
ESTIMATION FOR LINEAR MODULATIONS

Timing recovery is a challenging but very important task for reliable detection in synchronous receivers. To implement the receiver in a fully digital way, it requires the output waveform of the matched filter to be over-sampled by a free-running oscillator at a fixed rate faster than the symbol rate, and all further processing to be performed digitally based on these samples [75]. This means that the timing recovery consists of two distinct operations: timing estimation and timing correction, where the timing correction serves to provide the decision device with optimum decision metrics generated from the given samples by some sort of interpolation, which is controlled by the result of timing estimation [63], [75].

For bandwidth efficiency reasons, non-data aided or blind timing estimation architectures have received much attention during the last decade. Up until recently, a lot of blind timing estimators have been proposed for linear modulations transmitted through time non-selective flat-fading channels [41], [44], [63], [66], [71], [75], [78], [85] and [90]. In [85], feedback schemes are proposed. However, it is known that feedback schemes have good tracking performance and exhibit comparatively long acquisitions due to hangup phenomena, which is not desirable in short bursts [63], [71]. Therefore, blind feedforward hangup-free schemes have received considerable attention [41], [44], [63], [71], [75], [78] and [90].

Originally in [75], Oerder and Meyr proposed a blind feedforward square timing recovery technique for digital data transmission by linear modulation schemes, which we refer to as the O&M estimator. Several extensions as well as estimators similar in form to the O&M estimator were later reported in [41], [44] and [90]. It is not difficult

to observe that a subclass of blind feedforward timing estimators proposed in [41], [44] and [90] reduces to the O&M estimator provided that the timing lag is fixed to $\tau = 0$ in [41, Eq. 6], [44, Eq. 11] and [90, Eq. 2.18]. These estimators, along with the methods presented in [66], employ a second-law nonlinearity (SLN) on the received samples, and exhibit weak performance when operating with narrowband signaling pulses [58] and [71]. With the assumption of low SNR and PSK constellations, [71] proposes an *ad hoc* feedforward SNR-dependent ML-based timing estimator that assumes a logarithmic nonlinearity (LOGN) and is shown to exhibit better performance than the SLN (O&M) estimator. However, good estimates are obtained by fixing the SNR value to 5 dB. Moreover, since its performance analysis is not fully investigated, no thorough conclusions may be drawn [71]. Reference [78] proposes an approximate performance analysis of the SLN, fourth-law (FLN), and absolute value (AVN) nonlinearities based estimators assuming BPSK modulations and a stationary statistics framework.

Irrespective of the nonlinearity function used, one of the common features of all the above mentioned blind feedforward timing estimators is the exploitation of the cyclostationary (CS) statistics induced by oversampling the received signal. The role of cyclostationarity in synchronization was clearly acknowledged in [5] and [35], and a general CS framework for timing estimation was introduced by Gini and Giannakis in [44]. In this chapter, first we will analyze by exploiting the CS-statistics of the received signal the asymptotic performance of the estimators [41] and [44], which were proposed to estimate jointly the symbol timing and carrier frequency offset, then propose a CS-based general framework to develop efficient estimators, and rigorous and thorough performance analysis set-ups for the existing blind timing estimators. Several important and novel conclusions will be drawn. Finally, we will present an alternative two-sample-per-symbol based timing estimator, which exhibits very low computational complexity. This study relies on the novel cyclostationary signal

processing techniques developed in [19], [103].

A. Performance Analysis of Blind Frequency Offset and Symbol Timing Estimators GG and GSD

1. Introduction

The goal of this section is to analyze the performance of the feedforward non-data aided carrier frequency offset and symbol timing delay estimators [41] and [44] w.r.t. the pulse shape bandwidth and the oversampling factor. The theoretical asymptotic performance of the Gini-Giannakis (GG) [44] and Ghogho-Swami-Durrani (GSD) [41] estimators is established, and it is shown that the performance of these estimators does not improve by selecting a large value for the oversampling factor ($P > 3$), and the accuracy of the timing delay estimators can increase by choosing pulse shapes with larger bandwidths. By properly taking into account the aliasing effects, it is shown that the expressions of the symbol timing delay estimators take a slightly different form than the expressions reported in [41] and [44] when $P = 2$.

2. Modeling Assumptions

Consider the baseband representation of a linearly modulated signal transmitted through a flat-fading channel. The receiver output is expressed as (see e.g., [41] and [44]):

$$x_c(t) = \mu_c(t)e^{2i\pi F_e t} \sum_l w(l)h_c(t - \epsilon T - lT) + v_c(t), \quad (4.1)$$

where $\mu_c(t)$ is the fading-induced noise, $\{w(l)\}$ is a sequence of zero-mean unit variance i.i.d. symbols, $h_c(t)$ denotes the convolution of the transmitter's signaling pulse and the receiver filter, $v_c(t)$ is the complex-valued additive noise, T is the symbol period, F_e and ϵ stand for carrier frequency offset and symbol timing delay, respec-

tively, and represent the parameters to be estimated by exploiting the second-order cyclostationary-statistics of the received waveform.

By fractionally oversampling the received signal $x_c(t)$ with the sampling period $T_s := T/P$ ($P \geq 2$), the following discrete-time channel model is obtained:

$$x(n) = \mu(n)e^{2i\pi F_e T n/P} \sum_l w(l)h(n - lP) + v(n), \quad (4.2)$$

with $x(n) := x_c(nT_s)$, $\mu(n) := \mu_c(nT_s)$, $v(n) := v_c(nT_s)$, and $h(n) := h_c(nT_s - \epsilon T)$.

In order to derive the asymptotic performance of estimators [41], [44], without any loss in generality we assume the following:

(AS1) $w(n)$ is a zero-mean i.i.d. sequence with values drawn from a linearly modulated complex constellation with unit variance, i.e., $\sigma_w^2 := \mathbb{E}\{|w(n)|^2\} = 1$.

(AS2) $\mu(n)$ is a constant fading-induced noise with unit power. Later on, this assumption will be relaxed by considering that $\mu(n)$ is a time-selective fading process.

(AS3) $v(n)$ is a complex-valued zero-mean Gaussian process independent of $w(n)$, with variance σ_v^2 , which satisfies the mixing conditions [26], [44].

(AS4) the combined filter $h_c(t)$ is a raised cosine pulse of bandwidth $[-(1+\rho)/2T, (1+\rho)/2T]$, where the roll-off factor ρ satisfies $(0 \leq \rho < 1)$ [83, Ch. 9].

(AS5) frequency offset F_e is small enough so that the mismatch of the receive filter due to F_e can be neglected [44]. Generally, the condition $F_e T < 0.2$ is assumed. This assumption is required to ensure the validity of channel models (4.1), (4.2).

Based on these assumptions, in the ensuing subsection we introduce the non-data aided estimators of F_e and ϵ proposed in [44] (GG) and [41] (GSD).

3. Frequency Offset and Symbol Timing Estimators for Time-invariant Channels

a. Usual Definitions

The time-varying correlation of the nonstationary process $x(n)$ is defined as

$$r_{2x}(n; \tau) := \mathbb{E}\{x^*(n)x(n + \tau)\},$$

where τ is an integer lag. By exploiting Eq. (4.2) and taking into account the assumptions **(AS1)**–**(AS3)**, straightforward calculations lead to

$$r_{2x}(n; \tau) = r_{2x}(n + P; \tau), \quad \forall n, \tau.$$

Being periodic, $r_{2x}(n; \tau)$ admits a Fourier Series expansion

$$r_{2x}(n; \tau) = \sum_{k=0}^{P-1} R_{2x}(k; \tau) e^{2i\pi \frac{kn}{P}},$$

whose Fourier's coefficients, also termed cyclic correlations, are given for $k = 0, \dots, P-1$ by the following expression [41], [44]:

$$R_{2x}(k; \tau) := \frac{1}{P} \sum_{n=0}^{P-1} r_{2x}(n; \tau) e^{-2i\pi \frac{kn}{P}}.$$

The frequencies k/P (or simply k), for $k = 0, \dots, P-1$, are referred to as cyclic frequencies or cycles [43]. Furthermore, from these cyclic correlations, it is usual to define a cyclic spectrum for each cyclic frequency k , as follows:

$$S_{2x}(k; f) := \sum_{\tau} R_{2x}(k; \tau) e^{-2i\pi \tau f}. \quad (4.3)$$

We also define the conjugate second-order time-varying correlation of $x(n)$ as

$$\tilde{r}_{2x}(n; \tau) := \mathbb{E}\{x(n)x(n + \tau)\}.$$

It is easy to check that $\tilde{r}_{2x}(n; \tau)$ can be expressed as

$$\tilde{r}_{2x}(n; \tau) = \sum_{k=0}^{P-1} \tilde{R}_{2x}(k; \tau) e^{2i\pi \frac{(k+2F_e T)n}{P}},$$

and the conjugate cyclic correlation $\tilde{R}_{2x}(k; \tau)$ can be obtained by the generalized

Fourier Series expansion [43]:

$$\tilde{R}_{2x}(k; \tau) := \lim_{N \rightarrow \infty} \frac{1}{N} \sum_{n=0}^{N-1} \tilde{r}_{2x}(n; \tau) e^{-2i\pi \frac{(k+2F_e T)n}{P}}.$$

Similarly to Eq. (4.3), we can define the conjugate cyclic spectrum $\tilde{S}_{2x}(k; f)$ as the FT of the sequence $\{\tilde{R}_{2x}(k; \tau)\}_\tau$.

In practice, the cyclic correlations $R_{2x}(k; \tau)$ have to be estimated from a finite number of samples N , and the standard sample estimate of $R_{2x}(k; \tau)$ is given by (see e.g., [25], [43], [44]):

$$\hat{R}_{2x}(k; \tau) = \frac{1}{N} \sum_{n=0}^{N-\tau-1} x^*(n)x(n+\tau) e^{-2i\pi \frac{kn}{P}}, \quad \tau \geq 0,$$

which, under **(AS3)**, is asymptotically unbiased and mean square sense (m.s.s.) consistent.

b. Closed-form Expressions for the Second-order Statistics

We now focus on the closed-form expressions of the second order statistics of the received signal obeying the model (4.2).

According to Eq. (4.2), we obtain

$$R_{2x}(k; \tau) = \frac{\sigma_w^2}{P} e^{2i\pi \frac{F_e T \tau}{P}} \left(\sum_n h^*(n) h(n+\tau) e^{-2i\pi \frac{kn}{P}} \right) + \sigma_v^2 h_{rc}(\tau) \delta(k), \quad (4.4)$$

where $h_{rc}(n) := h_c(t)|_{t=nT_s}$. In order to show the dependency of $R_{2x}(k; \tau)$ on the timing delay ϵ , which is hidden in the expression of the discrete-time channel $h(n)$, an alternative expression for $R_{2x}(k; \tau)$ is next derived, based on the Parseval's relation.

First, the sum in (4.4) can be rewritten as

$$\sum_n h^*(n) h(n+\tau) e^{-2i\pi \frac{kn}{P}} = \int_{-\frac{1}{2}}^{\frac{1}{2}} H^*(f) H(f + \frac{k}{P}) e^{2i\pi (f + \frac{k}{P}) \tau} df,$$

where $H(f)$ denotes the FT of $h(n)$. In a similar way (see Eq. (4.4)), we obtain:

$$\tilde{R}_{2x}(k, \tau) = \frac{\sigma_{c,w}^2}{P} e^{2i\pi \frac{F_c T \tau}{P}} \left(\sum_n h(n) h(n + \tau) e^{-2i\pi \frac{kn}{P}} \right),$$

with $\sigma_{c,w}^2 := E\{w^2(n)\}$.

In order to point out the influence of the oversampling factor, we wish to express the cyclic correlations w.r.t. the continuous-time filter $h_c(t)$. Since the bandwidth of $h_c(t)$ is less than $1/T$ and the oversampling rate is equal to or larger than $2/T$, the oversampling does not introduce any aliasing for Fourier transform of $h(n)$. Therefore, thanks to Poisson's sum, it follows that for $|f| \leq 1/2$ [76, Ch. 3]:

$$\forall P \geq 2, \quad H(f) = \frac{1}{T_s} H_c \left(\frac{f}{T_s} \right) e^{-2i\pi f P \epsilon}, \quad (4.5)$$

where $H_c(F)$ stands for the FT of $h_c(t)$. As shown in [41] and [44], we can also express $H(f + k/P)$ for $|f| \leq 1/P$ and $k = \pm 1$ (the cycle $k = -1$ is equivalent to $k = P - 1$ by periodicity) as follows:

$$\forall P \geq 3, \quad H(f + k/P) = \frac{1}{T_s} H_c \left(\frac{f + k/P}{T_s} \right) e^{-2i\pi (f + \frac{k}{P}) P \epsilon}. \quad (4.6)$$

Based on the previous equations, we can obtain the following formula [44]:

$$\forall P \geq 3, \quad R_{2x}(k; \tau) = \frac{\sigma_w^2}{P} e^{2i\pi \frac{F_c T \tau}{P}} e^{i\pi \frac{k\tau}{P}} e^{-2i\pi k \epsilon} G(k; \tau) + \sigma_v^2 h_{rc}(\tau) \delta(k), \quad (4.7)$$

where

$$G(k; \tau) := \frac{P}{T} \int_{-1/2T}^{1/2T} H_c \left(F - \frac{k}{2T} \right) H_c \left(F + \frac{k}{2T} \right) e^{2i\pi \frac{\tau T F}{P}} dF.$$

Unlike [41] and [44], we have observed that Eq. (4.6) cannot be used in the case when $P = 2$. Indeed, if $P = 2$, then the aliasing effects due to frequency-shifting have to be taken into account. Therefore, Eq. (4.7) does not hold anymore except for

$k = 0$. For $P = 2$ and $|f| \leq 1/2$, the Poisson's sum leads to

$$H(f + 1/2) = \frac{1}{T_s} \left[H_c\left(\frac{f + 1/2}{T_s}\right) e^{-2i\pi\epsilon} + H_c\left(\frac{f - 1/2}{T_s}\right) e^{2i\pi\epsilon} \right] \cdot e^{-4i\pi f\epsilon}.$$

For $P = 2$ and $k = 1$, it follows that:

$$R_{2x}(k; \tau) = \sigma_w^2 e^{i\pi(F_e T + 1)\tau} \cos \left[2\pi \left(\epsilon + \frac{\tau}{4} \right) \right] G(k; \tau). \quad (4.8)$$

Due to the symmetry property of the raised-cosine function $h_c(t)$, one can notice that $H_c(F)$ is a real-valued even function [83, p. 546]. Then, it is easy to check that $G(k; \tau)$ is a real-valued function. Moreover, due to the band-limited property of the filter $h_c(t)$, $G(k; \tau)$ is nonzero only for cycles $k = 0, \pm 1$. In the same way, since $x(n)$ is given by the Eq. (4.2), it is well known that the cyclic spectrum of $x(n)$, can be expressed for $k \neq 0$ as (c.f. [100]):

$$S_{2x}(k; f) = \frac{\sigma_w^2}{P} H(f - F_e T_s) H^*(f - F_e T_s - k/P). \quad (4.9)$$

It follows that the supports of the functions $f \rightarrow H(f - F_e T_s)$ and $f \rightarrow H^*(f - F_e T_s - k/P)$ are disjoint as far as the cycles $|k| > 1$, which leads to no cyclic correlation information ($|S_{2x}(k; f)| = 0, \forall f$, and hence $|R_{2x}(k; \tau)| = 0$, for $|k| > 1$). In a similar way, the conjugate cyclic spectrum can be expressed as follows:

$$\tilde{S}_{2x}(k; f) = \frac{\sigma_{c,w}^2}{P} H(f - F_e T_s) H(F_e T_s + k/P - f).$$

c. The GG and GSD Estimators

The GG estimator determines the frequency offset F_e and the timing delay ϵ

based on the following equations [44, Eqs. (24), (25)]

$$\begin{cases} \hat{f}_e &= \frac{P}{4\pi T\tau} \arg\{\hat{R}_{2x}(1;\tau)\hat{R}_{2x}(-1;\tau)\}, \text{ for } P \geq 2, \\ \hat{\epsilon} &= -\frac{1}{2\pi} \arg\{\hat{R}_{2x}(1;\tau)e^{-2i\pi(\hat{f}_e T+1/2)\tau/P}\}, \text{ for } P \geq 3, \\ \hat{\epsilon} &= \frac{1}{2\pi} \arccos\left\{\operatorname{re}\left(\frac{\hat{R}_{2x}(1;\tau)e^{-i\pi(\hat{f}_e T+1)\tau}}{\sigma_w^2 G(1;\tau)}\right)\right\} - \frac{\tau}{4}, \text{ for } P = 2. \end{cases} \quad (4.10)$$

The last equation in the array (4.10) represents the right form of the GG symbol timing delay estimator in the case when $P = 2$, and its expression follows directly from the Eq. (4.8).

Note that the estimator presented in [90] can be obtained by choosing $\tau = P$ in (4.10). For sake of clarity, throughout this section, we choose $\tau = 1$ for the GG estimator. In this case, one can see that the GSD frequency offset estimator [41, Eq. (7)] coincides with the GG algorithm. Consequently, it is sufficient to analyze the GG frequency offset estimator. In contrast, the timing delay estimator corresponding to the GSD algorithm [41, Eq. (8)] is different than the GG symbol timing delay estimator and is given by the following equations

$$\begin{cases} \hat{\epsilon} = -\frac{1}{2\pi} \arg\{\hat{R}_{2x}(1;0)\}, \text{ for } P \geq 3, \\ \hat{\epsilon} = \frac{1}{2\pi} \arccos\left\{\operatorname{re}\left(\frac{\hat{R}_{2x}(1;0)}{\sigma_w^2 G(1;0)}\right)\right\}, \text{ for } P = 2. \end{cases} \quad (4.11)$$

In the next subsection, we establish the asymptotic variances of estimators (4.10)-(4.11), which are defined as follow:

$$\gamma_{F_e} := \lim_{N \rightarrow \infty} \operatorname{NE}\{(\hat{F}_e - F_e)^2\}, \quad \gamma_{\epsilon} := \lim_{N \rightarrow \infty} \operatorname{NE}\{(\hat{\epsilon} - \epsilon)^2\}.$$

4. Performance Analysis for Time-invariant Channels

In order to establish the asymptotic variance of the asymptotically unbiased and consistent estimators (4.10)-(4.11), it is necessary to evaluate the normalized unconjugate/conjugate asymptotic covariances of the cyclic correlations which are defined

as:

$$\begin{aligned}\Gamma_{u,v}^{(k,l)} &= \lim_{N \rightarrow \infty} NE\{(\hat{R}_{2x}(k; u) - R_{2x}(k; u))(\hat{R}_{2x}(l; v) - R_{2x}(l; v))^*\}, \\ \tilde{\Gamma}_{u,v}^{(k,l)} &= \lim_{N \rightarrow \infty} NE\{(\hat{R}_{2x}(k; u) - R_{2x}(k; u))(\hat{R}_{2x}(l; v) - R_{2x}(l; v))\}.\end{aligned}$$

As the estimators (4.10)-(4.11) are dealing only with the cyclic correlations at cycles $k = \pm 1$, we concentrate, in the sequel, on the derivation of the asymptotic covariances of the cyclic correlations for $k, l = \pm 1$. According to [15], we obtain:

$$R_{2x}(k; \tau) = e^{2i\pi \frac{k\tau}{P}} R_{2x}^*(-k; -\tau),$$

which implies that

$$\tilde{\Gamma}_{u,v}^{(k,l)} = e^{2i\pi \frac{lv}{P}} \Gamma_{u,-v}^{(k,-l)}. \quad (4.12)$$

Thus, it is sufficient to evaluate Γ since $\tilde{\Gamma}$ can be obtained directly based on Eq. (4.12). In [19], $\Gamma^{(1,1)}$ and $\tilde{\Gamma}^{(1,1)}$ are obtained only for circular input sequences (i.e., input sequences which satisfy the condition $E\{w(n)w(n + \tau)\} = 0$). The following proposition, which is an extension of the results presented in [19], is established in the Appendix E.

Proposition 3 *The asymptotic variances of the cyclic correlation estimates are given by:*

$$\begin{aligned}\Gamma_{u,v}^{(1,1)} &= \sum_{k=0}^{P-1} e^{2i\pi \frac{kv}{P}} \int_0^1 S_{2x}(k; f) S_{2x}^*(k; f - \frac{1}{P}) e^{2i\pi(u-v)f} df \\ &+ \sum_{k=0}^{P-1} e^{-2i\pi \frac{(1+k+2FeT)v}{P}} \int_0^1 \tilde{S}_{2x}(k; f) \tilde{S}_{2x}^*(k; f - \frac{1}{P}) e^{2i\pi(u+v)f} df + \kappa P R_{2x}(1; u) R_{2x}^*(1; v), \\ \Gamma_{u,v}^{(1,-1)} &= \sum_{k=0}^{P-1} e^{2i\pi \frac{kv}{P}} \int_0^1 S_{2x}(k; f) S_{2x}^*(k-2; f - \frac{1}{P}) e^{2i\pi(u-v)f} df \\ &+ \sum_{k=0}^{P-1} e^{2i\pi \frac{(1-k-2FeT)v}{P}} \int_0^1 \tilde{S}_{2x}(k; f) \tilde{S}_{2x}^*(k-2; f - \frac{1}{P}) e^{2i\pi(u+v)f} df + \kappa P R_{2x}(1; u) R_{2x}^*(-1; v),\end{aligned}$$

$$\Gamma_{u,v}^{(-1,1)} = \Gamma_{v,u}^{*(1,-1)}, \quad \Gamma_{u,v}^{(-1,-1)} = e^{2i\pi\frac{(v-u)}{P}} \Gamma_{-v,-u}^{(1,1)},$$

and κ denotes the kurtosis of $w(n)$.

In the above proposition, some terms within the sums may cancel out. Indeed, since the filter $h_c(t)$ is band-limited, the cyclic spectra at cycles $|k| > 1$ are zero. This remark implies, for example, that if $P > 2$, then only the terms driven by the index $k = 0$ remain in the expression of $\Gamma^{(1,1)}$ and $k = 1$ in $\Gamma^{(1,-1)}$. When $P = 2$, only $\Gamma^{(1,1)}$ is needed since $R_{2x}(1; \tau) = R_{2x}(-1; \tau)$.

a. Performance Analysis of the GG Estimator

The asymptotic performance of the GG estimator is established in the Appendix E. The following proposition sums up the expressions of the asymptotic variance of the GG frequency offset estimator.

Proposition 4 *For $P \geq 3$, the asymptotic variance of the frequency offset estimator (4.10) is given by:*

$$\gamma_{F_e} = \frac{P^4 \left(\Psi^T \Gamma \Psi^* - \text{re}\{e^{-4i\pi F_e T/P} \Psi^T \tilde{\Gamma} \Psi\} \right)}{32\pi^2 T^2 \sigma_w^4 G^2(1; 1)}$$

where

$$\Psi = [\psi, \psi^*]^T, \quad \psi = e^{2i\pi(\epsilon-1/2P)},$$

$$\Gamma = \begin{bmatrix} \Gamma_{1,1}^{(1,1)} & \Gamma_{1,1}^{(1,-1)} \\ \Gamma_{1,1}^{(-1,1)} & \Gamma_{1,1}^{(-1,-1)} \end{bmatrix},$$

and $\tilde{\Gamma}$ is defined in a similar way as Γ .

For $P = 2$, the asymptotic variance of the frequency offset estimator (4.10) is given by:

$$\gamma_{F_e} = \frac{\mathbf{1}^T \Gamma \mathbf{1} - \text{re}\{e^{-2i\pi F_e T} \mathbf{1}^T \tilde{\Gamma} \mathbf{1}\}}{8\pi^2 T^2 \sigma_w^4 \sin^2(2\pi\epsilon) G^2(1; 1)},$$

with $\mathbf{1} = [1, 1]^T$.

The closed-form expression of the GG timing symbol delay estimator is drawn in the following proposition.

Proposition 5 *For $P \geq 3$, the asymptotic variance of the timing delay estimator (4.10) is given by:*

$$\gamma_\epsilon = \frac{P^2 \operatorname{re}\{e^{-4i\pi F_e T/P} \tilde{\mathbf{\Gamma}}_{1,1}^{(1,-1)} - \psi^2 \mathbf{\Gamma}_{1,1}^{(1,-1)}\}}{8\pi^2 \sigma_w^4 G^2(1; 1)} + \frac{T^2}{P^2} \gamma_{F_e}.$$

For $P = 2$, the asymptotic variance of the timing delay estimator (4.10) is given by:

$$\gamma_\epsilon = \frac{\mathbf{\Gamma}_{1,1}^{(1,1)} + \operatorname{re}\{e^{-2i\pi F_e T} \tilde{\mathbf{\Gamma}}_{1,1}^{(1,1)}\}}{8\pi^2 \sigma_w^4 \cos^2(2\pi\epsilon) G^2(1; 1)}.$$

b. Performance Analysis of the GSD Estimator

When compared with the GG algorithm (4.10), the symbol timing delay estimators corresponding to the GSD algorithm are obtained from Eqs. (4.11) and by fixing $\tau = 0$. Note that such a choice of τ decouples the symbol timing delay estimators from the frequency offset estimator in the sense that the estimation of ϵ does not require an initial estimate of F_e [41]. The following result holds.

Proposition 6 *For $P \geq 3$, the asymptotic variance of the timing delay estimator (4.11) is given by:*

$$\gamma_\epsilon = \frac{P^2 \left(\mathbf{\Gamma}_{0,0}^{(1,1)} - \operatorname{re}\{e^{4i\pi\epsilon} \tilde{\mathbf{\Gamma}}_{0,0}^{(1,1)}\} \right)}{8\pi^2 \sigma_w^4 G^2(1; 0)}.$$

For $P = 2$, the asymptotic variance of the timing delay estimator (4.11) is given by:

$$\gamma_\epsilon = \frac{\mathbf{\Gamma}_{0,0}^{(1,1)} + \operatorname{re}\{\tilde{\mathbf{\Gamma}}_{0,0}^{(1,1)}\}}{8\pi^2 \sigma_w^4 \sin^2(2\pi\epsilon) G^2(1; 0)}.$$

We note that analyzing theoretically the influence of the system parameters such as oversampling factor or excess bandwidth factor from the equations displayed in the previous propositions is quite difficult. Therefore, we need numerical illustrations to highlight the contribution of each parameter to the performance. These simulation experiments show that selection of larger values for the oversampling factor P does not improve the performance of estimators (4.10)-(4.11). In addition, we also notice that the convergence rate of all the estimators (the mean-square error) decreases proportionally to $1/N$, where N stands for the number of available observations. In particular, the frequency offset estimators (4.10)-(4.11) converge slower than the estimator described in [18] and the previous two chapters, which exploits the conjugate cyclostationary statistics of the received waveform.

5. Extension to Time-selective Channels

Due to the assumption (**AS2**), the foregoing discussion applies only to time-invariant channels. In this subsection, we will see that the results obtained above can be extended to the case of time-selective fading effects as long as the fading distortion $\mu_c(t)$ is approximately constant over a pulse duration or, equivalently, the Doppler spread $B_\mu T$ is small, where B_μ denotes the bandwidth of $\mu_c(t)$ [44].

Assuming now that $\mu(n)$ is a stationary complex process with autocorrelation $r_\mu(\tau) := \text{E}\{\mu^*(n)\mu(n+\tau)\}$ [44], we can rewrite Eq. (4.4) for $k = \pm 1$ as:

$$R_{2x}(k; \tau) = \frac{\sigma_w^2}{P} r_\mu(\tau) e^{2i\pi \frac{F_e T \tau}{P}} \sum_n h^*(n) h(n+\tau) e^{-2i\pi \frac{kn}{P}}. \quad (4.13)$$

Based on Eq. (4.13), it is not difficult to find that all the previous estimators (Eqs. (4.10) and (4.11)) still hold true except that for $P = 2$ they take the form:

$$\hat{\epsilon} = \frac{1}{2\pi} \arccos \left\{ \text{re} \left(\frac{\hat{R}_{2x}(1; 1) e^{-i\pi(\hat{f}_e T + 1)}}{\sigma_w^2 G(1; 1) r_\mu(1)} \right) \right\} - \frac{1}{4},$$

$$\hat{\epsilon} = \frac{1}{2\pi} \arccos \left\{ \operatorname{re} \left(\frac{\hat{R}_{2x}(1; 0)}{\sigma_w^2 G(1; 0) r_\mu(0)} \right) \right\}, \quad (4.14)$$

respectively.

Compared with the performance analysis reported in the previous subsection, the exact asymptotic variance of GG and GSD estimators in the case of time-selective channels supports several modifications. Introduce now an additional assumption on the fading channel:

(AS6): the land-mobile channel is a Rayleigh fading channel, which means that $\mu(n)$ is a zero-mean complex-valued circular Gaussian process [83].

For general land-mobile channel models, the autocorrelation of $\mu(n)$ is proportional to the zero-order Bessel function, i.e., $r_\mu(\tau) \propto J_0(2\pi B_\mu \tau)$ (c.f. [84]). Based on the assumption **(AS6)**, $\tilde{r}_{2x}(n; \tau) = 0$ and the higher-order cumulants of $x(n)$ are also zero. Therefore, following the steps of Appendices E and E, one can find that in the presence of time-selective fading effects, the performance analysis can be established in a similar way as in the case of time-invariant fading channels. In fact, considering the assumption **(AS6)**, only the first terms of $\mathbf{\Gamma}_{u,v}^{(1,1)}$ and $\mathbf{\Gamma}_{u,v}^{(1,-1)}$ in Proposition 1 survive, and the asymptotic variances γ_{F_e} and γ_ϵ for the GG and GSD estimators in Propositions 2-4 still hold true except that some constants related to $r_\mu(1)$ or $r_\mu(0)$ should be added. For example, when $P = 2$, based on Eq. (4.14), we now obtain the following expressions for the asymptotic variances corresponding to the GG and GSD timing delay estimators:

$$\gamma_\epsilon = \frac{\mathbf{\Gamma}_{1,1}^{(1,1)} + \operatorname{re}\{e^{-2i\pi F_e T} \tilde{\mathbf{\Gamma}}_{1,1}^{(1,1)}\}}{8\pi^2 \sigma_w^4 \cos^2(2\pi\epsilon) G^2(1; 1) r_\mu^2(1)},$$

$$\gamma_\epsilon = \frac{\mathbf{\Gamma}_{0,0}^{(1,1)} + \operatorname{re}\{\tilde{\mathbf{\Gamma}}_{0,0}^{(1,1)}\}}{8\pi^2 \sigma_w^4 \sin^2(2\pi\epsilon) G^2(1; 0) r_\mu^2(0)},$$

respectively.

In closing this subsection, it is interesting to remark that for implementing the GG and GSD frequency-offset estimators no information regarding the time-varying fading process $\mu(n)$ is required. If the oversampling factor satisfies $P \geq 3$, then the implementation of the GG and GSD timing delay estimators does not require any knowledge of $\mu(n)$, too. However, when $P = 2$ knowledge of the second-order statistics $r_\mu(0)$ and $r_\mu(1)$ is required for implementing the GG and GSD timing delay estimators (4.14). However, simulation experiments, reported in the next subsection, show that from a computational complexity and performance viewpoint the best value of the oversampling factor is $P = 3$. Thus, estimation of parameters $r_\mu(0)$ and $r_\mu(1)$ can be avoided by selecting $P > 2$.

6. Simulation Experiments

In this subsection, the experimental MSE results and theoretical asymptotic bounds of estimators (4.10)-(4.11) are compared. The experimental results are obtained by performing a number of 400 Monte Carlo trials assuming that the transmitted symbols are i.i.d. linearly modulated symbols with $\sigma_w^2 = 1$. The transmit and receive filters are square-root raised cosine filters, and the additive noise $v(n)$ is generated by passing a Gaussian white noise through the square-root raised cosine filter to yield a discrete-time noise sequence with autocorrelation sequence $r_v(\tau) := E\{v^*(n)v(n + \tau)\} = \sigma_v^2 h_{rc}(\tau)$ [44]. The signal-to-noise ratio is defined as: $\text{SNR} := 10 \log_{10}(\sigma_w^2/\sigma_v^2)$. Experiments 1 to 4 assume BPSK symbols transmitted through time-invariant channels, while Experiments 5 to 6 are performed assuming time-selective Rayleigh fading and QPSK constellations. In our simulations, the Doppler spread is set to $B_\mu T = 0.005$ (very slow fading), $\mu(n)$ is created by passing a unit-power zero-mean white Gaussian noise process through a normalized discrete-time filter, obtained by bilinearly transforming a third-order continuous-time all-pole filter, whose poles are the roots of the

equation $(s^2 + 0.35\omega_0s + \omega_0^2)(s + \omega_0) = 0$, where $\omega_0 = 2\pi B_\mu/1.2$.

In all figures, the theoretical bounds of GG and GSD estimators are represented by the solid line and the dash line, respectively. The experimental results of GG and GSD estimators are plotted using dash-dot lines with stars and squares, respectively. Since the frequency offset estimators of GG and GSD are equivalent, only the former will be presented.

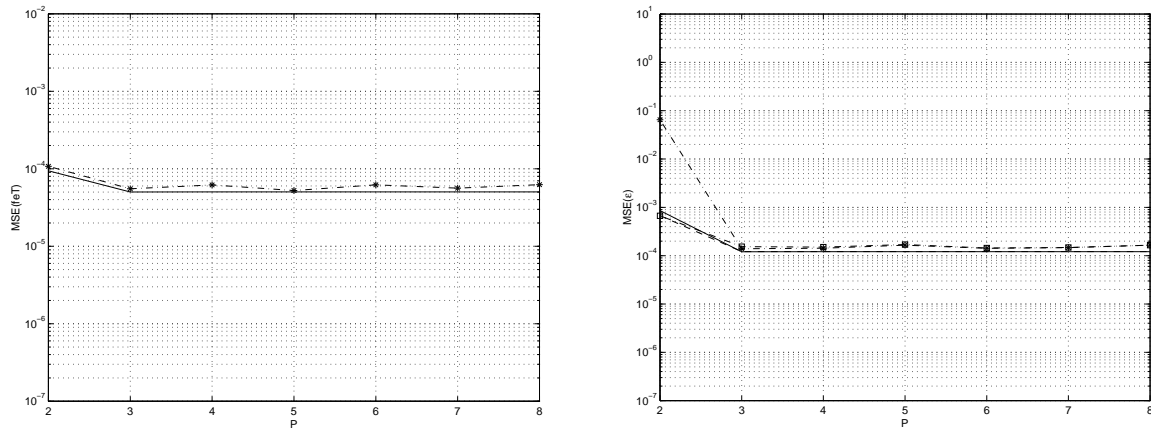


Fig. 31. MSE of $\widehat{F_e T}$ and $\widehat{\epsilon}$ vs. P for BPSK and time-invariant channel

Experiment 1 : *Performance versus the oversampling rate P for BPSK constellation.* By varying the oversampling rate P , we compare the MSE of GG and GSD estimators with their theoretical asymptotic variances. The number of symbols is set to $L = 200$, the roll-off factor of the pulse shape is $\rho = 0.5$, and SNR=10dB. The normalized frequency offset and timing delay are $F_e T = 0.05$ and $\epsilon = 0.37$, respectively. The results are depicted in Figure 31. It turns out that increasing the oversampling rate does not improve performance of the frequency offset and timing delay estimators as long as $P \geq 3$. This is a result which may be predicted by Shannon interpolation theorem, and since the estimators (4.10)-(4.11) exploit the second order statistics of the received signal $x(n)$, an oversampling rate larger than 2 is necessary to make the

cyclic spectra alias-free [50], [73]. Moreover, although more samples are collected as P increases, their correlation increases too, which is known to increase the variance of the estimators [44].

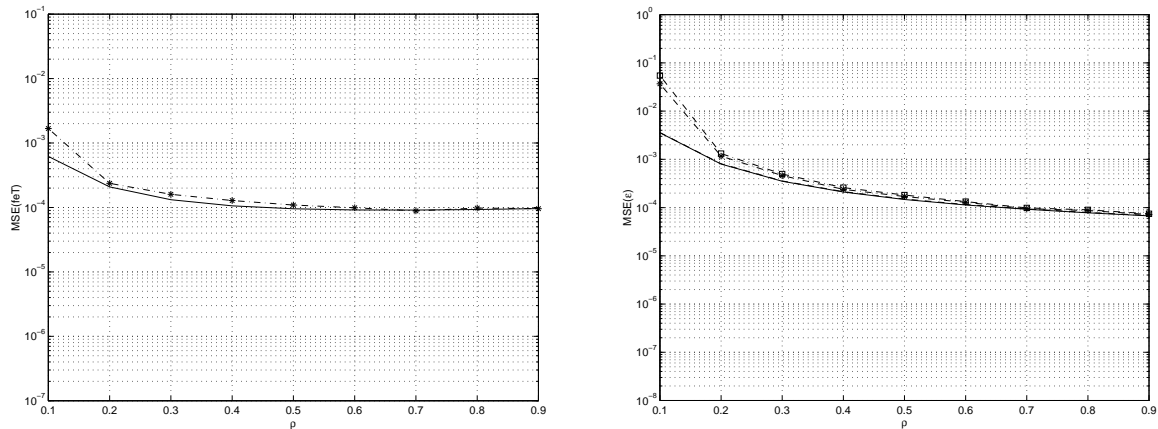


Fig. 32. MSE of $\widehat{F_e T}$ and $\widehat{\epsilon}$ vs. ρ for BPSK and time-invariant channel

Experiment 2 : *Performance versus the filter bandwidth for BPSK constellation.*

Figure 32 depicts the MSE of the estimators versus the roll-off factor ρ assuming oversampling rate $P = 4$, $L = 200$ transmitted symbols, SNR=10 dB, $F_e T = 0.1$ and $\epsilon = 0.37$. It can be seen that with ρ increasing, the performance of the timing delay estimators improves. This is an expected property, since physically, wideband pulses have comparatively short duration and, therefore, are better “seen” in the presence of noise [63, p. 65]. From another viewpoint, based on (4.9) and since $h_c(t)$ is bandlimited, it follows that as the bandwidth decreases, the second-order cyclic spectra are numerically weak, i.e., less cyclic correlation information is available.

Experiment 3 : *Performance versus the number of input symbols L for BPSK constellation.* In Figure 33, the theoretical and experimental MSE of the frequency offset and symbol timing delay estimators are plotted versus the number of symbols L , assuming the following parameters: $P = 4$, $\rho = 0.5$, SNR= 10 dB, $F_e T = 0.05$

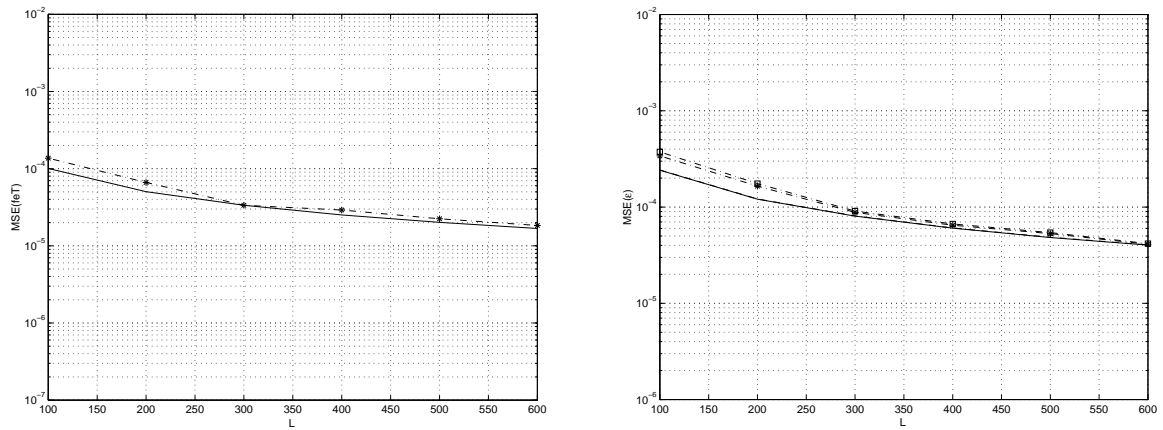


Fig. 33. MSE of $\widehat{F_e T}$ and $\widehat{\epsilon}$ vs. L for BPSK and time-invariant channel

and $\epsilon = 0.37$. Figure 33 shows that the experimental MSE of all the estimators are well predicted by the theoretical bounds derived in Subsection 4.

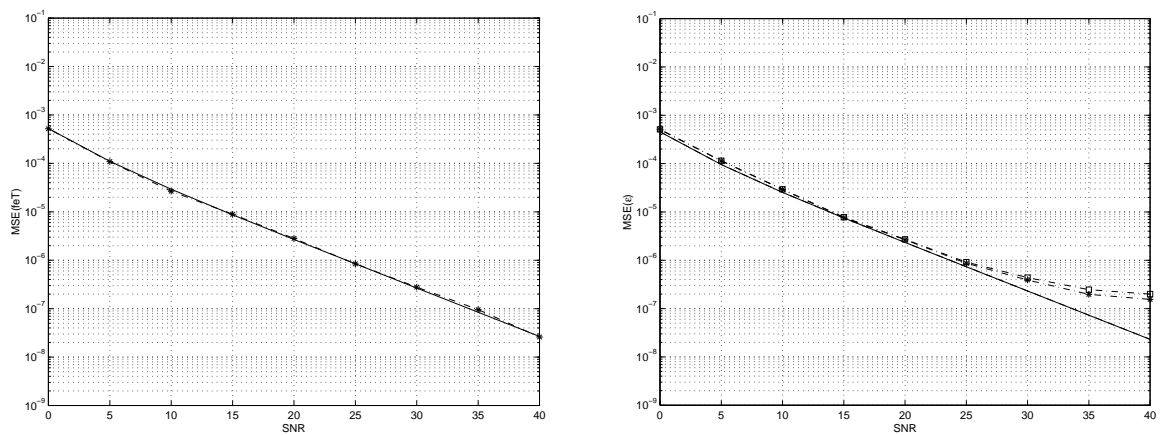


Fig. 34. MSE of $\widehat{F_e T}$ and $\widehat{\epsilon}$ vs. SNR for BPSK and time-invariant channel

Experiment 4: *Performance versus SNR for BPSK constellation.* Figure 34 depicts the experimental and theoretical MSE of the GG and GSD estimators versus SNR, assuming the parameters $P = 4$, $\rho = 0.9$, $L = 500$, $F_e T = 0.05$ and $\epsilon = 0.37$. The simulation results of timing estimators for high SNR range are supposed to agree with

the theoretical bounds when the number of samples N is sufficiently large to make the self noise negligible (c.f. [63, ch. 6]).

Experiment 5 : *Performance versus the oversampling rate P in time-selective channels for QPSK constellation.* We repeat the Experiment 1 by assuming QPSK symbols passing through a time-selective channel. The number of symbols is set to $L = 400$, the roll-off factor of the pulse shape is $\rho = 0.5$, SNR=10dB, $F_e T = 0.2$ and $\epsilon = 0.37$. The results are depicted in Figure 35. It turns out again that when $P \geq 3$, the performance of GG and GSD estimators does not depend on the oversampling factor P . So larger oversampling factors ($P = 4, \dots, 8$) are not justifiable from a computational and performance improvement viewpoint.

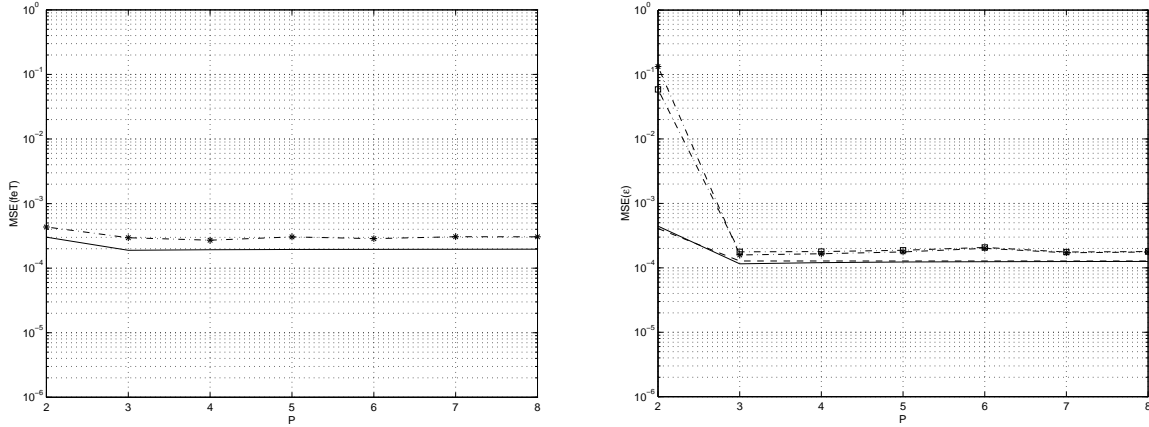


Fig. 35. MSE of $\widehat{F_e T}$ and $\hat{\epsilon}$ vs. P for QPSK and time-selective channel

Experiment 6 : *Performance versus the filter bandwidth in time-selective channels for QPSK constellation.* Figure 36 depicts the MSE of the estimators versus the roll-off factor ρ in the presence of time-varying fading effects, assuming oversampling rate $P = 4$, $L = 400$ transmitted symbols, SNR=10dB, $F_e T = 0.2$ and $\epsilon = 0.37$. Both the theoretical and experimental results corroborate again the conclusion of Experiment 2: pulse shapes with larger bandwidths can improve the performance of the timing

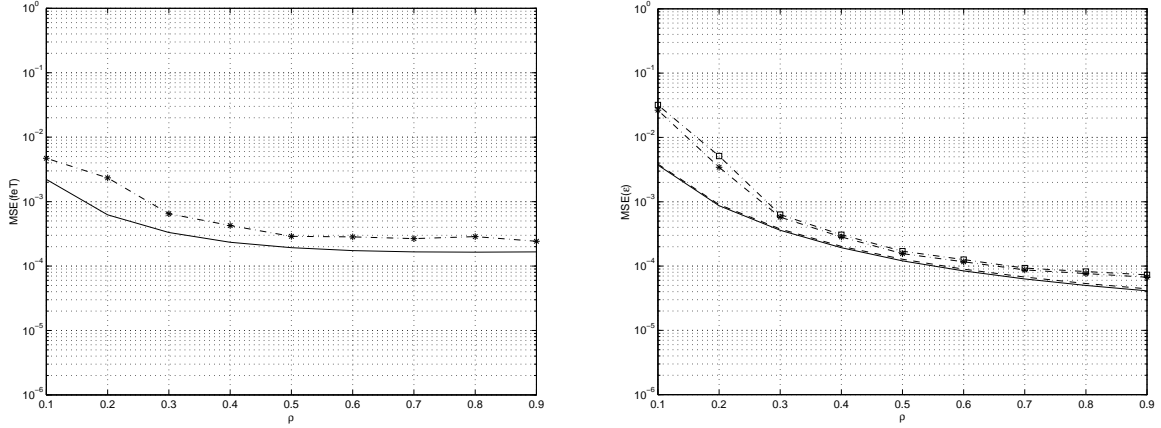


Fig. 36. MSE of $\widehat{F_e T}$ and $\widehat{\epsilon}$ vs. ρ for QPSK and time-selective channel

delay estimators.

7. Conclusions

In this section, we have analyzed the asymptotic performance of the blind carrier frequency offset and timing delay estimators introduced in [41] and [44]. Such estimators rely on the second-order cyclostationary statistics generated by oversampling the output of the receive filter. We have derived the asymptotic variance expressions of $\widehat{F_e}$ and $\widehat{\epsilon}$ and shown that a smaller oversampling rate ($P = 3$) can improve the estimation accuracy as well as reduce the computational complexity of the estimators.

By properly taking into account the aliasing effects, we have shown that when $P = 2$ the timing delay estimators take a different form than the expressions reported in [41] and [44]. which, however, exhibit unsatisfying performance (see Fig. 31 and 35). An alternative estimator with $P = 2$ and improved performance will be derived later in this chapter.

B. Blind Feedforward Symbol Timing Estimators: Further Results

1. System Model and Assumptions

Assuming in the absence of the frequency offset, the standard baseband system model (4.2) turns to:

$$x(n) = \sum_l w(l)h(n - lP) + v(n) . \quad (4.15)$$

In addition to **(AS1)**–**(AS5)**, we invoke the following assumptions [109]:

(AS7) To keep the presentation length to a minimum, the input modulating sequence $w(l)$ is also assumed circular (i.e., $E\{w^2(l)\} = 0$). These assumptions are not at all restrictive since all the derivations can be extended to non-circular modulations and symbol streams that assume arbitrary correlations.

(AS8) In [41], [44], [63], [71] and [75], the oversampling rate $P \geq 4$ is adopted to avoid certain aliasing effects. It was pointed out in the last section that when $P = 2$, the aliasing effects have to be taken into account, and a different form for the SLN timing estimator results. To avoid any overlapping, we assume $P \geq 3$.

All the assumptions are not stringent, therefore, the results presented here are quite general and suitable for many applications of practical interest.

Fig. 37 illustrates the common structure of the popular blind feedforward timing estimators mentioned above, which consists of filtering the received samples $\{x(n)\}_{n=0}^{N-1}$ through a nonlinearity that removes the modulation effects introduced by $w(l)$ and generates a data sequence $y(n)$ that contains spectral components whose phase information is exploited to recover the unknown timing epoch ϵ .

In the next subsection, first we briefly introduce a general form for the blind feedforward SLN timing estimators proposed in [41], [44], [75] and [90], and then propose a unifying ML-framework that will enable to establish some interesting links with some of the existing estimators and to analyze their asymptotic performance.



Fig. 37. Common structure of blind feedforward timing estimators

2. Second-Order CS Statistics-based Timing Estimators

a. SLN Timing Estimators

Let us rewrite Eq. (4.7) in a more compact form without frequency offset:

$$R_{2x}(k; \tau) = \frac{1}{P} e^{i\pi \frac{k\tau}{P}} e^{-2i\pi k\epsilon} G(k; \tau) + \sigma_v^2 h_{rc}(\tau) \delta(k). \quad (4.16)$$

Some straightforward calculations lead to the following explicit relations for $G(k; \tau)$ [109]: $G(-1; \tau) = G(1; \tau)$,

$$G(1; \tau) = \begin{cases} \frac{\rho P}{8} & \text{if } \tau = 0, \\ \frac{\rho P}{16} & \text{if } \tau = \pm \frac{P}{\rho}, \\ \frac{P^4 \sin \frac{\pi \tau \rho}{P}}{8\pi \tau (P^2 - \tau^2 \rho^2)} & \text{elsewhere,} \end{cases} \quad (4.17)$$

$$G(0; \tau) = \begin{cases} \frac{(4-\rho)P}{4} & \text{if } \tau = 0, \\ \frac{2\rho P}{\pi} \left(\frac{\pi}{4} \sin \frac{\pi}{2\rho} - \frac{1}{3} \cos \frac{\pi}{2\rho} \right) & \text{if } \tau = \pm \frac{P}{2\rho}, \\ \frac{\rho P}{\pi} \left(\frac{1}{3} \sin \frac{\pi}{\rho} - \frac{\pi}{8} \cos \frac{\pi}{\rho} \right) & \text{if } \tau = \pm \frac{P}{\rho}, \\ \frac{2P}{\pi} \left\{ \frac{P}{2\tau} \left[\frac{5}{8} \sin \frac{(1-\rho)\pi\tau}{P} + \frac{3}{8} \sin \frac{(1+\rho)\pi\tau}{P} \right] \right. \\ \left. + \frac{\tau \rho^2 P (\sin \frac{(1+\rho)\pi\tau}{P} + \sin \frac{(1-\rho)\pi\tau}{P})}{P^2 - 4\rho^2 \tau^2} + \frac{1}{16} \frac{\tau \rho^2 P (\sin \frac{(1-\rho)\pi\tau}{P} - \sin \frac{(1+\rho)\pi\tau}{P})}{P^2 - \rho^2 \tau^2} \right\} & \text{elsewhere.} \end{cases}$$

Observe also that between the set of second-order time-varying correlations $\{r_{2x}(n; \tau)\}$, $\forall n, \tau$, and the set of cyclic correlation coefficients $\{R_{2x}(k; \tau)\}$, $\forall k, \tau$, there is a one-to-one mapping, i.e., either of the two sets describes completely the second-order statistical properties of the received signal $x(n)$. Since $R_{2x}(k; \tau) =$

$\exp\{2i\pi k\tau/P\}R_{2x}^*(-k; -\tau)$, based on (4.16), it follows that only the subset $\{R_{2x}(1; \tau)\}$, $\forall \tau$, represents all the second-order statistics that may be used for estimating the unknown timing epoch ϵ . Note that the subset $\{R_{2x}(0; \tau)\}$, $\forall \tau$, assumes the knowledge of SNR and does not convey any information for estimating ϵ .

Based on Eq. (4.16), the following general SLN timing estimator may be proposed:

$$\hat{\epsilon} = -\frac{1}{2\pi} \arg\{\hat{R}_{2x}(1; \tau)e^{-i\pi\tau/P}\}. \quad (4.18)$$

The second-order CS-based timing estimators proposed in the literature choose different values for the timing lag τ in Eq. (4.18) (estimators [41] and [75] select $\tau = 0$, [44] assumes $\tau = 1$, and [90] considers $\tau = P$). The asymptotic performance of timing estimators [41] and [44] is derived and compared in the last section. Next, a ML-framework is proposed to analyze the performance of the general SLN timing estimator (4.18) and to possibly design improved performance estimators by exploiting the entire information provided by all the second-order statistics of the received signal.

b. ML Framework

Define the vector of correlations: $\mathbf{R}_{2x} := [R_{2x}(1; -\tau_m), \dots, R_{2x}(1; \tau_m)]^T$, where τ_m denotes an arbitrary non-negative integer. Denote the sample estimate of \mathbf{R}_{2x} by $\hat{\mathbf{R}}_{2x}$. According to [26], the sample cyclic correlation estimates $\{\hat{R}_{2x}(1; \tau)\}$, $\forall \tau$, are asymptotically jointly complex-valued and normally distributed. Thus, $\sqrt{N}[\hat{\mathbf{R}}_{2x} - \mathbf{R}_{2x}]$ is asymptotically jointly complex normal with zero-mean $\mathbf{0} := [0, \dots, 0]^T$, and its covariance and relation matrices are given by:

$$\mathbf{\Gamma} = \lim_{N \rightarrow \infty} NE\{(\hat{\mathbf{R}}_{2x} - \mathbf{R}_{2x})(\hat{\mathbf{R}}_{2x} - \mathbf{R}_{2x})^H\}, \quad \tilde{\mathbf{\Gamma}} = \lim_{N \rightarrow \infty} NE\{(\hat{\mathbf{R}}_{2x} - \mathbf{R}_{2x})(\hat{\mathbf{R}}_{2x} - \mathbf{R}_{2x})^T\},$$

respectively. Let $\mathbf{\Gamma}_{u,v}$ denote the (k, l) th-entry of $\mathbf{\Gamma}$, $u, v = -\tau_m, \dots, \tau_m$. The closed-

form expressions of $\mathbf{\Gamma}$ and $\tilde{\mathbf{\Gamma}}$ are established in Proposition 3, and with the assumption (AS7), can be expressed as:

$$\mathbf{\Gamma}_{u,v} = \int_{-\frac{1}{2}}^{\frac{1}{2}} S_{2x}(0; f) S_{2x}^*(0; f - \frac{1}{P}) e^{2i\pi(u-v)f} df + \kappa P R_{2x}(1; u) R_{2x}^*(1; v), \quad (4.19)$$

$$\tilde{\mathbf{\Gamma}}_{u,v} = \int_{-\frac{1}{2}}^{\frac{1}{2}} S_{2x}(1; f) S_{2x}^*(-1; f - \frac{1}{P}) e^{2i\pi(u+v)f} df + \kappa P R_{2x}(1; u) R_{2x}(1; v), \quad (4.20)$$

where for $|k| \leq 1$ (c.f. Eq. (4.9)):

$$S_{2x}(k; f) = \frac{1}{P} H_{rc}(f) H_{rc}(f - k/P) e^{-2i\pi k \epsilon} + \sigma_v^2 H_{rc}(f) \delta(k), \quad (4.21)$$

where $H_{rc}(f)$ denote the discrete-time FT of $h_{rc}(n)$.

Next, we transform the complex Gaussian pdf $\mathcal{CN}(\mathbf{0}, \mathbf{\Gamma}, \tilde{\mathbf{\Gamma}})$ into its equivalent algebraic form of the real Gaussian pdf $f_\epsilon(\hat{\mathbf{U}}_{2x})$ by defining the $(4\tau_m + 2) \times 1$ -dimensional vectors: $\mathbf{U}_{2x} := [\text{re}(\mathbf{R}_{2x})^T \text{ im}(\mathbf{R}_{2x})^T]^T$ and $\hat{\mathbf{U}}_{2x} := [\text{re}(\hat{\mathbf{R}}_{2x})^T \text{ im}(\hat{\mathbf{R}}_{2x})^T]^T$. Simple calculations show that the covariance matrix of $\hat{\mathbf{U}}_{2x}$ is given by:

$$\mathbf{\Lambda} := \lim_{N \rightarrow \infty} NE\{(\hat{\mathbf{U}}_{2x} - \mathbf{U}_{2x})(\hat{\mathbf{U}}_{2x} - \mathbf{U}_{2x})^T\} = \frac{1}{2} \begin{bmatrix} \text{re}(\mathbf{\Gamma} + \tilde{\mathbf{\Gamma}}) & \text{im}(\tilde{\mathbf{\Gamma}} - \mathbf{\Gamma}) \\ \text{im}(\tilde{\mathbf{\Gamma}} + \mathbf{\Gamma}) & \text{re}(\mathbf{\Gamma} - \tilde{\mathbf{\Gamma}}) \end{bmatrix}.$$

Generally, $\mathbf{\Lambda}$ depends on the unknown timing epoch ϵ . Now define the error vector $\mathbf{e} := \hat{\mathbf{U}}_{2x} - \mathbf{U}_{2x}$ and consider the following nonlinear regression model:

$$\hat{\mathbf{U}}_{2x} = \mathbf{U}_{2x}(\epsilon) + \mathbf{e}, \quad (4.22)$$

where both $\hat{\mathbf{U}}_{2x}$ and \mathbf{e} depend on the number of samples N , and \mathbf{U}_{2x} is a function of the unknown timing ϵ . The ABC estimator of ϵ for the above nonlinear regression problem is given by the nonlinear least-squares estimator weighted by the inverse of the asymptotic covariance matrix of the error vector \mathbf{e} , and takes the form [82, ch. 3],

[95, pp. 91–95]:

$$\hat{\epsilon} = \arg \min_{\epsilon} J(\epsilon) , \quad (4.23)$$

where

$$J(\epsilon) = \frac{1}{2} [\hat{\mathbf{U}}_{2x} - \mathbf{U}_{2x}(\epsilon)]^T \mathbf{\Lambda}(\epsilon)^{-1} [\hat{\mathbf{U}}_{2x} - \mathbf{U}_{2x}(\epsilon)] , \quad (4.24)$$

and ϵ means the trial value of ϵ . Using Eqs. (4.19), (4.20), and Parseval's relation, $\mathbf{\Gamma}$ and $\tilde{\mathbf{\Gamma}}$ can be expressed only in terms of $R_{2x}(k; \tau)$. Hence, a consistent estimate $\hat{\mathbf{\Lambda}}$ for $\mathbf{\Lambda}(\epsilon)$ can be obtained by using consistent sample estimates for $R_{2x}(k; \tau)$. In addition, it is well known that the replacement of $\mathbf{\Lambda}(\epsilon)$ in (4.24) by $\hat{\mathbf{\Lambda}}$ does not change the asymptotic properties of the resulting estimate $\hat{\epsilon}$ [82, p. 84]. Hence, the following reduced complexity estimator may be considered

$$\hat{\epsilon} = \arg \min_{\epsilon} \left\{ \frac{1}{2} [\hat{\mathbf{U}}_{2x} - \mathbf{U}_{2x}(\epsilon)]^T \hat{\mathbf{\Lambda}}^{-1} [\hat{\mathbf{U}}_{2x} - \mathbf{U}_{2x}(\epsilon)] \right\} , \quad (4.25)$$

which is asymptotically equivalent to (4.23) [82]. As \mathbf{e} is asymptotically normally distributed, one can observe that the ABC estimator (4.25) is nothing else than the asymptotic ML estimator of $\hat{\epsilon}$ in terms of the observations contained in the vector $\hat{\mathbf{U}}_{2x}$.

c. Asymptotic Performance Analysis

The ABC estimator is computationally very intensive and may suffer from possible local convergence problems. Next, we derive an efficient way to implement the ABC estimator. By exploiting (4.16), $\mathbf{U}_{2x}(\epsilon)$ takes the following expression [109]:

$$\mathbf{U}_{2x}(\epsilon) = \mathbf{\Phi} \cdot \boldsymbol{\theta} ,$$

where $\boldsymbol{\theta} := [\theta_0 \ \theta_1]^\top = [\cos(2\pi\epsilon) \ \sin(2\pi\epsilon)]^\top$, and

$$\boldsymbol{\Phi} := \frac{1}{P} \begin{bmatrix} G(1; -\tau_m) \cos(-\frac{\pi\tau_m}{P}) & G(1; -\tau_m) \sin(-\frac{\pi\tau_m}{P}) \\ \vdots & \vdots \\ G(1; \tau_m) \cos(\frac{\pi\tau_m}{P}) & G(1; \tau_m) \sin(\frac{\pi\tau_m}{P}) \\ G(1; -\tau_m) \sin(-\frac{\pi\tau_m}{P}) & -G(1; -\tau_m) \cos(-\frac{\pi\tau_m}{P}) \\ \vdots & \vdots \\ G(1; \tau_m) \sin(\frac{\pi\tau_m}{P}) & -G(1; \tau_m) \cos(\frac{\pi\tau_m}{P}) \end{bmatrix}.$$

Hence, (4.22) can be rewritten as:

$$\hat{\mathbf{U}}_{2x} = \boldsymbol{\Phi} \cdot \boldsymbol{\theta} + \mathbf{e}, \quad (4.26)$$

which means that the determination of the ABC-estimate of ϵ reduces to finding a Best Linear Unbiased Estimation (BLUE) of $\boldsymbol{\theta}$ for the linear model (4.26). It follows that in this case the BLUE estimator of $\boldsymbol{\theta}$ admits the closed-form expression [52, ch. 6], [95, ch. 4]:

$$\hat{\boldsymbol{\theta}} = (\boldsymbol{\Phi}^\top \boldsymbol{\Lambda}^{-1} \boldsymbol{\Phi})^{-1} \boldsymbol{\Phi}^\top \boldsymbol{\Lambda}^{-1} \hat{\mathbf{U}}_{2x}, \quad (4.27)$$

and the corresponding 2-by-2 asymptotic covariance matrix of $\hat{\boldsymbol{\theta}}$ is given by:

$$\boldsymbol{\Theta} := \lim_{N \rightarrow \infty} NE\{(\hat{\boldsymbol{\theta}} - \boldsymbol{\theta})(\hat{\boldsymbol{\theta}} - \boldsymbol{\theta})^\top\} = \begin{bmatrix} \Theta_{0,0} & \Theta_{0,1} \\ \Theta_{0,1} & \Theta_{1,1} \end{bmatrix} = (\boldsymbol{\Phi}^\top \boldsymbol{\Lambda}^{-1} \boldsymbol{\Phi})^{-1}. \quad (4.28)$$

Given the BLUE-estimate of $\boldsymbol{\theta}$, according to [52, Theorem 7.4], the ABC-estimate of ϵ can be expressed as:

$$\hat{\epsilon} = \frac{1}{2\pi} \arctan\left(\frac{\hat{\theta}_1}{\hat{\theta}_0}\right). \quad (4.29)$$

Considering a Taylor series expansion of the right-hand side of (4.29) and neglecting the terms of magnitude higher than $o(1/\sqrt{N})$, one can derive the asymptotic variance of $\hat{\epsilon}$, which is summarized in the result:

Theorem 8 *The asymptotic variance of the timing epoch estimator (4.29) is given by:*

$$\text{avar}(\hat{\epsilon}) := \lim_{N \rightarrow \infty} NE\{(\hat{\epsilon} - \epsilon)^2\} = \frac{\sin^2(4\pi\epsilon)}{16\pi^2} \left\{ \frac{\Theta_{0,0}}{\cos^2(2\pi\epsilon)} + \frac{\Theta_{1,1}}{\sin^2(2\pi\epsilon)} - \frac{4\Theta_{0,1}}{\sin(4\pi\epsilon)} \right\}. \quad (4.30)$$

It turns out that the O&M estimator is just a special case of the general estimator (4.23)-(4.29) with $\tau_m = 0$. Indeed, in this case: $\hat{\mathbf{U}}_{2x} = [\text{re}(\hat{R}_{2x}(1;0)) \quad \text{im}(\hat{R}_{2x}(1;0))]^T$, and

$$\mathbf{\Phi} = \frac{G(1;0)}{P} \begin{bmatrix} 1 & 0 \\ 0 & -1 \end{bmatrix}, \quad \mathbf{\Lambda} = \frac{1}{2} \begin{bmatrix} \mathbf{\Gamma}_{0,0} + \text{re}(\tilde{\mathbf{\Gamma}}_{0,0}) & \text{im}(\tilde{\mathbf{\Gamma}}_{0,0}) \\ \text{im}(\tilde{\mathbf{\Gamma}}_{0,0}) & \mathbf{\Gamma}_{0,0} - \text{re}(\tilde{\mathbf{\Gamma}}_{0,0}) \end{bmatrix}.$$

Eq. (4.27) leads to $\hat{\boldsymbol{\theta}} = (P/G(1;0))[\text{re}(\hat{R}_{2x}(1;0)) \quad -\text{im}(\hat{R}_{2x}(1;0))]^T$ and

$$\hat{\epsilon} = -\frac{1}{2\pi} \arctan \left\{ \frac{\text{im}(\hat{R}_{2x}(1;0))}{\text{re}(\hat{R}_{2x}(1;0))} \right\}, \quad (4.31)$$

which is just the estimator (4.18) with $\tau = 0$ (i.e., the O&M estimator). Also, based on Theorem 8, the asymptotic variance of the O&M estimator can be expressed as:

$$\text{avar}(\hat{\epsilon}) = \frac{P^2}{8\pi^2 G^2(1;0)} [\mathbf{\Gamma}_{0,0} - \text{re}(e^{4i\pi\epsilon} \tilde{\mathbf{\Gamma}}_{0,0})], \quad (4.32)$$

which coincides with the expression established earlier in Proposition 6.

As can be seen from the above derivations, the O&M estimator is an ABC-estimator, i.e., asymptotically an ML-estimator that exploits only one cyclic correlation ($\hat{\mathbf{R}}_{2x}(1;0)$). An additional feature of the O&M estimator regards its reduced computational complexity, by exploiting the information provided by the cyclic correlation $\hat{\mathbf{R}}_{2x}(1;0)$, the problem of estimating $\mathbf{\Lambda}$ is bypassed, which is a pleasing property for practical uses. Similar conclusions can be drawn on the other types of SLN timing estimators [41], [44] and [90].

Now it is of interest to ask whether the performance of the O&M estimator can be improved by exploiting additional second-order statistical information, i.e., whether exploiting additional cyclic correlations $\hat{\mathbf{R}}_{2x}(1; \tau)$ at lags $\tau \neq 0$ improves the performance. Surprisingly, from the plots shown in Figs. 38(a) and (b), the answer is no. In Figs. 38(a) and (b), we evaluate the theoretical MSE of SLN-estimate $\hat{\epsilon}$, which asymptotically takes the following form:

$$\text{MSE}(\hat{\epsilon}) := \text{E}\{(\hat{\epsilon} - \epsilon)^2\} = \frac{\text{avar}(\hat{\epsilon})}{N},$$

for different values of τ_m in the case of rolloff factors $\rho = 0.2$ and $\rho = 0.9$, respectively, assuming QPSK input symbols, the oversampling rate $P = 4$, the normalized timing epoch $\epsilon = 0.3$, and the number of samples $N = 400$ (i.e., the observation length $L = 100$ symbols). The modified CRB (MCRB) is adopted as a benchmark, and takes the expression $\text{MCRB}(\hat{\epsilon}) = 1/(8\pi^2 L \xi \text{SNR})$, where the parameter ξ , in the case of raised-cosine pulses, is given by [63, p. 65]: $\xi = (1/12) + \rho^2(0.25 - 2/\pi^2)$.

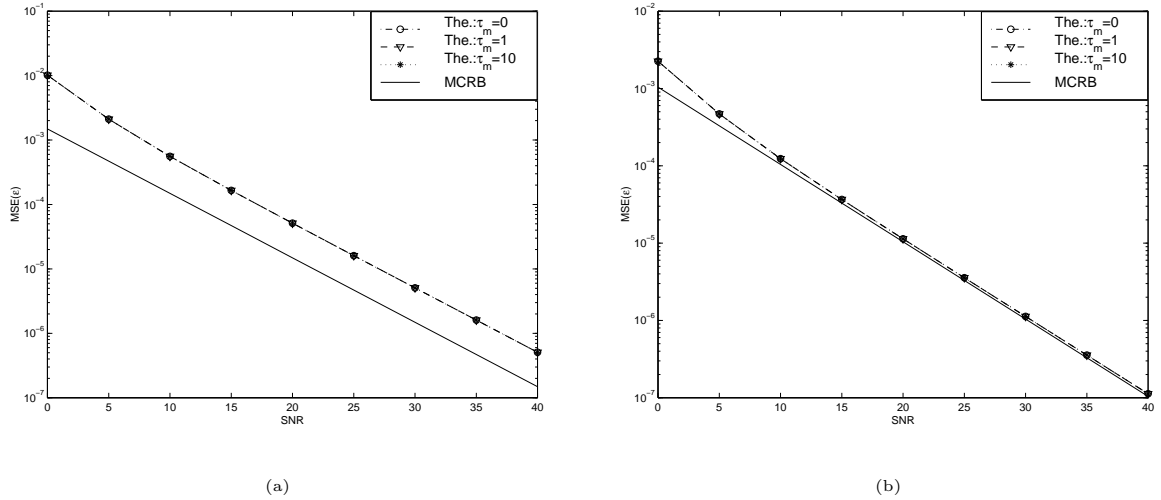


Fig. 38. Theoretical performance of SLN-estimate $\hat{\epsilon}$ for different values of τ_m with (a) $\rho = 0.2$ and (b) $\rho = 0.9$

To explain that the performance of the SLN timing epoch estimators for dif-

ferent τ_m 's is asymptotically the same, let us study the asymptotic behavior of the cost function $J(\hat{\epsilon})$ (4.24). Consider the following two random vectors $\hat{\mathbf{U}}_0 := [\text{re}(\hat{R}_{2x}(1;0)) \text{ im}(\hat{R}_{2x}(1;0))]^T$ and $\hat{\mathbf{U}}_1 := [\text{re}(\hat{R}_{2x}(1;1)) \dots \text{re}(\hat{R}_{2x}(1;\tau_m)) \text{ im}(\hat{R}_{2x}(1;1)) \dots \text{im}(\hat{R}_{2x}(1;\tau_m))]^T$, which correspond to the two sets of cyclic observations $\{\hat{R}_{2x}(1;0)\}$ and $\{\hat{R}_{2x}(1;1) \dots \hat{R}_{2x}(1;\tau_m)\}$, respectively. Let $\hat{\mathbf{U}}_2 := \mathbf{C} \cdot \hat{\mathbf{U}}_0$ denote the orthogonal projection of $\hat{\mathbf{U}}_1$ onto the subspace spanned by $\hat{\mathbf{U}}_0$, and define $\hat{\mathbf{U}}_0^\perp := \hat{\mathbf{U}}_1 - \hat{\mathbf{U}}_2$ as the error vector. According to the Projection Theorem, the following relation holds:

$$\text{cov}\{\hat{\mathbf{U}}_0^\perp, \hat{\mathbf{U}}_0\} = \mathbf{0} ,$$

from which, the projection matrix \mathbf{C} can be obtained and expressed in terms of the entries of $\mathbf{\Lambda}$ (cf. [52, ch. 12]). Since the sets $\{\hat{\mathbf{U}}_0 \ \hat{\mathbf{U}}_1\}$ and $\{\hat{\mathbf{U}}_0 \ \hat{\mathbf{U}}_0^\perp\}$ contain the same statistical information for estimating ϵ , and asymptotically $\hat{\mathbf{U}}_0$ and $\hat{\mathbf{U}}_0^\perp$ are independent and normally distributed, the cost function (4.24) decomposes into the sum of two terms as follows:

$$J(\hat{\epsilon}) = \underbrace{\frac{1}{2}[\hat{\mathbf{U}}_0 - \mathbf{U}_0(\hat{\epsilon})]^T \mathbf{\Lambda}_0(\hat{\epsilon})^{-1} [\hat{\mathbf{U}}_0 - \mathbf{U}_0(\hat{\epsilon})]}_{J_1(\hat{\epsilon})} + \underbrace{\frac{1}{2}[\hat{\mathbf{U}}_0^\perp - \mathbf{U}_0^\perp(\hat{\epsilon})]^T \mathbf{\Lambda}_0^\perp(\hat{\epsilon})^{-1} [\hat{\mathbf{U}}_0^\perp - \mathbf{U}_0^\perp(\hat{\epsilon})]}_{J_2(\hat{\epsilon})},$$

where \mathbf{U}_0 , $\mathbf{\Lambda}_0$, \mathbf{U}_0^\perp and $\mathbf{\Lambda}_0^\perp$ stand for the means and covariance matrices of $\hat{\mathbf{U}}_0$ and $\hat{\mathbf{U}}_0^\perp$, respectively. Choosing $\tau_m = 10$, Fig. 39 depicts the shapes of the cost functions $J_1(\hat{\epsilon})$, $J_2(\hat{\epsilon})$ and $J(\hat{\epsilon})$ for QPSK input symbols, assuming the following parameters: $P = 4$, $\epsilon = 0.3$, $\rho = 0.9$, SNR= 20dB and $L = 2,000$. It can be seen that the function $J_2(\hat{\epsilon})$ is much flatter than $J_1(\hat{\epsilon})$, and the cost function $J(\hat{\epsilon})$ is totally dominated by $J_1(\hat{\epsilon})$, which corresponds to the SLN timing estimator that relies only on the cyclic correlation $\hat{\mathbf{R}}_{2x}(1;0)$ (i.e., the O&M estimator). Furthermore, it turns out that the same conclusion holds true irrespective of the pulse shape excess bandwidth, oversampling factor, timing epoch and SNR. Therefore, it appears that w.r.t. the set

$\{\hat{R}_{2x}(1;0)\}$, the set of cyclic observations $\{\hat{R}_{2x}(1;1) \dots \hat{R}_{2x}(1;\tau_m)\}$ does not convey any additional information for estimating ϵ . Moreover, due to the normal distribution of the error vector \mathbf{e} , the BLUE is also the MVU estimator [52], which means that asymptotically, the O&M estimator achieves the best performance in the class of all estimators that exploit the second-order statistics of the received signal. This result justifies the following conclusion [109]: *The performance of all blind feedforward SLN timing estimators which exploit the second-order statistics of the received signal is asymptotically the same as long as the statistical information at timing lag $\tau = 0$ ($\hat{\mathbf{R}}_{2x}(1;0)$) has been considered.*

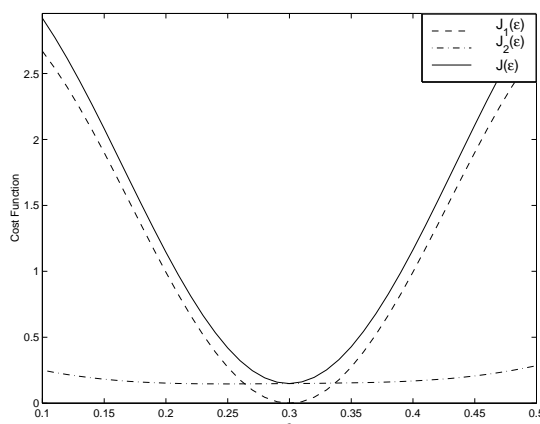


Fig. 39. Cost function of SLN estimator ($\rho = 0.9$, SNR=20dB)

d. Influence of the Oversampling Rate P

Now we analyze the effect of the oversampling rate P on the SLN timing estimators. Due to the conclusion obtained above, we only focus on the O&M estimator, whose asymptotic variance is given by (4.32). To properly inspect the influence of P , we need to evaluate the theoretical MSE of $\hat{\epsilon}$. Since the pulse shape $h_c(t)$ is bandlimited in $[-(1+\rho)/2T, (1+\rho)/2T]$ with $0 < \rho \leq 1$, according to [103], under the

assumption of $P \geq 3$, the following expressions hold [109]:

$$\begin{aligned} H_{rc}(f) &= \frac{1}{T_s} H_c \left(\frac{f}{T_s} \right) = \frac{P}{T} H_c(F) , \\ H_{rc}(f + k/P) &= \frac{1}{T_s} H_c \left(\frac{f + k/P}{T_s} \right) = \frac{P}{T} H_c \left(F + \frac{k}{T} \right) , \quad \text{for } |f| \leq 1/P \text{ and } k = \pm 1 . \end{aligned}$$

Therefore, based on (4.20) and (4.21), we can write:

$$\begin{aligned} \tilde{\Gamma}_{0,0} &= \int_{-\frac{1}{2}}^{\frac{1}{2}} S_{2x}(1; f) S_{2x}^*(-1; f - \frac{1}{P}) df + \kappa P R_{2x}(1; 0) R_{2x}(1; 0) \\ &= \frac{1}{P^2} e^{-4i\pi\epsilon} \int_{-\frac{1}{2}}^{\frac{1}{2}} H_{rc}^2(f) H_{rc}^2(f - \frac{1}{P}) df + \kappa P \frac{\rho^2}{64} e^{-4i\pi\epsilon} \\ &= \frac{P}{T^3} e^{-4i\pi\epsilon} \int_{-\frac{P}{2T}}^{\frac{P}{2T}} H_c^2(F) H_c^2(F - \frac{1}{T}) dF + \kappa P \frac{\rho^2}{64} e^{-4i\pi\epsilon} \\ &= \frac{P}{T^3} e^{-4i\pi\epsilon} \int_{-\frac{\rho}{2T}}^{\frac{\rho}{2T}} H_c^2(F + \frac{1}{2T}) H_c^2(F - \frac{1}{2T}) dF + \kappa P \frac{\rho^2}{64} e^{-4i\pi\epsilon} = P e^{-4i\pi\epsilon} \zeta_2 , \end{aligned}$$

where for the second equality we made use of (4.16) and (4.17), and

$$\zeta_2 := \frac{1}{T^3} \int_{-\frac{\rho}{2T}}^{\frac{\rho}{2T}} H_c^2(F + \frac{1}{2T}) H_c^2(F - \frac{1}{2T}) dF + \frac{\kappa \rho^2}{64} .$$

Similarly, we can obtain $\Gamma_{0,0} = P \zeta_1$, where:

$$\begin{aligned} \zeta_1 &:= \zeta_2 + \frac{2\sigma_v^2}{T^2} \int_{-\frac{\rho}{2T}}^{\frac{\rho}{2T}} H_c^2(F + \frac{1}{2T}) H_c(F - \frac{1}{2T}) dF \\ &\quad + \frac{\sigma_v^2}{T} \int_{-\frac{\rho}{2T}}^{\frac{\rho}{2T}} H_c(F + \frac{1}{2T}) H_c(F - \frac{1}{2T}) dF . \end{aligned}$$

Then, by exploiting (4.17) and (4.32), it yields that:

$$\text{MSE}(\hat{\epsilon}) = \frac{8(\zeta_1 - \zeta_2)}{\pi^2 \rho^2 L} . \quad (4.33)$$

Since ζ_1 and ζ_2 do not depend on P , $\text{MSE}(\hat{\epsilon})$ is independent of P whenever $P \geq 3$, which was shown in the previous section by computer simulations . One can observe

that in the noiseless case ($\sigma_v^2 \rightarrow 0$), $\zeta_1 = \zeta_2$, therefore, the asymptotic variance of the O&M estimate is equal to 0, which means that asymptotically in SNR and N , the variance of the O&M estimate converges to zero faster than $O(1/N)$. We remark that this result was first reported in [75] using a different analysis and certain approximations. Later in the next subsection, after introducing some necessary definitions, we will show further that the rate of convergence to zero of the asymptotic variance of the O&M estimate is even faster than $O(1/N^2)$ in the absence of additive noise.

3. Joint Second and Fourth-Order CS-based Timing Estimator

Pulses with small rolloff factors are of interest with bandwidth efficient modulations [71]. SLN timing epoch estimators exhibit bad performance with small rolloffs due to the lack of CS-information and their large self noise, especially in high SNR range [58], [63] and [103]. Hence, when dealing with strongly bandlimited pulses, nonlinearities other than the SLN may be considered to improve the performance of timing estimators. The most common used one is the FLN nonlinearity. Next, we briefly review the FLN-based timing estimator.

a. FLN Timing Estimator

The fourth-order time-varying correlation of $x(n)$ is defined as:

$$r_{4x}(n; \tau_1, \tau_2, \tau_3) := \mathbb{E}\{x^*(n)x^*(n + \tau_1)x(n + \tau_2)x(n + \tau_3)\} .$$

Consider only the case $\tau_1 = \tau_2 = \tau_3 = 0$, and based on [82, eq. 10.2.9], $r_{4x}(n; 0, 0, 0)$ can be alternatively expressed as:

$$\begin{aligned} r_{4x}(n; 0, 0, 0) &= \text{cum}(x^*(n), x^*(n), x(n), x(n)) + 2r_{2x}^2(n; 0) \\ &= \kappa \sum_l h^4(n - lP) + 2r_{2x}^2(n; 0) . \end{aligned}$$

It is not difficult to find that $r_{4x}(n; 0, 0, 0)$ is also periodic with respect to n with

period P , and its Fourier's coefficient at cycle $k = 1$ is given by:

$$\begin{aligned} R_{4x}(1; 0, 0, 0) &:= \frac{1}{P} \sum_{n=0}^{P-1} r_{4x}(n; 0, 0, 0) e^{-2i\pi \frac{n}{P}} = \frac{\kappa}{P} \sum_n h^4(n) e^{-2i\pi \frac{n}{P}} + 2R_{2x}(k; 0) \otimes R_{2x}(k; 0)|_{k=1} \\ &= \frac{\kappa}{P} \sum_n h^4(n) e^{-2i\pi \frac{n}{P}} + 4R_{2x}(0; 0)R_{2x}(1; 0), \end{aligned} \quad (4.34)$$

where \otimes stands for the circular convolution. Note that the following FT pairs hold:

$$h(n) \longleftrightarrow H_{rc}(f) e^{-2i\pi f \epsilon P}, \quad h^2(n) \longleftrightarrow e^{-2i\pi f \epsilon P} H_{rc}^{(2)}(f), \quad H_{rc}^{(2)}(f) := H_{rc}(f) * H_{rc}(f).$$

Based on Parseval's relation and (4.16), (4.34) can be expressed as:

$$\begin{aligned} R_{4x}(1; 0, 0, 0) &= \left\{ \frac{\kappa}{P} \int_{-1/2}^{1/2} H_{rc}^{(2)}(f) H_{rc}^{(2)}\left(f + \frac{1}{P}\right) df \right. \\ &\quad \left. + \frac{4}{P} G(1; 0) \left(\frac{1}{P} G(0; 0) + r_{2v}(0) \right) \right\} e^{-2i\pi \epsilon} = Q(1; 0) e^{-2i\pi \epsilon}, \end{aligned}$$

where the factor contained within braces, denoted by $Q(1; 0)$, is real-valued. Therefore, a timing estimator similar to (4.31) can be expressed as:

$$\hat{\epsilon} = -\frac{1}{2\pi} \arg\{\hat{R}_{4x}(1; 0, 0, 0)\}, \quad (4.35)$$

and whose asymptotic variance can be established in a similar expression to (4.32).

b. A New Optimal ABC Timing Estimator

Although the FLN estimator has a better performance than SLN in medium and high SNR ranges with small rolloffs, it is inferior to the latter at low SNRs. Estimators (4.31) and (4.35) suggest designing a new optimal (OPT) ABC timing estimator of the following form

$$\hat{\epsilon} = -\frac{1}{2\pi} \arg\{\boldsymbol{\alpha}^T \hat{\mathbf{R}}_x\}, \quad \boldsymbol{\alpha} := [1 \quad \alpha_1]^T, \quad \hat{\mathbf{R}}_x := [\hat{R}_{2x}(1; 0) \quad \hat{R}_{4x}(1; 0, 0, 0)]^T, \quad (4.36)$$

to improve the performance of both SLN and FLN estimators. The real-valued parameter α_1 is to be chosen so that the asymptotic variance of $\hat{\epsilon}$ in (4.36) is minimized.

Since the cyclic moment estimates $\hat{\mathbf{R}}_{2x}(1;0)$ and $\hat{\mathbf{R}}_{4x}(1;0,0,0)$ are asymptotically complex normal, so is any linear combination of them. By adopting the derivation presented in the previous subsection, we can obtain the following expression for the asymptotic variance of $\hat{\epsilon}$ in (4.36):

$$\text{avar}(\hat{\epsilon}) = \frac{\boldsymbol{\alpha}^T [\boldsymbol{\Pi} - \text{re}(e^{4i\pi\epsilon} \tilde{\boldsymbol{\Pi}})] \boldsymbol{\alpha}}{8\pi^2 |\boldsymbol{\alpha}^T \boldsymbol{\beta}|^2}, \quad (4.37)$$

where:

$$\begin{aligned} \boldsymbol{\Pi} &:= \lim_{N \rightarrow \infty} NE\{[\hat{\mathbf{R}}_x - \mathbf{R}_x][\hat{\mathbf{R}}_x - \mathbf{R}_x]^H\}, \quad \tilde{\boldsymbol{\Pi}} := \lim_{N \rightarrow \infty} NE\{[\hat{\mathbf{R}}_x - \mathbf{R}_x][\hat{\mathbf{R}}_x - \mathbf{R}_x]^T\}, \\ \mathbf{R}_x &:= [R_{2x}(1;0) \quad R_{4x}(1;0,0,0)]^T, \quad \boldsymbol{\beta} := \left[\frac{G(1;0)}{P} \quad Q(1;0) \right]^T. \end{aligned}$$

Hence, finding α_1 resorts to the standard Rayleigh quotient problem, whose solution is given by (c.f. [98, ch. 5]):

$$\hat{\alpha}_1^{(\text{OPT})} = \frac{[0 \quad 1] \cdot [\boldsymbol{\Pi} - \text{re}(e^{4i\pi\epsilon} \tilde{\boldsymbol{\Pi}})]^{-1} \boldsymbol{\beta}}{[1 \quad 0] \cdot [\boldsymbol{\Pi} - \text{re}(e^{4i\pi\epsilon} \tilde{\boldsymbol{\Pi}})]^{-1} \boldsymbol{\beta}}. \quad (4.38)$$

Plugging (4.38) back into (4.37), we obtain [109]:

$$\text{avar}(\hat{\epsilon}^{(\text{OPT})}) = \frac{1}{8\pi^2 \boldsymbol{\beta}^T [\boldsymbol{\Pi} - \text{re}(e^{4i\pi\epsilon} \tilde{\boldsymbol{\Pi}})]^{-1} \boldsymbol{\beta}}.$$

Now let us evaluate the entries of the asymptotic covariance matrices $\boldsymbol{\Pi}$ and $\tilde{\boldsymbol{\Pi}}$. Obviously, the first entries of $\boldsymbol{\Pi}$ and $\tilde{\boldsymbol{\Pi}}$ are given by $\boldsymbol{\Pi}_{0,0} = \boldsymbol{\Gamma}_{0,0}$, $\tilde{\boldsymbol{\Pi}}_{0,0} = \tilde{\boldsymbol{\Gamma}}_{0,0}$, respectively. Define the following mean-compensated stochastic processes:

$$e_2(n) := x^*(n)x(n) - r_{2x}(n;0), \quad e_4(n) := x^*(n)x^*(n)x(n)x(n) - r_{4x}(n;0,0,0),$$

and let $r_{2e_2}(n; \tau) := E\{e_2^*(n)e_2(n+\tau)\}$ and $R_{2e_2}(k; \tau)$ denote the time-varying and cyclic correlations of $e_2(n)$, respectively. In Appendix E, it was proved that $\boldsymbol{\Gamma}_{0,0} = S_{2e_2}(0; 1/P)$, $\tilde{\boldsymbol{\Gamma}}_{0,0} = S_{2e_2}(2; 1/P)$, whose expressions are given in (4.19) and (4.20).

Here we present a new method which makes use of the circular convolution of cyclic correlations of $x(n)$ in an iterative way and can be applied to more general cases.

Observe

$$\begin{aligned}
r_{2e_2}(n; \tau) &= \mathbb{E}\{x^*(n)x(n)x^*(n+\tau)x(n+\tau)\} - r_{2x}(n; 0)r_{2x}(n+\tau; 0) \\
&= \text{cum}(x^*(n), x(n), x^*(n+\tau), x(n+\tau)) + r_{2x}^2(n; \tau) \\
&= \kappa \sum_l h^2(n-lP)h^2(n+\tau-lP) + r_{2x}^2(n; \tau),
\end{aligned}$$

and

$$\begin{aligned}
R_{2e_2}(k; \tau) &= \frac{1}{P} \sum_{n=0}^{P-1} r_{2e_2}(n; \tau) e^{-2i\pi \frac{kn}{P}} = \frac{\kappa}{P} \sum_n h^2(n)h^2(n+\tau) e^{-2i\pi \frac{kn}{P}} \\
&\quad + R_{2x}(k; \tau) \otimes R_{2x}(k; \tau).
\end{aligned}$$

Thus, we obtain:

$$S_{2e_2}(k; f) = \sum_{\tau} \left(\frac{\kappa}{P} \sum_n h^2(n)h^2(n+\tau) e^{-2i\pi \frac{kn}{P}} + R_{2x}(k; \tau) \otimes R_{2x}(k; \tau) \right) e^{-2i\pi \tau f},$$

which can be used for accurately evaluating the matrices $\mathbf{\Gamma}_{0,0}$ and $\tilde{\mathbf{\Gamma}}_{0,0}$.

Similarly, the following expressions hold true:

$$\begin{aligned}
\mathbf{\Pi}_{0,1} &= S_{e_4e_2}(0; 1/P), \quad \mathbf{\Pi}_{1,0} = S_{e_2e_4}(0; 1/P), \quad \mathbf{\Pi}_{1,1} = S_{2e_4}(0; 1/P), \\
\tilde{\mathbf{\Pi}}_{0,1} &= S_{e_4e_2}(2; 1/P), \quad \tilde{\mathbf{\Pi}}_{1,0} = S_{e_2e_4}(2; 1/P), \quad \tilde{\mathbf{\Pi}}_{1,1} = S_{2e_4}(2; 1/P).
\end{aligned}$$

The evaluation of the above expressions is similar to that of $\mathbf{\Gamma}_{0,0}$ and $\tilde{\mathbf{\Gamma}}_{0,0}$, but involves the computation of higher-order (larger than second-order) cumulants and moments of $x(n)$, which is straightforward but exhibits too lengthy formulas, and therefore, will not be shown in this dissertation.

From (4.38), one can find that the OPT-estimate of $\hat{\alpha}_1$ requires the knowledge of the operating SNR and the value (or estimate) of timing epoch ϵ , which makes

the OPT estimator impractical. Fortunately, for most applications of interest, this difficulty can be circumvented with very little performance penalty, by fixing α_1 to a constant. Next, we present a case study which illustrates how to select α_1 .

c. Example (QPSK with Flat-fading Channel)

Consider an i.i.d. QPSK modulated symbol sequence transmitted through a time non-selective flat-fading channel corrupted by additive circular white Gaussian noise with variance σ_v^2 . Assuming the rolloff factor $\rho = 0.1$, $P = 4$ and the normalized timing epoch $\epsilon = 0.3$, the OPT-estimate $\hat{\alpha}_1$ in (4.38) is given in Table I (A) for various SNR levels. Table I (B) shows the optimal value of $\hat{\alpha}_1$ versus the timing epoch ϵ , assuming SNR= 20dB.

The results presented in Table I (A)–(B) and extensive simulation experiments suggest that in this application, we can always fix α_1 to a value in the range $[-0.13, -0.17]$ for implementing the estimator (4.36) without incurring any performance loss. This conclusion will be further corroborated by the simulation results shown later.

Table I. (a) OPT-estimate of $\hat{\alpha}_1$ versus SNR and (b) OPT-estimate of $\hat{\alpha}_1$ versus ϵ

SNR(dB)	0	5	10	15	20
$\hat{\alpha}_1$	-0.0386	-0.0880	-0.1326	-0.1559	-0.1649
SNR(dB)	25	30	35	40	
$\hat{\alpha}_1$	-0.1680	-0.1692	-0.1700	-0.1717	

(A)

ϵ	0.1	0.2	0.3	0.4	0.5
$\hat{\alpha}_1$	-0.1649	-0.1649	-0.1649	-0.1649	-0.1649
ϵ	0.6	0.7	0.8	0.9	
$\hat{\alpha}_1$	-0.1649	-0.1649	-0.1649	-0.1649	

(B)

d. Further Results on the Convergence Rate of the O&M Estimator

Before ending this subsection, let us study further the asymptotic behavior of O&M estimator in the noiseless case. Define the asymptotic variance of O&M estimate normalized by N^2 as:

$$\text{avar}_2(\hat{\epsilon}) := \lim_{N \rightarrow \infty} N^2 \mathbf{E}\{(\hat{\epsilon} - \epsilon)^2\}.$$

Based on (4.31), following a procedure similar to the one exploited in deriving Theorem 8, one can obtain the following expression for $\text{avar}_2(\hat{\epsilon})$:

$$\text{avar}_2(\hat{\epsilon}) = \frac{P^3}{8\pi^2 G^3(1; 0)} \text{re}\left\{e^{6i\pi\epsilon} S_{3e_2}\left(3; \frac{1}{P}, \frac{1}{P}\right) - e^{2i\pi\epsilon} S_{3e_2}\left(1; \frac{1}{P}, \frac{1}{P}\right)\right\},$$

where

$$\begin{aligned} S_{3e_2}(k; f_1, f_2) &:= \frac{1}{P} \sum_{n=0}^{P-1} \sum_{\tau_1, \tau_2} r_{3e_2}(n; \tau_1, \tau_2) e^{-2i\pi f_1 \tau_1} e^{-2i\pi f_2 \tau_2} e^{-\frac{2i\pi k n}{P}}, \\ r_{3e_2}(n; \tau_1, \tau_2) &:= \mathbf{E}\{e_2^*(n) e_2(n + \tau_1) e_2(n + \tau_2)\}, \end{aligned}$$

denote the third-order cyclic spectrum and time-varying correlation of $e_2(n)$, respectively.

Note that in the noiseless case, $x(n) = \sum_l w(l)h(n - lP) = x_0(n - \epsilon P)$, where $x_0(n) := \sum_l w(l)h_{rc}(n - lP)$ represents the oversampled output signal of the matched filter in the absence of timing epoch ϵ . Then, it is not difficult to find that the following relation holds:

$$S_{3e_2}(k; f_1, f_2) = S_{3e_2}^{(0)}(k; f_1, f_2) \cdot e^{-2i\pi k \epsilon},$$

where $S_{3e_2}^{(0)}(k; f_1, f_2)$ stands for the third-order cyclic spectrum of $e_2(n)$ corresponding to $x_0(n)$, and is independent of ϵ . After some lengthy and tedious manipulations, we can obtain the following expressions for both $S_{3e_2}^{(0)}(1; 1/P, 1/P)$ and $S_{3e_2}^{(0)}(3; 1/P, 1/P)$:

$$S_{3e_2}^{(0)}(1; 1/P, 1/P) = S_{3e_2}^{(0)}(3; 1/P, 1/P) = P^2 \kappa_6 \mathcal{H}_1^3 + 6P^2 \kappa \mathcal{H}_1 \mathcal{H}_2 + 2P^2 \mathcal{H}_3,$$

where $\kappa_6 := \text{cum}(w(l), w(l), w(l), w^*(l), w^*(l), w^*(l))$ and

$$\mathcal{H}_l := \frac{1}{T^{2l-1}} \int_{-\frac{\rho}{2T}}^{\frac{\rho}{2T}} H_c^l(F + \frac{1}{2T}) H_c^l(F - \frac{1}{2T}) dF, \quad l = 1, 2, 3.$$

Therefore, it turns out that $\text{avar}_2(\hat{\epsilon})$ is also equal to 0, which means that the O&M estimate exhibits a rate of convergence faster than $O(1/N^2)$ when the number of samples N and SNR are large enough. Finding the exact convergence rate of the O&M estimator in the absence of additive noise appears computationally very tedious and remains open.

4. Simulation Experiments

In this subsection, we conduct computer simulations to confirm the analysis presented above and to illustrate the performance of the proposed OPT estimator. All the experimental results are obtained by performing a number of 10^6 Monte-Carlo trials assuming QPSK constellation, the normalized timing epoch $\epsilon = 0.3$, and the additive noise $v(n)$ is generated by passing a Gaussian white noise through the square-root raised cosine filter to yield a discrete-time noise sequence with autocorrelation $r_v(\tau) = \sigma_v^2 h_{rc}(\tau)$.

Experiment 1-Comparison of asymptotic variances of estimators (4.31), (4.35) and (4.36) w.r.t. the MCRB: Fig. 40(a) and (b) depicts the asymptotic variances of the SLN (4.31), FLN (4.35), and OPT estimators (4.36), and MCRB, in two extreme cases: a strongly bandlimited pulse shape $\rho = 0.1$ and a pulse with large bandwidth $\rho = 0.9$. The performance of a practical implementation of (4.36) with fixed $\boldsymbol{\alpha}^T = [1 \quad -0.165]^T$, which is just an approximation of the OPT estimator, therefore termed APP, is also illustrated in Fig. 40(a) and (b). It can be seen that when dealing with narrowband pulse shapes, FLN is superior to SLN in medium and high SNR ranges, but worse than the latter at low SNRs. The OPT estimator outperforms

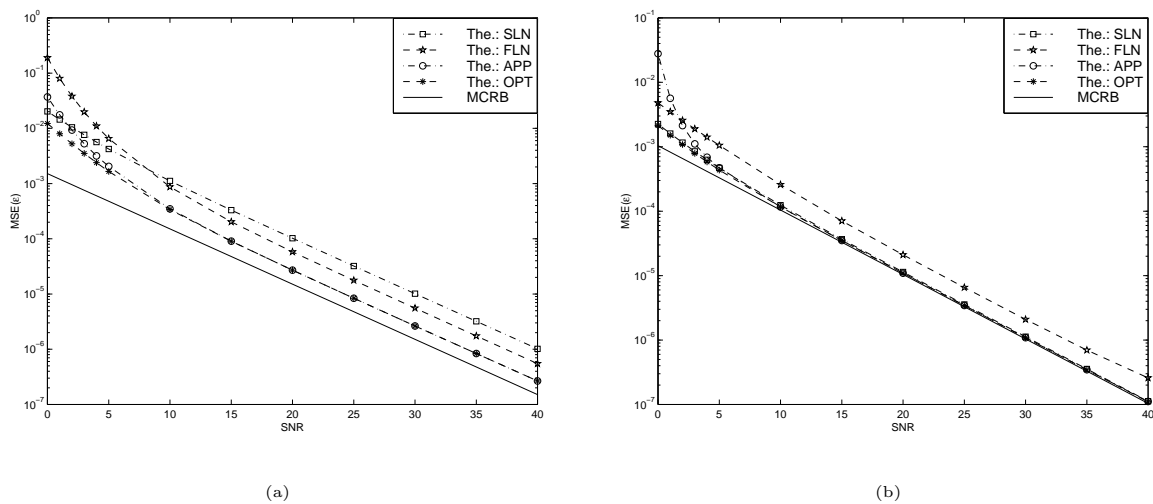


Fig. 40. Comparison of asymptotic variances versus SNR with (a) $\rho = 0.1$ and (b) $\rho = 0.9$

both SLN and FLN estimators, and is closer to MCRB. As expected, APP is a satisfying realizable alternative to OPT except at very low SNRs. In the case of large rolloffs, FLN is always inferior to the SLN estimator, while the latter is good enough to approach the performance of the OPT estimator. Fig. 41 shows the improvement exhibited by the OPT estimator w.r.t. the SLN estimator versus rolloff factor ρ assuming SNR= 20dB. It appears that the improvement is negligible when $\rho \geq 0.6$.

Experiment 2-Comparison of the MSE of estimators versus SNR: In Fig. 42(a) and (b), the experimental MSE of the proposed APP estimator is compared with those of the existing methods (SLN ($\tau_m = 0$), FLN, AVN [78] and LOGN [71]), assuming $\rho = 0.1$, $L = 400$, and $\rho = 0.9$, $L = 100$, respectively. These figures corroborate the results of Experiment 2 and show again the merit of the proposed APP estimator.

5. Conclusions

In this section, we have established a rigorous CS statistics-based ML-framework to design and analyze a class of blind feedforward timing estimators. We have shown

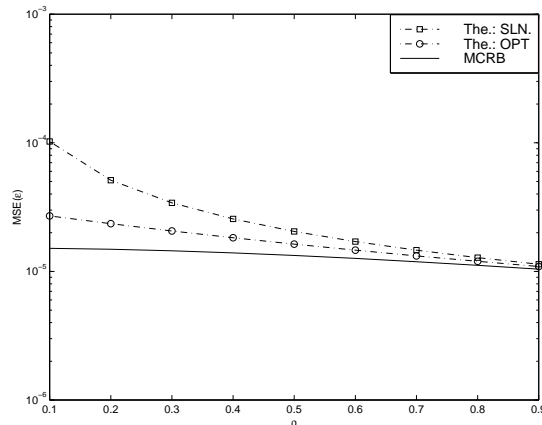


Fig. 41. Improvement of OPT over SLN versus ρ (SNR= 20dB)

that these estimators can be asymptotically interpreted as ML estimators and the O&M estimator achieves asymptotically the best performance in the class of SLN estimators, whose performance is insensitive to the oversampling rate P as long as $P \geq 3$. In the noiseless case, it has been shown that the rate of convergence is faster than $O(1/N^2)$. The asymptotic variance of these ML estimators is derived and can be employed as a benchmark for evaluating the system performance of the CS-based timing estimators proposed in the literature. The proposed analysis framework of timing estimators can be extended straightforwardly to the case of correlated symbol streams and time-selective flat-fading channels, and provides a systematic method to design optimal ML timing recovery schemes. Moreover, in this section, based on the proposed performance analysis, we have introduced an efficient estimator (OPT), which fully exploits the second and the fourth-order CS statistics of the received signal, that improves significantly the performance of the existing methods, when dealing with narrowband signaling pulses. One may ask whether the performance of timing estimators may be further improved if higher-order nonlinearities (i.e., higher than

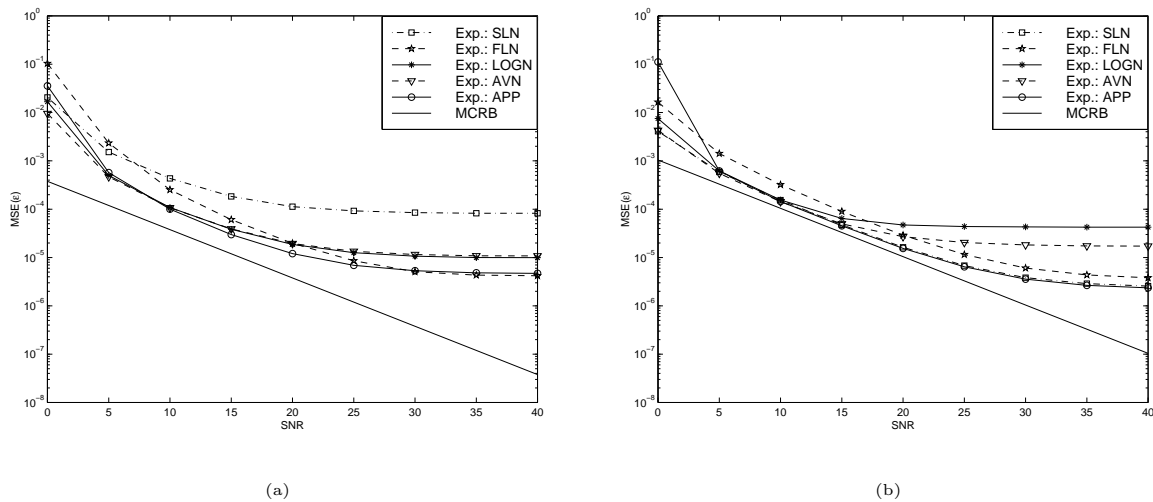


Fig. 42. Comparison of MSEs with (a) $\rho = 0.1$ and (b) $\rho = 0.9$

the fourth-order) are considered. We conjecture that the improvement is negligible, a fact that is corroborated by the plots depicted in Fig. 42 for the AVN and LOGN estimators, whose Taylor series expansions involve higher order terms.

C. An Alternative Blind Feedforward Symbol Timing Estimator Using Two Samples per Symbol

1. Introduction

Most of the methods mentioned previously require a sampling frequency of at least three times larger than the symbol rate [41], [44], [63], [71] and [75]. However, such high sampling rates are not desirable for high-rate transmissions, since the hardware cost of the receiver depends heavily on the required processing speed [115].

The two-sample-per-symbol based timing estimator (4.10) is shown to exhibit poor performance by simulations. Recently, Lee proposed a new blind feedforward timing estimation algorithm that requires only two samples per symbol. Compared with other two-samples per symbol based timing estimators [63] and [115], Lee's es-

imator has the advantage that it does not necessitate any low pass filters. Lee's estimator exhibits a reduced computational complexity comparable with that of the SLN estimator [75], which is known to be the simplest among the estimators using four samples per symbol and admits a very suitable digital implementation [55], [115]. However, Lee's estimator is asymptotically biased and its performance has not been analyzed thoroughly. The goal of this section is to analyze and evaluate the performance of Lee's estimator and to propose a new unbiased timing estimator with improved MSE performance. It is also shown that the proposed new estimator exhibits the same computational complexity as Lee's estimator, and significant MSE-improvements are observable especially in the case of pulse shapes with moderate and large excess bandwidth. The asymptotic (large sample) MSEs of these two estimators, together with the asymptotic bias of Lee's estimator, are established in closed-form. Computer simulations illustrate the merits of the proposed new timing estimator.

2. A New Blind Feedforward CS-based Symbol Timing Estimator

With $P = 2$, the system model (4.15) becomes:

$$x(n) := x_c(nT_s) = e^{j\phi} \sum_l w(l)h(n - 2l) + v(n), \quad n = 0, \dots, N - 1. \quad (4.39)$$

Based on the above model, Lee's estimator takes the following form (c.f. [55, Eq. (2)]):

$$\hat{\epsilon}_{\text{Lee}} := \frac{1}{2\pi} \arg \left\{ \sum_{n=0}^{N-1} |x(n)|^2 e^{-jn\pi} + \sum_{n=0}^{N-2} \text{Re}\{x^*(n)x(n+1)\} e^{-j(n-0.5)\pi} \right\}. \quad (4.40)$$

Based on (4.8), we obtain:

$$R_x(1; \tau) = e^{j\pi\tau} \cos \left[2\pi \left(\epsilon + \frac{\tau}{4} \right) \right] G(1; \tau). \quad (4.41)$$

Note that $G(1; \tau)$ and $R_x(1; \tau)$ are real-valued functions, since $e^{j\pi\tau} = (-1)^\tau$. Some straightforward calculations lead to the following more explicit expressions:

$$G(1; 0) = \frac{\rho}{4} \quad \text{and} \quad G(1; 1) = \frac{2 \sin \frac{\pi\rho}{2}}{\pi(4 - \rho^2)} .$$

From the expression of $\hat{R}_{2x}(k; \tau)$, one can observe that Lee's estimator (4.40) can be expressed as

$$\hat{\epsilon}_{\text{Lee}} = \frac{1}{2\pi} \arg \left\{ \hat{R}_x(1; 0) + j \operatorname{Re} \{ \hat{R}_x(1; 1) \} \right\} ,$$

and its asymptotic mean is given by:

$$\epsilon_0 := \lim_{N \rightarrow \infty} \mathbb{E} \{ \hat{\epsilon}_{\text{Lee}} \} = \frac{1}{2\pi} \arg \left\{ R_x(1; 0) + j R_x(1; 1) \right\} . \quad (4.42)$$

Based on (4.41) and (4.42), and for $\epsilon \in [0, 1/4]$, ϵ_0 can be expressed as:

$$\begin{aligned} \epsilon_0 &= \frac{1}{2\pi} \arctan \left\{ \frac{R_x(1; 1)}{R_x(1; 0)} \right\} = \frac{1}{2\pi} \arctan \left\{ \frac{G(1; 1)}{G(1; 0)} \tan(2\pi\epsilon) \right\} \\ &= \frac{1}{2\pi} \arctan \{ g(\rho) \tan(2\pi\epsilon) \} , \end{aligned}$$

with $g(\rho) := G(1; 1)/G(1; 0)$. Obviously, ϵ_0 is not equal to the true value of the timing delay ϵ except for several special values of ϵ , since in general $g(\rho) \neq 1$ whenever $\rho \in (0, 1]$. Now, it is not difficult to compute the asymptotic bias of Lee's estimator as:

$$\begin{aligned} \text{abias}(\rho, \epsilon) &:= \epsilon - \epsilon_0 = \frac{1}{2\pi} \left(\arctan \{ \tan(2\pi\epsilon) \} - \arctan \{ g(\rho) \tan(2\pi\epsilon) \} \right) \\ &= \frac{1}{2\pi} \arctan \left\{ \frac{1 - g(\rho)}{\cot(2\pi\epsilon) + \tan(2\pi\epsilon)g(\rho)} \right\} . \end{aligned} \quad (4.43)$$

When ϵ assumes values other than $[0, 1/4]$, the asymptotic bias of Lee's estimator can be obtained in a similar way and takes the same expression as (4.43). Fig. 43 plots $\text{abias}(\rho, \epsilon)$ versus ϵ for several values of ρ , which is similar to the plot [55, Fig. 2],

obtained by means of more laborious numerical calculations. From Fig. 43, it can be seen that the asymptotic bias is tolerable for small roll-off factors, but increases with ρ (bias is on the order of 10% of the timing epoch ϵ for $\rho = 0.9$).

The above derivation suggests that by compensating the term $g(\rho)$, we can design a new blind asymptotically unbiased feedforward symbol timing estimator of the following form:

$$\begin{aligned}\hat{\epsilon} &= \frac{1}{2\pi} \arg \left\{ g(\rho) \cdot \hat{R}_x(1; 0) + j \operatorname{Re} \{ \hat{R}_x(1; 1) \} \right\} \\ &= \frac{1}{2\pi} \arg \left\{ g(\rho) \cdot \sum_{n=0}^{N-1} |x(n)|^2 e^{-jn\pi} + \sum_{n=0}^{N-2} \operatorname{Re} \{ x^*(n)x(n+1) \} e^{-j(n-0.5)\pi} \right\}. \quad (4.44)\end{aligned}$$

Note that this new estimator (4.44) has the same implementation complexity as that of Lee's estimator (4.40). In the next subsection, we establish in closed-form expressions the asymptotic MSEs of estimators (4.40) and (4.44), which are defined as follows:

$$\gamma_{\text{Lee}} := \lim_{N \rightarrow \infty} \operatorname{NE} \{ (\hat{\epsilon}_{\text{Lee}} - \epsilon)^2 \}, \quad \gamma_{\text{new}} := \lim_{N \rightarrow \infty} \operatorname{NE} \{ (\hat{\epsilon} - \epsilon)^2 \}.$$

3. Performance Analysis for Estimators

Following the steps similar to that presented in Appendix E, one can obtain the asymptotic MSEs of the estimators (4.40) and (4.44) as [108]:

Theorem 9 *The asymptotic mean-square errors of the symbol timing delay estimators (4.44) and (4.40) are given by:*

$$\begin{aligned}\gamma_{\text{new}} &= \frac{1}{4\pi^2 G^2(1; 1)} \left\{ \frac{\cos^2(2\pi\epsilon)(\mathbf{\Gamma}_{1,1} - \mathbf{\Gamma}_{1,-1})}{2} + g^2(\rho) \sin^2(2\pi\epsilon) \mathbf{\Gamma}_{0,0} - g(\rho) \sin(4\pi\epsilon) \mathbf{\Gamma}_{1,0} \right\}, \\ \gamma_{\text{Lee}} &= \frac{\sin^2(4\pi\epsilon_0)}{\sin^2(4\pi\epsilon)} \gamma_{\text{new}} + N \cdot \text{bias}^2(\rho, \epsilon),\end{aligned}$$

respectively.

A direct analytical comparison between γ_{Lee} and γ_{new} seems intractable. Therefore, in the next subsection we will resort to numerical illustrations.

4. Simulation Experiments

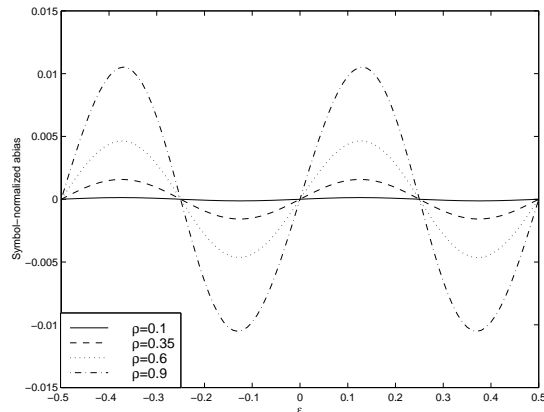


Fig. 43. Asymptotic bias of $\hat{\epsilon}_{Lee}$

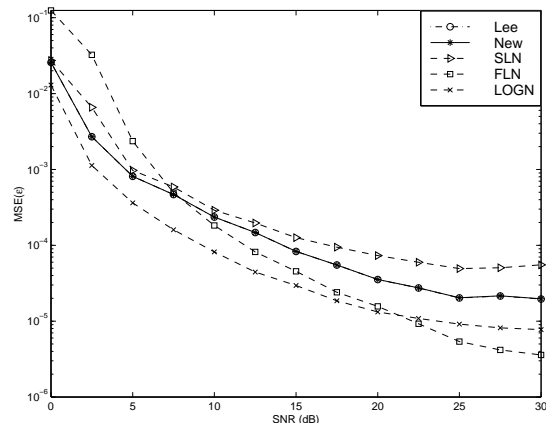


Fig. 44. MSEs versus SNR ($\rho = 0.1$)

To corroborate the proposed asymptotic performance analysis, we conduct computer simulations to compare the theoretical bounds of estimators (4.40) and (4.44) (i.e., γ_{Lee} and γ_{new} normalized with the number of samples N) with the experimental MSE-results. The performance of conventional four-samples/symbol-based blind feedforward symbol timing delay estimators: SLN [75], LOGN [71], FLN and AVN [78], is also illustrated. The experimental results are obtained by performing a number of 800 Monte Carlo trials assuming that the transmitted symbols are drawn from a QPSK constellation, the number of symbols $L = 512$ and the value of $\epsilon = 0.35$. Figs. 44–46 show the simulation results for the roll-off factors $\rho = 0.1$, $\rho = 0.35$, and $\rho = 0.5$, respectively. From these figures, the following conclusions can be drawn:

- The experimental MSE of the estimators (4.40) and (4.44) are well predicted

by the theoretical bounds derived above.

- The improvement of the proposed new estimator (4.44) over Lee's estimator (4.40) in medium and high SNR ranges is more and more significant when the roll-off factor ρ increases.
- At small roll-offs, both (4.40) and (4.44) outperform the SLN estimator, and are inferior to FLN, AVN and LOGN estimators, which however, exhibit much higher computational load than estimators (4.40) and (4.44), which require only two samples per symbol.
- With ρ increasing, the difference of the estimation accuracy between the proposed algorithm (4.44) and FLN, AVN and LOGN decreases, and further simulation results show that at large roll-offs ($\rho > 0.5$), the estimator (4.44) outperforms FLN, AVN and LOGN estimators.

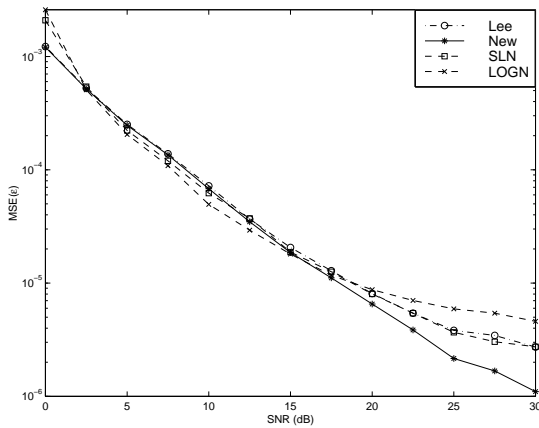


Fig. 45. MSEs versus SNR ($\rho = 0.35$)

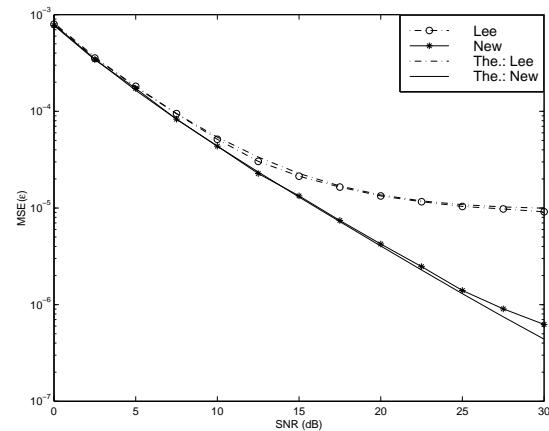


Fig. 46. MSEs versus SNR ($\rho = 0.5$)

5. Conclusions

In this section, we have analyzed Lee's symbol timing delay estimator using a cyclostationary statistics framework. Although, Lee's estimator presents the attractive property of a low computational load, it is asymptotically biased. To remedy this disadvantage, we have proposed a new unbiased estimator which outperforms significantly Lee's estimator at medium and high SNRs for large roll-off factors ($\rho > 0.5$), and which exhibits the same computational complexity as the latter. Moreover, the asymptotic MSEs of these two estimators, together with the asymptotic bias of Lee's estimator, are established in closed-form expressions. Computer simulations corroborate the theoretical performance analysis, and illustrate the merits of the proposed new timing delay estimator.

CHAPTER V

CONTINUOUS-MODE FRAME SYNCHRONIZATION FOR
FREQUENCY-SELECTIVE CHANNELS

A. Introduction

As mentioned in Chapter I, the problem of frame synchronization may arise in some specific applications after the symbol timing is obtained. In the past decades, there has been much research into continuous-mode frame synchronization, and the most widely used methods concentrate on locating a fixed frame synchronization pattern or “sync word” inserted periodically into the continuous data stream [16], [36], [37], [56], [57], [68], [74] and [88]. The optimum Maximum Likelihood (ML) rule for frame synchronization in AWGN channels with BPSK signaling was originally proposed by Massey [57]. Nielsen subsequently reported that this ML rule and its high Signal-to-Noise Ratio (SNR) approximation (high SNR ML rule) provided several dB improvement over the well-known correlation rule [74]. Many years later, Liu and Tan extended these results to M -ary PSK modulations and corroborated the conclusion of Nielsen [56]. Recently, based on ML rule, frame synchronization algorithms for flat fading channels were derived in [36] and [88].

Although it has been studied extensively for AWGN and flat fading channels, the problem of continuous-mode frame synchronization in the presence of frequency-selective channels has received much less attention. In [68], an ML-based frame synchronizer was derived assuming a binary pulse amplitude modulated system and known static dispersive intersymbol interference (ISI) channels. However, in many applications of interest, the channel is time varying and *a priori* unknown. This problem becomes further complicated in the presence of frequency offset, which is

the case due to the fact that frame synchronization sometimes has to be achieved before carrier recovery is performed [16]. The objective of the present chapter is to contribute filling this gap [105].

Generally, in the presence of other unknown variables (e.g., channel coefficients and frequency offset), two possible approaches may be derived to estimate the frame boundary according to the ML criterion. One is the *Bayesian* approach, which consists of modeling other unknowns as random variables with certain pdf and computing the average of joint likelihood function with respect to their pdfs to produce the marginal likelihood of the frame boundary, from which the ML estimate of frame boundary can be obtained (see e.g., [16], [36]). Another method aims at jointly estimating the frame boundary and other unknown variables [30], [53]. In this chapter, following the latter approach, we propose a computationally efficient synchronization scheme for joint frame synchronization, channel acquisition, and frequency offset estimation by exploiting the ML rule. Computer simulations show that the proposed algorithm exhibits low implementation complexity and good performance [105].

It is interesting to note that the problem of frame synchronization over unknown frequency-selective channels is well covered for the scenario of asynchronous or spontaneous packet transmission (“one-shot” or burst-mode synchronization) [30], [31], [53] and [54], where the sync word is prefixed to the data stream and is itself preceded by no signal or by a sequence of symbols to perform other synchronization tasks (a clock recovery sequence or an unmodulated sequence for carrier estimation) [57], [62]. There are two essential differences between the methods dealing with the “one-shot” synchronization and those of continuous-mode frame synchronization. First, the observation sequence of “one-shot” synchronization is chosen long enough to contain the complete frame sync word [62], while for the latter, an N -signal span of the received sequence, where N denotes the frame length [57], is usually processed. Second, for

the synchronization of spontaneous packet transmissions, it is always assumed that the position of the data packet is known up to an uncertainty in a finite interval which is centered about a coarse frame sync flag generated by the preceding automatic gain control unit [30], [53], [62]. This assumption guarantees that the frame sync word is contained entirely in the observation sequence and assumes its initial order. When tackling the problem of continuous-mode frame synchronization, it is generally assumed that the sync word is *a priori* equally likely to begin in any of the N positions of the received sequence (see e.g., [56], [57]).

After introducing the system model, an ML scheme for joint frame synchronization and channel acquisition is developed. Then, an extension of the proposed ML scheme to frequency-selective channels affected by Doppler shift/carrier frequency offset is presented. Finally, the performance of the proposed algorithms is demonstrated through computer simulations.

B. System Model

We consider a linear modulation (e.g., PSK or QAM) transmitted through a slow time-varying frequency-selective channel, whose coefficients $\mathbf{h} = [h_0, h_1, \dots, h_{L-1}]^T$ are assumed to remain constant over the duration of the observed sequence and L represents the channel memory. The frame of transmitted data consists of N symbols, where the first N_s symbols form a fixed frame synchronization pattern $\mathbf{s} = [s_0, s_1, \dots, s_{N_s-1}]^T$ followed by $P := N - N_s$ random data symbols $\mathbf{d} = [d_0, d_1, \dots, d_{P-1}]^T$ (see Fig. 47-a and b). We assume that the data symbols d_k are zero-mean i.i.d. with unit average energy per symbol, i.e., $\sigma_k^2 := \text{E}\{|d_k|^2\} = 1$, and the training symbols s_k are selected from the same set as that of data symbols d_k , so that no restriction is made on the frame structure to prohibit the replication of the frame synchronization pattern in

the portion of random data [56], [74]. It is generally desirable to choose a sync word with good autocorrelation property satisfying the condition

$$(s_0, s_1, \dots, s_{j-1}) \neq (s_{N_s-j}, s_{N_s-j+1}, \dots, s_{N_s-1}), \quad j = 1, 2, \dots, N_s - 1,$$

which ensures the number of replications of the sync word amid random data to be minimized [56], [62], [74].

The transmitted signal is passed through the channel \mathbf{h} , and sampled at the symbol period. It is reasonable to assume $P \geq L$ and $N_s \geq L$. The outputs of the channel corresponding to the i -th frame are modeled as (see Fig. 47-c)

$$x_k^{(i)} = \sum_{l=0}^{L-1} w_{k-l} h_l, \quad k = 0, 1, \dots, N - 1, \quad (5.1)$$

where

$$w_k = \begin{cases} d_{P+k}^{(i-1)}, & \text{if } -(L-1) \leq k \leq -1, \\ s_k, & \text{if } 0 \leq k \leq N_s - 1, \\ d_{k-N_s}^{(i)}, & \text{if } N_s \leq k \leq N - 1. \end{cases}$$

Based on (5.1), the positions of $x_0^{(i)}$, $-\infty < i < \infty$, are defined as the frame boundaries in the channel outputs, where the first training symbol s_0 is involved in the first path h_0 of the channel.

In the absence of *a priori* information, the received signal is a linear shift of the sequence $x_k^{(i)}$ with an arbitrary delay $\mu \in [0, 1, \dots, N - 1]$, rather than $x_k^{(i)}$ itself, and hence the frame boundaries may appear in any of the N positions (i.e., the location $N - \mu$ modulo N) with equal probability in an arbitrarily selected N -signal span $\mathbf{r} = [r_0, r_1, \dots, r_{N-1}]^T$ of the observed sequence (Fig. 47-d) [36], [56], [57]. Therefore, the frame synchronization problem that we pose resumes to estimating the index μ from the selected segment \mathbf{r} of channel output observations. Defining the linear

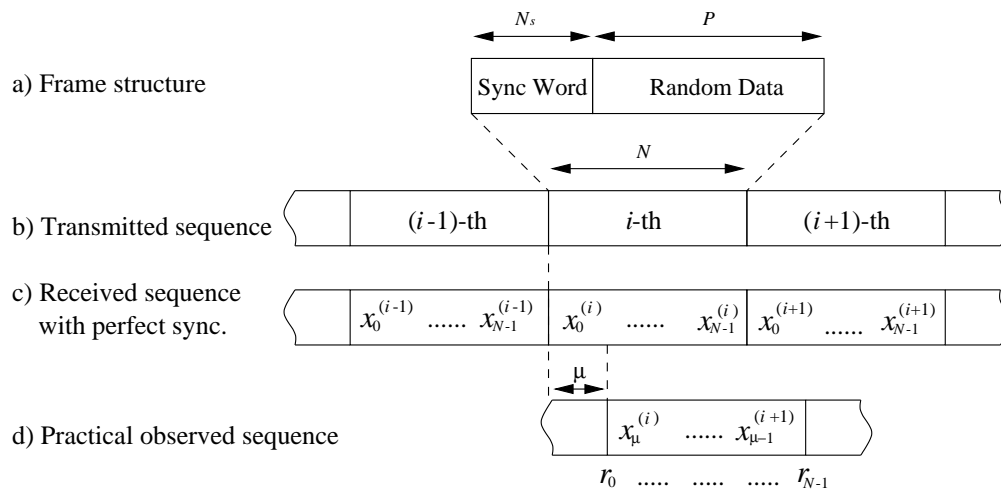


Fig. 47. Frame synchronization model

shift operator as $T(\mathbf{x}^{(i)}) := [x_1^{(i)}, x_2^{(i)}, \dots, x_{N-1}^{(i)}, x_0^{(i+1)}]^T$, we can express the received segment as

$$\mathbf{r} = T^\mu(\mathbf{x}^{(i)}) + \mathbf{n}, \quad (5.2)$$

where $\mathbf{n} := [n_0, n_1, \dots, n_{N-1}]^T$ and the components n_k are independent complex Gaussian random variables with zero-mean and variance N_0 . Note that when dealing with the problem of frame synchronization in AWGN and flat-fading channels, authors prefer to use (left) cyclic shift operator, which is defined by $T_{lc}(\mathbf{x}^{(i)}) := [x_1^{(i)}, x_2^{(i)}, \dots, x_{N-1}^{(i)}, x_0^{(i)}]^T$, instead of $T(\mathbf{x}^{(i)})$, since these two operations are statistically equivalent and the former makes the derivation more compact. However, this equivalence does not hold true in the case of frequency-selective channels. From (5.1), it is not difficult to find that $T_{lc}^m(\mathbf{x}^{(i)})$ and $T^m(\mathbf{x}^{(i)})$ do not always involve the same set of unknown random data when m varies, hence they exhibit different statistical properties due to the memory of the channel. For simplicity, we will omit the dummy variable i in the ensuing derivation.

C. Joint Frame Synchronization and Channel Acquisition

From (5.2), the optimum maximum-a-posteriori (MAP) algorithm maximizes the *posterior* probability $\Lambda_1 = p(m|\mathbf{r})$, $0 \leq m \leq N - 1$, which by the Bayes' theorem [79, p. 84] becomes $\Lambda_1 = f(\mathbf{r}|m) \cdot p(m)/f(\mathbf{r})$, where $f(\mathbf{r})$ stands for the pdf of \mathbf{r} . Since $p(m) = 1/N$ for all m , the MAP algorithm reduces to the ML estimator which maximizes

$$\Lambda_2 = f(\mathbf{r}|m) = \sum_{\text{all } \mathbf{d}_m} f(\mathbf{r}|m, \mathbf{d}_m) \cdot p(\mathbf{d}_m) = \sum_{\text{all } \mathbf{d}_m} \frac{1}{(\pi N_0)^N} e^{-\frac{1}{N_0}(\mathbf{r}-T^m(\mathbf{x}))^H \cdot (\mathbf{r}-T^m(\mathbf{x}))} \cdot p(\mathbf{d}_m), \quad (5.3)$$

where \mathbf{d}_m represents the set of unknown data involved in the operation $T^m(\mathbf{x})$. Note that the probability $p(\mathbf{d}_m)$ depends on the size of the symbol alphabet and the synchronization position m . Moreover, the averaging over all possible data vectors of length varying with m , whose complexity increases exponentially with the channel memory, is complicated enough to escape even an approximation, and hence the optimal estimator (5.3) appears computationally prohibitive. To circumvent this difficulty, next we propose a suboptimal but computationally efficient algorithm, which does not necessitate the averaging over the unknown data.

Exploiting (5.1), it is easy to observe that the subset $\mathbf{x}_s := [x_{L-1}, x_L, \dots, x_{N_s-1}]^T$ can be expressed as

$$\mathbf{x}_s = \mathbf{S} \cdot \mathbf{h}, \quad \mathbf{S} := \begin{pmatrix} s_{L-1} & s_{L-2} & \dots & s_0 \\ s_L & s_{L-1} & \dots & s_1 \\ \vdots & \vdots & \ddots & \vdots \\ s_{N_s-1} & s_{N_s-2} & \dots & s_{N_s-L} \end{pmatrix}, \quad (5.4)$$

and is affected by the sync word \mathbf{s} only and not by the random data. Define the (right) cyclic shift of the observed signals \mathbf{r} as $\mathbf{r}^{(m)} := T_{rc}^m(\mathbf{r})$, where $T_{rc}(\mathbf{r}) :=$

$[r_{N-1}, r_0, \dots, r_{N-2}]^T$, and choose a subwindow of length $N_s - L + 1$ of $\mathbf{r}^{(m)}$, namely $\mathbf{r}_s^{(m)} := [r_{L-1}^{(m)}, r_L^{(m)}, \dots, r_{N_s-1}^{(m)}]^T$. Under the assumption that m is the correct position of frame boundaries, $\mathbf{r}_s^{(m)}$ can be expressed in terms of the frame synchronization pattern \mathbf{s} as in (5.4). A reduced-complexity ML-based estimator of μ that exploits the information provided by $\mathbf{r}_s^{(m)}$ can be obtained by maximizing the likelihood function

$$\Lambda_3 = \frac{1}{(\pi N_0)^{N_s-L+1}} e^{-\frac{1}{N_0} (\mathbf{r}_s^{(m)} - \mathbf{x}_s)^H \cdot (\mathbf{r}_s^{(m)} - \mathbf{x}_s)},$$

or equivalently the log-likelihood function

$$\hat{\mu} = \arg \min_{0 \leq m \leq N-1} (\mathbf{r}_s^{(m)} - \mathbf{S} \cdot \mathbf{h})^H \cdot (\mathbf{r}_s^{(m)} - \mathbf{S} \cdot \mathbf{h}). \quad (5.5)$$

For a fixed m , the ML estimate of \mathbf{h} is given by (see e.g., [30], [53], [72])

$$\hat{\mathbf{h}}(m) = (\mathbf{S}^H \mathbf{S})^{-1} \mathbf{S}^H \mathbf{r}_s^{(m)}. \quad (5.6)$$

Substituting (5.6) into (5.5), we can obtain the following estimator equivalent to (5.5)

$$\hat{\mu} = \arg \max_{0 \leq m \leq N-1} \Lambda_4(m), \quad \Lambda_4(m) = \mathbf{r}_s^{H(m)} (\mathbf{B} - \mathbf{I}) \mathbf{r}_s^{(m)}, \quad (5.7)$$

where \mathbf{I} is the $(N_s - L + 1) \times (N_s - L + 1)$ identity matrix and $\mathbf{B} := \mathbf{S}(\mathbf{S}^H \mathbf{S})^{-1} \mathbf{S}^H$ denotes the projection matrix.

In summary, the proposed frame synchronization algorithm is as follows [105]:

- Step 1. Select an arbitrary length- N signal segment \mathbf{r} of the received signal.
- Step 2. For each $m \in [0, N - 1]$, choose the subwindow of observation $\mathbf{r}_s^{(m)}$ and compute the metric $\Lambda_4(m)$.
- Step 3. Find a value $\hat{\mu}$ such that the corresponding metric achieves the the maximum among the metrics (5.7).

Step 4. The channel estimate is given by (5.6) with $m = \hat{\mu}$.

Note that if $N_s - L = L - 1$ (i.e., $N_s = 2L - 1$), \mathbf{S} is an $L \times L$ square matrix

and nonsingular, then one can see that $\mathbf{B} = \mathbf{I}$. In this condition, $\Lambda_4(m)$ is always 0 and the estimator (5.7) is meaningless [72]. Therefore, the length of sync pattern has to be chosen as $N_s \geq 2L$. Physically, this means that the first $L - 1$ symbols of the sync pattern are guard symbols which prevent the remaining sync symbols from being affected by random data, and at least $L + 1$ uncorrupted sync symbols are required to estimate the $L + 1$ unknown parameters (μ, \mathbf{h}) .

The proposed synchronizer (5.7) is based on one frame length of channel observations. For certain applications where the constraint on the processing delay is not stringent, we may improve the performance of (5.7) by using multiple frames of channel observations to estimate the index μ . One method is to make individual estimates based on single-frame observations for K successive frames and then to use a majority decision rule which decides the estimate of μ on the majority of these K independent estimates (e.g., [56]). Another approach, which we will present here, is to jointly exploit the K successive frames of observations $\mathbf{r}_K := [r_0, r_1, \dots, r_{KN-1}]^T$ to obtain a single estimate of μ .

Assuming that the channel coefficients \mathbf{h} remain constant during the consecutive K frames of channel observations and following the procedure used to derive (5.7), one can obtain the K -frame based synchronizer, which takes a similar expression to (5.7) as

$$\hat{\mu} = \arg \max_{0 \leq m \leq N-1} \mathbf{r}_{Ks}^{\text{H}(m)} (\mathbf{B}_K - \mathbf{I}_K) \mathbf{r}_{Ks}^{(m)}, \quad (5.8)$$

where \mathbf{I}_K is the $K(N_s - L + 1) \times K(N_s - L + 1)$ identity matrix and

$$\begin{aligned} \mathbf{B}_K &:= \mathbf{S}_K (\mathbf{S}_K^H \mathbf{S}_K)^{-1} \mathbf{S}_K^H, \quad \mathbf{S}_K := \underbrace{[\mathbf{S}^T, \mathbf{S}^T, \dots, \mathbf{S}^T]}_K^T, \\ \mathbf{r}_{Ks}^{(m)} &= [r_K^{(m)}(L-1), \dots, r_K^{(m)}(N_s-1), r_K^{(m)}(N+L-1), \dots, r_K^{(m)}(N+N_s-1), \\ &\quad \dots, r_K^{(m)}((K-1)N+N_s-1)]^T, \quad \mathbf{r}_K^{(m)} := T_{rc}^m(\mathbf{r}_K). \end{aligned}$$

D. Synchronization in the Presence of Frequency offset

We now consider that there is a residual frequency offset in the received signal. Hence, the channel model (5.2) becomes

$$\mathbf{r} = \mathbf{\Omega}T^\mu(\mathbf{x}) + \mathbf{n}, \quad \mathbf{\Omega} := \text{diag}\{\boldsymbol{\omega}\}, \quad \boldsymbol{\omega} := [1, e^{j2\pi f_e}, \dots, e^{j2\pi(N-1)f_e}]^T, \quad (5.9)$$

where f_e stands for the unknown frequency offset normalized to the symbol rate.

Defining $\mathbf{\Omega}_s^{(m)} := \text{diag}\{\boldsymbol{\omega}_s^{(m)}\}$ with $\boldsymbol{\omega}_s^{(m)}$ chosen as the subwindow $[L-1, L, \dots, N_s-1]$ of $\boldsymbol{\omega}^{(m)} := T_{rc}^m(\boldsymbol{\omega})$, and adopting the procedure presented in the last section, we can obtain the following ML-based estimator for μ

$$\hat{\mu} = \arg \min_{0 \leq m \leq N-1} (\mathbf{r}_s^{(m)} - \mathbf{\Omega}_s^{(m)} \mathbf{S} \mathbf{h})^H \cdot (\mathbf{r}_s^{(m)} - \mathbf{\Omega}_s^{(m)} \mathbf{S} \mathbf{h}). \quad (5.10)$$

Similar to (5.6), the ML estimate of \mathbf{h} now takes the expression

$$\hat{\mathbf{h}}(m, f_e) = (\mathbf{S}^H \mathbf{S})^{-1} \mathbf{S}^H \mathbf{\Omega}_s^{H(m)} \mathbf{r}_s^{(m)}, \quad (5.11)$$

and the estimates of μ and f_e can be obtained by maximizing

$$\Lambda_5(m, f_e) = \mathbf{r}_s^{H(m)} (\mathbf{\Omega}_s^{(m)} \mathbf{B} \mathbf{\Omega}_s^{H(m)} - \mathbf{I}) \mathbf{r}_s^{(m)}. \quad (5.12)$$

To proceed, we derive an estimate of f_e as a function of m . Note that $\Lambda_5(m, f_e)$ can be expressed in the form

$$\Lambda_5(m, f_e) = 2\text{re} \left\{ \sum_{i=0}^{N_s-L} \sum_{j=i}^{N_s-L} \omega_s^{(m)}(i) \omega_s^{*(m)}(j) B_{i,j} r_s^{*(m)}(i) r_s^{(m)}(j) \right\} - \sum_{i=0}^{N_s-L} (B_{i,i+1} + 1) |r_s^{(m)}(i)|^2, \quad (5.13)$$

where $B_{i,j}$ is the (i, j) -entry of \mathbf{B} . The second term of the right hand side (RHS) of (5.13) is independent of f_e , and based on the definition of $\boldsymbol{\omega}_s^{(m)}$, the first term of the

RHS of (5.13) can be rewritten for $0 \leq m \leq L - 1$ or $N_s \leq m \leq N - 1$ as

$$2\text{re} \left\{ \sum_{k=0}^{N_s-L} \sum_{i=0}^{N_s-L-k} B_{i,i+k} r_s^{(m)}(i+k) r_s^{*(m)}(i) e^{-j2\pi k f_e} \right\} = 2\text{re} \left\{ \sum_{k=0}^{N-1} \rho_1(k) e^{-j2\pi k f_e} \right\},$$

where

$$\rho_1(k) := \begin{cases} \sum_{i=0}^{N_s-L-k} B_{i,i+k} r_s^{(m)}(i+k) r_s^{*(m)}(i), & \text{if } 0 \leq k \leq N_s - L, \\ 0, & \text{if } N_s - L < k \leq N - 1. \end{cases} \quad (5.14)$$

When m is in the range $[L, N_s - 1]$, defining $q := m - (L - 1)$, lengthy and tedious algebra manipulations lead to the following expressions for the first term of the RHS of (5.13)

$$2\text{re} \left\{ \sum_{k=0}^{N-1} (\rho_1(k) + \rho_2(k)) e^{-j2\pi k f_e} \right\},$$

where

$$\rho_1(k) = \rho_{11}(k) + \rho_{12}(k), \quad (5.15)$$

$$\rho_{11}(k) := \begin{cases} \sum_{i=0}^{q-1-k} B_{i,i+k} r_s^{(m)}(i+k) r_s^{*(m)}(i), & \text{if } 0 \leq k \leq q - 1, \\ 0, & \text{if } q \leq k \leq N - 1, \end{cases} \quad (5.16)$$

$$\rho_{12}(k) := \begin{cases} \sum_{i=q}^{N_s-L-k} B_{i,i+k} r_s^{(m)}(i+k) r_s^{*(m)}(i), & \text{if } 0 \leq k \leq N_s - L - q, \\ 0, & \text{if } N_s - L - q < k \leq N - 1, \end{cases} \quad (5.17)$$

$$\rho_2(k) := \begin{cases} 0, & \text{if } 0 \leq k < P + L, \\ \rho_3^*(N - k), & \text{if } P + L \leq k \leq N - 1, \end{cases} \quad (5.18)$$

$$\rho_3(k) := \sum_{i=0}^{q-1} \sum_{\substack{j=q \\ j-i=k}}^{N_s-L} B_{i,j} r_s^{(m)}(j) r_s^{*(m)}(i), \quad 1 \leq k \leq N_s - L. \quad (5.19)$$

Obviously, for each fixed m , $\hat{f}_e(m)$ can be estimated by

$$\hat{f}_e(m) = \arg \max_{f_e} \left\{ \text{re} \left\{ \sum_{k=0}^{N-1} (\rho_1(k) + \rho_2(k)) e^{-j2\pi k f_e} \right\} \right\}, \quad (5.20)$$

where $\rho_2(k)$ is equal to 0 or given by (5.18) depending on the value of m . It is easy to find that the estimator (5.20) can be efficiently implemented by FFT methods (see e.g., [53], [72]), and the estimation range of f_e is $|f_e| \leq 1/2$, the maximum range that can be expected for any frequency offset estimator operating on baud rate samples [72]. Finally, plugging (5.20) back into (5.12), the ML estimate of μ can be obtained

$$\hat{\mu} = \arg \max_{0 \leq m \leq N-1} \Lambda_6(m), \quad \Lambda_6(m) = \mathbf{r}_s^{\text{H}(m)} \left(\mathbf{\Omega}_s^{(m)}(\hat{f}_e(m)) \mathbf{B} \mathbf{\Omega}_s^{\text{H}(m)}(\hat{f}_e(m)) - \mathbf{I} \right) \mathbf{r}_s^{(m)}. \quad (5.21)$$

The proposed algorithm in the presence of frequency offset can be summarized as follows [105]:

Step 1. Select an arbitrary length- N signal segment \mathbf{r} of the received signal.

Step 2. For each $m \in [0, N-1]$, choose the subwindow of observation $\mathbf{r}_s^{(m)}$ and

- if $m \in [0, L-1]$ or $m \in [N_s, N-1]$, compute the term $\rho_1(k)$ according to (5.14) and set $\rho_2(k) = 0$.
- otherwise, compute the terms $\rho_1(k)$ and $\rho_2(k)$ according to (5.15)–(5.19).

Step 3. For each m , estimate f_e according to (5.20) and compute the metric $\Lambda_6(m)$ based on (5.21).

Step 4. Find a value $\hat{\mu}$ such that the corresponding metric achieves the maximum among the metrics.

Step 5. The frequency offset is obtained by (5.20) with $m = \hat{\mu}$.

Step 6. The channel estimate is given by (5.11) with $m = \hat{\mu}$ and $f_e = \hat{f}_e(\hat{\mu})$.

Exact theoretical analysis of frame synchronization algorithms does not generally appear to be tractable for the decision rules other than the correlation rule even for AWGN channels [56], [88]. Therefore, next we resort to computer simulations to evaluate the performance of the proposed synchronizers.

E. Simulation Results

In computer simulations, the false acquisition probabilities (FAP, i.e., $\hat{\mu} \neq \mu$) and the mean square channel estimation error (MSCEE) $E\{\|\hat{\mathbf{h}} - \mathbf{h}\|^2\}$ of the proposed joint frame synchronization and channel estimation algorithms are evaluated. In the presence of frequency offset, the mean square error (MSE) of \hat{f}_e (i.e., $\text{MSE}(\hat{f}_e) = E\{(\hat{f}_e - f_e)^2\}$) is investigated, too. All experiments are performed assuming 100,000 Monte Carlo trials, the transmitted symbols $\{d_k\}$ are taken from a QPSK constellation, the additive noise \mathbf{n} is generated as white Gaussian noise with variance N_0 and SNR is defined as $\text{SNR} := 10 \log_{10}(\sigma_k^2/N_0)$. The frequency-selective channel coefficients are modeled as i.i.d. complex Gaussian random variables with zero mean and variance $1/L$.

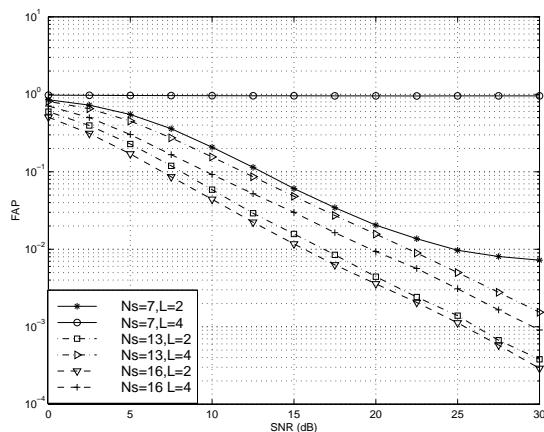


Fig. 48. FAP vs. SNR with fixed N

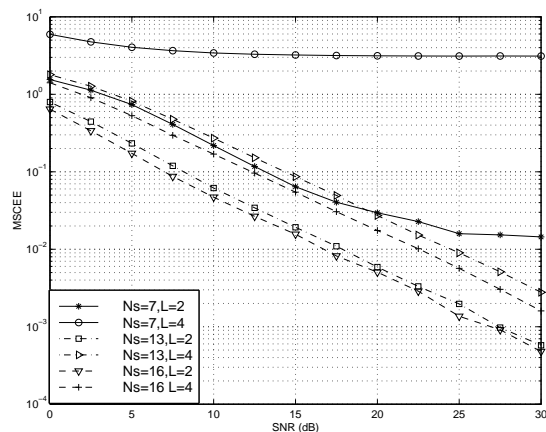


Fig. 49. MSCEE vs. SNR with fixed N

Experiment 1-Performance of the proposed synchronizer with fixed length N : Fixing the total length of frame $N = 64$, we plot the FAP and MSCEE of the synchronizer (5.7) versus SNR in Figs. 48 and 49, respectively, where two different channel orders $L = 2$ and $L = 4$ are assumed. The frame synchronization patterns used are the

7-symbol Barker sequence $\{1, 1, 1, 1, 1, 1, -1\}$, the 13-symbol Neuman-Hofman sequence $\{1, 1, 1, 1, 1, 1, -1, -1, 1, 1, -1, 1, -1\}$, and the midamble with length $N_s = 16$ adopted in the GSM system, i.e.,

$$\{1, -j, 1, j, 1, -j, -1, -j, -1, j, -1, -j, -1, j, -1, -j\}.$$

The results presented in Figs. 48 and 49 show that the performance of the proposed algorithm deteriorates when channel memory L increases or the length of sync words N_s decreases. The failure of (5.7) with $N_s = 7$ in the case of channel memory $L = 4$ is due to the fact that the condition of $N_s \geq L$ is not satisfied in this scenario.

Experiment 2-Performance of the proposed synchronizer with varying length N : Figs. 50 and 51 plot FAP and MSCEE versus SNR assuming 13-symbol Neuman-Hofman sequence and 16-symbol GSM midamble, channel memory $L = 4$, and different values of frame length N . It can be seen that the performance of the proposed synchronizer is not sensitive to the frame length, especially at medium and high SNRs, which is a pleasing property in the sense that we can increase the length P of useful data sequence to obtain a high transmission efficiency.

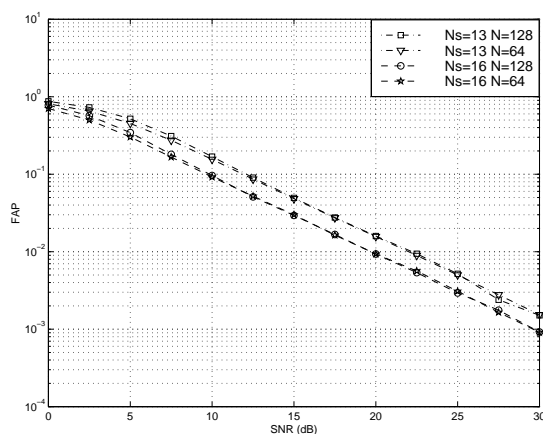


Fig. 50. FAP vs. SNR with varying N

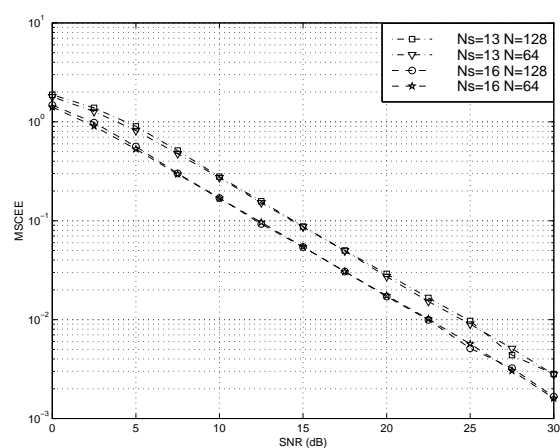


Fig. 51. MSCEE vs. SNR with varying N

Experiment 3-Multiple-frame synchronization: In Figs. 52 and 53, we compare the performance of multiple-frame synchronizer (5.8) ($K = 2$) with that of the single-frame based algorithm (5.7), assuming the following parameters: $N_s = 13$ and $N_s = 16$, $L = 4$ and $N = 128$. One can find that the former can provide 2 or 3 dB improvement over the latter with the price of a larger processing delay.

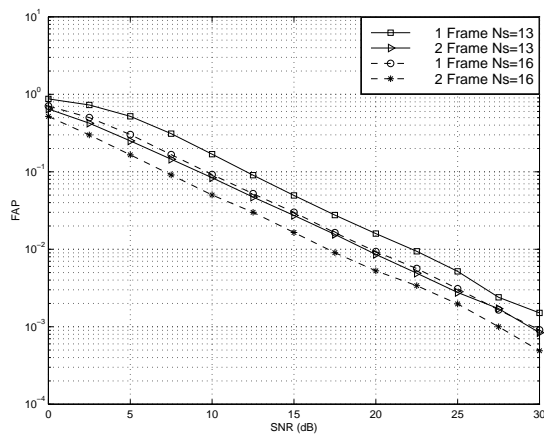


Fig. 52. Improvement of FAP with multiple-frame synchronization

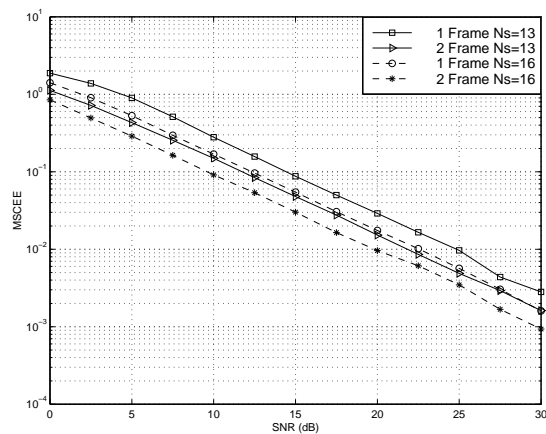
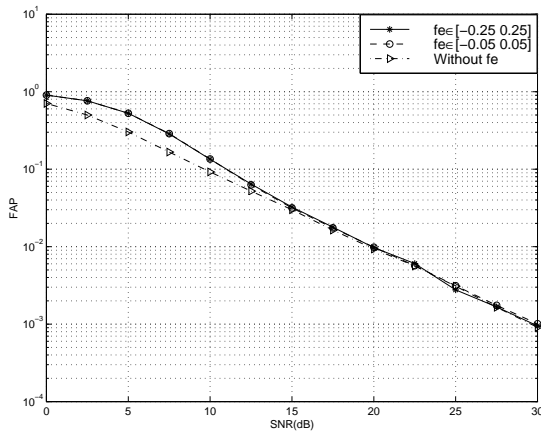
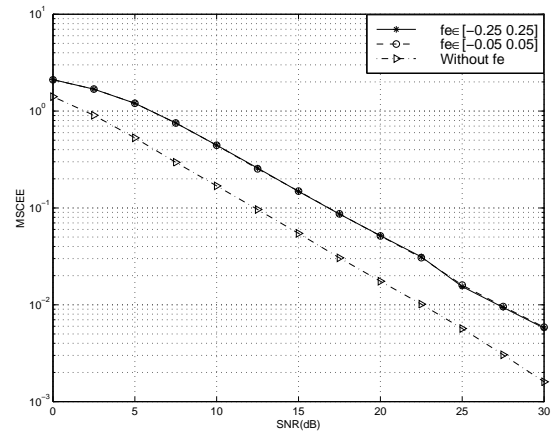
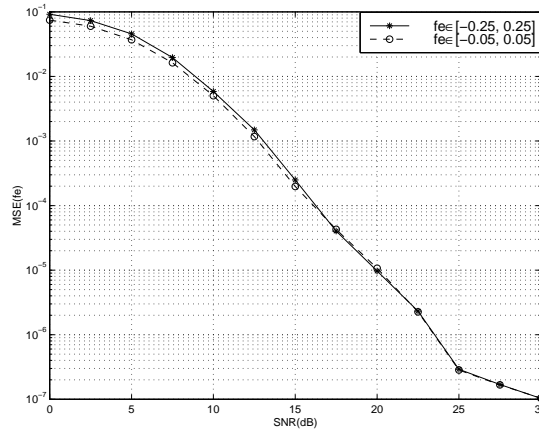


Fig. 53. Improvement of MSCEE with multiple-frame synchronization

Experiment 4-Performance of the proposed synchronizer in the presence of frequency offset: Fixing $L = 4$, $N_s = 16$ and $N = 64$, Figs. 54–56 illustrate the FAP, MSCEE and $MSE(\hat{f}_e)$ of the proposed algorithm in the presence and absence of frequency offset, respectively. In each simulation run, the frequency offset is selected randomly from the interval $[-f_0, f_0]$, assuming a uniform distribution. Two values of the upper-bound f_0 , $f_0 = 0.25$ (large frequency offset) and $f_0 = 0.05$ (small frequency offset), are used. Fig. 54 illustrates that the proposed frame acquisition algorithm is quite robust to frequency offsets, while Figs. 55-56 show that the proposed channel and frequency offset estimators exhibit almost the same performance in the presence of large and small frequency offsets.

Fig. 54. FAP in the presence of f_e Fig. 55. MSCEE in the presence of f_e Fig. 56. $MSE(\hat{f}_e)$ in the presence of f_e

F. Conclusion

We have proposed an ML synchronizer for joint frame, channel and frequency offset acquisition for continuous mode linearly modulated transmissions through frequency-selective channels affected by Doppler shift/carrier frequency offset. The proposed algorithms are computationally efficient, robust to frequency offsets, do not necessitate detection of the unknown data symbols, and exhibit good performance.

CHAPTER VI

SUMMARY

In this dissertation, several novel signal processing frameworks have been established to analyze and improve the performance of the existing synchronization algorithms for digital receivers. Moreover, unified methods for designing new computationally and statistically efficient feedforward synchronizers are developed for timing recovery, carrier estimation and frame synchronization. The topic of this dissertation covers most directions of synchronization problem, and it brings significant contribution and in-depth insights from both the performance analysis and design methodology points of view.

REFERENCES

- [1] M. Abramowitz and I. A. Stegun, Eds., *Handbook of Mathematical Functions*, Washington, DC: National Bureau of Standards, 1964.
- [2] A. N. D'Andrea, U. Mengali, and M. Morelli, "Symbol timing estimation with CPM modulation," *IEEE Transaction on Communications*, vol. 44, no. 10, pp. 1362-1371, October 1996.
- [3] S. Bellini, C. Molinari and G. Tartara, "Digital frequency estimation in burst mode QPSK transmission," *IEEE Transaction on Communications*, vol. 38, no. 7, pp. 959-961, July 1990.
- [4] S. Bellini, "Frequency estimators for M-PSK operating at one sample per symbol," in *Proc. GLOBECOM'94*, San Francisco, CA, 1994, pp. 962-966.
- [5] W. R. Bennet, "Statistics of regenerative digital transmission," *Bell Syst. Tech. J.*, vol. 37, no. 6, pp. 1501-1542, November 1958.
- [6] C. Bergogne, P. Sehier and M. Bousquet, "Reduced complexity frequency estimator for burst transmission," in *Proc. GLOBECOM'95*, vol. 2, Singapore, 1995, pp. 1318-1322.
- [7] C. Bergogne, P. Sehier and M. Bousquet, "Reduced complexity frequency estimator applied to burst transmission", in *Proc. IEEE International Conference on Universal Personal Communications*, Tokyo, Japan, 1995, pp. 231-235.
- [8] O. Besson, M. Ghogho, and A. Swami, "Parameter estimation for random amplitude chirp signals," *IEEE Transaction on Signal Processing*, vol. 47, no. 12, pp. 3208-3219, December 1999.

- [9] O. Besson and P. Stoica, "Frequency estimation and detection for sinusoidal signal with arbitrary envelope: a nonlinear least-squares approach," in *Proc. ICASSP'98*, Seattle, WA, USA, 1998, 2209-2212.
- [10] D. R. Brillinger, *Time Series Data Analysis and Theory*, San Francisco, CA: Holden Day, 1981.
- [11] D. R. Brillinger, "The comparison of least-squares and third-order periodogram procedures in the estimation of bifrequency," *Journal of Time Series Analysis*, vol. 1, no. 2, pp. 95–102, March 1980.
- [12] K. V. Cartwright, "Blind phase recovery in general QAM communication systems using alternative higher order statistics," *IEEE Signal Processing Letters*, vol. 6, no. 12, pp. 327-329, December 1999.
- [13] K. V. Cartwright, "Blind phase recovery in cross QAM communication systems with eighth-order statistics," *IEEE Signal Processing Letters*, vol. 8, pp. 304-306, December 2001.
- [14] L. Chen, H. Kusaka and M. Kominami, "Blind phase recovery in QAM communication systems using higher order statistics," *IEEE Signal Processing Letters*, vol. 3, no. 5, pp. 147-149, May 1996.
- [15] A. Chevreuil, E. Serpedin, P. Loubaton and G. B. Giannakis, "Blind channel identification and equalization using periodic modulation precoders: performance analysis," *IEEE Transaction on Signal Processing*, vol. 48, no. 6, pp. 1570-1586, June 2000.
- [16] Z. Y. Choi and Y. H. Lee, "Frame synchronization in the presence of frequency offset," *IEEE Transaction on Communications*, vol. 50, no. 7, pp. 1062-1065,

July 2002.

- [17] J. C.-I. Chuang and N. R. Sollenberger, "Burst coherent demodulation with combined symbol timing, frequency offset estimation, and diversity selection," *IEEE Transaction on Communications*, vol. 39, no. 7, pp. 1157-1164, July 1991.
- [18] P. Ciblat, P. Loubaton, E. Serpedin, and G. B. Giannakis, "Performance analysis of blind carrier frequency offset estimators for non-circular transmissions through frequency-selective channels," *IEEE Transaction on Signal Processing*, vol. 50, no. 1, pp. 130–140, January 2002.
- [19] P. Ciblat, P. Loubaton, E. Serpedin and G. B. Giannakis, "Asymptotic analysis of blind cyclic correlation based symbol-rate estimators," *IEEE Transaction on Information Theory*, vol. 48, no. 7, pp. 1922-1934, July 2002.
- [20] P. Ciblat, E. Serpedin, and Y. Wang, "On a blind fractionally-sampling based carrier frequency offset estimator for non-circular transmissions," *IEEE Signal Processing Letters*, vol. 10, no. 4, April 2003.
- [21] P. Ciblat and L. Vandendorpe, "Blind carrier frequency offset estimation for non-circular constellation based transmission," *IEEE Transaction on Signal Processing*, vol. 51, no. 5, pp. 1378–1389, May 2003.
- [22] H. A. Cirpan and M. K. Tsatsanis, "Maximum likelihood blind channel estimation in the presence of Doppler shifts," *IEEE Transaction on Signal Processing*, vol. 47, no. 6, pp. 1559-1569, June 1999.
- [23] F. Classen, H. Meyr, and P. Sehier, "Maximum likelihood open loop carrier synchronizer for digital radio," in *Proc. ICC'93*, Geneva, Switzerland, 1993, pp. 493-497.

- [24] S. N. Crozier, "Low complexity frequency estimator with close-to-optimum performance", in *Proc. IEEE International Conference on Universal Personal Communications*, vol. 1, Ottawa, Canada, 1993, pp. 426-430.
- [25] A. V. Dandawaté and G. B. Giannakis, "Nonparametric polyspectral estimators for k th-order (almost) cyclostationary processes," *IEEE Transaction on Information Theory*, vol. 40, no. 6, pp. 67-84, January 1994.
- [26] A. V. Dandawaté and G. B. Giannakis, "Asymptotic theory of mixed time average and k th-order cyclic-moment and cumulant statistics," *IEEE Transaction on Information Theory*, vol. 41, no. 1, pp. 216-232, January 1995.
- [27] Z. Ding, "Characteristics of band-limited channels unidentifiable from second-order cyclostationary statistics," *IEEE Signal Processing Letters*, vol. 3, no. 5, pp. 150-152, May 1996.
- [28] D. Efstathiou and A. H. Aghvami, "A comparison study of the estimation period of carrier phase and amplitude gain error for 16-QAM Rayleigh faded burst transmission," in *Proc. GLOBECOM'94*, San Francisco, CA, 1994, pp. 1904-1908.
- [29] D. Efstathiou and A. H. Aghvami, "Feedforward synchronization techniques for 16-QAM TDMA demodulations," in *Proc. ICC'96*, London, UK, 1996, pp. 1432-1436.
- [30] S. A. Fechtel and H. Meyr, "Fast frame synchronization, frequency offset estimation and channel acquisition for spontaneous transmission over unknown frequency-selective radio channels," in *Proc. PIMRC'93*, Yokohama, Japan, 1993, pp. 229-233.

- [31] S. A. Fechtel and H. Meyr, "Improved frame synchronization for spontaneous packet transmission over frequency-selective radio channels," in *Proc. PIMRC'94*, Hague, Holland, 1994, pp. 353-357.
- [32] G. Feyh, "Using cyclostationarity for timing synchronization and blind equalization," in *Proc. Asilomar'94*, Pacific Grove, CA, 1994, pp. 1448-1452.
- [33] M. P. Fitz, "Nonlinear digital carrier synchronization for Rician fading channels," in *Proc. GLOBECOM'90*, San Diego, CA, 1990, pp. 623-628.
- [34] J. M. Francos and B. Friedlander, "Bounds for estimation of multicomponent signals with random amplitude and deterministic phase," *IEEE Transaction on Signal Processing*, vol. 43, no. 5, pp. 1161-1172, May 1995.
- [35] L. E. Franks and J. P. Bubrouski, "Statistical properties of timing jitter in a PAM timing recovery scheme," *IEEE Transaction on Communications*, vol. 22, no. 7, pp. 913-920, July 1974.
- [36] J. A. Gansman, M. P. Fitz and J. V. Krogmeier, "Optimum and suboptimum frame synchronization for pilot-symbol-assisted modulation," *IEEE Transaction on Communications*, vol. 45, no. 10, pp. 1327-1337, October 1997.
- [37] C. N. Georghiades, "Chapter 19: Synchronization," in *The Communications Handbook*, J. D. Gibsson Ed., Boca Raton, FL: CRC Press, 2002.
- [38] C. N. Georghiades, "Blind carrier phase acquisition for QAM constellations," *IEEE Transaction on Communications*, vol. 45, no. 11, pp. 1477-1486, November 1997.
- [39] M. Ghogho, A. K. Nandi and A. Swami, "Cramèr-Rao bounds and maximum likelihood estimation for random amplitude phase-modulated signals," *IEEE*

- Transaction on Signal Processing*, vol. 47, no. 11, pp. 2905-2916, November 1999.
- [40] M. Ghogho and A. Swami, "Non-efficiency of the nonlinear least-squares estimator of polynomial phase signals in colored noise," in *Proc. Asilomar'98*, Pacific Grove, CA, 1998, pp. 1447-1451.
- [41] M. Ghogho, A. Swami and T. Durrani, "On blind carrier recovery in time-selective fading channels," in *Proc. Asilomar'99*, vol. 1, Pacific Grove, CA, 1999, pp. 243-247.
- [42] M. Ghogho, A. Swami, and T. Durrani, "Nonlinear least-squares estimation for harmonics in multiplicative and additive noise," *Signal Processing*, vol. 79, no. 2, pp. 43-60, October 1999.
- [43] G. B. Giannakis, "Cyclostationary Signal Analysis," Chapter in *Digital Signal Processing Handbook*, V. K. Madisetti and D. Williams, Eds., Boca Raton, FL: CRC Press, 1998.
- [44] F. Gini and G. B. Giannakis, "Frequency offset and symbol timing recovery in flat-fading channels: a cyclostationary approach," *IEEE Transaction on Communications*, vol. 46, no. 3, pp. 400-411, March 1998.
- [45] F. Gini and R. Reggiannini, "On the use of Cramér-Rao-like bounds in the presence of random nuisance parameters," *IEEE Transaction on Communications*, vol. 48, no. 12, pp. 2120-2126, December 2000.
- [46] I. S. Gradshteyn and I. M. Ryzhik, *Table of Integrals, Series, and Products*, New York: Academic, 1965.

- [47] T. Hasan, "Nonlinear time series regression for a class of amplitude modulated cosinusoids," *Journal of Time Series Analysis*, vol. 3, no. 2, pp. 109-122, 1982.
- [48] Y. Hongyi and B. Zhang, "Fully blind estimation of time delays and spatial signatures for cyclostationary signals," *Electronics Letters*, vol. 34, no. 25, pp. 2378-2380, December 1998.
- [49] Z.-T. Huang, Y.-Y. Zhou, W.-L. Jiang, and Q.-Z. Lu, "Joint estimation of Doppler and time-difference-of-arrival exploiting cyclostationary property," *IEE Proc. on Radar, Sonar and Navigation*, vol. 149, no. 4, pp. 161-165, August 2002.
- [50] L. Izzo and A. Napolitano, "Higher-order cyclostationary properties of sampled time-series," *Signal Processing*, vol. 54, no. 3, pp. 303-307, November 1996.
- [51] G. D. Jonghe and M. Moeneclaey, "Optimal averaging filter length of the Viterbi and Viterbi carrier synchronizer for a given frequency offset," in *Proc. GLOBE-COM'94*, San Francisco, 1994, pp. 1363-1368.
- [52] S. M. Kay, *Fundamentals of Statistical Signal Processing: Estimation Theory*, Paramus, NJ: Prentice-Hall, 1993.
- [53] Y. Koo and Y. H. Lee, "A joint maximum likelihood approach to frame synchronization in presence of frequency offset," in *Proc. ICC'02*, vol. 3, New York, 2002, pp. 1546-1550.
- [54] U. Lambrette, J. Horstmannshoff and H. Meyr, "Techniques for frame synchronization on unknown frequency selective channels," in *Proc. VTC'97*, vol. 2, Phoenix, AZ, 1997, pp. 1059-1063.

- [55] S. J. Lee, "A new non-data-aided feedforward symbol timing estimator using two samples per symbol," *IEEE Communications Letters*, vol. 6, No. 5, pp. 205-207, May 2002.
- [56] G. L. Liu and H. H. Tan, "Frame synchronization for Gaussian channels," *IEEE Transaction on Communications*, vol. 35, no. 8, pp. 818-829, August 1987.
- [57] J. L. Massey, "Optimum frame synchronization," *IEEE Transaction on Communications*, vol. 20, no. 2, pp. 115-119, April 1972.
- [58] J. E. Mazo, "Jitter comparison of tones generated by squaring and by fourth-power circuits," *Bell Syst. Tech. J.*, vol. 57, no. 5, pp. 1489-1498, May-June 1978.
- [59] F. Mazzenga and G. E. Corazza, "Blind least-squares estimation of carrier phase, Doppler shift, and Doppler rate for M-PSK burst transmission," *IEEE Communications Letters*, vol. 2, no. 3, pp. 73-75, March 1998.
- [60] F. Mazzenga and F. Vatalaro, "Parameter estimation in CDMA multiuser detection using cyclostationary statistics," *Electronics Letters*, vol. 32, no. 3, pp. 179-181, February 1996.
- [61] R. Mehlman, Y. Chen, and H. Meyr, "A fully digital feedforward MSK demodulator with joint frequency offset and symbol timing estimation for burst mode mobile radio," *IEEE Transaction on Vehicular Technology*, vol. 42, no. 4, pp. 434-443, November 1993.
- [62] R. Mehlman, and H. Meyr, "Optimum frame synchronization for asynchronous packet transmission," in *Proc. ICC'93*, vol. 2 Geneva, Switzerland, 1993, pp. 826-830.

- [63] U. Mengali and A. N. D' Andrea, *Synchronization Techniques for Digital Receivers*, New York: Plenum Press, NY, 1997.
- [64] H. Meyr, M. Moeneclaey, and S. A. Fechtel, *Digital Communication Receivers: Synchronization, Channel Estimation, and Signal Processing*, New York: Wiley, NY, 1998.
- [65] K. S. Miller, *Some Eclectic Matrix Theory*, Malabar, FL: Robert E. Krieger Publishing Company, 1987.
- [66] M. Moeneclaey and G. de Jonghe, "Tracking performance comparison of two feedforward ML-oriented carrier-independent NDA symbol synchronizers," *IEEE Transaction on Communications*, vol. 40, no. 9, pp. 1423-1425, September 1992.
- [67] M. Moeneclaey and G. de Jonghe, "ML-oriented NDA carrier synchronization for general rotationally symmetric signal constellations," *IEEE Transaction on Communications*, vol. 42, no. 8, pp. 2531-2533, August 1994.
- [68] B. H. Moon, and S. S. Soliman, "ML frame synchronization for the Gaussian channel with ISI," in *Proc. ICC'91*, Denver, CO, 1991, pp. 1698-1702.
- [69] M. Morelli, "Doppler-rate estimation for burst digital transmission," *IEEE Transaction on Communications*, vol. 50, no. 5, pp. 707-710, May 2002.
- [70] M. Morelli, A. N. D' Andrea, and U. Mengali, "Feedforward estimation techniques for carrier recovery in 16-QAM modulation," in *Broadband Wireless Communications*, M. Luise and S. Pupolin, Eds., New York: Springer, 1998.
- [71] M. Morelli, A. N. D' Andrea and U. Mengali, "Feedforward ML-based timing estimation with PSK signals," *IEEE Communications Letters*, vol. 1, no. 3,

- pp. 80-82, May 1997.
- [72] M. Morelli, and U. Mengali, "Carrier-frequency estimation for transmissions over selective channels," *IEEE Transaction on Communications*, vol. 48, no. 9, pp. 1580-1589, September 2000.
- [73] A. Napolitano, "Cyclic higher-order statistics: input/output relations for discrete- and continuous-time MIMO linear almost-periodically time-variant systems," *Signal Processing*, vol. 42, no. 2, pp. 147-166, March 1995.
- [74] P. T. Nielsen, "Some optimum and suboptimum frame synchronizers for binary data in Gaussian noise," *IEEE Transaction on Communications*, vol. 21, pp. 770-772, June 1973.
- [75] M. Oerder and H. Meyr, "Digital filter and square timing recovery," *IEEE Transaction on Communications*, vol. 36, no. 5, pp. 605-612, May 1988.
- [76] A. V. Oppenheim and R. W. Schaffer, *Discrete-Time Signal Processing*. Englewood Cliffs, NJ: Prentice-Hall, 1989.
- [77] B. E. Padon, "A matched nonlinearity for phase estimation of a PSK-modulated carrier," *IEEE Transaction on Information Theory*, vol. 32, no. 3, pp. 419-422, May 1986.
- [78] E. Panayirci and E. Y. Bar-Ness, "A new approach for evaluating the performance of a symbol timing recovery system employing a general type of nonlinearity," *IEEE Transaction on Communications*, vol. 44, no. 1, pp. 29-33, January 1996.
- [79] A. Papoulis, *Probability, Random Variables, and Stochastic Processes*, Third edition, New York: WCB/McGraw-Hill, 1991.

- [80] D. R. Pauluzzi and N. C. Beaulieu, "A comparison of SNR estimation techniques for the AWGN channel," *IEEE Transaction on Communications*, vol. 48, no. 10, pp. 1681-1691, October 2000.
- [81] B. Picinbono and P. Bondon, "Second-order statistics of complex signals," *IEEE Transaction on Signal Processing*, vol. 45, no. 2, pp. 411-420, February 1997.
- [82] B. Porat, *Digital Processing of Random Signals*, Paramus, NJ: Prentice-Hall, 1994.
- [83] J. G. Proakis, *Digital Communications*, 3rd ed. New York: McGraw Hill, 1995.
- [84] T. S. Rappaport, *Wireless Communications: Principles and Practice*, Upper Saddle River, NJ: Prentice Hall, 1996.
- [85] J. Riba, J. Sala and G. Vázquez, "Conditional maximum likelihood timing recovery: estimators and bounds," *IEEE Transaction on Signal Processing*, vol. 49, no. 4, pp. 835-850, April 2001.
- [86] F. Rice, B. Cowley, B. Moran and M. Rice, "Cramér-Rao lower bound for QAM phase and frequency estimation," *IEEE Transaction on Communications*, vol. 49, no. 9, pp. 1582-1591, September 2001.
- [87] F. Rice, B. Cowley, and M. Rice, "A new bound and algorithm for star 16QAM carrier phase estimation," *IEEE Transaction on Communications*, vol. 51, no. 2, pp. 161-165, February 2003.
- [88] P. Robertson, "Maximum likelihood frame synchronization for flat fading channels," in *Proc. ICC'92*, Chicago, IL, 1992, pp. 1426-1430.

- [89] H. Sari and S. Moridi, "New phase and frequency detectors for carrier recovery in PSK and QAM systems," *IEEE Transaction on Communications*, vol. 36, no. 9, pp. 1035-1043, September 1988.
- [90] K. E. Scott and E. B. Olasz, "Simultaneous clock phase and frequency offset estimation," *IEEE Transaction on Communications*, vol. 43, no. 7, pp. 2263-2270, July 1995.
- [91] E. Serpedin, A. Chevreuil, G. B. Giannakis, and P. Loubaton, "Blind channel and carrier frequency offset estimation using periodic modulation precoders," *IEEE Transaction on Signal Processing*, vol. 48, no. 8, pp. 2389-2405, August 2000.
- [92] E. Serpedin, P. Ciblat, G. B. Giannakis and P. Loubaton, "Performance analysis of blind carrier phase estimators for general QAM constellations," *IEEE Transaction Signal Processing*, vol. 49, no. 8, pp. 1816-23, August 2001.
- [93] J. P. Seymour and M. P. Fitz, "Nonlinear digital phase estimation for mobile communications," in *Proc. PIMRC'92*, Boston, MA, 1992, pp. 194-198.
- [94] R. A. Scholtz, "Frame synchronization techniques," *IEEE Transaction on Communications*, vol. 28, no. 8, pp. 1204-1213, August 1980.
- [95] T. Söderström and P. Stoica, *System Identification*, Paramus, NJ: Prentice-Hall, 1989.
- [96] C. M. Spooner, "Chapter 2: Higher-order statistics for nonlinear processing of cyclostationary signals," in *Cyclostationary in Communications and Signal Processing*, W. A. Gardner Ed., New York: IEEE Press, 1993.

- [97] C. M. Spooner and W. A. Gardner, "The cumulant theory of cyclostationary time-series, Part II: Development and applications," *IEEE Transaction on Signal Processing*, vol. 42, no. 12, pp. 3409-3429, December 1994.
- [98] P. Stoica and R. Moses, *Introduction to Spectral Analysis*, Paramus, NJ: Prentice-Hall, 1997.
- [99] L. Tong, "Joint blind signal detection and carrier recovery over fading channel," in *Proc. ICASSP'95*, Detroit, MI, 1995, pp. 1205-1208.
- [100] L. Tong, G. Xu, B. Hassibi and T. Kailath, "Blind channel identification based on second-order statistics: a frequency-domain approach," *IEEE Transaction on Signal Processing*, vol. 41, no. 1, pp. 329-334, January 1995.
- [101] G. Vazquez and J. Riba, "Non-data aided digital synchronization," Chapter 9 in *Signal Processing Advances in Wireless and Mobile Communications*, G. B. Giannakis, Y. Hua, P. Stoica and L. Tong, Eds., vol. 1, pp. 357-402, Paramus, NJ: Prentice-Hall, 2001.
- [102] A. J. Viterbi and A. M. Viterbi, "Nonlinear estimation of PSK-modulated carrier phase with application to burst digital transmissions," *IEEE Transaction on Information Theory*, vol. 29, no. 4, pp. 543-551, July 1983.
- [103] Y. Wang, P. Ciblat, E. Serpedin and P. Loubaton, "Performance analysis of a class of non-data aided frequency offset and symbol timing estimators for flat-fading channels," *IEEE Transaction on Signal Processing*, vol. 50, no. 9, pp. 2295-2305, September 2002.
- [104] Y. Wang and E. Serpedin, "A class of blind phase recovery techniques for higher-order QAM modulations: estimators and bounds," *IEEE Signal Processing*

Letters, vol. 9, no. 10, pp. 301–304, October 2002.

- [105] Y. Wang and E. Serpedin, “Continuous-mode frame synchronization for frequency-selective channels,” *IEEE Transactions on Vehicular Technology* (accepted), 2002.
- [106] Y. Wang and E. Serpedin, “Non-data aided feedforward carrier frequency offset estimators for QAM constellations: a nonlinear least-squares approach,” *EURASIP Journal on Applied Signal Processing*, Elsevier, Netherlands (submitted), 2003.
- [107] Y. Wang and E. Serpedin, “Optimal matched blind carrier phase estimators for star 16QAM constellations,” in *Proc. Conference on Information, Sciences and Systems*, Princeton, NJ, March 2002, CDROM.
- [108] Y. Wang, E. Serpedin, and P. Ciblat, “An alternative blind feedforward symbol timing estimator using two samples per symbol,” *IEEE Transactions on Communications*, vol. 51, no. 9, pp. 1451–1455, September, 2003.
- [109] Y. Wang, E. Serpedin, and P. Ciblat, “Blind feedforward cyclostationary-based timing estimation for linear modulations,” *IEEE Transactions on Wireless Communications* (accepted), 2002.
- [110] Y. Wang, E. Serpedin, and P. Ciblat, “Optimal blind carrier recovery for M-PSK burst transmissions,” *IEEE Transactions on Communications*, vol. 51, no. 9, pp. 1571–1581, September, 2003.
- [111] Y. Wang, E. Serpedin, and P. Ciblat, “Optimal blind nonlinear least-squares carrier phase and frequency offset estimation for general QAM modulations,”

- IEEE Transactions on Wireless Communications*, vol. 2, no. 5, pp. 1040–1054, September, 2003.
- [112] Y. Wang, E. Serpedin, P. Ciblat, and P. Loubaton, “Non-data-aided feedforward cyclostationary statistics based carrier frequency offset estimators for linear modulations,” in *Proc. GLOBECOM’01*, vol. 2, San Antonio, TX, 2001, pp. 1386-1390.
- [113] W. T. Webb and L. Hanzo, *Modern Quadrature Amplitude Modulation : Principles and Applications for Fixed and Wireless Channels*, New York: IEEE Press and London: Pentech Press, 1994.
- [114] G. Zhou and G. B. Giannakis, “Harmonics in multiplicative and additive noise: performance analysis of cyclic estimators,” *IEEE Transaction on Signal Processing*, vol. 43, no. 6, pp. 1445–1460, June 1995.
- [115] W.-P. Zhu, M. O. Ahmad and M. N. S. Swamy, “A fully digital timing recovery scheme using two samples per symbol,” in *Proc. IEEE Int. Symp. on Circuits and systems*, vol. 2, Sydney, Australia, 2001, pp. 421-424.

APPENDIX A

DERIVATION OF EQUATIONS (2.8) AND (2.16)

Using (2.5), we can express $E\{y(n)\}$ as follows:

$$\begin{aligned}
E\{y(n)\} &= E\{F(\rho(n))e^{jM\varphi(n)}\} \\
&= \frac{1}{M} \sum_{m=0}^{M-1} \int_0^\infty \frac{\rho(n)F(\rho(n))}{\pi\sigma_v^2} e^{-\frac{\rho^2(n)+1}{\sigma_v^2}} \int_{-\pi}^\pi e^{jM\varphi(n)} e^{\frac{2\rho(n)}{\sigma_v^2} \cos[\varphi(n) - \frac{2\pi m}{M} - \phi(n)]} d\varphi(n) d\rho(n) \\
&= \frac{1}{M} \sum_{m=0}^{M-1} e^{j2\pi m} e^{jM\phi(n)} \int_0^\infty \frac{2\rho(n)F(\rho(n))}{\sigma_v^2} e^{-\frac{\rho^2(n)+1}{\sigma_v^2}} I_M\left(\frac{2\rho(n)}{\sigma_v^2}\right) d\rho(n), \\
&= e^{jM\phi(n)} \int_0^\infty F(\rho(n)) \frac{I_M\left(\frac{2\rho(n)}{\sigma_v^2}\right)}{I_0\left(\frac{2\rho(n)}{\sigma_v^2}\right)} \cdot \frac{2\rho(n)}{\sigma_v^2} e^{-\frac{\rho^2(n)+1}{\sigma_v^2}} I_0\left(\frac{2\rho(n)}{\sigma_v^2}\right) d\rho(n), \tag{A.1}
\end{aligned}$$

where in deriving the third equality we made use of the definition of $I_M(\cdot)$ [1, eq. (9.6.19)]. Then, by exploiting (2.6), equations (2.8) and (2.9) follow. Similar to (A.1), the following expression can be derived:

$$\begin{aligned}
E\{y^2(n)\} &= E\{F^2(\rho(n))e^{j2M\varphi(n)}\} \\
&= e^{j2M\phi(n)} \int_0^\infty F^2(\rho(n)) \frac{I_{2M}\left(\frac{2\rho(n)}{\sigma_v^2}\right)}{I_0\left(\frac{2\rho(n)}{\sigma_v^2}\right)} \cdot \frac{2\rho(n)}{\sigma_v^2} e^{-\frac{\rho^2(n)+1}{\sigma_v^2}} I_0\left(\frac{2\rho(n)}{\sigma_v^2}\right) d\rho(n),
\end{aligned}$$

which proves (2.16).

APPENDIX B

PROOF OF THEOREM 1

In order to establish the Theorem 1, let us first study the second-order statistics of additive noise $u(n)$. From (2.10), $u(n)$ can be expressed as:

$$u(n) := y(n) - \mathbb{E}\{y(n)\} = F(\rho(n))e^{jM\varphi(n)} - \mathbb{E}\{F(\rho(n))e^{jM\varphi(n)}\} .$$

Define the second-order unconjugate/conjugate autocorrelations of $u(n)$ as:

$$\begin{aligned} r_u(n; \tau) &:= \mathbb{E}\{u^*(n)u(n + \tau)\} = \mathbb{E}\left\{F(\rho(n))e^{-jM\varphi(n)}F(\rho(n + \tau))e^{jM\varphi(n + \tau)}\right\} \\ &\quad - \mathbb{E}\left\{F(\rho(n))e^{-jM\varphi(n)}\right\}\mathbb{E}\left\{F(\rho(n + \tau))e^{jM\varphi(n + \tau)}\right\} , \\ \tilde{r}_u(n; \tau) &:= \mathbb{E}\{u(n)u(n + \tau)\} = \mathbb{E}\left\{F(\rho(n))e^{jM\varphi(n)}F(\rho(n + \tau))e^{jM\varphi(n + \tau)}\right\} \\ &\quad - \mathbb{E}\left\{F(\rho(n))e^{jM\varphi(n)}\right\}\mathbb{E}\left\{F(\rho(n + \tau))e^{jM\varphi(n + \tau)}\right\} , \end{aligned}$$

respectively. Due to (2.7), it turns out that $r_u(n; \tau)$ and $\tilde{r}_u(n; \tau)$ are both equal to zero if $\tau \neq 0$. Hence, we obtain from (2.9), (2.15) and (2.16) the following relations:

$$r_u(n; \tau) = \left[\mathbb{E}\{F^2(\rho(n))\} - \left| \mathbb{E}\{F(\rho(n))e^{jM\varphi(n)}\} \right|^2 \right] \delta(\tau) = (\mathcal{B} - \mathcal{C}^2)\delta(\tau) , \quad (\text{B.1})$$

$$\begin{aligned} \tilde{r}_u(n; \tau) &= \left[\mathbb{E}\{F^2(\rho(n))e^{j2M\varphi(n)}\} - \mathbb{E}^2\{F(\rho(n))e^{jM\varphi(n)}\} \right] \delta(\tau) \\ &= (\mathcal{D} - \mathcal{C}^2)e^{j2M\phi(n)}\delta(\tau) . \quad (\text{B.2}) \end{aligned}$$

Next, we begin the derivation of the Theorem 1. Considering the Taylor series expansion of $\hat{\mathcal{C}} \exp(j \sum_{l=0}^2 \hat{\omega}_l n^l)$ in the neighborhood of the true value $[\mathcal{C} \ \omega_0 \ \omega_1 \ \omega_2]^T$, we can write:

$$\hat{\mathcal{C}} e^{j \sum_{l=0}^2 \hat{\omega}_l n^l} = \mathcal{C} e^{j \sum_{l=0}^2 \omega_l n^l} + (\hat{\mathcal{C}} - \mathcal{C}) e^{j \sum_{l=0}^2 \omega_l n^l} + j \sum_{k=0}^2 n^k (\hat{\omega}_k - \omega_k) \mathcal{C} e^{j \sum_{l=0}^2 \omega_l n^l} + \text{rem} ,$$

where rem stands for the high-order remainder terms which asymptotically as $N \rightarrow \infty$ can be neglected. Thus, we can approximate (2.12) by:

$$J(\hat{\boldsymbol{\omega}}) \doteq \frac{1}{2} \sum_{n=0}^{N-1} \left| y(n) - \mathcal{C} e^{j \sum_{i=0}^2 \omega_i n^i} - (\hat{\mathcal{C}} - \mathcal{C}) e^{j \sum_{i=0}^2 \omega_i n^i} - j \sum_{k=0}^2 n^k (\hat{\omega}_k - \omega_k) \mathcal{C} e^{j \sum_{i=0}^2 \omega_i n^i} \right|^2.$$

Setting the derivatives of $J(\hat{\boldsymbol{\omega}})$ w.r.t. $\hat{\boldsymbol{\omega}}$ to 0, we obtain:

$$\begin{aligned} \sum_{n=0}^{N-1} \text{re} \left\{ u(n) e^{-jM\phi(n)} \right\} - N(\hat{\mathcal{C}} - \mathcal{C}) &= 0, \\ \sum_{n=0}^{N-1} n^k \text{im} \left\{ u(n) e^{-jM\phi(n)} \right\} - \mathcal{C} \sum_{l=0}^2 (\hat{\omega}_l - \omega_l) \sum_{n=0}^{N-1} n^{k+l} &= 0, \quad k = 0, 1, 2. \end{aligned}$$

We normalize the above equations by $N^{1/2}$ and $N^{k+1/2}$, $k = 0, 1, 2$, respectively, and obtain that asymptotically ($N \rightarrow \infty$) the following relations hold (c.f. [40]):

$$\frac{1}{\sqrt{N}} \sum_{n=0}^{N-1} \text{re} \left\{ u(n) e^{-jM\phi(n)} \right\} = \sqrt{N}(\hat{\mathcal{C}} - \mathcal{C}), \quad (\text{B.3})$$

$$\begin{aligned} \frac{1}{\sqrt{N}} \sum_{n=0}^{N-1} \left(\frac{n}{N}\right)^k \text{im} \left\{ u(n) e^{-jM\phi(n)} \right\} &= \mathcal{C} \sum_{l=0}^2 N^{l+1/2} (\hat{\omega}_l - \omega_l) \left(\frac{1}{N} \sum_{n=0}^{N-1} \left(\frac{n}{N}\right)^{k+l} \right) \\ &= \sum_{l=0}^2 \frac{\mathcal{C}}{k+l+1} N^{l+1/2} (\hat{\omega}_l - \omega_l), \quad k = 0, 1, 2, \end{aligned} \quad (\text{B.4})$$

where in deriving the last equality, we made use of the well-known limit [47]:

$$\lim_{N \rightarrow \infty} \frac{1}{N} \sum_{n=0}^{N-1} \left(\frac{n}{N}\right)^k = \frac{1}{k+1}.$$

Next, we express the equations (B.3) and (B.4) in the matrix compact form equation:

$$\begin{aligned} \mathbf{K}_N(\hat{\boldsymbol{\omega}} - \boldsymbol{\omega}) &= \boldsymbol{\Lambda}^{-1} \boldsymbol{\varepsilon}, \quad (\text{B.5}) \\ \mathbf{K}_N &:= \begin{bmatrix} N^{\frac{1}{2}} & 0 & 0 & 0 \\ 0 & N^{\frac{1}{2}} & 0 & 0 \\ 0 & 0 & N^{\frac{3}{2}} & 0 \\ 0 & 0 & 0 & N^{\frac{5}{2}} \end{bmatrix}, \end{aligned}$$

$$\begin{aligned}
\mathbf{\Lambda} &:= \begin{bmatrix} 1 & 0 & 0 & 0 \\ 0 & \mathcal{C} & \frac{\mathcal{C}}{2} & \frac{\mathcal{C}}{3} \\ 0 & \frac{\mathcal{C}}{2} & \frac{\mathcal{C}}{3} & \frac{\mathcal{C}}{4} \\ 0 & \frac{\mathcal{C}}{3} & \frac{\mathcal{C}}{4} & \frac{\mathcal{C}}{5} \end{bmatrix}, \\
\boldsymbol{\varepsilon} &:= \begin{bmatrix} \frac{1}{\sqrt{N}} \sum_{n=0}^{N-1} \operatorname{re} \left\{ u(n) e^{-jM\phi(n)} \right\} \\ \frac{1}{\sqrt{N}} \sum_{n=0}^{N-1} \operatorname{im} \left\{ u(n) e^{-jM\phi(n)} \right\} \\ \frac{1}{\sqrt{N}} \sum_{n=0}^{N-1} \left(\frac{n}{N} \right) \operatorname{im} \left\{ u(n) e^{-jM\phi(n)} \right\} \\ \frac{1}{\sqrt{N}} \sum_{n=0}^{N-1} \left(\frac{n}{N} \right)^2 \operatorname{im} \left\{ u(n) e^{-jM\phi(n)} \right\} \end{bmatrix}. \tag{B.6}
\end{aligned}$$

Since in (B.5) only $\boldsymbol{\varepsilon}$ is random, the asymptotic covariance matrix of $\hat{\boldsymbol{\omega}}$ can be expressed as:

$$\boldsymbol{\Sigma}_{\hat{\boldsymbol{\omega}}} := \lim_{N \rightarrow \infty} \mathbb{E} \left\{ \mathbf{K}_N (\hat{\boldsymbol{\omega}} - \boldsymbol{\omega}) (\hat{\boldsymbol{\omega}} - \boldsymbol{\omega})^T \mathbf{K}_N^T \right\} = \lim_{N \rightarrow \infty} \mathbb{E} \left\{ \boldsymbol{\Lambda}^{-1} \boldsymbol{\varepsilon} \boldsymbol{\varepsilon}^T \boldsymbol{\Lambda}^{-1} \right\} = \boldsymbol{\Lambda}^{-1} \mathbf{R}_{\boldsymbol{\varepsilon}} \boldsymbol{\Lambda}^{-1},$$

where $\mathbf{R}_{\boldsymbol{\varepsilon}} := \lim_{N \rightarrow \infty} \mathbb{E} \{ \boldsymbol{\varepsilon} \boldsymbol{\varepsilon}^T \}$.

Observe that:

$$\begin{aligned}
\mathbf{R}_{\boldsymbol{\varepsilon}}(1, 1) &= \lim_{N \rightarrow \infty} \frac{1}{N} \mathbb{E} \left[\left(\sum_{n=0}^{N-1} \operatorname{re} \{ u(n) e^{-jM\phi(n)} \} \right)^2 \right] \\
&= \lim_{N \rightarrow \infty} \frac{1}{4N} \sum_{n_1, n_2=0}^{N-1} \mathbb{E} \left\{ \left[u(n_1) e^{-jM\phi(n_1)} + u^*(n_1) e^{jM\phi(n_1)} \right] \left[u(n_2) e^{-jM\phi(n_2)} + u^*(n_2) e^{jM\phi(n_2)} \right] \right\}.
\end{aligned}$$

Using (B.1) and (B.2), $\mathbf{R}_{\boldsymbol{\varepsilon}}(1, 1)$ can be written as:

$$\mathbf{R}_{\boldsymbol{\varepsilon}}(1, 1) = \lim_{N \rightarrow \infty} \frac{1}{2N} \sum_{n=0}^{N-1} (\mathcal{D} + \mathcal{B} - 2\mathcal{C}^2) = \frac{1}{2} (\mathcal{D} + \mathcal{B} - 2\mathcal{C}^2).$$

Similarly, we obtain $\mathbf{R}_{\boldsymbol{\varepsilon}}(1, k) = 0$, $k = 2, 3, 4$, which means that the NLS estimators of the amplitude and phase parameters are asymptotically decoupled.

To evaluate the asymptotic variance of $\hat{\omega}_l$, $l = 0, 1, 2$, we need to compute for $k, m = 0, 1, 2$:

$$\begin{aligned} \mathbf{R}_{\boldsymbol{\varepsilon}}(2+k, 2+m) &= \lim_{N \rightarrow \infty} \frac{1}{N} \sum_{n_1, n_2=0}^{N-1} \left(\frac{n_1}{N}\right)^k \left(\frac{n_2}{N}\right)^m \\ &\quad \cdot \mathbb{E} \left[\text{im}\{u(n_1)e^{-jM\phi(n_1)}\} \text{im}\{u(n_2)e^{-jM\phi(n_2)}\} \right]. \end{aligned}$$

Using the same technique as for $\mathbf{R}_{\boldsymbol{\varepsilon}}(1, 1)$, we obtain:

$$\mathbf{R}_{\boldsymbol{\varepsilon}}(2+k, 2+m) = \frac{1}{2(k+m+1)} (\mathcal{B} - \mathcal{D}), \quad k, m = 0, 1, 2.$$

Thus, the matrix $\mathbf{R}_{\boldsymbol{\varepsilon}}$ can be expressed as:

$$\mathbf{R}_{\boldsymbol{\varepsilon}} = \frac{1}{2} \begin{bmatrix} \mathcal{B} + \mathcal{D} - 2\mathcal{C}^2 & 0 \\ 0 & (\mathcal{B} - \mathcal{D})\mathbf{H} \end{bmatrix}, \quad (\text{B.7})$$

where $\mathbf{H} := \{1/(k+l+1)\}_{k, l=0}^2$ is the so-called Hilbert matrix [65]. Note that:

$$\boldsymbol{\Lambda}^{-1} = \begin{bmatrix} 1 & 0 \\ 0 & \mathcal{C}^{-1}\mathbf{H}^{-1} \end{bmatrix}.$$

Therefore, the asymptotic covariance matrix of $\hat{\boldsymbol{\omega}}$ is obtained as:

$$\begin{aligned} \boldsymbol{\Sigma}_{\hat{\boldsymbol{\omega}}} &= \boldsymbol{\Lambda}^{-1} \mathbf{R}_{\boldsymbol{\varepsilon}} \boldsymbol{\Lambda}^{-1} \\ &= \frac{1}{2} \begin{bmatrix} \mathcal{B} + \mathcal{D} - 2\mathcal{C}^2 & 0 \\ 0 & (\mathcal{B} - \mathcal{D})\mathcal{C}^{-2}\mathbf{H}^{-1} \end{bmatrix}, \end{aligned} \quad (\text{B.8})$$

where the inverse of the Hilbert matrix \mathbf{H} is given by [65]:

$$\mathbf{H}^{-1}(k, l) = (-1)^{k+l} \frac{(k+3)!(l+3)!}{(k!)^2(l!)^2(2-k)!(2-l)!(k+l+1)}. \quad (\text{B.9})$$

Based on (B.8) and (B.9), some direct computations lead to the sought asymptotic variances (2.14). This concludes the proof of Theorem 1.

APPENDIX C

DERIVATION OF THEOREM 7

Considering the Taylor series expansion of $\sum_{k=0}^{P-1} \dot{\lambda}_k \exp(j\dot{\phi}_k + j2\pi(\dot{\alpha} + k/P)n)$ in the neighborhood of the true value $\boldsymbol{\theta} := [\lambda_0 \cdots \lambda_{P-1} \phi_0 \cdots \phi_{P-1} \alpha_0]^T$, we can write:

$$\begin{aligned} \sum_{k=0}^{P-1} \dot{\lambda}_k e^{j\dot{\phi}_k} e^{j2\pi(\dot{\alpha} + \frac{k}{P})n} &= \sum_{k=0}^{P-1} \lambda_k e^{j\phi_k} e^{j2\pi(\alpha_0 + \frac{k}{P})n} + \sum_{k=0}^{P-1} (\dot{\lambda}_k - \lambda_k) e^{j\phi_k} e^{j2\pi(\alpha_0 + \frac{k}{P})n} \\ &+ j \sum_{k=0}^{P-1} (\dot{\phi}_k - \phi_k) \lambda_k e^{j\phi_k} e^{j2\pi(\alpha_0 + \frac{k}{P})n} + j2\pi n (\dot{\alpha} - \alpha_0) \sum_{k=0}^{P-1} \lambda_k e^{j\phi_k} e^{j2\pi(\alpha_0 + \frac{k}{P})n} + \text{rem}, \end{aligned}$$

where rem is the high-order remainder term which can be neglected. Then we can approximate (3.16) by:

$$\begin{aligned} J(\dot{\boldsymbol{\theta}}) &\doteq \frac{1}{2N} \sum_{n=0}^{N-1} \left| x^4(n) - \sum_{k=0}^{P-1} \lambda_k e^{j\phi_k} e^{j2\pi(\alpha_0 + \frac{k}{P})n} - \sum_{k=0}^{P-1} (\dot{\lambda}_k - \lambda_k) e^{j\phi_k} e^{j2\pi(\alpha_0 + \frac{k}{P})n} \right. \\ &\left. - j \sum_{k=0}^{P-1} (\dot{\phi}_k - \phi_k) \lambda_k e^{j\phi_k} e^{j2\pi(\alpha_0 + \frac{k}{P})n} - j2\pi n (\dot{\alpha} - \alpha_0) \sum_{k=0}^{P-1} \lambda_k e^{j\phi_k} e^{j2\pi(\alpha_0 + \frac{k}{P})n} \right|^2. \end{aligned} \quad (\text{C.1})$$

Setting $\partial J(\dot{\boldsymbol{\theta}})/\partial \dot{\lambda}_k = 0$ for $k = 0, \dots, P-1$, we obtain:

$$\begin{aligned} \hat{\lambda}_k &= \text{re} \left\{ \frac{1}{N} \sum_{n=0}^{N-1} x^4(n) e^{-j\phi_k} e^{-j2\pi(\alpha_0 + \frac{k}{P})n} \right\} - \sum_{\substack{l=0 \\ l \neq k}}^{P-1} \hat{\lambda}_l \text{re} \left\{ \frac{1}{N} \sum_{n=0}^{N-1} e^{j(\phi_k - \phi_l)} e^{j2\pi \frac{k-l}{P} n} \right\} \\ &+ \sum_{\substack{l=0 \\ l \neq k}}^{P-1} \hat{\lambda}_l (\hat{\phi}_l - \phi_l) \text{im} \left\{ \frac{1}{N} \sum_{n=0}^{N-1} e^{j(\phi_k - \phi_l)} e^{j2\pi \frac{k-l}{P} n} \right\} \\ &+ 2\pi N (\hat{\alpha} - \alpha_0) \sum_{\substack{l=0 \\ l \neq k}}^{P-1} \hat{\lambda}_l \text{im} \left\{ \frac{1}{N} \sum_{n=0}^{N-1} \frac{n}{N} e^{j(\phi_k - \phi_l)} e^{j2\pi \frac{k-l}{P} n} \right\}. \end{aligned} \quad (\text{C.2})$$

To compute the individual factors in the R.H.S. of (C.2), the following well-known result will be used extensively [47]:

Lemma 1. *With k denoting a positive integer and $\delta(\omega)$ denoting Kronecker delta, it holds that:*

$$\lim_{N \rightarrow \infty} \frac{1}{N} \sum_{n=0}^{N-1} \left(\frac{n}{N}\right)^k e^{j(\omega n + \phi)} = \frac{e^{j\phi} \delta(\omega)}{k+1}. \quad (\text{C.3})$$

Using (C.3), we can further approximate (C.2) by:

$$\hat{\lambda}_k = \frac{1}{N\lambda_k} \operatorname{re} \left\{ \sum_{n=0}^{N-1} x^4(n) \lambda_k e^{-j\phi_k} e^{-j2\pi(\alpha_0 + \frac{k}{P})n} \right\}. \quad (\text{C.4})$$

Following the same procedure, i.e., by setting:

$$\frac{\partial J(\hat{\boldsymbol{\theta}})}{\partial \hat{\phi}_k} = 0, \quad k = 0, \dots, P-1, \quad \frac{\partial J(\hat{\boldsymbol{\theta}})}{\partial \hat{\alpha}} = 0,$$

and using Lemma 1, the following expressions can be obtained:

$$\hat{\phi}_k - \phi_k = \frac{1}{N\lambda_k} \operatorname{im} \left\{ \sum_{n=0}^{N-1} x^4(n) e^{-j\phi_k} e^{-j2\pi(\alpha_0 + \frac{k}{P})n} \right\} - \pi N(\hat{\alpha} - \alpha_0), \quad (\text{C.5})$$

$$\begin{aligned} N(\hat{\alpha} - \alpha_0) &= \frac{3}{2\pi N\Lambda^2} \operatorname{im} \left\{ \sum_{n=0}^{N-1} \frac{n}{N} x^4(n) \sum_{l=0}^{P-1} \lambda_l e^{-j\phi_l} e^{-j2\pi(\alpha_0 + \frac{l}{P})n} \right\} \\ &\quad - \frac{3}{4\pi\Lambda^2} \sum_{l=0}^{P-1} \lambda_l^2 (\hat{\phi}_l - \phi_l), \end{aligned} \quad (\text{C.6})$$

where $\Lambda^2 := \sum_{k=0}^{P-1} \lambda_k^2$. Solving (C.5) and (C.6), we can express $\hat{\phi}_k$, $k = 0, \dots, P-1$ and $\hat{\alpha}$ in terms of the true value $\boldsymbol{\theta}$ and $x^4(n)$ by:

$$\begin{aligned} \hat{\phi}_k - \phi_k &= \frac{1}{N\lambda_k^2} \operatorname{im} \left\{ \sum_{n=0}^{N-1} x^4(n) \lambda_k e^{-j\phi_k} e^{-j2\pi(\alpha_0 + \frac{k}{P})n} \right\} \\ &\quad + \frac{3}{N\Lambda^2} \operatorname{im} \left\{ \sum_{n=0}^{N-1} x^4(n) \sum_{l=0}^{P-1} \lambda_l e^{-j\phi_l} e^{-j2\pi(\alpha_0 + \frac{l}{P})n} \right\} \\ &\quad - \frac{6}{N\Lambda^2} \operatorname{im} \left\{ \sum_{n=0}^{N-1} \frac{n}{N} x^4(n) \sum_{l=0}^{P-1} \lambda_l e^{-j\phi_l} e^{-j2\pi(\alpha_0 + \frac{l}{P})n} \right\}, \end{aligned} \quad (\text{C.7})$$

$$\begin{aligned} N(\hat{\alpha} - \alpha_0) &= \frac{6}{\pi N\Lambda^2} \operatorname{im} \left\{ \sum_{n=0}^{N-1} \frac{n}{N} x^4(n) \sum_{l=0}^{P-1} \lambda_l e^{-j\phi_l} e^{-j2\pi(\alpha_0 + \frac{l}{P})n} \right\} \\ &\quad - \frac{3}{\pi N\Lambda^2} \operatorname{im} \left\{ \sum_{n=0}^{N-1} x^4(n) \sum_{l=0}^{P-1} \lambda_l e^{-j\phi_l} e^{-j2\pi(\alpha_0 + \frac{l}{P})n} \right\}. \end{aligned} \quad (\text{C.8})$$

Next, let us write the above expressions in matrix form¹:

$$\hat{\boldsymbol{\theta}} - \boldsymbol{\theta} = \mathbf{m} + \mathbf{H}\mathbf{b}, \quad \mathbf{m} := [-\lambda_0 \ \cdots \ -\lambda_{P-1} \ 0 \ \cdots \ 0]^T,$$

$$\mathbf{H} := \begin{bmatrix} \frac{1}{\lambda_0} & 0 & 0 & \cdots & 0 & 0 & \cdots & \cdots & \cdots & 0 & 0 \\ 0 & \frac{1}{\lambda_1} & 0 & \cdots & 0 & 0 & \cdots & \cdots & \cdots & 0 & 0 \\ \vdots & \vdots & \ddots & \vdots & \vdots & \vdots & \ddots & \ddots & \ddots & \vdots & \vdots \\ 0 & 0 & \cdots & 0 & \frac{1}{\lambda_{P-1}} & 0 & 0 & \cdots & \cdots & 0 & 0 \\ 0 & 0 & \cdots & 0 & 0 & \frac{1}{\lambda_0^2} + \frac{3}{\Lambda^2} & \frac{3}{\Lambda^2} & \cdots & \cdots & \frac{3}{\Lambda^2} & -\frac{6}{\Lambda^2} \\ 0 & 0 & \cdots & 0 & 0 & \frac{3}{\Lambda^2} & \frac{1}{\lambda_1^2} + \frac{3}{\Lambda^2} & \frac{3}{\Lambda^2} & \cdots & \frac{3}{\Lambda^2} & -\frac{6}{\Lambda^2} \\ \vdots & \vdots & \ddots & \vdots & \vdots & \vdots & \vdots & \ddots & \vdots & \vdots & \vdots \\ 0 & 0 & \cdots & 0 & 0 & \frac{3}{\Lambda^2} & \frac{3}{\Lambda^2} & \cdots & \frac{3}{\Lambda^2} & \frac{1}{\lambda_{P-1}^2} + \frac{3}{\Lambda^2} & -\frac{6}{\Lambda^2} \\ 0 & 0 & \cdots & 0 & 0 & -\frac{3}{\pi\Lambda^2} & -\frac{3}{\pi\Lambda^2} & \cdots & -\frac{3}{\pi\Lambda^2} & -\frac{3}{\pi\Lambda^2} & \frac{6}{\pi\Lambda^2} \end{bmatrix},$$

$$\mathbf{b} := \begin{bmatrix} \frac{1}{N} \text{re} \left\{ \sum_{n=0}^{N-1} x^4(n) \lambda_0 e^{-j\phi_0} e^{-j2\pi\alpha_0 n} \right\} \\ \frac{1}{N} \text{re} \left\{ \sum_{n=0}^{N-1} x^4(n) \lambda_1 e^{-j\phi_1} e^{-j2\pi(\alpha_0 + \frac{1}{P})n} \right\} \\ \vdots \\ \frac{1}{N} \text{re} \left\{ \sum_{n=0}^{N-1} x^4(n) \lambda_{P-1} e^{-j\phi_{P-1}} e^{-j2\pi(\alpha_0 + \frac{P-1}{P})n} \right\} \\ \frac{1}{N} \text{im} \left\{ \sum_{n=0}^{N-1} x^4(n) \lambda_0 e^{-j\phi_0} e^{-j2\pi\alpha_0 n} \right\} \\ \frac{1}{N} \text{im} \left\{ \sum_{n=0}^{N-1} x^4(n) \lambda_1 e^{-j\phi_1} e^{-j2\pi(\alpha_0 + \frac{1}{P})n} \right\} \\ \vdots \\ \frac{1}{N} \text{im} \left\{ \sum_{n=0}^{N-1} x^4(n) \lambda_{P-1} e^{-j\phi_{P-1}} e^{-j2\pi(\alpha_0 + \frac{P-1}{P})n} \right\} \\ \frac{1}{N} \text{im} \left\{ \sum_{n=0}^{N-1} \frac{n}{N} x^4(n) \sum_{l=0}^{P-1} e^{-j\phi_l} e^{-j2\pi(\alpha_0 + \frac{l}{P})n} \right\} \end{bmatrix}. \quad (\text{C.9})$$

Using (3.12) and Lemma 1, it is straightforward to verify that $\lim_{N \rightarrow \infty} \mathbf{E}\{\mathbf{b}\} = [\lambda_0^2 \ \lambda_1^2 \ \cdots \ \lambda_{P-1}^2 \ 0 \ \cdots \ 0]^T$, hence the asymptotic unbiasedness of $\hat{\boldsymbol{\theta}}$ follows, i.e., $\lim_{N \rightarrow \infty} \mathbf{E}\{\hat{\boldsymbol{\theta}} - \boldsymbol{\theta}\} = \mathbf{0}$.

¹In the following we replace $\hat{\alpha}$ and α_0 by $N\hat{\alpha}$ and $N\alpha_0$ in $\hat{\boldsymbol{\theta}}$ and $\boldsymbol{\theta}$, respectively.

Since in (C.9) only \mathbf{b} is random, the asymptotic covariance matrix of $\hat{\boldsymbol{\theta}}$ can be simplified as:

$$\boldsymbol{\Sigma} := \lim_{N \rightarrow \infty} N \text{cov}(\hat{\boldsymbol{\theta}}) = \mathbf{H} \lim_{N \rightarrow \infty} [N \text{cov}(\mathbf{b})] \mathbf{H}^T := \mathbf{H} \mathbf{B} \mathbf{H}^T. \quad (\text{C.10})$$

There are $(2P+1) \times (2P+1)$ entries $\boldsymbol{\Sigma}_{k,l}$, $k, l \in [0, 2P]$, but we are only interested in $\gamma = \boldsymbol{\Sigma}_{2P,2P}$. Due to the special structure of \mathbf{H} , it is not difficult to find that:

$$\gamma = \mathbf{u}^T \mathbf{B}^{(s)} \mathbf{u}, \quad \mathbf{u} := \left[-\frac{3}{\pi \Lambda^2} \quad -\frac{3}{\pi \Lambda^2} \quad \dots \quad -\frac{3}{\pi \Lambda^2} \quad \frac{6}{\pi \Lambda^2} \right]^T, \quad (\text{C.11})$$

$$\mathbf{B}^{(s)} := \lim_{N \rightarrow \infty} [N \text{cov}(\mathbf{b}_s)],$$

$$\mathbf{b}_s := \begin{bmatrix} \frac{1}{N} \text{im} \left\{ \sum_{n=0}^{N-1} x^4(n) \lambda_0 e^{-j\phi_0} e^{-j2\pi\alpha_0 n} \right\} \\ \frac{1}{N} \text{im} \left\{ \sum_{n=0}^{N-1} x^4(n) \lambda_1 e^{-j\phi_1} e^{-j2\pi(\alpha_0 + \frac{1}{P})n} \right\} \\ \vdots \\ \frac{1}{N} \text{im} \left\{ \sum_{n=0}^{N-1} x^4(n) \lambda_{P-1} e^{-j\phi_{P-1}} e^{-j2\pi(\alpha_0 + \frac{P-1}{P})n} \right\} \\ \frac{1}{N} \text{im} \left\{ \sum_{n=0}^{N-1} \frac{n}{N} x^4(n) \sum_{l=0}^{P-1} e^{-j\phi_l} e^{-j2\pi(\alpha_0 + \frac{l}{P})n} \right\} \end{bmatrix}.$$

The entries $\mathbf{B}_{l_1, l_2}^{(s)}$, $l_1, l_2 \in [0, P-1]$ of matrix $\mathbf{B}^{(s)}$ can be expressed as:

$$\begin{aligned} \mathbf{B}_{l_1, l_2}^{(s)} &= \lim_{N \rightarrow \infty} N \text{cov} \left(\frac{1}{N} \text{im} \left\{ \sum_{n=0}^{N-1} x^4(n) \lambda_{l_1} e^{-j\phi_{l_1}} e^{-j2\pi(\alpha_0 + \frac{l_1}{P})n} \right\}, \right. \\ &\quad \left. \frac{1}{N} \text{im} \left\{ \sum_{n=0}^{N-1} x^4(n) \lambda_{l_2} e^{-j\phi_{l_2}} e^{-j2\pi(\alpha_0 + \frac{l_2}{P})n} \right\} \right) \\ &= \lim_{N \rightarrow \infty} \frac{1}{2N} \left\{ \text{re} \left\{ \text{cov} \left(\sum_{n=0}^{N-1} x^4(n) \lambda_{l_1} e^{-j\phi_{l_1}} e^{-j2\pi(\alpha_0 + \frac{l_1}{P})n}, \right. \right. \right. \\ &\quad \left. \left. \sum_{n=0}^{N-1} x^{*4}(n) \lambda_{l_2} e^{j\phi_{l_2}} e^{j2\pi(\alpha_0 + \frac{l_2}{P})n} \right) \right\} \\ &\quad \left. - \text{re} \left\{ \text{cov} \left(\sum_{n=0}^{N-1} x^4(n) \lambda_{l_1} e^{-j\phi_{l_1}} e^{-j2\pi(\alpha_0 + \frac{l_1}{P})n}, \right. \right. \right. \\ &\quad \left. \left. \sum_{n=0}^{N-1} x^4(n) \lambda_{l_2} e^{-j\phi_{l_2}} e^{-j2\pi(\alpha_0 + \frac{l_2}{P})n} \right) \right\} \right\}. \quad (\text{C.12}) \end{aligned}$$

From (3.13), we can obtain the following time-varying covariances:

$$\text{cov}\{x^4(n_1), x^4(n_2)\} = \mathbb{E}\{e(n_1)e(n_2)\} = \tilde{c}_{2e}(n_2; n_1 - n_2), \quad (\text{C.13})$$

$$\text{cov}\{x^4(n_1), x^{*4}(n_2)\} = \mathbb{E}\{e(n_1)e^*(n_2)\} = c_{2e}(n_2; n_1 - n_2). \quad (\text{C.14})$$

Since $v(n)$ satisfies the mixing condition **(AS4)**, $w(n)$ has finite moments and $h(n)$ has finite memory, it follows that $e(n)$ (defined in (3.13)) also has finite moments, i.e., $\tilde{c}_{2e}(n; \tau) < \infty$ and $c_{2e}(n; \tau) < \infty$. Substituting (C.13) and (C.14) into (C.12), we can express the first term of the R.H.S. of (C.12) as follows:

$$\begin{aligned} & \lim_{N \rightarrow \infty} \frac{1}{2N} \left\{ \text{re} \left\{ \text{cov} \left(\sum_{n=0}^{N-1} x^4(n) \lambda_{l_1} e^{-j\phi_{l_1}} e^{-j2\pi(\alpha_0 + \frac{l_1}{P})n}, \right. \right. \\ & \quad \left. \left. \sum_{n=0}^{N-1} x^{*4}(n) \lambda_{l_2} e^{j\phi_{l_2}} e^{j2\pi(\alpha_0 + \frac{l_2}{P})n} \right) \right\} \\ &= \text{re} \left\{ \lim_{N \rightarrow \infty} \frac{1}{2N} \sum_{n_1=0}^{N-1} \sum_{n_2=0}^{N-1} \lambda_{l_1} \lambda_{l_2} e^{-j(\phi_{l_1} - \phi_{l_2})} e^{-j2\pi[\alpha_0(n_1 - n_2) + \frac{l_1 n_1 - l_2 n_2}{P}] } c_{2e}(n_2; n_1 - n_2) \right\} \\ &= \text{re} \left\{ \lim_{N \rightarrow \infty} \frac{1}{2N} \sum_{\tau=-(N-1)}^{N-1} \sum_{n=0}^{N-1-|\tau|} \lambda_{l_1} \lambda_{l_2} e^{-j(\phi_{l_1} - \phi_{l_2})} e^{-j2\pi(\alpha_0 + \frac{l_1}{P})\tau} e^{-j2\pi \frac{l_1 - l_2}{P} n} c_{2e}(n; \tau) \right\} \\ &= \frac{1}{2} \text{re} \left\{ \lambda_{l_1} \lambda_{l_2} e^{-j(\phi_{l_1} - \phi_{l_2})} \lim_{N \rightarrow \infty} \sum_{\tau=-(N-1)}^{N-1} \left[\frac{1}{N} \sum_{n=0}^{N-1-|\tau|} c_{2e}(n; \tau) e^{-j2\pi \frac{l_1 - l_2}{P} n} \right] e^{-j2\pi(\alpha_0 + \frac{l_1}{P})\tau} \right\} \\ &= \frac{1}{2} \text{re} \left\{ \lambda_{l_1} \lambda_{l_2} e^{-j(\phi_{l_1} - \phi_{l_2})} \lim_{N \rightarrow \infty} \sum_{\tau=-(N-1)}^{N-1} C_{2e} \left(\frac{l_1 - l_2}{P}; \tau \right) e^{-j2\pi(\alpha_0 + \frac{l_1}{P})\tau} \right\} \\ &= \frac{1}{2} \text{re} \left\{ \lambda_{l_1} \lambda_{l_2} e^{-j(\phi_{l_1} - \phi_{l_2})} S_{2e} \left(\frac{l_1 - l_2}{P}; \alpha_0 + \frac{l_1}{P} \right) \right\} \\ &= \frac{1}{2} \text{re} \left\{ \tilde{C}_{4x}^* \left(\alpha_0 + \frac{l_1}{P}; \mathbf{0} \right) \tilde{C}_{4x} \left(\alpha_0 + \frac{l_2}{P}; \mathbf{0} \right) S_{2e} \left(\frac{l_1 - l_2}{P}; \alpha_0 + \frac{l_1}{P} \right) \right\}, \end{aligned}$$

where we have replaced the double sum over n_1 and n_2 by the double sum over $n := n_2$ and $\tau := n_1 - n_2$, and used the Lemma 1. $C_{2e}(\alpha; \tau)$ stands for the unconjugate cyclic correlation of $e(n)$. Similarly, the second term of the R.H.S. of (C.12) can be expressed

as:

$$\begin{aligned} & \lim_{N \rightarrow \infty} \frac{1}{2N} \left\{ \operatorname{re} \left\{ \operatorname{cov} \left(\sum_{n=0}^{N-1} x^4(n) \lambda_{l_1} e^{-j\phi_{l_1}} e^{-j2\pi(\alpha_0 + \frac{l_1}{P}n)}, \right. \right. \\ & \quad \left. \left. \sum_{n=0}^{N-1} x^4(n) \lambda_{l_2} e^{-j\phi_{l_2}} e^{-j2\pi(\alpha_0 + \frac{l_2}{P}n)} \right) \right\} \\ &= \frac{1}{2} \operatorname{re} \left\{ \tilde{C}_{4x}^* \left(\alpha_0 + \frac{l_1}{P}; \mathbf{0} \right) \tilde{C}_{4x}^* \left(\alpha_0 + \frac{l_2}{P}; \mathbf{0} \right) \tilde{S}_{2e} \left(2\alpha_0 + \frac{l_1 + l_2}{P}; \alpha_0 + \frac{l_1}{P} \right) \right\}. \end{aligned}$$

Therefore, for $l_1, l_2 \in [0, P - 1]$, we obtain:

$$\begin{aligned} \mathbf{B}_{l_1, l_2}^{(s)} &= \frac{1}{2} \operatorname{re} \left\{ \tilde{C}_{4x}^* \left(\alpha_0 + \frac{l_1}{P}; \mathbf{0} \right) \tilde{C}_{4x} \left(\alpha_0 + \frac{l_2}{P}; \mathbf{0} \right) S_{2e} \left(\frac{l_1 - l_2}{P}; \alpha_0 + \frac{l_1}{P} \right) \right\} \\ &\quad - \frac{1}{2} \operatorname{re} \left\{ \tilde{C}_{4x}^* \left(\alpha_0 + \frac{l_1}{P}; \mathbf{0} \right) \tilde{C}_{4x}^* \left(\alpha_0 + \frac{l_2}{P}; \mathbf{0} \right) \tilde{S}_{2e} \left(2\alpha_0 + \frac{l_1 + l_2}{P}; \alpha_0 + \frac{l_1}{P} \right) \right\}. \end{aligned}$$

Using similar arguments, the following expression can be derived for $l \in [0, P - 1]$:

$$\begin{aligned} \mathbf{B}_{P, l}^{(s)} &= \mathbf{B}_{l, P}^{(s)} = \frac{1}{4} \sum_{k=0}^{P-1} \left\{ \operatorname{re} \left\{ \tilde{C}_{4x}^* \left(\alpha_0 + \frac{l}{P}; \mathbf{0} \right) \tilde{C}_{4x} \left(\alpha_0 + \frac{k}{P}; \mathbf{0} \right) S_{2e} \left(\frac{l - k}{P}; \alpha_0 + \frac{l}{P} \right) \right\} \right. \\ &\quad \left. - \frac{1}{4} \sum_{k=0}^{P-1} \operatorname{re} \left\{ \tilde{C}_{4x}^* \left(\alpha_0 + \frac{l}{P}; \mathbf{0} \right) \tilde{C}_{4x}^* \left(\alpha_0 + \frac{k}{P}; \mathbf{0} \right) \tilde{S}_{2e} \left(2\alpha_0 + \frac{l + k}{P}; \alpha_0 + \frac{l}{P} \right) \right\} \right\}, \end{aligned}$$

and

$$\begin{aligned} \mathbf{B}_{P, P}^{(s)} &= \frac{1}{6} \sum_{k, l=0}^{P-1} \left\{ \operatorname{re} \left\{ \tilde{C}_{4x}^* \left(\alpha_0 + \frac{l}{P}; \mathbf{0} \right) \tilde{C}_{4x} \left(\alpha_0 + \frac{k}{P}; \mathbf{0} \right) S_{2e} \left(\frac{l - k}{P}; \alpha_0 + \frac{l}{P} \right) \right\} \right. \\ &\quad \left. - \frac{1}{6} \sum_{k, l=0}^{P-1} \operatorname{re} \left\{ \tilde{C}_{4x}^* \left(\alpha_0 + \frac{l}{P}; \mathbf{0} \right) \tilde{C}_{4x}^* \left(\alpha_0 + \frac{k}{P}; \mathbf{0} \right) \tilde{S}_{2e} \left(2\alpha_0 + \frac{l + k}{P}; \alpha_0 + \frac{l}{P} \right) \right\} \right\}. \end{aligned}$$

Based on (C.11), after some lengthy calculations, we express γ as:

$$\begin{aligned} \gamma &= \frac{3}{2\pi^2 \Lambda^4} \sum_{l_1, l_2=0}^{P-1} \left\{ \operatorname{re} \left\{ \tilde{C}_{4x}^* \left(\alpha_0 + \frac{l_1}{P}; \mathbf{0} \right) \tilde{C}_{4x} \left(\alpha_0 + \frac{l_2}{P}; \mathbf{0} \right) S_{2e} \left(\frac{l_1 - l_2}{P}; \alpha_0 + \frac{l_1}{P} \right) \right\} \right. \\ &\quad \left. - \operatorname{re} \left\{ \tilde{C}_{4x}^* \left(\alpha_0 + \frac{l_1}{P}; \mathbf{0} \right) \tilde{C}_{4x}^* \left(\alpha_0 + \frac{l_2}{P}; \mathbf{0} \right) \tilde{S}_{2e} \left(2\alpha_0 + \frac{l_1 + l_2}{P}; \alpha_0 + \frac{l_1}{P} \right) \right\} \right\}, \end{aligned}$$

and when the above expression is rewritten in matrix form, the equation (3.17) follows.

APPENDIX D

DERIVATION OF PROPOSITIONS 1 AND 2 (SKETCH)

Our purpose is to evaluate the unconjugate/conjugate cyclic spectra $S_{2e}(\alpha; f)$ and $\tilde{S}_{2e}(\alpha; f)$ corresponding to two oversampling factors $P = 1$ and $P > 1$, respectively.

According to the definition of the additive noise $e(n)$ (3.13), we can express its unconjugate/conjugate time-varying correlations as:

$$\begin{aligned}
c_{2e}(n; \tau) &:= \mathbb{E}\{e^*(n)e(n + \tau)\} \\
&= \mathbb{E}\left\{[x^4(n) - \tilde{c}_{4x}(n; \mathbf{0})]^*[x^4(n + \tau) - \tilde{c}_{4x}(n + \tau; \mathbf{0})]\right\} \\
&= 16m_{2x}(n; \tau)m_{6x}(n; 0, 0, \tau, \tau, \tau) + 18m_{4x}^2(n; 0, \tau, \tau) \\
&\quad - 144m_{2x}^2(n; \tau)m_{4x}(n; 0, \tau, \tau) + 144m_{2x}^4(n; \tau) \\
&\quad + \text{cum}\left\{\underbrace{x^*(n), \dots, x^*(n)}_4, \underbrace{x(n + \tau), \dots, x(n + \tau)}_4\right\}, \tag{D.1}
\end{aligned}$$

$$\begin{aligned}
\tilde{c}_{2e}(n; \tau) &:= \mathbb{E}\{e(n)e(n + \tau)\} \\
&= \mathbb{E}\left\{[x^4(n) - \tilde{c}_{4x}(n; \mathbf{0})][x^4(n + \tau) - \tilde{c}_{4x}(n + \tau; \mathbf{0})]\right\} \\
&= 16\mathbb{E}\{x(n)x^3(n + \tau)\}\mathbb{E}\{x^3(n)x(n + \tau)\} + 18\mathbb{E}^2\{x^2(n)x^2(n + \tau)\} \\
&\quad + \text{cum}\left\{\underbrace{x(n), \dots, x(n)}_4, \underbrace{x(n + \tau), \dots, x(n + \tau)}_4\right\}, \tag{D.2}
\end{aligned}$$

respectively.

Case 1. Evaluation of $S_{2e}(\alpha_0)$ for $P = 1$

Note that when $P = 1$, the moments m_{lx} are independent of the time index n and:

$$\text{cum}\left\{\underbrace{x^*(n), \dots, x^*(n)}_4, \underbrace{x(n + \tau), \dots, x(n + \tau)}_4\right\} = \kappa_8 e^{j2\pi\alpha_0\tau} \sum_l h^{*4}(l)h^4(l + \tau),$$

then $S_{2e}(\alpha_0)$ in Proposition 1 can be obtained by plugging the above expression into (D.1) and taking the Fourier transform of the sequence $\{c_{2e}(\tau)\}_\tau$.

Case 2. Evaluation of $\tilde{S}_{2e}(2\alpha_0; \alpha_0)$ for $P = 1$

The following expressions can be derived due to the circularity of the transmitted signal $w(n)$:

$$\begin{aligned}
\mathbb{E}\{x(n)x^3(n+\tau)\} &= \text{cum}\{x(n), x(n+\tau), x(n+\tau), x(n+\tau)\} \\
&= \tilde{\kappa}_4 e^{j2\pi f_e(4n+3\tau)} \sum_l h(l)h^3(l+\tau), \\
\mathbb{E}\{x^3(n)x(n+\tau)\} &= \text{cum}\{x(n), x(n), x(n), x(n+\tau)\} \\
&= \tilde{\kappa}_4 e^{j2\pi f_e(4n+\tau)} \sum_l h^3(l)h(l+\tau), \\
\mathbb{E}\{x^2(n)x^2(n+\tau)\} &= \text{cum}\{x(n), x(n), x(n+\tau), x(n+\tau)\} \\
&= \tilde{\kappa}_4 e^{j2\pi f_e(4n+2\tau)} \sum_l h^2(l)h^2(l+\tau), \\
\text{cum}\{\underbrace{x(n), \dots, x(n)}_4, \underbrace{x(n+\tau), \dots, x(n+\tau)}_4\} &= \tilde{\kappa}_8 e^{j2\pi f_e(8n+4\tau)} \sum_l h^4(l)h^4(l+\tau).
\end{aligned}$$

Then, the conjugate cyclic correlation $\tilde{C}_{2e}(2\alpha_0; \tau)$ can be obtained as:

$$\begin{aligned}
\tilde{C}_{2e}(2\alpha_0; \tau) &:= \lim_{N \rightarrow \infty} \frac{1}{N} \sum_{n=0}^{N-1} \tilde{c}_{2e}(n; \tau) e^{-j4\pi\alpha_0 n} \\
&= e^{j2\pi\alpha_0\tau} \left[\tilde{\kappa}_8 \sum_l h^4(l)h^4(l+\tau) + 16\tilde{\kappa}_4^2 \sum_l h(l)h^3(l+\tau) \cdot \sum_l h^3(l)h(l+\tau) \right. \\
&\quad \left. + 18\tilde{\kappa}_4^2 \left(\sum_l h^2(l)h^2(l+\tau) \right)^2 \right].
\end{aligned}$$

Finally, the expression of $\tilde{S}_{2e}(2\alpha_0; \alpha_0)$ follows by taking the Fourier transform of the sequence $\{\tilde{C}_{2e}(2\alpha_0; \tau)\}_\tau$ at the frequency α_0 .

Case 3. Evaluation of $S_{2e}(k/P; \alpha_0 + l/P)$ for $P > 1$

When $P > 1$, the last term of (D.1) can be expressed as:

$$\text{cum}\{\underbrace{x^*(n), \dots, x^*(n)}_4, \underbrace{x(n+\tau), \dots, x(n+\tau)}_4\}$$

$$= \kappa_8 e^{j2\pi\alpha_0\tau} \sum_l h^{*4}(n-lP)h^4(n+\tau-lP).$$

The cyclic correlation coefficient at cycle k/P and the cyclic spectrum at frequency $\alpha_0 + l/P$ of $e(n)$ can be expressed as:

$$\begin{aligned} C_{2e}\left(\frac{k}{P}; \tau\right) &= \frac{1}{P} \sum_{n=0}^{P-1} c_{2e}(n; \tau) e^{-j2\pi\frac{kn}{P}}, \\ S_{2e}\left(\frac{k}{P}; \alpha_0 + \frac{l}{P}\right) &= \sum_{\tau} C_{2e}\left(\frac{k}{P}; \tau\right) e^{-j2\pi(\alpha_0 + \frac{l}{P})\tau}. \end{aligned}$$

Since $m_{lx}(n; \boldsymbol{\tau}) = \sum_{k=0}^{P-1} M_{lx}(k; \boldsymbol{\tau}) \exp(j2\pi kn/P)$ for $l = 4, 6$, we obtain:

$$\begin{aligned} C_{2e}\left(\frac{k}{P}; \tau\right) &= 16\mathcal{V}_1 + 18\mathcal{V}_2 - 144\mathcal{V}_3 + 144\mathcal{V}_4 \\ &\quad + \frac{\kappa_8}{P} e^{j2\pi\alpha_0\tau} \sum_n h^{*4}(n)h^4(n+\tau) e^{-j2\pi\frac{kn}{P}}, \end{aligned}$$

where \mathcal{V}_i , $i = 1, \dots, 4$, are defined as in Proposition 2. Hence, we obtain:

$$\begin{aligned} S_{2e}\left(\frac{k}{P}; \alpha_0 + \frac{l}{P}\right) &= \sum_{\tau} (16\mathcal{V}_1 + 18\mathcal{V}_2 - 144\mathcal{V}_3 + 144\mathcal{V}_4) e^{-j2\pi(\alpha_0 + \frac{l}{P})\tau} \\ &\quad + \sum_{\tau} \frac{\kappa_8}{P} e^{j2\pi\alpha_0\tau} \sum_n h^{*4}(n)h^4(n+\tau) e^{-j2\pi\frac{kn}{P}} e^{-j2\pi(\alpha_0 + \frac{l}{P})\tau}. \end{aligned} \quad (\text{D.3})$$

Note that the last term of (D.3) can be expressed as:

$$\begin{aligned} &\sum_{\tau} \frac{\kappa_8}{P} e^{j2\pi\alpha_0\tau} \sum_n h^{*4}(n)h^4(n+\tau) e^{-j2\pi\frac{kn}{P}} e^{-j2\pi(\alpha_0 + \frac{l}{P})\tau} \\ &= \frac{\kappa_8}{P} \sum_{\tau} \sum_n h^{*4}(n)h^4(n+\tau) e^{-j2\pi\frac{kn}{P}} e^{-j2\pi\frac{l}{P}\tau} \\ &= \frac{\kappa_8}{P} \sum_{\tau_1} h^4(\tau_1) e^{-j2\pi\frac{l}{P}\tau_1} \sum_n h^{*4}(n) e^{-j2\pi\frac{(k-l)n}{P}} \\ &= \frac{\kappa_8 P}{\tilde{\kappa}_4^2} \tilde{C}_{4x}\left(\alpha_0 + \frac{l}{P}; \mathbf{0}\right) \tilde{C}_{4x}^*\left(\alpha_0 + \frac{l-k}{P}; \mathbf{0}\right), \end{aligned}$$

then, $S_{2e}(k/P; \alpha_0 + l/P)$ in Proposition 2 is obtained.

Case 4. Evaluation of $\tilde{S}_{2e}(2\alpha_0 + k/P; \alpha_0 + l/P)$ for $P > 1$

Following the similar procedure presented in Case 2, it is not difficult to show:

$$\begin{aligned}
\lim_{N \rightarrow \infty} \frac{1}{N} \sum_{n=0}^{N-1} \mathbb{E}\{x(n)x^3(n+\tau)\} e^{-j2\pi(\alpha_0 + \frac{k}{P})n} &= e^{j6\pi f_e \tau} \tilde{C}_{4x_1}(k; \tau), \\
\lim_{N \rightarrow \infty} \frac{1}{N} \sum_{n=0}^{N-1} \mathbb{E}\{x^2(n)x^2(n+\tau)\} e^{-j2\pi(\alpha_0 + \frac{k}{P})n} &= e^{j4\pi f_e \tau} \tilde{C}_{4x_2}(k; \tau), \\
\lim_{N \rightarrow \infty} \frac{1}{N} \sum_{n=0}^{N-1} \mathbb{E}\{x^3(n)x(n+\tau)\} e^{-j2\pi(\alpha_0 + \frac{k}{P})n} &= e^{j2\pi f_e \tau} \tilde{C}_{4x_3}(k; \tau), \\
\lim_{N \rightarrow \infty} \frac{1}{N} \sum_{n=0}^{N-1} \underbrace{\text{cum}\{x(n), \dots, x(n), x(n+\tau), \dots, x(n+\tau)\}}_{\substack{4 \quad 4}} e^{-j2\pi(2\alpha_0 + \frac{k}{P})n} \\
&= e^{j8\pi f_e \tau} \tilde{C}_{8x}(k; \tau),
\end{aligned}$$

where $\tilde{C}_{4x_i}(k; \tau)$, $i = 1, 2, 3$, and $\tilde{C}_{8x}(k; \tau)$ are defined as in Proposition 2.

Based on (D.2) and the above equations, the conjugate cyclic spectrum $\tilde{S}_{2e}(2\alpha_0 + k/P; \alpha_0 + l/P)$ of Proposition 2 can be established.

APPENDIX E

DERIVATION OF PROPOSITION 3

In [19], a powerful approach has been developed for calculating the asymptotic covariance matrices of the cyclic correlation estimates. In order to derive $\mathbf{\Gamma}^{(1,1)}$ and $\mathbf{\Gamma}^{(1,-1)}$, we strongly refer to the method introduced in the afore-mentioned reference.

Define the mean-compensated $(2\Upsilon + 1)$ -dimensional stochastic process:

$$\mathbf{e}_2(n) = \mathbf{x}_2(n) - \mathbf{r}_x(n) ,$$

where

$$\mathbf{x}_2(n) = [x(n - \Upsilon)x^*(n), \dots, x(n + \Upsilon)x^*(n)]^T ,$$

and

$$\mathbf{r}_x(n) = [r_{2x}(n; -\Upsilon), \dots, r_{2x}(n; \Upsilon)]^T .$$

Let $\mathbf{r}_{\mathbf{e}_2}(n, \tau) := \mathbb{E}\{\mathbf{e}_2(n + \tau)\mathbf{e}_2^H(n)\}$ be the time-varying correlation where the superscript H denotes complex-conjugation and transposition. Furthermore, let $\mathbf{R}_{\mathbf{e}_2}(k, \tau)$ and $\mathbf{S}_{\mathbf{e}_2}(k; f)$ represent the cyclic correlation and cyclic spectrum of $\mathbf{e}_2(n)$, respectively. In [19], it is shown that

$$\mathbf{\Gamma}^{(1,1)} = \mathbf{S}_{\mathbf{e}_2}(0; 1/P).$$

Based on similar arguments as the ones developed in [19], it is not difficult to prove that

$$\mathbf{\Gamma}^{(1,-1)} = \mathbf{S}_{\mathbf{e}_2}(2; 1/P).$$

Next, we will only concentrate on the derivation of $\mathbf{\Gamma}^{(1,1)}$. The derivation of $\mathbf{\Gamma}^{(1,-1)}$ can be done similarly. First, we characterize the cyclic spectrum of the process $\mathbf{e}_2(n)$.

For a general noncircular input, the time-varying correlation of $\mathbf{e}_2(n)$ can be expressed as:

$$\begin{aligned} [\mathbf{r}_{\mathbf{e}_2}(n; \tau)]_{u,v} &= r_{2x}(n+v; \tau+u-v)r_{2x}^*(n; \tau) \\ &+ \text{cum}\{x(n+u+\tau), x^*(n+\tau), x^*(n+v), x(n)\} + \tilde{r}_{2x}(n; \tau+u)\tilde{r}_{2x}^*(n+v; \tau-v), \end{aligned}$$

where $(u, v) \in \{-\Upsilon, \dots, \Upsilon\}^2$. Let the notation $[\mathbf{M}]_{u,v}$ stand for the (u, v) th-entry of an arbitrary matrix \mathbf{M} . It follows that the cyclic correlations of $\mathbf{e}_2(n)$ at the cyclic frequency $k=0$ are given by

$$\begin{aligned} [\mathbf{R}_{\mathbf{e}_2}(0; \tau)]_{u,v} &= \sum_{k=0}^{P-1} R_{2x}(k; \tau+u-v)R_{2x}^*(k; \tau)e^{2i\pi kv/P} + C_{2x}(0; u+\tau, -\tau, -v) \\ &+ \sum_{k=0}^{P-1} \tilde{R}_{2x}(k; \tau+u)\tilde{R}_{2x}^*(k; \tau-v)e^{-2i\pi(k+2f_eT)v/P}, \end{aligned}$$

where the cyclic cumulant sequence $C_{2x}(k; \boldsymbol{\tau})$, $\boldsymbol{\tau} := [\tau_1, \tau_2, \tau_3]$, can be expressed as:

$$C_{2x}(k; \boldsymbol{\tau}) := \int_{-1/2}^{1/2} S_{4,x}(k; \mathbf{f})e^{2i\pi\boldsymbol{\tau}\mathbf{f}^T} d\mathbf{f},$$

where $S_{4,x}(k; \mathbf{f})$ stands for the cyclic trispectrum of the discrete-time signal $x(n)$ at cyclic frequency k/P and frequency $\mathbf{f} := [f_1, f_2, f_3]$.

Thus:

$$\boldsymbol{\Gamma}_{u,v}^{(1,1)} = [\mathbf{S}_{\mathbf{e}_2}(0; 1/P)]_{u,v} = \sum_{k=0}^{P-1} \mathcal{R}_{k,u,v} + \mathcal{C}_{u,v} + \sum_{k=0}^{P-1} \tilde{\mathcal{R}}_{k,u,v},$$

with:

$$\begin{aligned} \mathcal{R}_{k,u,v} &= e^{2i\pi kv/P} \sum_{\tau \in \mathbb{Z}} R_{2x}(k; \tau+u-v)R_{2x}^*(k; \tau)e^{-2i\pi\tau/P}, \\ \mathcal{C}_{u,v} &= \sum_{\tau \in \mathbb{Z}} C_{2x}(0; u+\tau, -\tau, -v)e^{-2i\pi\tau/P}, \\ \tilde{\mathcal{R}}_{k,u,v} &= e^{-\frac{2i\pi(k+2f_eT)v}{P}} \sum_{\tau \in \mathbb{Z}} \tilde{R}_{2x}(k; \tau+u)\tilde{R}_{2x}^*(k; \tau-v)e^{-\frac{2i\pi\tau}{P}}. \end{aligned}$$

It remains to express $\mathcal{C}_{u,v}$. We recall that

$$\mathcal{C}_{u,v} = \int_{-\frac{1}{2}}^{\frac{1}{2}} S_{4,x}(0; f_1, f_2, f_3) \sum_{\tau \in \mathbb{Z}} e^{2i\pi(f_1(u+\tau) - f_2\tau - f_3v)} e^{-2i\pi\tau/P} df_1 df_2 df_3. \quad (\text{E.1})$$

Let $S_{4,x_c}(k/T; \mathbf{F})$ be the cyclic trispectrum of $x_c(t)$ at cyclic frequency k/T and frequency $\mathbf{F} := [F_1, F_2, F_3]$. From [50], [73] and [97], $S_{4,x}(k; \mathbf{f})$ can be expressed in terms of $S_{4,x_c}(k/T; \mathbf{F})$ by the following relation:

$$S_{4,x}(k; \mathbf{f}) = \frac{1}{T_s^3} \sum_{l \in \mathbb{Z}} \sum_{\boldsymbol{\mu} \in \mathbb{Z}^3} S_{4,x_c} \left(\frac{l}{T}; \frac{\mathbf{f} - \boldsymbol{\mu}}{T_s} \right) \delta \left(\frac{k-l}{P} \bmod 1 \right),$$

for all $(f_1, f_2, f_3) \in (-1/2, 1/2]^3$. The notation $(a \bmod b)$ denotes a modulo b , and by convention, $(a \bmod b)$ belongs to $(-b/2, b/2]$.

Since $x_c(t)$ is given by Eq. (4.1), it is well known that ([19, Appendix C], [96]):

$$\begin{aligned} S_{4,x_c} \left(\frac{k}{T}; \mathbf{F} \right) &= \frac{\kappa}{T} H_c(F_1 - f_e) H_c^*(F_2 - f_e) \\ &\quad \cdot H_c^*(F_3 - f_e) H_c \left(\frac{k}{T} - F_1 + F_2 + F_3 - f_e \right) e^{-2i\pi\kappa e}, \end{aligned} \quad (\text{E.2})$$

with $H_c(F)$ representing the FT of $h_c(t)$. As $h_c(t)$ is bandlimited in $[-(1+\rho)/2T, (1+\rho)/2T]$ with $0 \leq \rho < 1$, $S_{4,x_c}(k/T; \mathbf{F})$ will be nonzero only for cycles $\{k/T, |k| \leq 3\}$.

We deduce that

$$S_{4,x}(k; \mathbf{f}) = \frac{1}{T_s^3} \sum_{l=-3}^3 \sum_{\boldsymbol{\mu} \in \mathbb{Z}^3} S_{4,x_c} \left(\frac{l}{T}; \frac{\mathbf{f} - \boldsymbol{\mu}}{T_s} \right) \delta \left(\frac{k-l}{P} \bmod 1 \right), \quad (\text{E.3})$$

for all $(f_1, f_2, f_3) \in (-1/2, 1/2]^3$.

According to Eqs. (E.1) and (E.3), we obtain that for $P \geq 3$

$$\mathcal{C}_{u,v} = \frac{1}{T_s^3} \sum_{\substack{l=-3 \\ l=(0 \bmod P)}}^3 \int_{-\frac{1}{2}}^{\frac{1}{2}} S_{4,x_c} \left(\frac{l}{T}; \frac{f_1}{T_s}, \frac{f_1 - 1/P}{T_s}, \frac{f_3}{T_s} \right) e^{2i\pi(f_1 u - f_3 v)} df_1 df_3.$$

Replacing the cyclic spectra of $x_c(t)$ with their expressions given by Eq. (E.2) and then expressing $H_c(F)$ in terms of $H(f)$ by means of Eq. (4.5) leads to

$$\begin{aligned} \mathcal{C}_{u,v} = & \frac{\kappa T_s}{T} \int_{-\frac{1}{2}}^{\frac{1}{2}} H(f_1 - f_e T_s) H^*(f_1 - \frac{1}{P} - f_e T_s) \\ & \cdot H^*(f_3 - f_e T_s) H(f_3 - \frac{1}{P} - f_e T_s) e^{2i\pi(f_1 u - f_3 v)} df_1 df_3. \end{aligned}$$

Using Eq. (4.9), we obtain finally:

$$\mathcal{C}_{u,v} = \frac{\kappa T}{T_s} \int_{-\frac{1}{2}}^{\frac{1}{2}} S_{2x}(1; f_1) e^{2i\pi f_1 u} df_1 \int_{-\frac{1}{2}}^{\frac{1}{2}} S_{2x}^*(1; f_3) e^{-2i\pi f_3 v} df_3 = \frac{\kappa T}{T_s} R_{2x}(1; u) R_{2x}^*(1; v).$$

The expressions in the case of $P = 2$ can be obtained using a similar approach.

APPENDIX F

PROOF OF PROPOSITION 4

We establish next the asymptotic performance of the GG estimators for $P \geq 3$.

For $\tau = 1$, Eq. (4.10) can be rewritten as:

$$\hat{f}_e = \frac{P}{4\pi T} \arg\{\hat{R}_{2x}(1; 1)\hat{R}_{2x}(-1; 1)\} = \frac{P}{4\pi T} \arctan\left\{\frac{\hat{\alpha}_1}{i\hat{\beta}_1}\right\}, \quad (\text{F.1})$$

where

$$\begin{aligned} \hat{\alpha}_1 &:= \hat{R}_{2x}(1; 1)\hat{R}_{2x}(-1; 1) - \hat{R}_{2x}^*(1; 1)\hat{R}_{2x}^*(-1; 1), \\ \hat{\beta}_1 &:= \hat{R}_{2x}(1; 1)\hat{R}_{2x}(-1; 1) + \hat{R}_{2x}^*(1; 1)\hat{R}_{2x}^*(-1; 1). \end{aligned}$$

For convenience, we define the following:

$$\begin{aligned} \alpha_1 &:= R_{2x}(1; 1)R_{2x}(-1; 1) - R_{2x}^*(1; 1)R_{2x}^*(-1; 1), \\ \beta_1 &:= R_{2x}(1; 1)R_{2x}(-1; 1) + R_{2x}^*(1; 1)R_{2x}^*(-1; 1), \end{aligned}$$

and $\Delta\alpha_1 := \hat{\alpha}_1 - \alpha_1$, $\Delta\beta_1 := \hat{\beta}_1 - \beta_1$. Eq. (F.1) can be equivalently expressed as:

$$\hat{f}_e = \frac{P}{4\pi T} \arctan\left(\frac{\alpha_1}{i\beta_1} \cdot \frac{1 + \frac{\Delta\alpha_1}{\alpha_1}}{1 + \frac{\Delta\beta_1}{\beta_1}}\right). \quad (\text{F.2})$$

According to [19], $\Delta\alpha_1$ and $\Delta\beta_1$ are on the order of $o(1/\sqrt{N})$. Considering a Taylor series expansion of the RHS of (F.2) and neglecting the terms of magnitude higher than $o(1/\sqrt{N})$, it follows that:

$$\hat{f}_e = \frac{P}{4\pi T} \left[\arctan\left(\frac{\alpha_1}{i\beta_1}\right) + \frac{\alpha_1}{i\beta_1} \frac{1}{1 + \left(\frac{\alpha_1}{i\beta_1}\right)^2} \left(\frac{\Delta\alpha_1}{\alpha_1} - \frac{\Delta\beta_1}{\beta_1}\right) \right]. \quad (\text{F.3})$$

Simple manipulations of (F.3) lead to:

$$\gamma_{f_e} = \zeta_1^2 \lim_{N \rightarrow \infty} \text{NE} \left(\frac{\Delta\alpha_1}{\alpha_1} - \frac{\Delta\beta_1}{\beta_1} \right)^2 = \zeta_1^2 \left(\frac{V_{11}}{\alpha_1^2} + \frac{V_{12}}{\beta_1^2} - \frac{2V_{13}}{\alpha_1\beta_1} \right),$$

where

$$\zeta_1 := P \tan(4\pi T f_e / P) / [4\pi T (1 + \tan^2(4\pi T f_e / P))],$$

$$V_{11} := \lim_{N \rightarrow \infty} \text{NE}\{(\Delta\alpha_1)^2\}, \quad V_{12} := \lim_{N \rightarrow \infty} \text{NE}\{(\Delta\beta_1)^2\}, \quad V_{13} := \lim_{N \rightarrow \infty} \text{NE}\{\Delta\alpha_1 \Delta\beta_1\}.$$

Since $\hat{R}_{2x}(k; \tau) = R_{2x}(k; \tau) + o(1/\sqrt{N})$, the previous terms can be easily computed as follows:

$$V_{11} = 2\text{re}\{\mathbf{R}^T(1)\tilde{\mathbf{\Gamma}}\mathbf{R}(1) - \mathbf{R}^T(1)\mathbf{\Gamma}\mathbf{R}^*(1)\},$$

$$V_{12} = 2\text{re}\{\mathbf{R}^T(1)\tilde{\mathbf{\Gamma}}\mathbf{R}(1) + \mathbf{R}^T(1)\mathbf{\Gamma}\mathbf{R}^*(1)\},$$

$$V_{13} = 2i\text{im}\{\mathbf{R}^T(1)\tilde{\mathbf{\Gamma}}\mathbf{R}(1)\},$$

with $\mathbf{R}(1) := [R_{2x}(-1; 1) \ R_x(1; 1)]^T$. According to Eq. (4.7), one can check also that:

$$\alpha_1 = 2i \frac{\sigma_w^4}{P^2} \sin(4\pi f_e T / P) G^2(1; 1),$$

$$\beta_1 = 2 \frac{\sigma_w^4}{P^2} \cos(4\pi f_e T / P) G^2(1; 1),$$

which enables us to conclude the derivation of γ_{f_e} , after some simple algebra manipulations of the Eq. (4.7).

The derivation of the asymptotic performance of $\hat{\epsilon}$ is more complicated because the expression (4.10) depends on the estimate of f_e when τ is not equal to 0. Similarly to the derivation presented in Eqs. (F.1) and (F.2), we obtain

$$\hat{\epsilon} = -\frac{1}{2\pi} \arctan \left(\frac{\alpha_2}{i\beta_2} \cdot \frac{1 + \frac{\Delta\alpha_2}{\alpha_2}}{1 + \frac{\Delta\beta_2}{\beta_2}} \right),$$

where

$$\begin{aligned}
\alpha_2 &= R_{2x}(1; 1)e^{-2i\pi(f_e T + 1/2)/P} - R_{2x}^*(1; 1)e^{2i\pi(f_e T + 1/2)/P}, \\
\beta_2 &= R_{2x}(1; 1)e^{-2i\pi(f_e T + 1/2)/P} + R_{2x}^*(1; 1)e^{2i\pi(f_e T + 1/2)/P}, \\
\Delta\alpha_2 &= \hat{R}_{2x}(1; 1)e^{-2i\pi(\hat{f}_e T + 1/2)/P} - \hat{R}_{2x}^*(1; 1)e^{2i\pi(\hat{f}_e T + 1/2)/P} \\
&\quad - R_{2x}(1; 1)e^{-2i\pi(f_e T + 1/2)/P} + R_{2x}^*(1; 1)e^{2i\pi(f_e T + 1/2)/P}, \\
\Delta\beta_2 &= \hat{R}_{2x}(1; 1)e^{-2i\pi(\hat{f}_e T + 1/2)/P} + \hat{R}_{2x}^*(1; 1)e^{2i\pi(\hat{f}_e T + 1/2)/P} \\
&\quad - R_{2x}(1; 1)e^{-2i\pi(f_e T + 1/2)/P} - R_{2x}^*(1; 1)e^{2i\pi(f_e T + 1/2)/P}.
\end{aligned}$$

Then, the asymptotic variance of $\hat{\epsilon}$ can be expressed as:

$$\gamma_\epsilon = \zeta_2^2 \lim_{N \rightarrow \infty} NE \left(\frac{\Delta\alpha_2}{\alpha_2} - \frac{\Delta\beta_2}{\beta_2} \right)^2 = \zeta_2^2 \cdot \left(\frac{V_{21}}{\alpha_2^2} + \frac{V_{22}}{\beta_2^2} - \frac{2V_{23}}{\alpha_2\beta_2} \right), \quad (\text{F.4})$$

with

$$\begin{aligned}
\zeta_2 &:= \tan(2\pi\epsilon) / [2\pi(1 + \tan^2(2\pi\epsilon))], \\
V_{21} &:= \lim_{N \rightarrow \infty} NE\{(\Delta\alpha_2)^2\}, \\
V_{22} &:= \lim_{N \rightarrow \infty} NE\{(\Delta\beta_2)^2\}, \\
V_{23} &:= \lim_{N \rightarrow \infty} NE\{\Delta\alpha_2\Delta\beta_2\}.
\end{aligned}$$

The term V_{21} can be re-written as:

$$\begin{aligned}
V_{21} = \lim_{N \rightarrow \infty} NE \left\{ \left[e^{-2i\pi(\hat{f}_e T + 1/2)/P} \delta_1 - e^{2i\pi(\hat{f}_e T + 1/2)/P} \delta_1^* \right. \right. \\
\left. \left. + e^{-i\frac{\pi}{P}} R_{2x}(1; 1) \delta_2 - e^{i\frac{\pi}{P}} R_{2x}^*(1; 1) \delta_2^* \right]^2 \right\}
\end{aligned}$$

with

$$\delta_1 = \hat{R}_{2x}(1; 1) - R_{2x}(1; 1),$$

and

$$\delta_2 = e^{-2i\pi\hat{f}_e T/P} - e^{-2i\pi f_e T/P} .$$

A first-order Taylor series expansion implies further:

$$\delta_2 = -\frac{2i\pi T}{P} e^{-2i\pi f_e T/P} (\hat{f}_e - f_e) = -\frac{2i\pi T}{P} e^{-2i\pi f_e T/P} \zeta_1 \left(\frac{\Delta\alpha_1}{\alpha_1} - \frac{\Delta\beta_1}{\beta_1} \right).$$

After defining the intermediary variables:

$$\begin{aligned} \lambda_1 &:= \frac{2i\pi T}{P} \zeta_1 \lambda e^{2i\pi f_e T/P}, \\ \lambda_2 &:= -\frac{2i\pi T}{P} \zeta_1 \lambda e^{-2i\pi f_e T/P}, \end{aligned}$$

and

$$\begin{aligned} \lambda &:= \left(\frac{1}{\alpha_1} - \frac{1}{\beta_1} \right) \left[R_{2x}(1; 1) \tilde{\Gamma}_{1,1}^{(1,-1)} + R_{2x}(-1; 1) \tilde{\Gamma}_{1,1}^{(1,1)} \right] \\ &\quad - \left(\frac{1}{\alpha_1} + \frac{1}{\beta_1} \right) \left[R_{2x}^*(1; 1) \Gamma_{1,1}^{(1,-1)} + R_{2x}^*(-1; 1) \Gamma_{1,1}^{(1,1)} \right], \end{aligned}$$

it follows that:

$$\begin{aligned} V_{21} &= 2\text{re} \left(e^{-4i\pi(f_e T/P + 1/2P)} \tilde{\Gamma}_{1,1}^{(1,1)} \right) - 2\Gamma_{1,1}^{(1,1)} + 4\text{re} \left(e^{-2i\pi(f_e T/P + 1/2P)} \lambda_2 R_{2x}(1; 1) \right) \\ &\quad - 4\text{re} \left(e^{-2i\pi f_e T/P} \lambda_1 R_{2x}^*(1; 1) \right) - 4\text{im}^2 \left(\frac{2i\pi T}{P} e^{-2i\pi(f_e T/P + 1/2P)} R_{2x}(1; 1) \right) \gamma_{f_e}. \end{aligned} \quad (\text{F.5})$$

The expressions of V_{22} and V_{23} as well as the remaining parts of the other propositions can be derived using similar arguments. Moreover, according to Eq. (4.7), we obtain that

$$\alpha_2 = -2i \frac{\sigma_w^2}{P} \sin(2\pi\epsilon) G(1; 1), \quad (\text{F.6})$$

and

$$\beta_2 = 2 \frac{\sigma_w^2}{P} \cos(2\pi\epsilon) G(1; 1). \quad (\text{F.7})$$

Finally, plugging Eqs. (F.6), (F.7), and (4.7) back into (F.5) and (F.4) concludes the proof.

VITA

Yan Wang was born in Wuhan, Hubei Province, China. His permanent address is: Tai Yue Yuan 901, Haidian District, Beijing, 100876, China. He received the B.S. degree from the Department of Electronics, Peking University, Beijing, China, in 1996 and the M.Sc. degree from the School of Telecommunications Engineering, Beijing University of Posts and Telecommunications (BUPT), in 1999. From 1999 to 2000, he was a member of BUPT-Nortel R&D Center, Beijing. Since 2000, he has been a Research Assistant under Prof. Erchin Serpedin with the Department of Electrical Engineering, Texas A&M University, College Station. His research interests are in the area of statistical signal processing and its applications in wireless communication systems.

The typist for this thesis was Yan Wang.